NTNU
Norwegian University of
Science and Technology

Design and Optimization of a Miniature Autonomous Drilling Rig

Contribution to the Drillbotics Competition

2018

Andreas Thuve

Petroleum Geoscience and Engineering

Submission date: June 2018
Supervisor: Alexey Pavlov, IGP
Co-supervisor: Tor Berge Gjersvik, IGP
Sigve Hovda, IGP

Norwegian University of Science and Technology
Department of Geoscience and Petroleum

Abstract

Drillbotics is an international drilling competition hosted by DSATS for the fourth consecutive year, arranged to accelerate advancement in drilling automation. NTNU was one of nine universities that based on a design report got accepted to the 2018 finals. This report will portray NTNU's Phase II contribution to the competition, including design calculations, technical considerations and key findings, as well as describing the competition day.

A report was made for Phase I of the competition which serves as a foundation to the work done in this release [1]. The changes introduced in Phase I are implemented on the rig and described here, in addition to several new ideas. The miniature rig has been improved through four different design focuses: safety, performance & reliability, simplicity and digitalization.

By adding an acrylic plexiglass to surround the drill pipe and pump shaft, drilling HSE has been improved. A semi-closed system was implemented on the rig's circulation system, removing water from the rig floor, and separating it further from the electronics.

Through designing a non-aggressive bit, the miniature rig was able to drill with increased weight at lower torque, shielding the drill pipe from twist-off while increasing ROP. Stiffness of the rig was improved by the addition of structural support to the rig framework as well as a cylindrical load cell. Together with a new ball screw, this resulted in reduced drilling vibrations while improving control responsiveness. A low-wear bearing was implemented to reduce damage on the drill pipe, while a universal coupling was added below the top drive to absorb vibrations stemming from misalignment.

The rig design has been simplified. With a newly designed downhole sensor card solution, four components were removed from the stabilizer in the BHA while maintaining hydraulic integrity. An automatic balancing unit sub has been proposed and tested, however proved to be under-dimensioned and failed during testing. A shorter stabilizer design was incorporated, reducing BHA weight and the pipe's tendency to twist-off, by reducing the difference in torsional inertia between drill pipe and BHA.

A framework for digitalization has been established. This includes fit-for-purpose software in a transition from MATLAB SimuLink to NI LabVIEW, and data lake-access of automatic well reporting. An improved GUI design was implemented, improving QoL for the driller. Additional sensors are added, including downhole accelerometer and gyroscope, and a topside ultra-sonic intelligent sensor unit, for formation boundary analysis. The control system may now run two different scripts: a competition script designated to performance in the Drillbotics competition, and a full autonomous script. The autonomous script is capable of detecting and estimating drilled formation from a selection of different rock, and optimize drilling accordingly.

The Drillbotics 2018 competition day was held on June 4th. The NTNU rig was successfully able to drill through the entirety of the competition rock, with total drilling time of

195 seconds. The competition rock included a variety of formations of different hardness, and a detrimental 45° inclination. The rig proved its ability by drilling without any dysfunctions, showcasing smooth layer transition through integrator reset and ability to handle over-torquing. Utilizing a best-fit compromise PID tuning allowed the rig to handle both soft sandstone as well as a hard section of flatstone.

Sammendrag

Drillbotics er en internasjonal borekonkurranse grunnlagt av DSATS holdt for fjerde år på rad, designet for å akselerere utviklingen innen boreautomatisering. NTNU var et av ni universiteter som ble, basert på høstens designrapport, akseptert til finalen i 2018. Denne rapporten skildrer NTNUs bidrag til konkurransen, inkludert designberegninger, tekniske hensyn og nøkkelfunn, samt beskrivelse av konkurransedagen.

En rapport ble laget for fase I i konkurransen som fungerer som grunnlag for arbeidet i denne utgivelsen. Endringene som ble introdusert i fase I er implementert på riggen og beskrevet, i tillegg til flere nye ideer. Miniatyrriggen har blitt forbedret gjennom fire hovedfokuspunkt: sikkerhet, ytelse og pålitelighet, simplifisering og digitalisering.

Helse, miljø og sikkerhet på riggen er økt ved å legge til et sikkerhetsglass rundt borerøret og pumpeakselen. Riggens sirkulasjonssystem er også forbedret ved å implementere et avløpssystem som tar seg av returstrømmen av boreslammet og fjerner unødvendig søl fra gulvet samt skjermer det elektriske systemet.

Ved å designe en ikke-aggressiv borekrone, kan miniatyrriggen bore med økt matekraft ved lavere dreiemoment som beskytter borrøret fra avrivning samtidig som man øker penetrasjonsrate. Stivheten i riggen ble forbedret med strukturell støtte til riggrammen samt en sylindrisk lastcelle. Sammen med en ny kuleskrue resulterte dette i reduserte borevibrasjoner samtidig som kontrollen økte. Et slitesterkt lager ble implementert for å redusere skade på borerøret, mens en universalkopling ble lagt under hoved-boremotoren for å absorbere vibrasjoner som skyldes skjevheter i oppsettet.

Riggdesignet har også blitt forenklet. Ved å benytte en nyutviklet løsning for nedihullssensorkort ble fire komponenter fjernet fra stabilisatoren i nedihullskonfigurasjonen (BHA) samtidig som hydraulisk integritet er opprettholdt. En automatisk balanseenhet er blitt foreslått og testet, men viste seg å være underdimensjonert og ble ødelagt under testing. Et kortere stabilisatordesign ble innarbeidet. Det nye designet har lavere vekt som har minket sjansen for avrivning ved å redusere forskjellen i treghetsmoment mellom borerør og BHA.

Et rammeverk for digitalisering er etablert. Dette inkluderer tilpasset programvare i en overgang fra MATLAB SimuLink til NI LabVIEW, og data lake-tilgang fra automatisk brønnrapportering. Et forbedret grafisk brukergrensesnitt har blitt implementert med økt

brukervennlighet for borelederen. Ekstra sensorer er lagt til, inkludert nedihullsakselerometer og gyroskop, og en ultrasonisk intelligent overflatesensor, for formasjonsgrenseanalyse. Kontrollsystemet kan nå kjøre to forskjellige skript: et konkurranseskript med formål om økt ytelse i Drillbotics-konkurransen, og et fullstendig autonomt skript. Det autonome skriptet er i stand til å oppdage og estimere hvilken formasjon som blir boret fra et begrenset utvalg av kjente bergarter, og optimaliser boringen deretter.

Konkurransdagen for Drillbotics 2018 ble avholdt 4. juni. NTNU-riggen avla en vellykket boreoperasjon og fullførte hele konkurrasesteinen uavbrutt med en total boretid på 195 sekunder. Konkurransesteinen inkluderte en rekke formasjoner av forskjellig hardhet og en baderomsflis med 45° helning. Riggen viste sin evne til å bore uten problemer, deriblant glatt lagovergang gjennom integratortilbakestilling og evne til å håndtere overmomentering. Ved å bruke en kompromissutgave for PID-justering kunne riggen håndtere både myk sandstein og harde fliser.

Acknowledgement

Table of Contents

List of Tables

List of Figures

Chapter 1

Introduction

With record-high global crude oil production rates of 3.95 *M thousand toe per year*, petroleum resources are depleted faster than ever [2]. The demand for petroleum products is only growing: daily demand worldwide has increased 16% over the last 10 years [3]. As long as the human dependency on petroleum products remains, the industry seeks to continuously develop and invent techniques to maintain production and increase recovery. Inspired by other industries, the petroleum industry does so by an increased level of automation in all its sectors, one of which is drilling.

Automation in the drilling industry allows for more precise and reliable drilling, enabling access to remote and complex reservoirs. In the last 20 years, only one new discovery, the Johan Sverdrup field, ranks among the 30 largest oil field on the Norwegian continental shelf (NCS) [4]. On NCS, and estimated 45% of total recoverable petroleum resources have already been recovered. While forecasts expect production to last for yet another 50 years, maintained production relies on improved recovery rates, new techniques, innovations and development of new fields [5]. Low-hanging fruits are already under production. The remaining resources are more complex in structure, located in remote environments under tough conditions.

Automation of drilling systems allows for more precise, reliable and responsive drilling, enabling drilling of longer, accurate and complex wells. The Norwegian Petroleum Directorate reports that out of all expenses in the oil and gas industry in Norway in 2016, 25% is spent on developing wells [6]. With increased levels of automation, drilling time is shortened, risk of failure is reduced and there is less need for manpower. By eliminating the need of human intervention, people are removed away from the hazardous drill floor and harsh environments of drilling rigs. Through automation, drilling as a profession and petroleum as an industry becomes safer.

In 2008, a group of Society of Petroleum Engineers (SPE) members formed Drilling Systems Automation Technical Section (DSATS). DSATS is a sub-committee dedicated to

"accelerate the development and implementation of systems automation in the well drilling industry" [7]. In 2015, the annual competition Drillbotics was organized by DSATS for the first time. The competition encourages multi-disciplinary teams of students worldwide to develop, craft and program a miniature drilling rig and related technologies capable of autonomous drilling. To compete, each team is sent an enclosed unknown rock formation replicating geology of real oil fields. Pressing only a start button, the teams will employ their machine to drill fast and efficiently while optimizing borehole quality and avoiding drilling dysfunctions. The competition aims to introduce aspiring students to drilling automation while at the same time initiating development of new innovative technologies and control processes.

2018 marks the fourth successive year of the Drillbotics competition. The Norwegian University of Science and Technology (NTNU) entered for the first time in 2017. Out of the nine teams competing in the final, NTNU's contribution landed the second place. Last year's work included design and construction of a miniature drilling rig from scratch. Without experience in the competition, the team built a functioning machine and developed a control system capable of automatic drilling that maintains integrity and avoids drilling dysfunctions. After the competition, during the fall of 2017, NTNU's drilling rig was evaluated, tested and analysed as described in a project report [1]. Based on that evaluation, new technologies, improvements and algorithms have been implemented in an updated version of the rig. This thesis elaborates on the evaluation process and discusses results of drilling autonomously the new features.

Mechanical improvements include stiffening of the structure, alignment of components that surrounds the drill string, a hydraulic system, added safety features, standardized formations for systematic testing, new tooljoint, customized bit and bottomhole assembly (BHA) and other measures that improve convenience of use, reliability and drilling performance. An updated control system allows the drilling rig to run different control algorithms for different purposes. To some extent, it is capable of detecting and estimating drilled rock formations, using a library of pre-determined optimal drilling parameters to drill efficiently. The control system is implemented in a new, fit-for-purpose software with improved graphical user interface (GUI). A system for automatic well reporting is now an integral part of testing. Data lake solutions enable efficient data analytics. New instrumentation both downhole and topside give enhanced drilling data. The work described in this thesis is motivated by performance in the Drillbotics competition. However, equally important, the thesis attempts to look at the wider picture and use the miniature rig to develop autonomous solutions that are applicable in full-scale operations in the industry.

The mechanical design of the rig, test formations, hydraulics, drill bit and bottom hole assembly (BHA) are described in section 6. Operational limitations and constraints are discussed in section 7. Algorithms, software and instrumentation on the rig are described in section 8. Results from various tests described throughout the thesis are found in section 9. Section 10 discusses NTNU's performance and results from the on-site competition held on the 4th of June, 2018. Challenges encountered throughout the project, ranging from hardware-related issues to difficulties with project management and time-planning,

are discussed in section 11. The project has potential for improvement and further development of technologies and solutions. Recommendations for future work are found in section 12.

Chapter 2

Organization

The Drillbotics competition is a team project with a maximum of five students on each team. The NTNU Drillbotics team 2018 has been fortunate enough to recruit five students. A structured organization is required to make a team work together. A precise plan is necessary to make sure that the whole team has the same vision and at all time works towards the same goal. Working in a team project as comprehensive as Drillbotics is new to all the team members and the learning outcome of this process has been immense in terms of team management and time planning.

2.1 Team

The team consists of four students from the petroleum department specialized in drilling engineering and one from the cybernetic department. The team is supported by three supervisors from the petroleum department and one from the Cybernetic department. Furthermore, the team has a support team at the lab. The team at the lab support the everyday work including both the mechanical and the electrical work.

2.2 Roles

To ensure that the potential of team is used as efficiently as possible, every team member has been dedicated a specific role. The roles are displayed in **Fig. 2.1**. The team management was discussed in a meeting early in Phase I of the competition with the purpose of making use of the interests and the pre-knowledge of every individual constructively. The roles were set to make sure that every team member should know who to inquire with questions related to the different fields. The team felt it was important with an open work environment and as some of the roles are broader and more time consuming than others, it has been necessary to communicate and work across the roles.

2.3 Project Management

The Drillbotics competition is divided into two phases. In Phase I, the team should make a design proposal for the rig. The design proposal should include a detailed plan for the mechanical setup, programming, safety and cost estimate. In Phase II, the purpose has been to implement the plan made in Phase I, including ordering parts and building the rig. When the rig was completed, the mechanical limits of the rig needed to be evaluated before moving into the programming phase. It has been extremely important for the team to document the progress to learn from earlier events. Documenting the progress also makes it easier for next year's team to keep track of what has already been done making the handover as smooth as possible.

Continuous information flow within the team is key for good progress. To provide this, morning meetings have been held regularly. The duration of the morning meetings have been about half an hour. The meetings have mainly been for each team members to present what they have produced and to discuss any problems or issues that may have occurred since last meeting. The team has continued meeting the supervisors every second week, mainly to give status on the rig. Central aspects of the future work has also been discussed during these meetings an how to handle any time delays.

The team has taken certain measures to organize and keep track of progression. One of the measures has been creating online documents as a simple and fast way of keeping the whole team updated. Amongst the documents that has been made, the following are the most crucial:

- **Lessons Learned Log:** Last semester a Lessons Learned document was made after request from the supervisors. The document is a great way of logging steps in the process. In the document every event should be logged with a comment on the outcome. It is important to log both positive and negative incidents to see what is working and what needs to be improved.
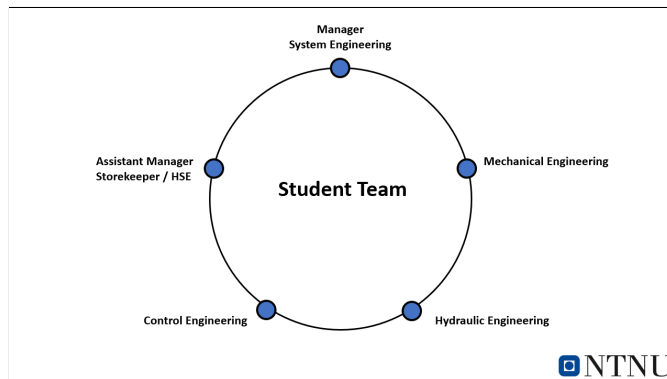
Figure 2.1: Different roles in the Drillbotics team 2018. The team is divided into specific roles to ensure systematic work and constant progress in all aspects of the project.

- **Inventory List:** To keep track of equipment on the rig, an inventory list was made in Phase I. The list is meant to be a resource preventing any delays related to lack of equipment.

- **Action Log:** An action log was created with the intention of logging every detailed plan and work done on the rig. Action logs are common in the industry especially for larger companies to make sure that people from different departments can see what has been done at the project at any given time. The action log has not been utilized as much as first intended due to various reasons. Mostly the team felt the time spent on paper work did not pay off in terms of simplicity.

- **Drilling Report:** For the testing phase it is important for the team to have a consistent and well organized template on how to run tests and systematize the logging of parameters. To make the most of the results, a standard sheet has been made to log every test run. **Fig. 2.2** shows the drilling report. The drilling parameters for every run are logged such as WOB, RPM and make-up torque. The logged parameters are also saved on the computer with date and number. To keep track of the hole quality, dimensions of the hole are logged in the "comments" section. For post-analysis both analytically and visually, the position of the test runs are made in a specific system, making it easy to compare the test data with the actual hole.

- **Time Planner:** To keep track of the time in the project a time planner was created. All plans are included in the document with an estimate of how long time it should take. To make sure that the project will meet the final deadline it is also important to include a safety margin to encounter any unexpected delays.

The Drillbotics Guidelines state that a monthly project report should be submitted to DSATS to document progress, issues and key learnings. The report has been a great way of forcing the team to collecting and systematize data and present it to a third party. Due to the measures listed above, the monthly project report has mainly been a summary of the documents listed above, and how we are keeping up with the time planner.

2.4 Time Planning

The team took use of a time planner already early in Phase I of the competition. The Drillbotics project is built up of many small projects which all depend on each other. Experienced from last semester, it is extremely important to make use of the time planner

Test 2			Team members present			
Purpose of test	Test LabVIEW drilling					
Run Number/File name	Excel file "Drilling data 140318" Run 2			Y	N	Description
Formasjon	Cement		Twistoff?		x	
Bit	Alibaba		Whirl?		x	
M/U Torque	17	Nm	Other dysfunctions?		x	
WOB	15	kg	Comments			
RPM	1000	RPM				
Trykk	6	bar	Smooth drilling, but too low WOB, approx. 5 kg measured			
Max hoist torque	0,3	Nm				

Figure 2.2: Layout of the drilling report used for systematic logging of drilling tests.

as early as possible. For Phase II , this was done early January where the team gathered a meeting discussing all the aspects of the competition and where the bottle necks might occur. The expected time for every event was estimated including a safety margin. The expected time was the minimum time and the expected time combined with the safety margin was set to be the absolute worst case scenario. Last semester, the team learned that making a time planner can be challenging. The challenging part mostly related to aspects that was not controllable within the group. In Phase I most of the work were related to the design of the rig and minor reworks. The design was made by the team members with assistance from the support team at the workshop. The crew at the workshop is assisting several other projects and is not always available despite their efficiency. This caused some delays, but rarely more than a couple of days. In Phase II many of the plans were made with external companies, turning out to be more time consuming than expected.

An important part of Phase II in the Drillbotics competition has been ordering parts for the drilling rig. The team identified this as a potential source of delays, and therefore wanted to order parts as early as possible. Orders were written down in the time planner, each with their expected delivery date as given by vendors. The team added a conservative extension to the delivery dates, to be on the safe side should there be any delays. However, ordering parts turned out to be more difficult in practice. The team has experienced delays surpassing even the safety margins. For instance, the team did not take into account difficulties contacting vendors and delays before ordering, only that post-order.

Compared to Phase I, the delays in Phase II have been significantly larger. While a delay in Phase I caused hours or days of downtime, the delays of orders made during Phase II have lasted up to several weeks. This has caused delays in the plans, despite a safety margin of up to 50%. Measures have been made to keep up with the deadlines and to maintain progress on other fields while the rig has been waiting on parts.

Progress in LabVIEW strongly depends on a functioning rig. The script needs to be tested in order to check for errors and bugs. This is not possible to do during reconstruction of mechanical parts of the rig. These delays were taken into account. After the mechanical design was finished, the rig still experienced longer periods of downtime due to unexplained software issues. The problems related to recommended software from National Instrument that did not work as first assumed. The back-up solution of PLC and OPC saw problems updating data and sometimes shutting off, still without a discovered pattern. Unfortunately, these delays have affected the amount of tests that has been run. To compensate for this, the team has made a structured future work plan.

Chapter 3

Safety

Working in the petroleum industry includes flammable chemicals, powerful machines and high pressure processes which can all be dangerous if not treated with respected or with incorrect handling. According to EHSToday the fatale rates in the petroleum industry is seven times higher than any other industry [8] where transportation and contact injuries from falling objects are the most frequent hazards. Occupational Safety and Health Administration, OSHA, presents graphically how to avoid hazards in hierarchy of controls in **Fig. 3.1**. The hierarchy rates measured from low to high efficiency where PPE is the lowest efficient and eliminating the hazard is the highest efficiency. Introducing automation using machines in high risk zones is placed in the middle of the hierarchy as it does not take away the danger completely, but still eliminate the presence of human personnel.

Drillbotics is a multidisciplinary master project involving both manual and theoretical work. Rig construction and operations are new to most of the team members as the education does not provide this. Luckily the students have a support team of qualified personnel helping and instructing during these processes. Despite the help from the support team it is important to take precautions to avoid dangerous situations. As in any project with potential hazards, safety of personnel is the number one priority.

Even though the miniature rig operates at lower drilling parameters with less forces involved, the chance of minor injuries are still present. In Phase I, the major focus was improving the mechanical design of the rig. For Phase II, testing of the rig has been the main priority, but in order to do so, a lot of mechanical work has been necessary which involved heavy equipment, high temperature and spinning objects. Prior to the lab work, the team from the workshop held a full safety course for the students including regulations and procedures in case of an emergency. A new safety course was held early in Phase II as this phase involves more test drilling and requires team members working at the lab without supervision by lab personnel. OSHS states that two of the biggest threats to oil rig workes are human errors and worker culture. To ensure a healthy and safe mindset of the team members, safety guidelines have been made with operating procedures while
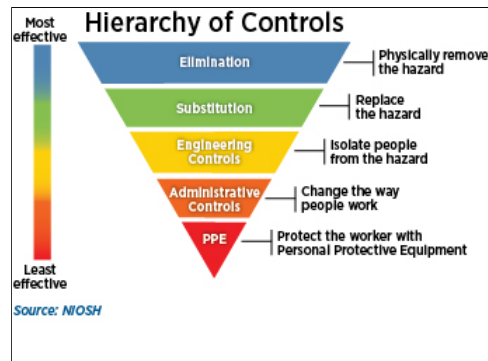
Figure 3.1: Shows OSHS's hierarchy triangle of controls explaining measures for avoiding hazards and the correlating efficiency. The triangle sheds light on the effect of changing working procedures and extracting personnel from dangerous situations.

working on the rig site. A risk assessment can also be found in appendix B.

Section 3.1 and 3.2 discuss safety during construction and operation of the rig. This master thesis is building on the work done in Phase I of the competition, thus many of the measures rule for this semester as well. The sections are therefore an extended version of the safety section in Thuve et. al. (2017).

3.1 Hazards During Rig Construction

Safety hazards related to rig construction are mechanical. They include cuts, pinching injuries, debris, heavy lifting and operating machinery. Most of the rig construction was completed last year, so the risks are low for injuries during construction. Also, construction of the rig is only to be done by qualified personnel. Should the Drillbotics team members help with the construction, they must wear protective equipment such as gloves, glasses, helmets, boots and lab coats.

In accordance with NTNU safety regulations, all high voltage setup on the rig must be performed by qualified personnel. Potential incidents with electrical equipment include shocks and damage to equipment. Risk reducing measures include keeping water away from electrical sources and making sure power is cut off while connecting wires and components. In addition, all wiring shall be insulated.

3.2 Hazards During Operations

As the team has spent considerable time testing the rig and drilling rock samples, the safety hazards during operation of the rig are important to identify and mitigate. Most of the hazards are linked to handling the rock samples, moving parts on the rig, high internal

pressure and buckling of drill pipe. Risk reducing measures are mainly the use of proper personal protective equipment (PPE) and overall awareness.

Last year, the rock samples were nonuniform and strapped in place in a wooden cage. No wheels were placed on the cage for easy handling of the rock. Last year's team justified this by having caster wheels on the rig itself, stating that it would allow for easy positioning above the rock sample. In practice, this was a poor solution as there is limited space for the rig in the lab. Therefore, to correctly place the rock sample under the rig several people were required to push and pull it in place. Potential incidents when moving heavy rock samples include back injury, muscle strain, cuts and crushing of fingers or toes. It is therefore important to wear gloves and shoes when moving the rock sample. A new solution for rock samples to be drilled was designed and constructed in Phase I. It is essentially a wooden box with casters that can be filled with cement and other desired rock types that allows for easy handling and placement of the rock sample. In Phase II several similar rock samples have been made. Since the team only have one set of wheels, the design has been slightly changed. The caster wheels have been replaced with two pairs of wooden beams underneath the rock sample allowing transportation using a pallet jack.

Applying weight on bit through the drill pipe is imperative for any success in Drillbotics. Employing too much weight can lead to buckling of the pipe with risk of injury to personnel from debris. Mitigation of the risks include following drilling procedures, testing buckling limits including design factors. For the testing phase, a maximum limit for WOB is implemented in the script set to shut off all motors if reached. To decrease the chance of reaching the maximum set points of the motors, the integral windup is bounded decreasing the chance of overshooting due to accumulated errors. For the competition, reaching the maximum top drive torque limit will not stop the hoisting motor, but rather pull up a certain length before continuing the drilling process.

The new setup for return flow directs water from the well through a hose directly to the drain. Last year's setup had no control of the return flow. Water ended up on the floor, and was further diverted to the drain through a path made of tape and cable. This system had poor control of the water and also left a mess of cuttings. The upgraded system diverts the return flow in tubing from the rig site to the drain, eliminating any chance of water being in contact with the electrical system.

The circulation system includes a water pump to increase the pressure in the circulation system. For safety reasons burst calculations are done on the drill pipe including a safety factor. The previous team believed that by increasing the internal pressure in the drill pipe one could avoid buckling and therefore wanted as high internal pressure in the pipe as possible. This theory was thoroughly investigated by this year's team in Phase I. The conclusion after several buckling tests was that the internal pressure does not increase the buckling limit as they assumed and a high internal pressure pressure is therefore not desired any more. The wall thickness of the pipe this year has been increased by 30%. The combination of higher burst limit and lower internal pressure gives a low chance of bursting the pipe. During drilling, the pump pressure is set to a constant 15 bar. If, by any

chance, the hydraulic system should get clogged, a relief valve is implemented after the water pump with a maximum limit of 100 bar. This valve should eliminate the chance of pressure damage to the system.

To prevent the drill string from drilling beyond the rock formation, a maximum limit for position is included in the script. The maximum limit has a reference point from the kelly bushing and is set to stop 10 cm above the floor. For extra safety, the system has two stop switches, one at the top and one at the bottom of the roller guide. The top switch prevents the guide frame going over the top of the roller guide and is also used for running a positional homing sequence. The bottom switch works as a double barrier stopping the rig from drilling through the floor.

According to the US Bureau of Labor Statistics, roughly 20% of injuries in the oil and gas industry are caused by being caught in objects, equipment or material [9]. The rig contains several moving and rotating parts. Serious injury might occur if someone is caught. Loose clothing is therefore prohibited in the vicinity of the rig. In addition, it is important that all power is shut off before connecting or reconnecting the drill pipe or BHA.

To distance the personnel from any possible danger, an acrylic safety glass is installed surrounding all moving objects and high pressure zones. The acrylic glass has two sections, one surrounding the test rock under the drill floor and one surrounding the drill string from the drill floor up and above top drive. The first section has a door which can easily be opened when changing rock sample or when doing adjustments on the BHA. The second section uses a hoisting mechanism which allows for full access to the drill string when opened. It is strictly forbidden to pressurize the system or start rotation of the drill string before both sections are closed.

A major hazard when operating electrical equipment such as motors is the possibility of fire due to improper electrical wiring or overheating of motors. All personnel have familiarized themselves with the emergency exits and procedures in case of a fire. Only qualified personnel is to modify the electrical equipment. Other general hazards include tripping, damage to hearing and falling objects. It is important to maintain a clean working environment, ensure good housekeeping and use proper PPE.

Emergency Stop Button

The rig is operated by the driller who monitors the drilling process closely. The driller has the possibility to stop the rig at any time, should something unwanted happen during a run. Using the GUI to stop a drilling run has a lag time as the rotations and the WOB will ramp down to zero. In an emergency situation it is important with quick reaction time. As a second and faster barrier, an emergency stop button placed outside the electrical cabinet is implemented in the control system. For safer drilling, one person is always in charge of the stop button during test runs. The stop button should be pushed if drill pipe failure or other situations that may damage personnel or the equipment occur.

Chapter 4

Automation in the Industry

According to the Cambridge Dictionary, automation is defined as machines acting automatically [10]. The term saw first widespread use in 1947, in conjunction with Ford Motor Company building an automated department for automobile production [11]. Whereas earlier facilities took in use manpower to treat, assemble and paint the various car parts, a new setup used tailored machines or *robots* instead. This made the manufacturing facilities safer, and improved production rates. Various degrees of automation exist, ranging from fully human control to complete autonomy. Macpherson et al. discussed in their 2013 paper [12] such a model, where they divide this range into ten categories, as shown in **Fig. 4.1**.

The figure from Macpherson is interesting when considering automation in the drilling industry. Generally, it can be said that the ultimate goal is LOA 10 - no human interaction necessary. This would first and foremost eliminate the need of human presence in dangerous locations such as a drilling rig, thus improving safety of operations. Furthermore, the use of artificial intelligence and machine learning could generate smart algorithms to allow for drilling through tighter mud windows, reaching targets otherwise out of range.

Levels of Automation	Functions			
	Monitoring	Generating	Selecting	Implementing
1. Manual Control	Human	Human	Human	Human
2. Action Support	Human/Computer	Human	Human	Human/Computer
3. Batch Processing	Human/Computer	Human	Human	Computer
4. Shared Control	Human/Computer	Human/Computer	Human	Human/Computer
5. Decision Support	Human/Computer	Human/Computer	Human	Computer
6. Blended Decision Making	Human/Computer	Human/Computer	Human/Computer	Computer
7. Rigid System	Human/Computer	Computer	Human	Computer
8. Automated Decision Making	Human/Computer	Human/Computer	Computer	Computer
9. Supervisory Control	Human/Computer	Computer	Computer	Computer
10. Full Automation	Computer	Computer	Computer	Computer

Figure 4.1: Macpherson et al. divided the levels of automation into ten categories, from manual control to full automation [12].

Cost is an important factor, and fully automated drilling operations could turn out to be beneficial in this aspect too. A valid counterpoint is that the added complexity of the equipment would surely add an extra initial investment cost, as compared to equipment at lower LOA. However, eliminating human presence could cut down on operational expenditures, arguably making automation economically beneficial in the long run.

As of today, it can be seen that E&P companies have been implementing automation more and more over the years [12]. At the highest LOA is most noticeably Rotary Steerable Systems. A study conducted in 2013 by de Wardt et al. showed that the mean time between failure increased by 100%, and that the automated control system delivered smoother drilling performance with less shocks and vibrations as compared to manual control [13]. Another example from the industry is the NOVOS system. This automation package from National Oilwell Varco has algorithms to select drilling parameters to maximize rate of penetration (ROP), automated tagging sequence, among other features. Doing connections with NOVOS as opposed to manually allowed for time savings of up to 41% [14].

Automated downhole equipment generates a large stream of data up and down the drill string as opposed to lower LOA equipment, ultimately reaching the bandwidth limit of the mud pulse systems readily available today. This includes the traditional poppet valve technology, but also newer telemetry applying frequency modulation. The average transfer rates of such mud pulse systems are in the range of 5 - 10 BPS [15]. With the introduction of wired drill pipes, users can enjoy transfer rates up to 57 600 BPS [15]. It is evident that this increase in transfer rates allows for more sophisticated control between downhole and surface, possibly allowing for the highest LOA.

As an example, the french E&P company Total took use of wired drill pipe on the Martin Linge Field. This resulted in an average reduction of 5.87 hours/1000 m drilled, solely due to improvements in telemetry time [16]. All this was done with an uptime of impressive 91%. However, rigs on the NCS are widely different when it comes to technology and LOA. As an example of an older rig, there is Transocean Arctic (TOA). Built in 1986, the rig is still going strong, however with low LOA and no major processes being automated. To initiate a build section and communicate a signal down hole, the directional driller has to manually alter the pump in a binary sequence. This unique pressure characteristic is recorded down hole and translated into a meaningful configuration on the rotary steerable system (RSS), generating desired dog legs. Through higher LOA and wired drill pipe this could be done quite similar to how the Drillbotics rig is operated, with a surface located control system communicating electrically to the downhole equipment. The result would be cut time and thus economic savings, and improved quality of life (QoL) for the driller.

Living in this decade of digitalization with intelligent computers and touch screens virtually everywhere, it can be quite amazing to visit a drilling rig to realize just how much is done in an old-fashioned way. An example of this is offshore logistics: On the same semi-sub as mentioned earlier, the TOA, all the containers on deck are kept track of through human inspection. That is, a crew member walks around the different decks and notes the location of different containers on a piece of paper. The list is later handed over to the

Storekeeper, who feeds the data into a computer. However, this method relies on humans interacting with each other, leading to misunderstandings and incomplete lists. In short, the library is never fully updated, and thus useless. This has led to increased costs, for instance where a supply ship has to stay put longer due to lack of space on the rig deck. If the crane operator simply transferred the different crates from boat to rig directly on a tablet with a virtual rig deck, this problem could be easily solved.

4.1   A Critique on Automation

The drilling industry can be said to be in a unique position regarding automation. Where many industries are already automated, the drilling industry is in many ways lagging behind. However, a question one should ask is: Does automation only bring along positive aspects? An example related to this is how Tesla - the electronic car manufacturer - has handled production of their latest Model 3. After not being able to reach previously set production goals, their CEO, Elon Musk, recently admitted in a tweet: "Yes, excessive automation at Tesla was a mistake (...) Humans are underrated" [17]. Even though car manufacturing and drilling are two different industries, this still adds an interesting aspect to the discussion. Could it be the case that excessively automating the drilling industry could be a mistake just like at Tesla?

The Paradox of Automation says that the more efficient the automated system, the more crucial the human contribution of the operators [18]. This can be directly transferred to the various LOA as discussed by Macpherson et al. [12], where more automation equals higher LOA. An example that is easy to relate to, can be cruise control versus autopilot in a car. Whereas the cruise control only adjusts throttle and the driver is always ready to intervene, trusting the vehicle's autopilot could prove to be a greater pitfall should it fail. This would also be the case for drilling equipment. Should computers be trusted to a full LOA 10 for all processes? Dangerous situations like handling and bleeding out a kick could be done by the computer, but some would argue a human touch on the choke is preferable. In this debate it is important to remember that humans can and will make mistakes. And for automation to be successful, it only has to overcome man, not reach perfection.

Chapter 5

Downscaling to a Miniature Rig

Downscaling is the act of reducing a system to some smaller version. This is exactly what is done in the Drillbotics competition: A miniature drilling rig is to be built, replicating a full scale drilling rig. The small scale rig should essentially do the same thing - drill a hole through rock formations. The processes are similar in many aspects, only that the dimensions of equipment, distances and loads are smaller. The miniature rig and accordingly drilled well are *downscaled* versions of the full scale. The important question to answer is: What is necessary to take into account when downscaling a drilling process, and are there any major changes to be wary about when planning the operation?

5.1 Drilling Environment

The length of a subsea well on the NCS can be several kilometres, with typical vertical depths to the reservoir between one and two kilometres. Because the formation is filled with liquid, this will be pressurized due to the hydrostatic coloumn above. An important factor when drilling is to keep formation fluids out of the well and maintain well integrity, which is done partly by keeping the well pressure above the formation pressure. Other barriers include casings and safety valves. However, even though the pressure in the well is high, the pressure *difference* between well and formation is not necessarily substantial. The well pressure is controlled by adjusting the weight of the drilling mud, or by applying a back-pressure to a lighter mud through Managed Pressure Drilling (MPD). Drilling fluid can be either water- or oil-based, where the latter in particular have a lubricating effect on the drilling equipment. The well pressure will have an upper limit equal that of the formation fracture gradient. Drilling speed is affected by the differential pressure between the well and the formation, where higher drilling rates are generally found with lower well pressure. A high well pressure will induce both static and dynamic hold down-effects that make it more difficult to remove cuttings [19]. The upper and lower limit of the well pressure make up the drilling window. At times this can be narrow, allowing for only a small overbalance in the well.

For the miniature Drillbotics rig, the size of the formation to be drilled at the competition sets an upper limit for well depth to 35 cm. This means that the bottom hole pressure will be limited by a 35 cm tall hydrostatic column of water, yielding a pressure of 0.035 bar. Further, there is no formation fluid inside the rock. This means that the pressure difference between well and formation will be directly given by the well pressure. The absolute value in pressure will be much higher for a full scale well, where pressures might reach the range of several hundred bar. However, for wells with a tight drilling window, or in the use of MPD and underbalanced drilling, the pressure differential between well and formation for the miniature rig and a real well is similar. Moreover, the drilling fluid used in the miniature rig is for the NTNU team limited to water. In addition to circulating out cuttings, the fluid offers some cooling and lubricating effect, although less than oil based compounds.

5.2 Drill Pipe

The natural difference in well length between a full scale well and the miniature rig leads to differences in the drill pipes used. Two of the main hazards for a drill pipe are buckling and twist-off, which happen when exceeding the mechanical limits of the pipe. This is discussed in detail in 7.1. Buckling limit is a strong function of pipe length, where buckling is more likely for growing lengths. This is not the case for twist-off: the torque limit is independent of pipe length. This suggests that for a full scale well, buckling should be more of a problem than twist-off. The buckling limit is also a function of pipe diameter.

The Drillbotics guidelines state that the drilling rig must use a 3' long pipe [20]. The pipe should have a 3/8" outer diameter (OD) and a wall thickness of 0.049". A typical full scale drill pipe has an OD of 5", with wall thickness of 0.875" [21]. A drill pipe joint is usually 30' long, and is often racked in stands of three joints. When drilling, the total length of the string will reach to the bottom of the well, which can be up to 10,000' or more. The drill string used in the miniature rig only consists of one pipe joint, meaning connections during drilling are not necessary. Further, this implies that the pipe length in a real world well can be over 3,000 times longer than the miniature string. Comparing diameters, the miniature pipe is about 13 times thinner. Despite this difference they both count as thick-walled pipes, having a diameter greater than 20 times the wall thickness.

Drill pipes used by the miniature rig are limited to aluminum with grade 6061-T6. The Young's Modulus of such aluminum is around 69 GPa, with an ultimate tensile strength (UTS) of 310 MPa. A real world drill pipe is made of steel, which may typically have a Young's Modulus around 200 GPa with UTS of 580-1180 MPa [22]. The difference in material properties has huge impact on the mechanical limits of the pipes.

The relationship between a pipe's parameters will determine what kind of failure it will see first. For instance, a very long pipe will tend to buckle before it twists off, whereas a short pipe otherwise identical is more likely to twist off. The miniature rig is equipped with two stabilizing sleeves, restricting lateral movement. The stabilizers further reduce the effective length of the already short pipe. Comparing the ratio between effective length and

diameter of a real drill string to that on the miniature rig, it is evident that the real world drill pipe is much longer compared to how wide it is. This geometry leads to a tendency to buckle.

When drilling with the miniature rig, the team has had more issues with twist-off as opposed to buckling of the drill pipe. Twist-offs do not seem to occur at peaks in drill pipe torque, but rather after sustained drilling with vibrations and possibly due to fatigue in the pipe. This is supported by Constantin et al., finding twist-off is usually a result of fatigue [23]. A tendency to twist-off before buckling makes sense in light of the discussion in the previous paragraph. It is reasonable to choose a weaker pipe material in the Drillbotics Guidelines, to down-scale the drilling scenario and have the material in use closer reflect the drilling loads. However, the large difference in pipe lengths accounts for more than the difference in materials. Considering this imbalance, the Drillbotics team conclude that downscaling from full scale to a miniature rig shifts the failure criterion of the drill pipe from a tendency to buckle to a tendency to twist off.

5.3   Drilling Algorithm

The NTNU Drillbotics rig uses a suite of techniques in order to operate truly autonomously. Some full scale drilling rigs operate largely on a manual basis, where others encompass more advanced and autonomous features [14]. Even though equipment and drilling environment differ between the miniature rig and full scale, software techniques for controlling and optimizing the drilling process are interchangeable. Digitalization and automation are already hot topics in the drilling industry [13], and the Drillbotics competition acts as a catalyst for development in the area. The techniques described later in this report, especially those regarding rock estimator and event detection, should be applicable for a full scale rig too.

5.4   Drilling Parameters

Some of the most important parameters during drilling are weight on bit (WOB), RPM and torque. In most cases, the first two are chosen by the driller, whereas torque is a resulting parameter. The value of this torque will firstly be a function of applied WOB and RPM, but also dependent on different variables such as bit design and formation type. For a full-scale drilling rig, the method of drilling through control of WOB is used. For the miniature drilling rig to be used in Drillbotics, a part of the discussion is to use a torque-based controller, varying WOB and RPM to achieve a constant torque even through different formations.

Regarding weight on the drill bit, the conventional method is to hang the top drive from a draw works system, which has an electronic brake attached, controlled by the driller. By adjusting the brake force, the driller can apply more or less WOB. The maximum theoretically possible weight would be the total buoyed weight of the entire drill string assembly, including topside components such as bails and top drive. Most of the weight stems from

Table 5.1: Comparison of typical drilling parameters for the miniature and a full scale rig, presenting the different orders of magnitude.

Item	Full Scale	Drillbotics	Unit
Bit Size	6 - 36	1.125	"
WOB	1,000 - 15,000	10 - 60	kg
RPM	100 - 200	1,000 - 2,000	r/min
Torque	1,000 - 10,000	1 - 7	Nm
ROP	0 - 100	0 - 40	cm/min

the heavy BHA. The weight in a drill string is distributed such that the neutral point (without any tension or compression) is axially placed well inside the heavy duty drill collar section, which is much more tolerant to loads as compared to normal drill pipe.

As for the Drillbotics miniature drilling rig, such a system using draw works to control weight *is* a theoretical possibility. Using the aforementioned criterion that weight of the drill string plus attached components have to surpass maximum desired WOB, the Drillbotics rig would at the moment be capable of around 50 kg applied WOB, which is how many kg of hardware that sit atop the drill bit. Because of drill string limitations the desired weight would most likely never reach 100 kg, and the rig's carriage could easily be modified to be heavier than it is. However, such a method was not chosen for the Drillbotics rig. The team is implementing a weight controller, which requires a possibility to control and adjust weight at a sample rate of 100 Hz. Doing such adjustments at this pace requires precise control of the weight, which the team believes would be difficult to achieve through a draw works system. Therefore, the rig is operating through a ball screw setup, applying weight on bit through pushing the bit down by rotating a ball screw with an electric motor.

The WOB difference between a full scale rig and the miniature Drillbotics rig is large, as seen in **Table 5.1**. The natural reason for the weight difference comes down to pipe limitations: whereas a full scale rig use long steel drill pipes in the size range of 5-6" OD, the miniature rig is limited to a 3' aluminum drill pipe with 3/8" OD. Moreover, the torque will be naturally higher, due to the massive load difference, as well as larger bit contact area. The torque and weight differences are reasonable and somewhat easy to accept. However, explaining why the typical RPM ranges should be this different may be less intuitive. An analogue may be comparing revs on two vehicles with different cylinder size, where the vehicle with a larger cylinder will operate at a lower RPM range to produce the same power.

5.4.1 Mechanical Specific Energy

Mechanical specific energy (MSE) is defined as the ratio between total input energy and removed rock volume when drilling. Minimizing MSE is beneficial, because more rock is dug away with less energy used. Of course, MSE has a lower limit. You cannot drill without doing work. The lower limit of MSE is numerically equivalent to the confined

comperssive strength (CCS) of the rock being drilled. However, MSE can remain constant through different drilling parameters. MSE being minimized towards CCS of the rock is an indication that the bit is operating in its *efficient zone*, as first introduced by Teale in 1965 [24], further discussed by Dupriest et al. [25]. To obtain the best ROP possible while drilling in the efficient zone, parameters such as WOB and RPM should be increased all the way to the point where MSE starts increasing. MSE is used as a tool during drilling to ensure efficiency. After presenting the governing equation, this section will use MSE to investigate the efficiency of the miniature rig from an actual drilling test run in Portland cement, and present suggestions to improve the drilling efficiency.

Deriving the Equation

By definition, MSE can be written as

$$MSE = \frac{Total\ Energy\ Input}{Volume\ Rock\ Removed}. \tag{5.1}$$

This can be decomposed into vertical and rotational energy,

$$MSE = \frac{Vertical\ Energy\ Input}{Volume\ Rock\ Removed} + \frac{Rotational\ Energy\ Input}{Volume\ Rock\ Removed}, \tag{5.2}$$

where vertical and rotational energy are respectively delivered through WOB and torque. The drilled volume will be the bit cross-sectional area (A), multiplied with differential depth of drilling (Δh). Further, the vertical energy can be seen as the work done through applying a force (F) over the differential depth Δh, so that

$$MSE = \frac{F \cdot \Delta h}{A \cdot \Delta h} + \frac{2\pi \cdot T \cdot n}{A \cdot \Delta h}, \tag{5.3}$$

where T is the drilling torque and n is number of revolutions from the bit. The second fraction can be expanded by evaluating the denominator and numerator on a *per time*-basis, yielding

$$MSE = \frac{F}{A} + \frac{2\pi \cdot T \cdot \frac{n}{s}}{A \cdot \frac{\Delta h}{s}}. \tag{5.4}$$

Revolutions per second is by definition the rotational frequency of the drill string, and same goes for $\frac{\Delta h}{s}$, which is the ROP. Further inputting WOB for the bit force F yields the final equation, as presented by Teale [24]:

$$MSE = \frac{WOB}{A} + \frac{2\pi \cdot T \cdot RPM}{A \cdot ROP}. \tag{5.5}$$

Investigating MSE and Drilling Efficiency

Using equation 5.5, the MSE during drilling can be calculated - regardless of size of the rig. Given that both rigs drill in the efficient zone of their drill bit, the miniature and a full scale should approach similar MSE values when drilling through the same rock. As discussed by Teale (1965), MSE should further be numerically equivalent to the compressive strength of the rock for efficient drilling. In the industry, the *unconfined* strength was
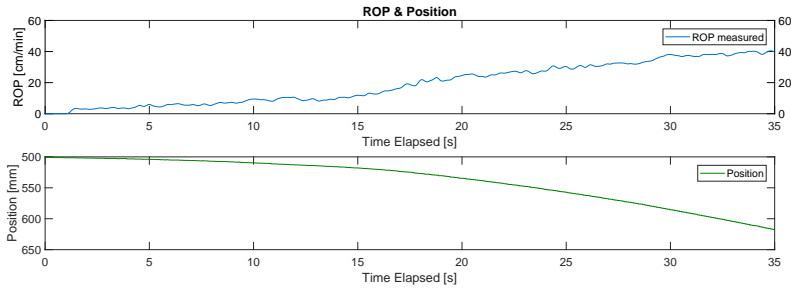
Figure 5.1: ROP and drill bit position from RKB in cement. ROP value at 35 seconds (40 cm/min) used in MSE calculation.
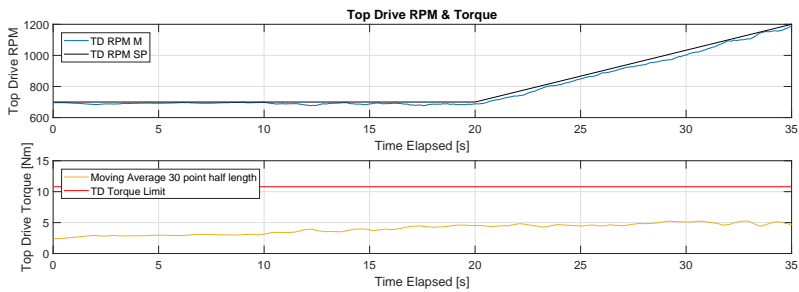
Figure 5.2: Top Drive RPM and drill string torque in cement. RPM and torque values at 35 seconds (1200 RPM, 5 Nm) used in MSE calculation.

initially used. However, operators found that rocks seemed to be more persistent when drilling them in situ, as compared to in lab experiments. Xiangchao Shi et al. (2015) published a paper, introducing a model using the stronger confined strength of the rock instead of unconfined strength, yielding better results [26]. Comparing the situation for the miniature rig and a full scale, it is evident that the miniature test rock is not supported at all, with no pore pressure or confining rock surrounding it. Therefore, the NTNU team believes that the *unconfined* compressive strength is the better choice to use in relation with MSE for the miniature rig.

The unconfined compressive strength (UCS) of regular Portland cement is a strong function of curing time. According to Pavement Interactive, the unconfined compressive strength increases from 8.3 MPa after 3 days of curing to 20.7 MPa 25 days later [27]. **Fig. 5.1**,**5.2** and **5.3** show drilling parameters for a run through regular Portland cement with the miniature rig. Extracting values for WOB, RPM, ROP and torque at 35 seconds yields an MSE value of 147 MPa, as shown in **Table 5.2**. Comparing this with even the maximum UCS listed by Pavement Interactive of 20.7 MPa suggests that the drilling is not efficient, as the MSE at 147 MPa is clearly not numerically equivalent to the UCS of 20.7 MPa. Further analysing equation 5.5 reveals that WOB has a minimal impact on MSE. In fact, mathematically increasing WOB from the drilling run above with a factor of 10 from
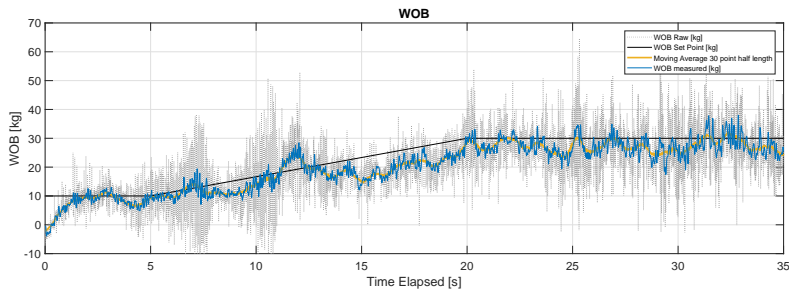
Figure 5.3: WOB for drilling in cement. WOB value at 35 seconds (25 kg) used in MSE calculation.

25 to 250 kg yields an increase in MSE of only 2.7%. On the other hand, changing the drill bit RPM has massive impact: reducing with a factor of 10 from 1200 to 120 RPM yields 89.8 % decrease in MSE. Also, MSE is very sensitive to changes in ROP. The rig is clearly drilling inefficiently with regards to MSE. Could drilling with different parameters lead to increased efficiency, bringing MSE down and numerically close to the UCS?

To reduce the MSE, the numerators of equation 5.5 (WOB, torque and RPM) have to decrease, or the denominators (bit area and ROP) have to grow. As shown by Thuve et al. (2017), the miniature rig operates poorly at RPM values less than 1000 for WOB of 20 kg and above, suffering from axial vibrations with the combination of high WOB and low RPM [1]. Additionally, the natural frequency range of the rig is hit, and the string sees severe lateral vibrations. The Drillbotics rig use a WOB-based controller. Consequently, the top drive torque is not an input parameter, and is difficult to reduce without slacking off weight. Using a less aggressive drill bit could have an impact, but this might slow down the ROP, as investigated in 9.4. The reduced MSE from lowering torque would be counteracted by an MSE increased from lower ROP. The bit area is limited by the bit diameter of 1.125" as stated in the Drillbotics guidelines [20]. Should the rig drill more efficiently, the parameter to change would have to be WOB. The team has discovered no tendency to founder in cement, and increasing WOB yields a more or less linear increase in ROP, as shown by Thuve et al. (2017) [1]. This leads to the conclusion that efficient drilling in cement for the miniature rig is unobtainable due to the weak mechanical limits of the drill pipe.

Table 5.2: Calculating MSE with equation 5.5. Parameters for miniature rig are extracted from second 35 in Portland cement (**Fig.** 5.1, 5.2, 5.3). Parameters for the full scale are not from an actual well, but are realistic in size. This combination gives an MSE comparable to that found for the miniature rig.

Item	Full Scale	Drillbotics	Unit
Bit Size	8	1.125	"
WOB	10,000	25	kg
RPM	180	1200	r/min
Torque	4,000	5	Nm
ROP	100	40	cm/min
MSE	143	147	MPa

Chapter 6

Mechanical Design

Autonomous drilling requires smart technologies and algorithms. However, drilling efficiency, stability, hole quality, integrity and overall performance is optimized by construction of a robust and reliable mechanical foundation. Clever and elegant solutions allow the control system to push involved equipment to its physical limits and extend the operating window for drilling parameters. A miniature rig and related equipment was inherited from last year's Drillbotics team. This year, the rig has been evaluated and redesigned to improve the mechanical aspects of the autonomous machine. Equipment has been replaced or upgraded and new parts have been added. Additional features include standardized formations for systematic and quantitative testing, a hydraulic system as well as design and manufacturing of a custom drill bit and BHA.

6.1 Miniature Drilling Rig

A miniature automatic drilling rig was designed and constructed last year. It replicates a full-scale drilling rig in the petroleum industry, incorporating unique solutions to enable downscaled functionality. This year, the rig has been evaluated, redesigned and upgraded in a two-phase process. This two-phase process is motivated by the structure of the Drillbotics competition, which requires submission of an initial Phase I design report to qualify for the Phase II on-site test. During Phase I, which is referred to as a design phase, the old rig was evaluated through extensive testing and improvements to the design were proposed. Phase II is a construction phase, and involved ordering, manufacturing and assembling of new parts, as well as testing of the new setup. Some features proved not to suffice, requiring continuous development of new innovative solutions throughout the phase.

This section is a brief description of the original rig with attention to features that remain in the final design. It elaborates on all improvements that were planned in Phase I and why some proposed new features were not implemented in Phase II. Most importantly, this section fully describes the final design of the drilling rig that was used in the competition. Schematics for all drilling equipment related to the rig are found in appendix C.5.

6.1.1   Original Rig

The rig from last year is built according to restrictions in the guidelines with focus on safety, mobility, drilling functionality and performance. The overall functionality of the rig is unchanged, and several features of the original rig remain in the final design. These include the rig framework, hoisting motor, top drive motor, pump, roller guides and guide frame, ball screw, hydraulic swivel, electrical swivel and several safety features. **Fig. 6.1** illustrates all rig equipment that remains from the original design.
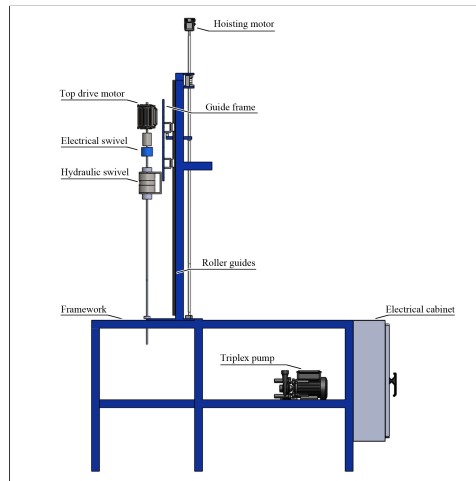
Figure 6.1: Original rig and associated equipment inherited from last year's team.

Framework

The framework is customized to integrate motors, pumps and other equipment that is required to drill in solid rock. It is made of 5 by 5 cm hollow steel beams. The rig is 70 cm wide and 285 cm tall when considering all equipment mounted on it. The framework is constructed so that it divides the rig into four different compartments. As shown in **Fig. 6.2**, steel beams form a horizontal rig floor and a vertical derrick. The derrick separates the area above the rig floor into an active compartment for the rotating drill string and travelling block, and a compartment for the computer that runs the control system and allows users to monitor drilling. The two compartments underneath the rig floor are used for accommodating rock samples and the pump and hoses. The rig floor is elevated 90 cm above the laboratory floor to enable drilling of rock samples of size similar to the rock sample that was provided for the 2017 on-site test, which was 60 cm tall. **Fig. 6.3** illustrates how the derrick may fold down for transportation, which is made possible by hinges. The rig is 253 cm long when folded down. Transportation is enabled by caster wheels mounted on each leg.
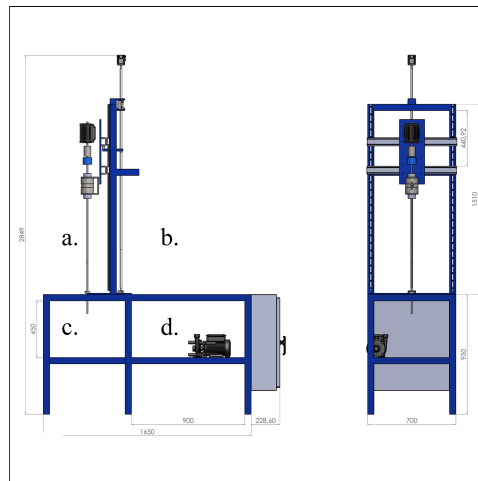
Figure 6.2: Front and side view of the miniature rig. Compartments: **a.** active drilling area for drill string and travelling block, **b.** compartment for computer, **c.** compartment for rock samples and lower end of drill string and **d.** compartment for pump and hoses. Dimensions in mm.
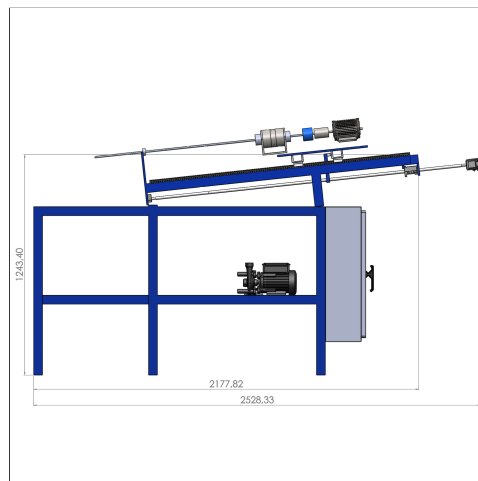
Figure 6.3: Side view of rig with derrick folded down. Dimensions in mm.

Hoisting Motor and Ball Screw

Traditional hoisting systems in the industry apply WOB by gravitational forces acting on heavy drill collars controlled by drawworks. The drilling assembly including top drive and swivel weighs in at 50 kg, and additional weight could be added to achieve more WOB. However, due to strict requirements regarding weight adjustment in the control system, the rig applies weight to the bit by a motor. A Lenze GST AC gear motor, which is referred to as the hoisting motor, is mounted on the derrick and acts through a ball screw. WOB is

achieved as rotational energy generated by the motor is transferred from rotational motion in the ball screw to linear, vertical movement in the drill string. Ball screw drive is selected for this purpose due to its high precision, step resolution and efficiency [28]. The hoisting motor is shown in **Fig. 6.1**.

Top Drive Motor

The miniature rig uses a top drive motor to provide rotation and torque to the drill string. The top drive motor is a 400 V ABB AC engine that is mounted above the drill string and may travel up and down along the derrick. Top drive is selected in favour of a rotary table and kelly drive due to the fact that the aluminum pipe is round and slick. This fact means that rotary kelly bushing would require excessive engineering to be viable. Furthermore, the top drive motor is directly connected to the drill pipe, making it more energy efficient. The top drive motor is shown in **Fig. 6.1**.

Pump and Swivel

As in the industry, drilling fluid is circulated down the drill string and out of the annulus when drilling. The rig uses water from the water supply network provided by outlets in the laboratory. Water enters the hydraulic system of the rig at 5.3 bar before being pressurized in a HAWK triplex pump. Hoses guide high-pressure water into a hydraulic swivel placed between the top drive motor and the drill string, down the rotating drill string and out of hole through the annulus. The original setup involves no handling of return flow, and drilling fluid with cuttings used to be collected in drains on the laboratory floor. The swivel provides backpressure by oil at 7.4 bar. A piston allows hydraulic connection from the water supply network and oil. The triplex pump and hydraulic swivel are shown in **Fig. 6.1**.

Roller Guides and Guide Frame

The drill string must travel vertically when rocks are drilled. To enable vertical movement, two linear roller guides are mounted on the derrick, guiding a guide frame. The roller guides hold the guide frame fixed horizontally while allowing vertical motion. The top drive motor, swivels and drill pipe are mounted on the guide frame, and follow its movements. The setup is somewhat similar to the travelling block used in full-scale operations. A horizontal steel beam, ball screw nut and nut bracket connect the guide frame to the ball screw. When the hoisting motor is engaged to provide WOB, rotation in the ball screw causes the guide frame to move vertically. The roller guides and guide frame are shown in **Fig. 6.1**.

Safety Considerations

Several risk-mitigating considerations are included in the original rig design. Acrylic glass is mounted around the rock sample compartment to physically separate it from the surrounding environment. Working personnel, electrical components and other parts of the rig are guarded from drilling fluid and debris. The front acrylic glass is made with hinges

to allow insertion and extraction of rock samples between operations. Acrylic glass is also mounted on the derrick to protect components above the rig floor in case of burst pipe or other incidents. An electrical cabinet stores all electronic equipment at a distance from the active drilling area to protect it from fluids. An emergency stop button located on the cabinet immediately overrides all electronic signals to stop all action when triggered. The electrical cabinet is shown in **Fig. 6.1**.

The original rig also features a load cell to measure WOB and two independent stabilizers to support the drill string: one mounted on the rig and one mounted on rock samples. After thorough evaluation of the original rig, these solutions have been redesigned and replaced by new solutions.

6.1.2   Improved Rig

Several features of the original rig have been redesigned with new solutions. The changes include a new load cell, ball screw, support beams to stiffen the rig framework, new solutions for stabilizing and aligning the drill string, protective glass and treatment of return flow.

Load Cell

WOB applied by the hoisting motor is measured and recorded by a load cell. In the original structure, the load cell was mounted on the horizontal steel beam connecting the ball screw and guide frame. The original load cell is shown in **Fig. 6.4** together with an illustration of its location on the original structure. This solution caused several issues. Firstly, due to absence of vertical support, the joint comprising the load cell and horizontal steel beam was flexible. Efforts to increase or reduce WOB would result in flexing of the steel beam and ball screw rather than motion in the travelling block and drill string. As a result, the control system was slow, unresponsive and unreliable. The full analysis of the original load cell configuration that was conducted in Phase I and different proposed solutions are found in appendix C.2.

The original load cell setup is removed and replaced by a sturdier solution. Now, a new cylindrical and hollow load cell is mounted on the ball screw nut bracket around the ball screw. To suppress flexing, the horizontal steel beam is welded directly onto the guide frame. A slanted steel beam connects the horizontal beam and the guide frame to provide vertical support and stiffen the previously flexible joint. The new load cell configuration is illustrated in **Fig. 6.5**.

Ball Screw

The previously mentioned ball screw has been replaced. Drilling with the old rig caused the horizontal steel beam to flex, which, in turn, caused permanent damage to the old ball screw by bending it. The damage was evident when the new load cell solution was implemented: the stiff setup recorded erratic WOB measurements when hoisting up and down. WOB plotted with depth when hoisting with the old ball screw is analysed further
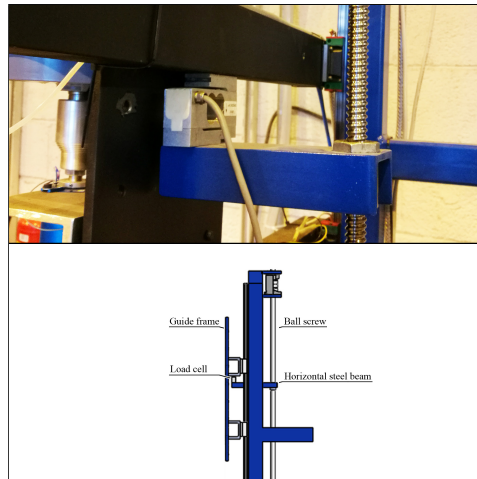
Figure 6.4: Photography of original load cell and schematic of the setup.
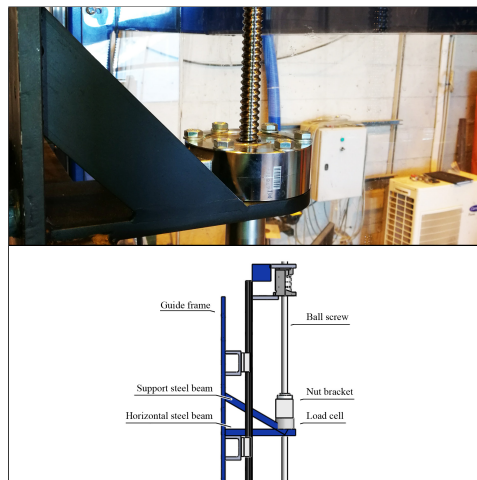
Figure 6.5: Photography of cylindrical load cell and schematic of the setup.

in section 9.8. The team intended to upgrade to a thicker and more robust ball screw. However, due to absence of larger hollow load cells on the market, the new ball screw is the same as the old one: HIWIN ball screw with 5 mm lead and 16 mm nominal diameter.

Stabilizers

The rig has two topside stabilizers mounted along the drill string. The stabilizers improve drilling performance by mitigating vibrations and reducing the effective length of free pipe, essentially reducing the risk of buckling. Both stabilizers are roller bearings separated at a distance from each other. The upper stabilizer remains at the same location as

in the original design: it is attached to the framework at the rig floor below the travelling block, as shown in **Fig. 6.6**.

The lower stabilizer solution has been redesigned. The previous solution used a *riser* - a cylinder housing for the roller bearing - that was mounted directly on top of rock samples, separated from the rig. The solution required a lot of time to properly align the lower riser with the rig and drill string prior to drilling. The lower bearing would seldom land properly in the riser. This caused several issues resulting in wear on the drill pipe and vibrations. Due to different alignment from experiment to experiment, the method was inconsistent and not very scientific. A full analysis of all problems related to the old riser from Phase I is found in appendix C.3.

The new lower stabilizer uses a riser that is attached to the rig instead of to rock samples. Now, both stabilizers are always centered around the drill string. The working principle of the new stabilizer is the working principle of the old one: a roller bearing is housed in a riser below the rig floor. The new riser is mounted on a linear riser guide attached to the rig. The linear riser guide allows the riser to move vertically along the drill string, even with drill pipe, BHA and bit installed. The solution is flexible in that the stabilizer may be placed atop rocks of varying sizes. Assembly and intervention with the drill string between operations is faster and more convenient. Before drilling, the riser is hoisted down to the rock surface and firmly locked onto it by bolts. Rings with threaded connections of different lengths fit into the lower end of the riser. They are used to extend the riser all the way down to drilled rocks. The lower stabilizer, riser and linear riser guide are shown in **Fig. 6.6**.
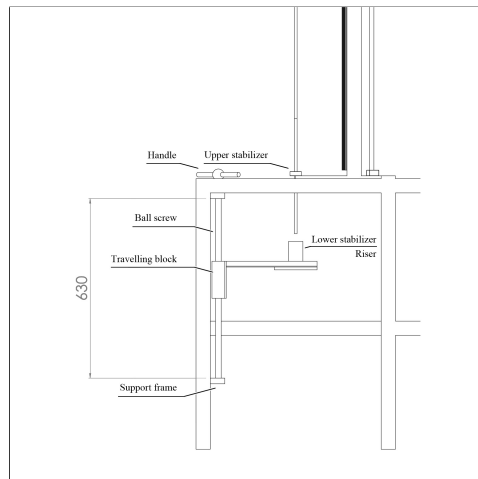
Figure 6.6: Upper and lower topside stabilizer. Both stabilizers use a roller bearing. The lower stabilizer uses a riser and linear riser guide.

The riser solves a second issue: control of return flow while drilling. Return flow is con-

tained within the riser by a neoprene layer that seals between the riser and formation. A bell nipple guides drilling fluids in the annulus out of the riser and into a hose that transports it away from the rig site.

The linear riser guide consists of a ball screw, travelling block, rotating handle and support frame on the rig. The ball screw reaches from 4 to 67 cm below the drill floor. The travelling block mounted to the ball screw is 13 cm tall, allowing the riser to travel a total distance of 50 cm. The riser is a 20 cm tall cylinder mounted on a 1 cm thick aluminum plate penetrated with multiple holes dedicated to bolts that fasten it to rock samples. An internal restriction in the riser prohibits bearings from falling into drilled holes. The restriction has an ID close to the OD of stabilizers in the BHA. The quality of pilot holes has shown to be strongly dependant on the stabilizing effect of the lower part of the riser. The roller bearing is prevented from falling out of the top of the cylinder by two tiny screws that are inserted before drilling. The bell nipple is located at the lower end of the riser. It is placed below the rotating bearing to prevent drilling fluids with cuttings from intervening with its rotation.

Support Beams

Support beams have been added to stiffen the rig structure. The beams are constructed at 45° angle between the rig floor and derrick to provide lateral support. The beams are based 52 cm from the derrick and reach 52 cm above the drill floor. Heavy-duty screws are used to mount the support beams, which are easily disassembled to allow the derrick to fold down for transportation. The support beams are shown in **Fig. 6.7**.
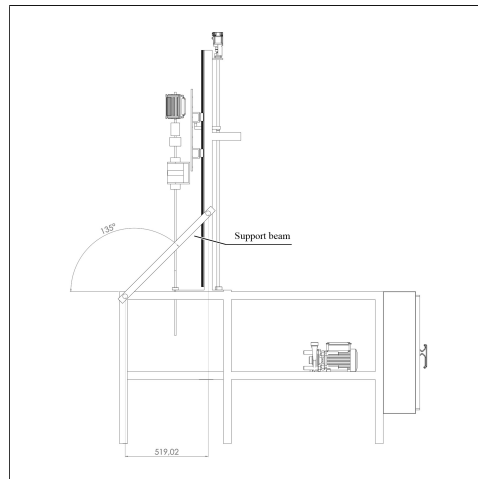
Figure 6.7: Support beams. Dimensions in mm.

Wildemanns (2017) showed by a finite element method (FEM) analysis of the rig structure that the natural frequency range of the rig is shifted from between 8 and 19 Hz (480 and

1140 RPM) to between 28 and 47 Hz (1680 and 2820 RPM) when adding the support beams [29]. The rig is excited when drilling primarily by rotation in the top drive motor. When drilling, the operating window of the top drive is generally below 1800 RPM. This implies that when adding support beams, the natural frequencies of the rig structure are seldom reached when drilling. The FEM concludes that after drilling a few centimeters, the natural frequencies are entirely outside the top drive operating window. Conclusively, the support beams potentially reduce rig vibrations.

Universal Coupling and Alignment

A universal coupling is added between the top drive motor and electrical swivel. Analyses of the original rig proved various problems regarding alignment of all components around to the drill string. These issues were evident in several ways, one of which was lateral vibrations when rotating the drill string. The lateral vibrations occurred both when drilling and when rotating in free air. A full analysis on rig alignment is found in appendix C.3.

The universal coupling intends to remove all misalignments caused by machinery in the top drive by decoupling rotation in the top drive from that in the components below. The universal coupling is shown in **Fig. 6.8**. During the construction phase, other alignment issues occurred due to the guide frame, which was slightly bent. The guide frame has been dismantled, straightened and reassembled, and all components mounted on it have been carefully aligned.

Figure 6.8: Universal coupling mounted below the top drive motor.

Protective Glass

On the original rig, acrylic glass is included as a safety measure to separate the active drilling area from working personnel and other equipment on the rig and laboratory. Orig-

inally, five separate acrylic glass pieces were mounted around the rock sample compartment and one on the derrick between the drill string and computer. In the new design, additional acrylic glass is mounted to also surround the drill string above the rig floor. The added protective glass may be pulled aside when handling drill pipes or working with other equipment on the derrick.

Final Rig

The final rig entered for the 2018 competition is shown in **Fig. 6.9** (schematic) and **Fig. 6.10** (photography).
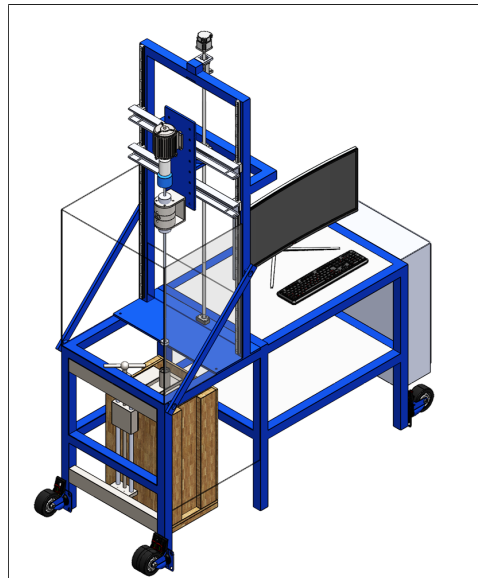
Figure 6.9: Schematic of final rig entered for the Drillbotics competition.

Figure 6.10: Photography of final rig entered for the Drillbotics competition.

6.2   Rock Formation

Phase I started with changing the setup for the test rocks from individual rock layers strapped together to boxes cemented in place containing different rock types. The setup showed great potential and has been decided to take into use for testing in Phase II as well. The most important improvements have been the setup time, repeatability of the tests and avoiding movement between the rock layers.

In Phase I, the team was working most on getting a robust and smooth rig which should be easy and quick to make ready for test drilling. The highest priority was becoming comfortable using the rig. The first rock sample was therefore made using softer rocks containing only shale and cement. Retractable wheels were mounted onto the wooden box for increased mobility. As the heaviest rock samples can be up to 60 kg, this feature has decreased the setup time and the amount of personnel needed for test drilling as it now can be handled by only one person.

The guidelines for the competition state that the scope is to drill a 60 cm tall rock as fast as possible. After receiving the competition rock, is was clear that the rock sample for the 2018 competition was only 35 cm tall. Anyhow it is just as important for the NTNU team to be able to handle any type of rock configurations that may occur. The team has tried to recreate as many rock configurations that may be given in the competition rock as possible. Last year's competition rock contained several rock layers including both harder and softer rocks. Some of the layers were also inclined making it extra difficult drilling a perfectly vertical hole.

This year, several new features have been added to the computer algorithm including layer detection and a rock estimator. A lot of test drilling is required to optimize the drilling algorithm. Several rock formations have been built, including different rock layers and configurations to have prepare for the competition.

In total, the team has built ten different test rocks. Two rock samples made up by 10 cm cement for optimizing pilot holes only, and eight rock formation of 50 cm made for general test drilling. All the test samples are made in solid wooden boxes providing space and stability when mounting the riser onto the formation. Further the retractable wheels have been replaced by wooden beams under the formation making them possible to move using a pallet jack. The new design of the box can be seen in **Fig. 6.11** This saves the team some time not having to mount on the wheels every time changing from one rock formation to another.

The rock estimator is run over a time interval of 35 seconds. This requires layer with a thickness large enough to prevent the drill bit entering the next layer before finishing the recognition phase. After estimating the rock the rig should use optimal parameters for the specific rock layer. To make the estimator robust requires a lot of test runs logging the theta values for every type of rock in a digital library. The first rock formation built contained shale layers of 4.5 cm. Some of the new rock samples have been made with thicker layers to obtain more data from one test run. These rocks have been made of only cement

and one specific rock type.

To test the rock estimator and the layer detection, two new rock samples are made. One consisting of several different rock types and one with tilted rock layers. The first rock sample can be seen in **Fig. 6.12**. This rock is the final test before the competition housing layers which should already be familiar to the system. Different shale types are also included in this rock to test how the system responds on almost similar rock types. The second rock is made with inclined layers which was a common configuration in the competition rock last year. When drilling into a transition zone in the horizontal layered formation, the whole area of the bottom hole will meet a new rock layer at the same time. This is not the case when drilling into a tilted layer. Now the transition zone will be longer and dependant on the inclination angle. Drilling into a tilted layer may also change the verticality of the well. Drilling into a new layer much harder than the previous can cause the well to build an angle as the bit will tend to follow the weakest path and therefore sliding along the harder layer instead of penetrating it.

Both in Phase I Phase II the rock samples have been donated from local vendors. This semester the team has been in contact with more supplies as the team wanted to make a comprehensive database of rock types. Shale has been donated from Sorte Skiferbrudd and Heimdal Naturstein. Heimdal Naturstein also provided the team with marble, basalt and larvikite. Nidaros Domkirke Restaureringsarbeid donated granite. The tiles are gathered from Modena Fliser Trondheim and the cement has, as last semester, been bought from local suppliers. Due to lack of time, the team has not been able to do test drilling in all the rock samples, and has decided to focus on cement, shale, and basalt as this is most similar to what one would expect to find in real drilling operations. Since Drillbotics culminate in the drilling competition, tiles and granite have also been put in focus as these are some of the rock types with lowest drillability and therefore are expected to cause the most
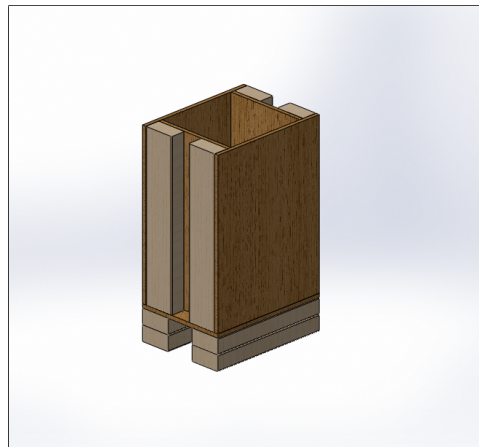
Figure 6.11: Wooden box used to make rock formations. The double set of wooden beams under the box is added to fit a pallet jack under it for transportation.

problems. The remaining rocks are kept in a storage to use for next year's team.

6.3 Hydraulics

In the industry, the hydraulics are extremely important for improving the drilling performance of the rig with less risk of stuck pipe due to hole cleaning and increasing ROP[30]. Improper hydraulic system using less optimal mud or insufficient hole cleaning may also impact the production of the well. This chapter will describe the hydraulic system of the miniature rig including choice of drilling mud, slip velocity calculation and required flow rate with corresponding pump pressure. In Phase I, a proposed layer detection system using cutting analysis was discusses. The team has decided to delay this project as the time spent on making a proper camera detecting cutting analysis program requires a lot of work load and will not pay off in rig performance in the Drillbotics competition. The system is presented in appendix C.1.

6.3.1 Drilling Mud

For Drillbotics, the main purpose of the drilling mud is hole cleaning and cooling the bit. The competition rock is no more than 35 cm tall and problems regarding hole stability and swelling are not likely to occur. Oil based mud (OBM) has been considered, but due to lack of resources and need of a sophisticated closed loop system including shale shakers, desanders and desilters an open loop system using fresh water as drilling fluid has been used. The viscosity of the drilling fluid is an important parameter regarding hole cleaning and can be changed using additives. The viscosity of water is lower than in OBM. The downhole situation for the miniature rig is not as complex regarding well pressure. Thus, the lack of viscosity for cutting transportation can simply be compensated for by increas-
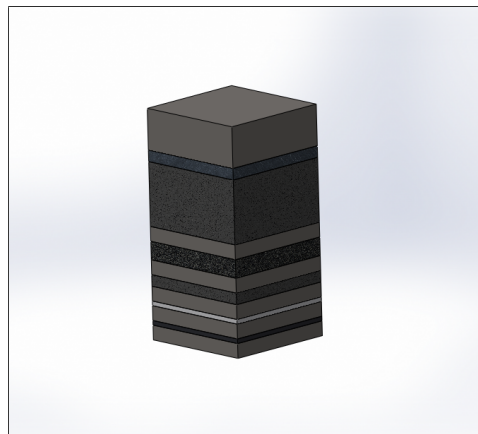
Figure 6.12: Example of a test formations. This test rock is a combination of different types of tiles and shale, basalt and cement holding the rocks together. The total height of the rock sample is 60 cm consisting of 50 cm rock and 10 cm of wooden beams underneath.

Figure 6.13: Semi-closed loop system with neoprene layer sealing the interface between rock formations and the riser guide. The water is guided through the rubber hose directly to the drain.

ing the flow rate of the mud without exceeding the mud window. Water is also more cost efficient and cleaner for the environment than using oil based mud.

6.3.2   Circulation System

The circulation system is mainly an extended version of the system used in Phase I of the competition. The water is supplied using a standard water outlet in the lab of 5.3 bar. The water then divides into two tubes, one for back pressure of the swivel and the other being pressurized in a pump, increasing the pump rate to obtain desired flow rate. The pump is a Hawk HC980A displacement pump. The choice of pump has been thoroughly described by Thuve et al. (2017). The drilling fluid then goes in a hydraulic tube, through the water swivel before entering the pipe and out into the annulus. The new design consists of a sealed riser on top of the formation diverting the flow through a bell nipple into a hose which guides the water to the drain. This feature mitigates problems with spill of water and cuttings, leaving a cleaner and less slippery rig site. The new water handling system is illustrated in **Fig. 6.13**.

6.3.3   Cutting Transportation in the Annulus

Having a clean wellbore is critical during drilling operations to decrease the chance of stuck pipe. In Drillbotics, an aluminum is used as the drill string. As discussed in section 5.2, our main problem during drilling is twist-off. Twist-offs occurs due to high torque or friction in the rotation of the BHA. The team is therefore looking for ways to reduce any unnecessary friction. Sufficient hole cleaning is one way of reducing the friction on the

BHA, thus it is of high priority.

To remove cuttings, the force of the water on the cuttings need to be greater than the gravitational force working downwards. The force of the water is a function of flow velocity and the minimum velocity is referred to as the slip velocity. The slip velocity is dependant both on fluid parameters and property of cuttings. The flow regime of the water surrounding the cuttings also impact the lifting capacity, where turbulent flow has proved to be more efficient [31].

The calculation of slip velocity is an iterative process. The initial value first needs to be calculated. This slip velocity is then reused to calculate a new friction number yielding a new flow regime and more accurate slip velocity. **Eq. 6.1**, **Eq. 6.2** and **Eq. 6.3** all use SI-units and give the slip velocity for laminar, transitional and turbulent flow respectively.

$$v_s = \frac{4}{3} \frac{g d_s^2}{30 f} \frac{\rho_s - \rho_f}{\rho_f} \tag{6.1}$$

$$v_s = \left(\frac{2g}{33}\right)^{\frac{2}{3}} \frac{d_s (\rho_s - \rho_f)^{\frac{2}{3}}}{(\rho_f \mu_a)^{\frac{1}{3}}} \tag{6.2}$$

$$v_s = \sqrt{\frac{8}{9} \frac{g d_s (\rho_s - \rho_f)}{\rho_f}} \tag{6.3}$$

where g $[m/s^2]$ is the gravitational constant, d_s $[m]$ is the cutting diameter, f is the friction constant which depends on Reynolds number, ρ_s $[kg/m^3]$ and ρ_f $[kg/m^3]$ are densities of cuttings and the drilling fluid. The derivation of the equations for slip velocity can be found in *Design Considerations for a Miniature Autonomous Drilling Rig*, by Thuve et al. (2017).

Cutting Size

Drillbotics is a downscaled version of a drilling rig. This goes for the cutting size as well. The slip velocity equations are calculated for a spherical object and depend strongly on the size of the object. The cutting size for cement, shale and granite is small and has not been experienced to become larger than 2 mm in diameter. Problems have occurred when drilling in multiple layers of tiles. For a single layer of tile surrounded by cement, the tile has a confining support, and will not crack. For multiple layers, small air gaps will be present in the intersections, allowing for the tile to break, resulting in much larger cuttings. Last semester, larger cuttings were assumed to be crushed by the stabilizer into smaller cuttings. Testing done in Phase II has shown that this does not happen for tiles, where the rig reaches its maximum torque limit and stops rotation. The desired scenario would be to grind through the tiles only producing smaller cuttings. As this is not guaranteed to be the case, an alternative solution is to operate with a flow rate which can remove these larger cuttings. An increase in flow rate does not necessarily get rid of the stuck pipe entirely as it is not possible to clean the hole for cuttings larger than what can fit in the annulus. Cutting size of this dimension will need a reaming operation, crushing the
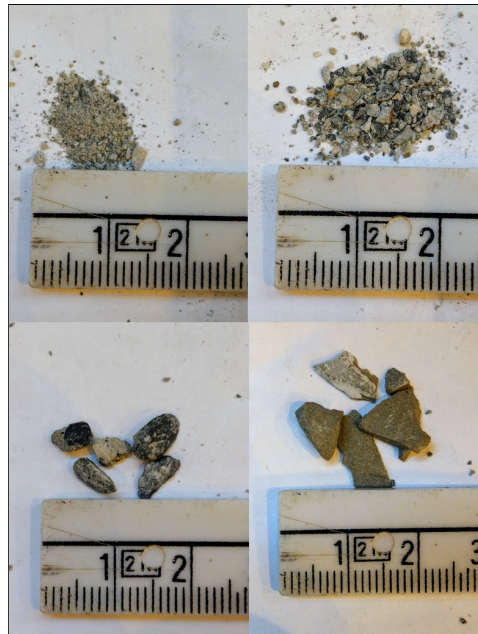
Figure 6.14: Cutting size from different rocks. From left to right on top: cement and shale. Bottom left shows larger grains from cement. Bottom right shows cuttings from broken tiles, which lead to stuck pipe.

cuttings into suitable size.

Increased ROP with Increased Flow Rate

Optimizing the ROP is important in the Drillbotics competition. The rock estimator uses WOB and RPM as the only drilling parameters for predicting ROP (as discussed in section 8.5). However, hole cleaning is important for progression in the rock. There are several factors which influence hole cleaning such as deviation, mud type, and also the percentage of drilling, sliding, reaming and circulating. The concentration of cuttings will change according to these parameters. In big scale drilling operations, the well path can be several kilometres long including deviated and horizontal sections. With limited pump capacity and restrictive mud window, normally, drilling needs to be stopped at certain points to circulate out the cuttings before continuing further. For the miniature rig, the cutting size is relatively small. The well section is only 35 cm at its longest with no inclination. Due to a rather high flow rate, cutting accumulation down hole is not considered to become a problem. Still, as higher flow rate will not affect the drilling performance negatively in any way, the team has decided to choose a large safety factor.

6.3.4 Nozzle Size

Last year's team postulated that high internal pressure in the drill pipe could not only reduce, but eliminate buckling problems completely. The theory is further described in Thuve et al. (2017) and section 7.1.1. To increase the internal pressure in the pipe, a replaceable nozzle was installed in the BHA with a range from 0.6 mm to 1.5 mm. The threaded connection between the BHA and the nozzle had a diameter of 5 mm. This year's team has through literature studies and buckling tests falsified this theory. Tests have been done with and without a high internal pressure in the pipe resulting in the same buckling limit for identical pipes. An increase in pressure in the system will have a higher potential of causing leakage in the hydraulic system and a hypothetical leak can cause more damage with high pressure. The replaceable nozzle is therefore removed from the system allowing higher flow rates at a lower pressure.

6.3.5 Pressure Loss in the System

The hydraulic system is driven by the pump circulating drilling fluid from the rig through the wellbore, cooling the bit and removing cuttings. When water is going through the system, friction in the components it's passing through causes a pressure drop. The pressure drop is dependent on the geometry of the pipe system, fluid characteristics and the flow velocity. Pressure drop is divided into two main categories: major and minor pressure losses. Major pressure losses consist of loss in the pipe and tubes, whereas minor pressure losses include fittings, valves, bends, inlets and outlets. The pressure in the wellbore is approximately 1 bar as the hydrostatic column in the well can be neglected. The pressure drop in the system can be written as:

$$\Delta p_{system} = p_{pump},$$ (6.4)

where Δp_{system} included both minor and major losses in the system.

Major losses includes pressure loss in the hydraulic tube, the pipe and the BHA. The tube has an inner diameter of 1.2 cm. The BHA has a inner diameter of 1.4 cm with some configurations inside, but these are not expected to have any significant impact on the pressure drop. The pressure loss in pipes is given as:

$$p_{major} = \sum_i f_i \frac{L_i}{D_i} \frac{V_i^2}{2} \rho_f,$$ (6.5)

where $\frac{L_i}{D_i}$ is the ratio between the length and the inner diameter of the pipe section, V_i (m/s) is the flow velocity and $\rho_f (kg/m^3)$ is the density of the fluid which in our case is fresh water with density of 1000 kg/m^3. Minor losses are calculated using the empirical loss coefficient K_L. The loss coefficient is based on the geometry of the pipe configuration and the pressure loss through these are expressed as

$$p_{minor} = \sum_j K_j \frac{V_j^2}{2} \rho_f.$$ (6.6)

The hydraulic system on the miniature rig has two smooth bends, one in the swivel connection and one inside the swivel. Both these smooth bends have $K_L = 0.9$. The highest pressure drop in the system is over the bit nozzle and is derived using equation for velocity out of the nozzle[32]:

$$v_n = \sqrt{\frac{2\Delta p_b}{\rho_w}}, \tag{6.7}$$

where Δp_b (bar) is the pressure drop over the nozzle. The theoretical and the actual discharge is not equal. To compensate for this, a discharge coefficient is used:

$$C_d = \frac{Q_{actual}}{Q_{theoretical}} \tag{6.8}$$

By using **Eq. 6.8** and $v_n = Q_{theoretical}/A_{nozzle}$, Δp_b can be written as:

$$\Delta p_b = \frac{8Q^2\rho_w}{\pi^2 C_d^2 d^4}, \tag{6.9}$$

where Q (m^3/s) is flow rate and d (m) is the inner diameter of the pipe. Pressure drop over the nozzle is significantly larger than the rest of the pressure drop in the system combined. Pressure drop is strongly dependent on the diameter of the nozzle and will increase drastically when the diameter size is under 1 mm. To get a more exact measurement of the pressure drop, the pressure drop over the nozzle is calculated by using:

$$\Delta p_b = p_{pump} - p^*_{system}, \tag{6.10}$$

where p^*_{system} is the pressure loss in the system from the pump all the way through the BHA, not including the bit nozzle. Last year the nozzle had an inner diameter of 0.5 mm. This year, a diameter of 5 mm has been chosen. A larger diameter allows for increased flow rate at a lower system pressure.

Twist-off Detection

During test drilling, the drill pipe has twisted off several times. As per now, the operational procedure for twist-off has been pushing the red emergency button, shutting down the whole system. Since the drilling rig is to operate autonomously, events such as pipe failure should be included in the script. The pump used in the hydraulic system is a positive displacement pump. The characteristics for such pumps are that they deliver the same flow rate for a constant RPM regardless of the pressure drop in the system. Before twist-offs occur, the drilling fluid goes through the circulation system creating a pressure drop which the pump counteracts. The largest pressure drop in the system happens over the bit nozzle. When the pipe twists off, the water will leave the system before entering the nozzle, thus the pressure will decrease. By using an electronic pressure gauge connected to the operation computer, twist-offs can be detected and reacted to instantaneously by the system.

6.3.6 Applications for the Pressure Sensor

The pressure in the system is a function of flow rate. A flow test has been done to understand the relationship between the flow rate and the pressure in the system. The test was done with the Alibaba drill bit for three different nozzle sizes. The tests were run for one minute each, measuring the flow rate with a 20 L bucket and the corresponding pump pressure from the pressure gauge. The pressure sensor is implemented into the control system. By increasing the pump rate, thus the flow rate, the pressure will also increase. Knowing the flow rate for different pump pressures allows the driller to adjust the pump rate to ensure proper hole cleaning. By implementing this in the code, it is possible to regulate the pump as a function of ROP. Furthermore, regulating pump pressure could be useful in conjunction with the Rock Estimator. Different lithologies feature unique cuttings both in size and weight, and changing pump rate depending on which formation is drilled could allow the pump to run at an optimal rate, not wasting unnecessary power. The current control system only reads the pump pressure and the rig operates at a constant pump rate.

6.4 Drill Bit

A polycrystalline diamond compact (PDC) bit is provided by DSATS to be used in the Phase II on-site test. The Drillbotics guidelines state that "students are also allowed to design and use their own bits for the Phase II on-site test, within the dimensional limits (...)" [20]. In collaboration with Lyng Drilling AS, Drillbotics NTNU has designed and manufactured a customized miniature PDC bit in accordance with stated requirements.

Design and production of a custom PDC bit requires effort and time. It has been a priority in Phase II of the project due to several anticipated benefits. Firstly, design of a custom bit allows the team to test and tune the control system and mechanical aspects of the rig prior to the on-site test with the same setup that is used during the test. Consequently, there are necessarily no discrepancies in response related to differences in the bit. Secondly, design parameters have been selected based on experience from extensive test drilling with other bits, as well as on knowledge from literature studies, industry professionals and supervisors. The design is customized for NTNU's miniature drilling rig and aims at mitigating dysfunctions and problems frequently encountered with it and to optimize hole quality and drilling efficiency.

This section will elaborate on the complete bit design process. This includes general theory on PDC bits, challenges when relating industry theory to a miniature bit, design specifications of the custom bit and a summary of the modelling and manufacturing process. Test results and comparison with other bits are found in 9.4. Schematics of the final bit design is found in appendix C.5.3.

6.4.1 Drill Bit Theory

The custom miniature bit design is based on theory and know-how from the industry. Theory is incorporated in the design aiming to optimize drilling performance. Drilling performance can be measured by several different parameters, such as drilling speed (ROP), drilling efficiency, safety, hole quality and failure. Several of these parameters are directly related to and may be optimized through considerations in the bit design. This section will discuss industry theory about full-scale PDC bits and focus on design features that impact drilling performance.

PDC Bit

PDC bits are fixed-head bits that use PDC cutters [33]. **Fig. 6.15** shows an overview of drill bit nomenclature on a 6-bladed PDC bit commonly used in the industry. To optimize drilling performance, bit design considerations are mainly influenced by mechanical design parameters, bit materials, hydraulics and properties of the formation being drilled. Cutter structure characteristics are important mechanical design parameters. These include cutter geometry, placement and density, as well as hydraulic requirements and well geometry. Another important design feature is the bit profile. The bit profile impacts stability and cleaning efficiency, and lays the foundation for cutter placement [34].

Traditional roller-cone bits cause formation to fail in compressive stress. When drilling with PDC bits, formation fails in shear stress. When shearing, vertical penetrating force from applied WOB and horizontal force from rotation in the drill string are transmitted to the cutters. The resultant force defines a plane for cutter thrust. Cuttings are sheared of at an angle relative to that plane. Formation fails either due to brittle or plastic failure. When shearing with a PDC bit, the energy to reach the plastic limit for rupture is relatively low. This means that PDC bits require less WOB compared to roller-cone bits [34]. This is beneficial when drilling with a miniature rig that operates with WOB that seldom exceeds 100 kg, and motivates the design of a PDC bit in advantage of roller-cone.

Cutter Profile

Cutter structure characteristics of a bit are specified by a cutter profile. A cutter profile is a planar representation of cutter geometry, placement and density, as shown by the example in **Fig. 6.16**. Cutters are placed on the bit face to completely cover the bottomhole, ranging from the apex to the gauge. The number of cutters in a design is expressed by cutter density. Cutter density depends on cutter profile shape and length, and on cutter size, type and quantity. When drilling, cutters near the gauge travel a longer distance than those close to the center. They travel faster, remove more rock, and are more exposed to wear. Consequently, bits are usually designed with greater cutter density close to the gauge. Depth of cut of a bit is reduced by increasing the overall cutter density. Naturally, decreased depth of cut is analogous to decreased ROP. However, it also leads to a reduction in bit torque and less vibrations, resulting in less damage to the bit, pipe and BHA and prolonged bit life [34]. The weak, twist-off-susceptible aluminum drill pipe benefits from
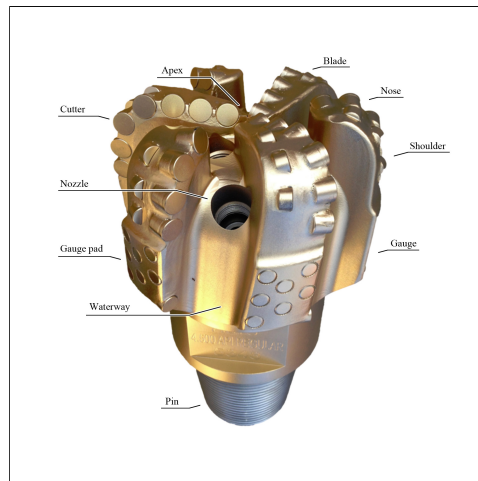
Figure 6.15: Nomenclature for PDC bits [35].

such a non-aggressive design.
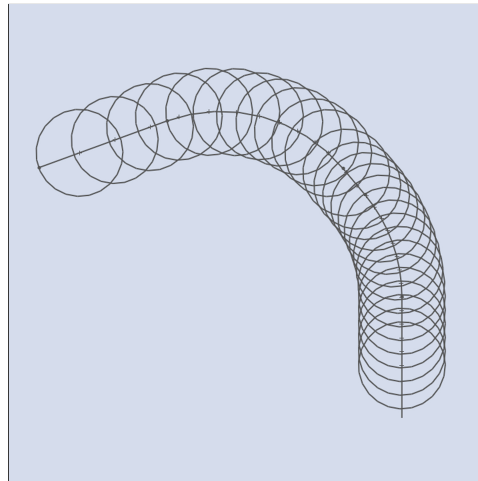
Figure 6.16: Cutter profile for a PDC bit. Note that cutters are placed along the bit profile, and that cutter density is greatest near the gauge.

Cutters are also specified by orientation. One important orientation parameter is the attack angle, or *rake angle* of a cutter. In drill bit terminology, rake angle is referred to as cutter back rake, and is defined as the angle between a cutter's face and the plane perpendicular to formation being drilled. In other words, it is the tilt of a cutter in the direction of bit rotation, as shown in **Fig. 6.17**. When increasing cutter back rake, depth of cut and bit aggressiveness is reduced. This leads to a decrease in bit vibration and bit whirl and pro-

longed bit life. Higher back rake is also beneficial for hole cleaning due to a reduction in tendency of cuttings to stick to the cutter face. However, one should also keep in mind that less aggressive bits cause lower ROP: with higher cutter back rake, more WOB is required to maintain ROP. Consequently, aggressive bits are more energy efficient [36]. Bits in the industry are commonly made with back rake angles ranging from 0° to 30°, depending on properties of the formation being drilled. Lower back rake angles are used to maximize ROP in softer formations where bit wear is less of an issue [37].
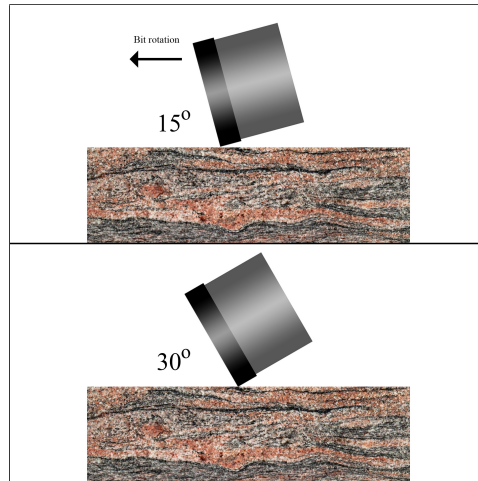
Figure 6.17: 15° and 30° back rake angles of a PDC cutter. Bit seen from the side.

Cutter orientation is also specified by side rake. When looking at a bit face from the front, side rake is the angle between a cutter's face and the orthogonal of the bit face, as illustrated in **Fig. 6.18**. In the industry, general consensus is that bits with side rake features drill faster than bits without it. A cutter with side rake has improved cleaning properties as it reduces the tendency of cuttings to stick to the cutter face. This is especially true in soft and plastic formations prone to bit balling [38]. Cutters on full-scale bits are rarely orthogonally oriented. However, large side rake angles quickly require great amounts of input energy to drill [39]. Side rake angles around 10° are common.

Bit Profile

With PDC bits, the cutters are supported by a fixed-head bit body. The bit body shape is referred to as its bit profile. The bit profile is significant for drilling performance due to its influence on stability, durability, cleaning efficiency, cutter density, steerability, thermal properties and ROP. The geometry of a bit, as established by the bit profile, dictates hydraulic flow across the face and along the body. Hydraulic flow, in turn, affects ROP. When drilling, cuttings are generated at the bit face. If the cuttings are removed slower than the speed they are generated in, they will accumulate and reduce ROP. If bit hydraulics allow
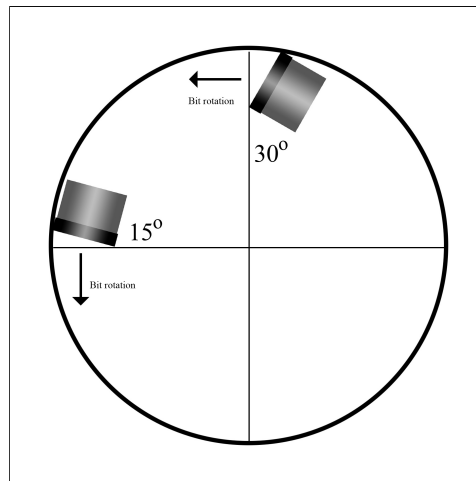
Figure 6.18: $15°$ and $30°$ side rake angles of a PDC cutter. Bit seen from the front.

for faster flow, ROP is relatively higher. Hydraulic flow across the bit is also beneficial for cooling and lubrication during drilling. The bit profile has direct influence on possibilities of cutter placement and density. As seen in **Fig. 6.16**, the bit profile must support the cutter profile. Bits range from being classified as flat profiles to long parabolic profiles. Flatter profiles are less aggressive, generating less abrasive wear and lower ROP [34]. A flat profile is illustrated in **Fig. 6.19**. In the industry, bits are usually designed somewhere in between flat and long parabolic, i.e. with short or medium parabolic profiles [40]. Results from tests of commercially available bits show that deep coned bits have a tendency of less whirl compared to other bits [41].

6.4.2 Design Specifications

The custom miniature bit is designed based on theory and experience from the industry in accordance to design requirements stated in the competition guidelines. Parts of the design are directly motivated by full-scale concepts, while others try to account for differences between a full-scale and miniature environment. Some features are incorporated in the design specifically to mitigate problems that have been frequently encountered during previous drilling. This section will describe design specifications of NTNU's miniature bit and elaborate on considerations for the choice of design. A summary of design parameters is given in **Table 6.1**. For comparison, design parameters of the bit provided by DSATS are also listed. Both bits are depicted in **Fig. 6.20**.

When designing a miniature bit, it is important to fully understand the environment of a miniature rig and differences between drilling in a lab and operations in full-scale oil fields. Overall differences between the two environments have been discussed in 5. What is important for bit design is that the aluminum pipe is weak and prone to twist-off. The
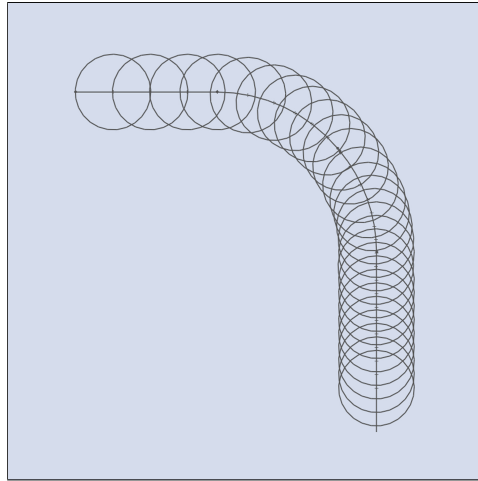
Figure 6.19: Cutter profile along a flat bit profile. Solid line represents bit profile.
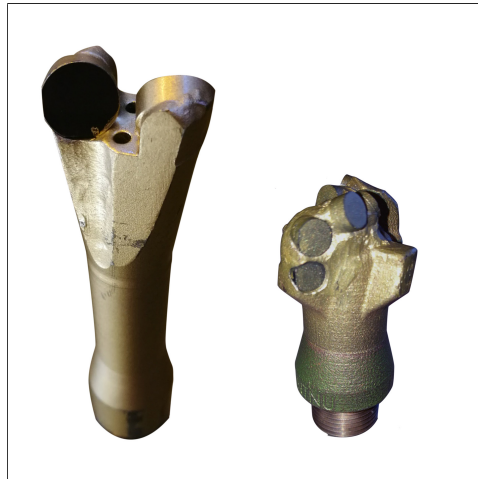
Figure 6.20: Picture of bit provided by DSATS (left) and custom bit (right) (not to scale).

rig operates at relatively low WOB and high RPM. Drilled rocks are at atmospheric con-
ditions, and there is no in-situ formation pressure. In fact, there is no formation fluid.
This means that there is no pore pressure to consider when applying internal pressure in
the drill string. Downhole temperature is also at atmospheric conditions, so all thermal
effects are related to bit-rock interaction. Consequently, drilling fluid is mainly used to
clean the bit face and remove cuttings. It also helps lubricating and cooling the bit. Drilled
hole are measured by verticality, which means that steerability is irrelevant. Bit wear dur-
ing a single run is of little importance, since drilled holes are never longer than 60 cm.
Available space for features on the miniature bit is a challenge: bits in the industry drill

Table 6.1: Comparison of design parameters of NTNU's custom bit and the bit provided by DSATS.

Bit specification		
	NTNU bit	**DSATS bit**
Bit diameter	1.125"	1.125"
Effective length	1.75"	5.5"
with cross-over	*NA*	6.9"
Weight	109 g	280 g
with cross-over	*NA*	380 g
Blades	2	2
Cutters	8	2
Nozzles	2	2
Cutter specification		
	NTNU bit	**DSATS bit**
Diameter	0.235"	0.529"
Siderake angle	10°	0°
Backrake angle	20°	20°
Nozzle specification		
	NTNU bit	**DSATS bit**
Diameter	2.4 mm	2.35 mm
Spacing	180°	180°

holes commonly ranging from 36" conductors to 5 1/2" sections in the production zone. Comparatively, the miniature bit is 1.125".

Cutter Profile

Extensive drilling with the miniature rig proves frequent issues related to vibrations. Post-drilling analyses reveal that torque spikes that significantly exceed intended levels occur regularly. More importantly, torque over time cause fatigue. This results in twist-off at the aluminium pipe just above the BHA. To account for this, the custom bit is designed to be non-aggressive. As discussed in section 6.4.1, this is achieved by high cutter density and high cutter back rake angle. In an attempt to maximize cutter density, an early bit proto-type was designed with three blades and four cutters on each blade in a spiral structure. When modelling the bit, it was difficult to fit all cutters on the bit face. This illustrates the major challenge of designing a downscaled bit; there is limited space at the bit face. PDC cutters are available down to around 5 mm OD. In the industry, e.g. a 17 1/2" drill bit with multiple blades can in theory fit over a hundred cutters. With a gauge of 1.125" in the miniature environment, the story is different. As a result, the custom bit is designed with two blades, each with four 6 mm cutters. The blades are symmetric. The cutter density is significantly different than that of the bit provided by DSATS, which has two blades with one cutter each. The cutter profiles of the custom bit and the bit provided by DSATS are shown in **Fig. 6.21**.
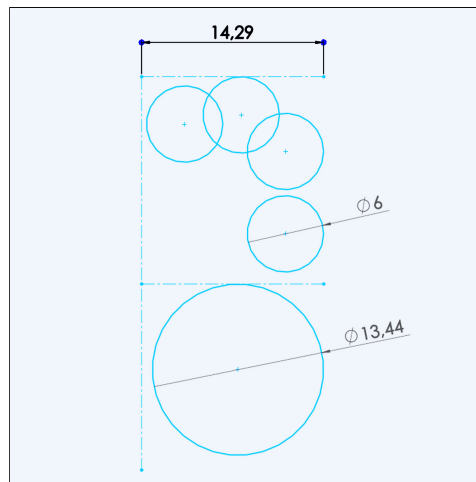
Figure 6.21: Cutter profile of the custom bit (top) and bit provided by DSATS (bottom). Dimensions in mm.

Cutter Orientation

Bit aggressiveness is reduced by high cutter back rake angles. All cutters are designed with back rake of $20°$. Although this means that more WOB is required to increase ROP, the rig operates below the pipe buckling limit, and pipes seldom buckle during testing. The cutters are designed with $10°$ side rake.

Low-friction Wear Pad

The bit is designed with specific features that attempt to improve bit stability. One of those features is a slightly parabolic profile: the center cutter is slightly withdrawn at the bit face. More importantly, the bit is designed with large, non-cutting, low-friction wear pads. Two metal pads are located on shoulders on the bit between the blades. This is illustrated by the schematic in **Fig. 6.22**. The shoulders are shorter than the blades to avoid interaction with rock at the bit face, but rather with the borehole wall at the wear pads. The shoulders are placed $85°$ offset of the blades to improve bit stability. In the industry, the technique of using a wear pad has proven to balance forces created by the cutters, evidently improving stability and reducing bit whirl. Warren et. al. (1990) modified a four-bladed 8 1/2" bit with reamer to include a wear pad on the stabilizer. When comparing performance, the conclusion was that "after modification, the bit was retested and all evidence of whirl was eliminated (...)" [41].

Length

The custom bit is shorter, lighter and more compact than the provided bit. Several benefits are achieved by shortening the length of the bit. Firstly, there is only 30 cm space avail-
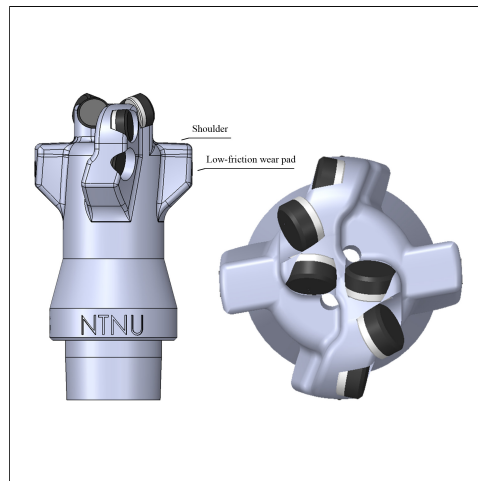
Figure 6.22: Low-friction wear pads as seen from a side view and bit face.

able between a 60 cm tall formation and the rig floor. This constitutes an upper physical limit for available total BHA length. In addition to the length of BHA components, some additional space is required for handling of pipe and BHA prior to drilling. A short bit frees up space for stabilizers and other subs, and makes it more convenient to operate the rig. A second benefit of a short bit is that it reduces the length of unsupported BHA prior to drilling by allowing the roller bearing in the lower topside stabilizer to be placed closer to the formation surface. Thirdly, a shorter distance must be drilled before the stabilizer sub in the BHA enters the hole. This restricts lateral vibrations below the stabilizer, improving hole quality through a reduction in gauge of drilled holes. The effective length of the custom bit, excluding the threads at the pin, is 44.1 mm (1.74"). Compared to the bit provided by DSATS, which is 139.7 mm (5.5") long, the length is reduced by 68 %. The competition guidelines were misinterpreted. As a result, the threads of the BHA and DSATS bit are incompatible and a cross-over sub is needed. The cross-over sub adds 36 mm (1.42"). Considering this additional length, the custom bit reduces bit length by 75 %.

Weight

The custom bit is lighter than the provided bit. As seen in table 6.1, the custom bit weighs 109 g, 171 g less than the DSATS bit alone and 271 g less than the DSATS bit and the required cross-over sub. During preliminary testing, twist-off at the connection between the BHA and pipe was the most common failure [1]. To strengthen the system with regards to twist-off, the custom bit is intentionally made significantly lighter to reduce the discrepancy in torsional inertia between the drill pipe and BHA.

Threads

The bit is designed with short threads. The length of threads of the provided bit is 0.6"
(15.24 mm). The NTNU team has extensive experience of drilling with threads as short
as 7 mm in components in the BHA without experiencing any form of failure, suggesting
that these threads provide sufficient strength. Based on this, all threads in the BHA have
been shortened. The threads at the pin in the custom bit are 0.3" (7.62 mm). Correspond-
ing female parts in other subs in the BHA have been shortened equivalently, resulting in
an overall shorter BHA. An integrity analysis of the threads could reveal a possibility of
reducing the lengths even further.

Nozzle

The internal part of the custom bit's pin is threaded. Previously, a threaded nut has been
placed inside a downhole stabilizer above the bit to restrict fluid flow. The threaded nut
acted as a replaceable nozzle. This nut is now placed inside the bit at the internally
threaded pin. When fluid enters the bit from the nozzle, two 2.4 mm OD channels 180°
opposite of each other transmit the fluid out of the bit into the annulus. The bit nozzles are
placed close to the bit center to transport cuttings radially away from the bit face.

6.4.3   3D-Modelling and Manufacturing

The bit has been designed by the NTNU team in collaboration with Lyng Drilling AS
(a Schlumberger company) in the 3D-modelling software SolidWorks. The bit was 3D-
printed by The ExOne Company before being shipped to Lyng Drilling AS who added the
cutters and threads. This section is a walkthrough of the design process in SolidWorks and
how the previously discussed specifications have formed the final design.

The 3D-modelling process can be summarized as a three-step procedure. First, a 2D sketch
that includes the basis for all components and features of the bit is made. Then, a 3D model
is made from the features in the 2D sketch to ensure there is proper available space in a
3D environment, and that it is physically possible to manufacture the bit. Finally, the 2D
sketch and 3D model is modified and tuned in an iterative process until the design satisfies
all criteria.

2D Sketch

The 2D sketch encompasses the basis for all features of the bit. This includes the main bit
body, blades, gauge pad, threads, nozzles and cutter profile, which includes cutter place-
ment, back rake and side rake angles.

Three separate sketch entities in the 2D sketch define the main functionality of the bit.
These are sketches for the main bit body, blades and cutter profile. The cutter profile is
of highest importance, whereas the blade is modelled to support the desired profile. For

the miniature bit, the bit body and blade profile must be designed to support cutters that cover a 1.125" OD hole. Blades and low-friction gauge pads are among the features that dictate overall length of the bit body. The bit body is slimmer than the blades, and forms waterways for return flow. The main bit body sketch includes the pin, which is designed according to threads specifications. **Fig. 6.23** shows the final 2D sketch of the bit body, blade profile and cutter profile of the custom bit. The figure includes 2D sketches for metal insertions in the low-friction gauge pad and nozzles for fluid flow through the bit.
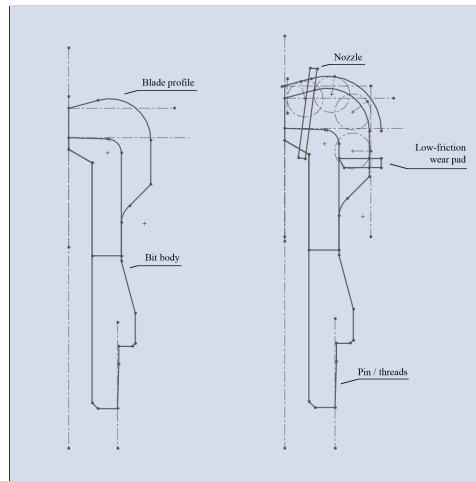
Figure 6.23: 2D sketch of bit body and blade profile (left) and 2D sketch that includes sketches for nozzles, wear pads and cutters (right).

A detailed view of the cutter profile is shown in **Fig. 6.24**. It includes four 6 mm OD cutters: three at the bit face and one gauge cutter below the others. All cutters at the bit face are displaced 2 mm from the blade profile to ensure that they interact with drilled rock before the bit matrix. The center-to-center distance between each upper cutter is 4.5 mm. Collision between cutters on different blades is avoided by allowing a minor gap of 0.38 mm at the center cutter. The edge of the gauge cutters is placed 14.29 mm from the centerline to ensure that drilled holes have an OD of 1.125".

Cutter back rake and side rake angles are defined relative to the cutter profile. This ensures that the cutters are placed correctly in the final 3D-model. Back rake and side rake angles are specified in the 2D sketch as vectors in the 3D-space: one vector specifies back rake while another specifies side rake angle. Together, these vectors produce a final vector that fully defines trajectory of a cutter socket on a blade. Side rake angle is implemented by drawing a vector on the bit face, i.e. the plane perpendicular to the top of the cutter profile. **Fig. 6.25** shows the vector specifying 10° side rake for the center cutter. Back rake angle is implemented by drawing a vector *into* the plane of the cutter profile. **Fig. 6.26** shows the vector specifying 20° back rake for the center cutter, as well as the vector specifying cutter socket trajectory.
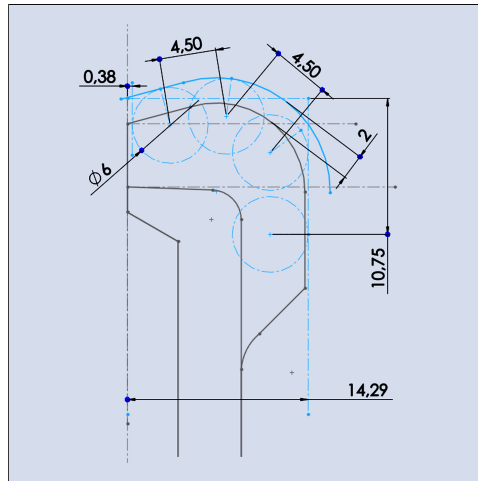
Figure 6.24: Cutter profile of the custom bit. Dimensions in mm.
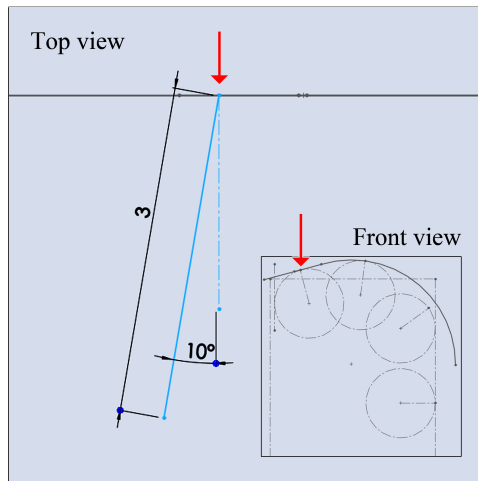
Figure 6.25: 2D sketch of vector specifying 10° side rake for the center cutter. Red indicators mark the same point on the sketch from a top and front view. Dimension in mm.

3D Model

A 3D model of the bit is made based on the 2D sketch presented above. In succession, the modelling process involves making the bit body, blades, cutter sockets, wear pads, nozzles and a finalizing process. A bit body foundation is made by extruding the bit body sketch (see **Fig. 6.23**) around the centerline (axis of rotation). The result of this action is shown
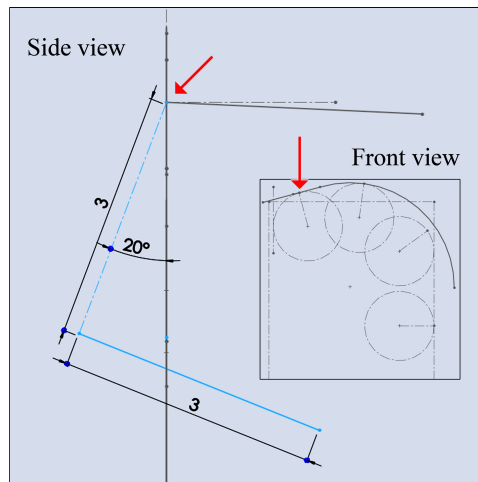
Figure 6.26: 2D sketch of vector specifying 20° back rake for the center cutter. Red indicators mark the same point on the sketch from a side and front view. The bottom blue line define cutter socket trajectory. Dimension in mm.

in **Fig. 6.27**.
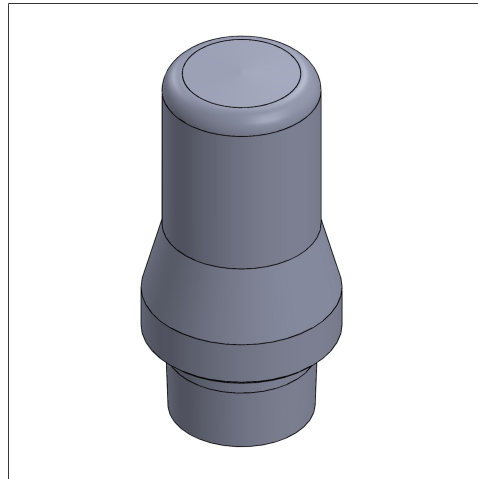
Figure 6.27: 3D model of bit body foundation.

Blades are made by drawing a new sketch on top of the 3D bit foundation. This sketch is drawn by free hand. However, the sketch must be drawn so that it fits all four cutter sockets with proper support from the matrix behind each cutter. This is achieved in an iterative trial-and-error process. Once the sketch satisfies the criteria, the blade is created by extruding the sketch along the exterior of the bit body. The blade is extruded along a

helix to form waterways in the direction of bit rotation. This is shown in **Fig. 6.28**. Finally, the blade is completed by trimming it according to the blade profile (from the 2D sketch in **Fig. 6.23**). This is shown in **Fig. 6.29**.
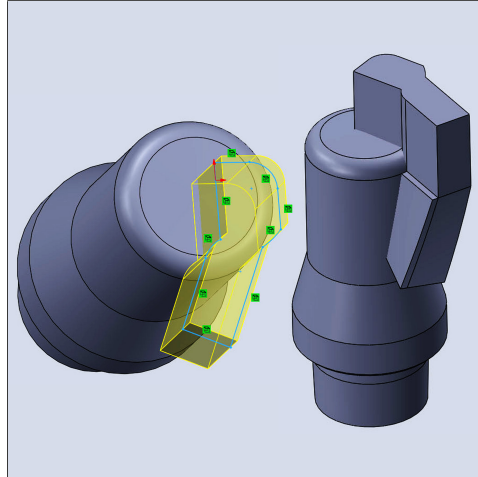
Figure 6.28: 2D sketch of blade drawn above the bit body (left) and 3D model of blade when the sketch is extruded downwards along a helix.
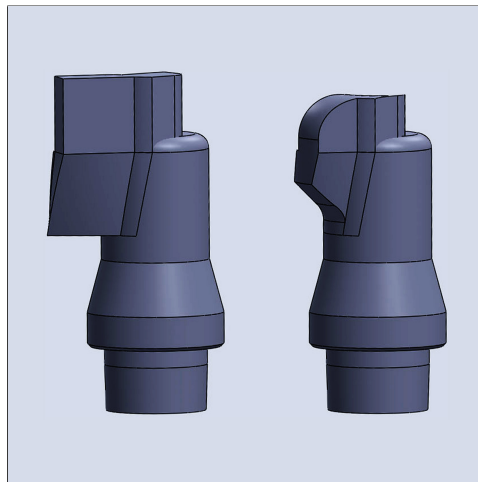
Figure 6.29: 3D model of blade before (left) and after (right) being moulded by the blade profile.

Cutter sockets for the cutters are then added to the blade body. Cutter sockets are made by extruding placeholder cylinders along the trajectory vector specified by side rake and back rake angles (as was shown in **Fig. 6.25** and **Fig. 6.26**). Placeholder cylinders are used to visualize cutter placement on the blade body and to avoid colliding cutters. If cutters

collide, collision is avoided by rotating the cylinders around the centerline. The result is shown in **Fig. 6.30**.
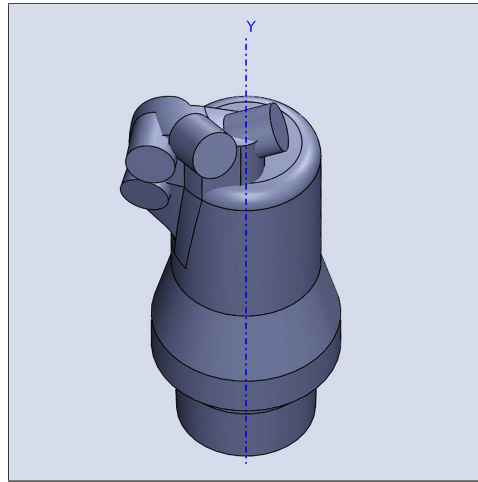
Figure 6.30: 3D model of placeholder cylinders representing cutter sockets on the blade.

The process for modelling a low-friction wear pad is the same as for the blade: draw a sketch on top of the bit body, extrude the sketch downwards along a helix and mould it. The wear pad shoulder is moulded after the blade profile. However, recall that the wear pad shoulder is shorter than the blade. This is achieved by modifying the blade profile sketch. Once a wear pad shoulder is created, the single blade and shoulder is duplicated and rotated around the centerline to form pairs. The result is shown in **Fig. 6.31**.

To finalize the bit, sharp edges are chamfered and nozzles are placed properly on the bit face. The chamfered bit with placeholders is shown in **Fig. 6.32**. By subtracting all placeholder objects from the main bit object, the final custom bit model that is sent for 3D-printing is made. The model is shown in **Fig. 6.33**. Cutters, metal inserts, coating and logos can be added in an assembly to visualize the bit when processed after printing. The final assembly is shown in **Fig. 6.34**. The manufactured bit is depicted in **Fig. 6.35**.
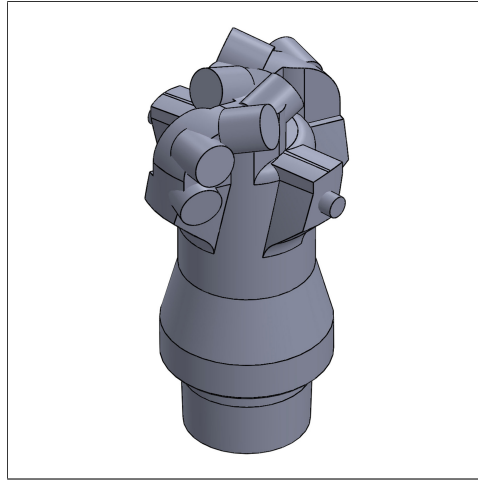
Figure 6.31: 3D model of bit with two blades and two wear pads. Placeholder cylinders represent cutters on the blades and metal inserts on the wear pads.
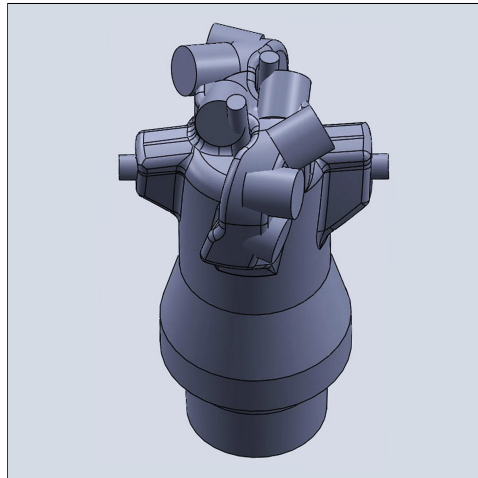
Figure 6.32: 3D model of chamfered bit with placeholders for cutters, metal inserts and nozzles.
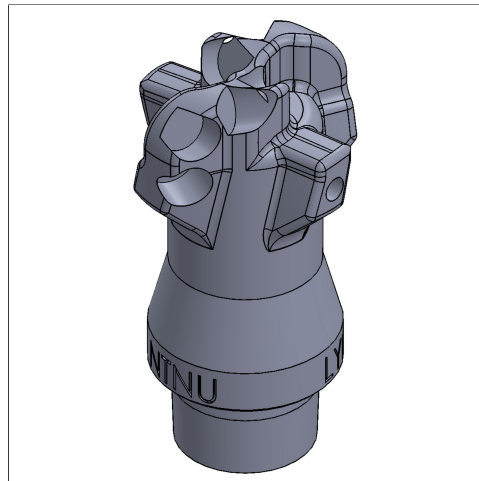
Figure 6.33: Model of custom bit ready for 3D-printing.

Figure 6.34: Final custom bit 3D model, including cutters, metal inserts, coating and logos.

Figure 6.35: Photography of bit manufactured by Lyng Drilling AS.

6.5 Bottom Hole Assembly

Bottom hole assembly (BHA) is a term used for the components of a drill string located below the drill pipe. In the industry, a properly equipped BHA is essential for the success of any drilling operation. Performance of the miniature rig can be improved by accurately configuring the BHA and including certain key components in it. Design of a custom BHA is not required by the competition guidelines, and commercially available alternatives are suggested. However, by designing a unique custom BHA, requirements of NTNU's rig and envisioned features are considered. This section includes BHA theory from the industry and the functionality of different available components. It will focus on functionality that is relevant for the miniature rig and present the custom design. A custom BHA was crafted last year, and the section clarifies and motivates differences between the old and new design.

6.5.1 BHA Theory

Depending on the intention of a drilling operation, a BHA consists of different subs with different functionalities. Common subs include drill collars, stabilizers, shocks, hole-openers, reamers, sensors, bit sub and bit. They are included in a BHA depending on the goal of an operation. Wellbore trajectory and directional drilling is controlled by flexibility in the BHA, which depends on configuration of stabilizers. Proper configuration of the BHA is crucial for maximizing ROP and lowering drilling costs [42].

The miniature rig drills short, straight holes in small rock samples. Thus, considerations when designing the BHA are somewhat limited compared to the design process for full-scale operational assemblies. Key functionality that should be included is specified in the competition guidelines. The provided aluminium pipe is slick. Tooljoints of arbitrary type are required at either end of the pipe to attach it to the rig and BHA. Downhole stabilizers are allowed; however, they may not exceed a combined length of 3.5" (8.9 cm). Any other subs cannot have an OD of over 90% of the OD of the bit (i.e 90% of 1.125"). Weight may be added through the BHA to increase drill string tension and compression; however, the guidelines state that "(...) the additional weight shall not directly impose lateral forces to stabilize the drill string". The rig must incorporate downhole sensors and solutions for telemetry to topside. Downhole sensors transmitting data of vibrations, verticality, tortuousity or other parameters are part of the evaluation during the competition. The BHA design is also evaluated on solutions for how the weight and stabilizers are designed and attached to the drill string and bit sub [20].

6.5.2 BHA Design

Envisioned functionality for the custom miniature BHA is to connect to the drill pipe, stabilize the drill string, house downhole sensors, transmit downhole signals to topside, transmit high-pressure drilling fluids downhole and connect to the bit. A custom BHA was made last year. The new design is inspired by the old one, but it incorporates new solutions and improvements. Schematics for all components in both the old and new BHA are found in appendix C.5.2.

Old BHA

The old BHA is depicted in **Fig. 6.36** and a schematic of it is shown in **Fig. 6.37**. It consists of a stabilizing sub, a tool joint connecting the stabilizer to the drill pipe and the bit. The tool joint comprises a hydraulic connection with an internal metal sleeve for the drill pipe. The total length of the BHA, measuring from above the connection to the bit face, is 142 mm. The stabilizer sub is 80 mm long, where 60 mm is considered as a stabilizer by competition rules stated in the guidelines. The exterior has helically shaped grooves to allow return flow of drilling fluid with cuttings up the annulus and out of the hole. Sensors are housed inside the sub and are hydraulically sealed by three components that form a chamber. Signals are transmitted to topside by wires extending through the drill pipe. The sub has a restricted ID below the sensor housing with a threaded wall. A replaceable threaded nut can be inserted in the restriction to act as a nozzle. To enable connection to the drill pipe and bit, both ends of the sub are threaded. Some bits require a cross-over sub due to incompatible threads.

Figure 6.36: Photography of the old BHA.

New BHA

The new BHA design is modular and consists of several subs. The primary stabilizing sub is similar to the old BHA. It has the same helical grooves on its exterior and is used to house downhole sensors. However, it has been redesigned and is shorter and lighter with a simpler solution for sensor housing. The stabilizing sub schematic is shown in **Fig. 6.38**. It is 51 mm long, and the full length is considered as a stabilizer by competition guidelines. The significant reduction in length compared to the old BHA is possible for two reasons; the threads at the top and bottom are shorter, and the nozzle has been removed from the stabilizer and placed in the bit instead. The stabilizer sub weighs 121 g, 31% less than the old stabilizer (177 g). The bottom threads are 3/8" BSP and are compatible
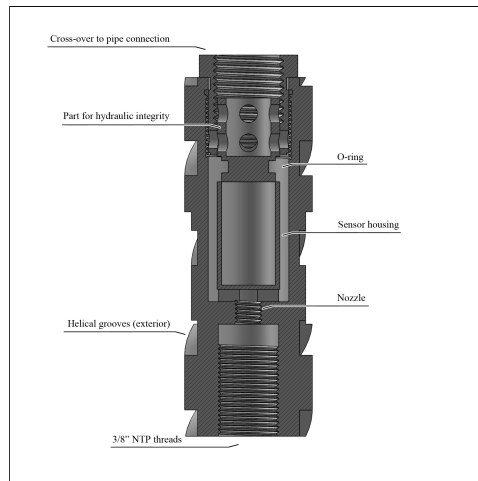
Figure 6.37: Schematic of the primary stabilizer sub of the old BHA. It houses downhole sensors and enables connection to the drill pipe above and the bit below.

with the custom bit. Bits with 3/8" NTP threads require a cross-over sub, such as the bit provided by DSATS. The top threads are 3/8" BSP to accommodate the pipe connection sub. Downhole sensors are placed in a slim sensor card that is inserted into designated tracks on the stabilizer wall. The card is unable to pass an internal restriction below and is locked in place from above by the upper connection. Drilling fluids may easily flow past the slim card and out of the drill string. Hydraulic integrity of the sensors is secured by using a water repellent coating. The downhole sensor card is depicted in **Fig. 6.39**.

Downhole Sensor Communication

An electrical wire with a quick connection socket at the top end of the sensor card enables signal transmission to topside. The wire has three parts: the top end connects to the control system and extends from the swivel at the top end of drill pipes. The bottom part is attached to the sensor card. The middle part has quick connection sockets at either end connecting the control system to the sensor card. The middle part of the wire is easily replaceable. In case of twist-off in the pipe just above the BHA (where most of the twist-offs occur), the quick connection socket is designed to detach before the wire snaps. If the wire snaps, it does so above the connection socket at the replaceable middle part.

Tooljoint

The hydraulic connection tooljoint used in the old BHA design is replaced. The previous solution caused issues where the metal fitting attached to the drill pipe would bite into and deform the aluminum at high torques. This would severely weaken the pipe, eventually causing twist-off. If pipes - for any reason - needed to be replaced, the connection would
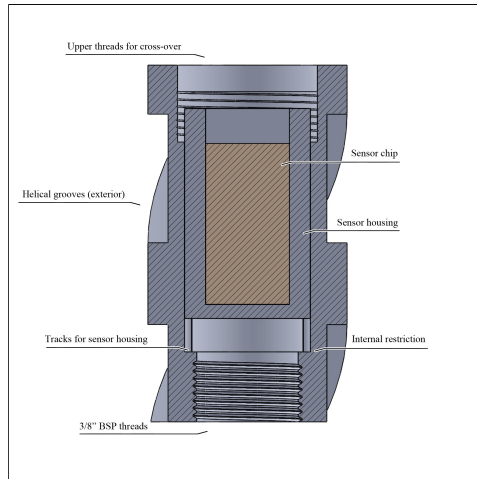
Figure 6.38: Schematic of stabilizer sub of the new BHA. It houses downhole sensors and enables connection to the drill pipe above and the bit below. The sensor chip is illustrative: the chip and card are one integral part.

Figure 6.39: Downhole sensor card with accelerometer, gyroscope and thermometer.

rarely come off without causing damage. The new BHA uses a mechanical connection that secures the pipe over a longer distance with a larger contact area. Hydraulic integrity is retained by an o-ring. The mechanical connection causes less damage, is quicker to assemble and may be disassembled without leaving marks on the pipe. The old hydraulic and new mechanical connection are shown in **Fig. 6.40**.

Figure 6.40: Old and new BHA tooljoint.

Modular BHA

Other stabilizing subs have been designed that may be connected at the bottom end of the primary stabilizing sub if desired. A modular BHA solution is chosen because it is uncertain whether a long and heavy or short and light BHA perform best when drilling with a miniature rig. With a modular BHA, different combinations may be tested. When adding the additional subs, more of the allowed 8.9 cm of downhole stabilization are exploited. However, more weight is added. The upper threads at the upper sub fits into the primary stabilizer, and the bottom sub threads are 3/8" BSP, equivalent to the threads of the primary stabilizer. The top and bottom sub effectively add 10 and 14 mm of downhole stabilizers,

Table 6.2: Weights and lengths of the old and new BHA.

	Weight	Length
Old BHA	177 g	80 mm
New BHA	121 g	51 mm
With secondary subs	195 g	75 mm

respectively. They are helically grooved on the exterior in a continuation of the pattern of the primary sub. A fully assembled BHA is 75 mm long and weighs 195 g. **Fig. 6.41** shows a picture of the primary sub and secondary subs. Weight and length of the old and new BHA is listed in **Table 6.2**.

Primary stabilizer   Secondary stabilizer

Figure 6.41: Photography of the primary and secondary stabilizer subs of the new BHA.

Dynamic Stabilizer

The subs are designed with matching circular grooves at the surface between them. When assembled, the BHA is loaded with balls that are free to move in the circular groove. Their purpose is to act as a dynamic stabilizer that mitigates lateral vibrations in the drill string. The working principle of a dynamic stabilizer is rather simple; if the center of mass of a rotating system is shifted away from the axis of rotation, the system will oscillate. By allowing some of the mass to move freely, any mass imbalance will be naturally shifted towards the center of rotation, potentially eliminating the imbalance. In this case the rotating system is the drill string, and the freely moving masses are the balls in the circular groove. The balls are depicted in **Fig. 6.42**.

Figure 6.42: Freely moving balls in the dynamic stabilizer.

7

Mechanical Limits and Constraints

There were several limitations affecting the rig and control system design. This section attempts to highlight the most significant limitations related to mechanical and operational limits and restrictions from the competition guidelines. Handeland et. al (2017) discussed the design consideration for the miniature drilling rig. Theoretical discussion on the drill string failure modes buckling, burst, twist-off and power consumption are similar to that of chapter 3.2 and 3.3 [1]. The competition guidelines stipulate the rules and constrains including a maximum stabilizer length of 89 mm, limiting the length of the BHA, and a maximum power consumption of 25 Hp (18.64 kW). Another major limitation is the pipe geometry and material. All teams must use a 3' pipe with an outer diameter of 3/8" and a maximum wall thickness of 0.049". It must be an aluminum pipe, specifically the alloy type 6061-T6.

7.1 Buckling

Applying sufficient weight to the drill string is essential for effective drilling operations. As described in section 6.1.1, WOB applied by the miniature rig by a hoisting motor and ball screw. Nonetheless, compression of the drill string is critical as too much WOB increases the risk of buckling the pipe. Sinusoidal or helical buckling of the drill string occurs when the load increases beyond a critical value [43]. Under static conditions, buckling of a vertical drill pipe is described in its simplest form by Euler's equation (**Eq. 7.1**) for critical load [44], [43].

$$F_{cr} = \frac{\pi^2 EI}{(KL)^2} \qquad (7.1)$$

In **Eq. 7.1** E is the material's Yong's Modulus (Pa), I is the minimum area moment of inertia (also known as second moment of area) (m^4), K the effective length factor, L is the unsupported pipe length (m) and, F_{cr} is the critical load before buckling occurs (N). The equation relies on many idealized assumptions, such as a perfectly straight pipe. It is also assumed that all load is applied through the pipe centroid, i.e, no eccentricity effects are

taken into account.

As described in the project report [1], Long, S & Bennet, D. (1996) differentiates vertical buckling in three different modes of equilibrium [45].

1. Stable equilibrium of a pipe occurs when the applied compressive load is less than the Euler critical load. Any deflection caused by an applied lateral load to the pipe will not remain once the lateral load is removed.

2. The second mode is when the pipe is under neutral equilibrium. This occurs when the axial load equals Euler's critical load. Any lateral force applied to the pipe will result in irreversible deflection of the pipe.

3. The last mode describes buckling as a result of pure axial forces. When the axial load exceeds the critical load, the pipe will buckle even without any lateral forces.

The minimum second moment of area for a hollow cylindrical shaft is the one about the x- and y-axis and is given by **Eq. 7.2** where OD and ID are the outer and inner diameter of the pipe (m) [46].

$$I = \frac{\pi}{64} \left(OD^4 - ID^4 \right) \tag{7.2}$$

The effective length factor K is included in the Euler's formula to incorporate the effects of different end conditions on the critical buckling load. **Fig. 7.1** summarizes the four end conditions: rounded-rounded, fixed-fixed, fixed-free, and fixed-rounded. **Eq. 7.1** is suitable for calculating critical loads for relative long columns. However, for shorter columns, the critical load differs from the predictions of Euler's equation. Note that the critical load given in **Eq. 7.1** diverges to extreme values as the length decreases towards zero. In reality, short columns will yield before the calculated buckling force. The failure limit is linked to the slenderness ratio, the length of the pipe relative to the radius of gyration, k (m). J.B. Johnson's empirical equation takes into account the slenderness ratio and its effect on critical stress when the ratio is below a critical value. The critical stress is given by **Eq. 7.3**, where C is an end-condition constant, E is Young's Modulus (Pa), L is the pipe length and k is the radius of gyration.

$$\sigma_{cr} = \frac{P_{cr}}{A} = \frac{C\pi^2 EI}{AL^2} = \frac{C\pi^2 E}{\left(\frac{L}{k}\right)^2} \tag{7.3}$$

The relation between the second moment of area to the radius of gyration, and the end-condition constant to the effective length factor is given in **Eq. 7.4**, while the slenderness ratio is given in **Eq. 7.5**. Johnson's empirical parabolic formula is given in **Eq. 7.6**, where σ_{ys} is the material yield strength (Pa).

$$I = Ak^2, \quad C = 1/K^2 \tag{7.4}$$
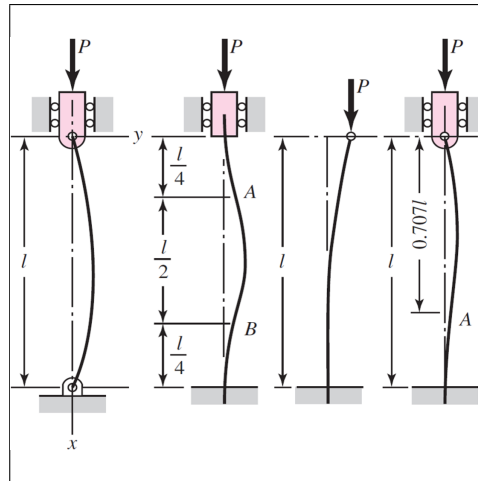
Figure 7.1: Pipe end conditions. From left to right: rounded-rounded, fixed-fixed, fixed-free, and fixed-rounded [46].

$$\frac{L}{k} = L\sqrt{\frac{A}{I}} \tag{7.5}$$

$$\sigma_{cr} = \sigma_{ys} - \left(\frac{\sigma_{ys}}{2\pi}\frac{L}{k}\right)^2 \frac{1}{CE}, \frac{L}{k} \leq \left(\frac{L}{k}\right)_{cr} \tag{7.6}$$

Note that the parabolic equation is defined when the slenderness ratio is equal or less than the critical slenderness ratio given in **Eq. 7.7**, and that the critical stress for intermediate and short columns are dependent on the material properties as well as geometry. **Table 7.1** gives a summary of the end conditions and their theoretical, conservative and recommended value [46].

$$\left(\frac{L}{k}\right)_{cr} = \sqrt{\frac{2\pi^2 CE}{\sigma_{ys}}} \tag{7.7}$$

Fig. 7.2 shows how the the critical buckling load increases as the slenderness ratio is decreased, equivalent to decreasing the pipe length for a given OD and thickness. Due to high rotational speeds and vibrations during drilling, one of the main concerns of drill pipe failure is fatigue. The critical load has been plotted when using aluminum 6061-T6 yield strength and fatigue strength. Note that Johnson's parabola has lower critical loads when using the fatigue strength. Comparison of the critical loads for two different pipe thicknesses are also given in **Fig. 7.2**. Last year, the drill pipe had a wall thickness of 0.035", compared to 0.049" this year. The increase in wall thickness increases the critical buckling load evident by the square and circle shifting to the left on the buckling curve. All squares and circles are plotted for a slenderness ratio corresponding to the maximum

Table 7.1: Theoretical, conservative and recommended values of the end-condition constant C. The table is modified from Budynas, R.G & Nisbett, J.K (2011) Table 4-2.

Column End Condition	End-Condition Constant C		
	Theoretical	Conservative	Recommended
Rounded-Rounded	1	1	1
Fixed-Fixed	4	1	1.2
Fixed-Free	0.25	0.25	0.25
Fixed-Rounded	2	1	1.2

Table 7.2: Length at which Euler critical buckling equals Johnson's parabola. The values are calculated for a pipe thickness of 0.0049" and outer diameter of 3/8".

Strength	C	L/k	Length (cm)
Yield - 276 MPa	1.2	76.9	22.7
	4	140.4	41.5
Fatigue - 96.5 MPa	1.2	133.0	38.5
	4	237.4	70.3

unsupported pipe length of 0.68 meter. Note that the Euler buckling curves are identical for the two pipe thicknesses (see **Eq. 7.3**). The difference in theoretical buckling load occurs as a result of change in pipe area and moment of area.

The drill pipe will go through a stabilizing kelly bushing at the drill floor. The theoretical and recommended value for the end condition constant C for this setup is 4 and 1.2 respectively, given by the fixed-fixed column end condition in **Table 7.1**. The pipe is weakest with respect to buckling at the onset of drilling when the unsupported pipe length is at its longest. As drilling commences, the unsupported length of the drill pipe changes until half the pipe has passed the bushing. **Table 7.2** gives a summary at which length the critical load is equal for both Euler buckling and Johnson's parabola for yield and fatigue strength, and different values of C. The maximum WOB that can be applied by the hoisting motor is given by **Eq. 7.8**. **Fig. 7.3** shows the maximum applicable static WOB as a function of unsupported pipe length for different values of C.

$$F_{WOB,max} = \sigma_{cr} A \tag{7.8}$$

The results of the static buckling test are discussed in section 9.1.1 and show that the best fit value for C equals 3 for the new pipe with wall thickness 0.049". The results matched the pipe with wall thickness 0.016". As a result of the rig design, there are three section of unsupported drill pipe. These include the free pipe above the kelly bushing, the intermediate pipe between the kelly bushing and riser bearing, and the lower part under the riser bearing which is connected to the BHA. It is assumed that the longest of the three sections will determine the buckling limit of the system. Therefore the maximum
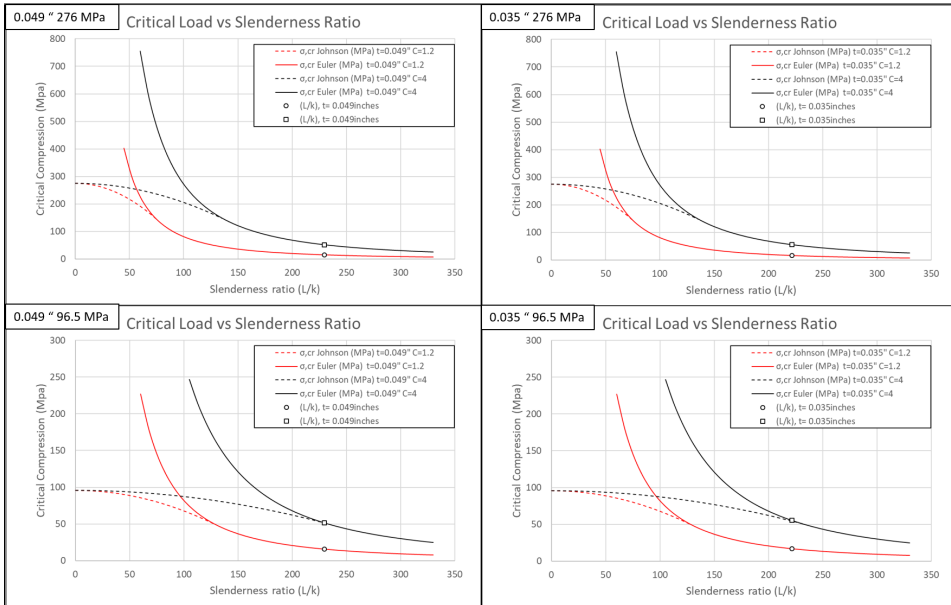
Figure 7.2: Critical buckling load as a function of slenderness ratio. Note that all the squares and circles mark the slenderness ratio at 68 cm.
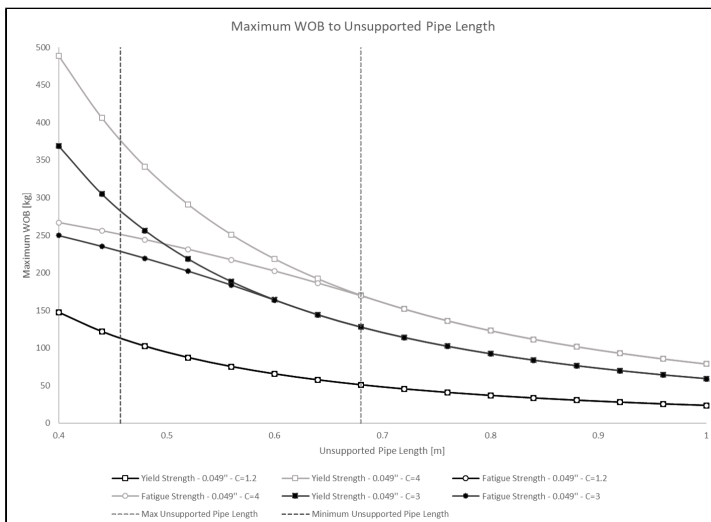
Figure 7.3: Maximum applicable WOB as a function of unsupported pipe length for a 0.049" thick drill pipe with 3/8" OD.
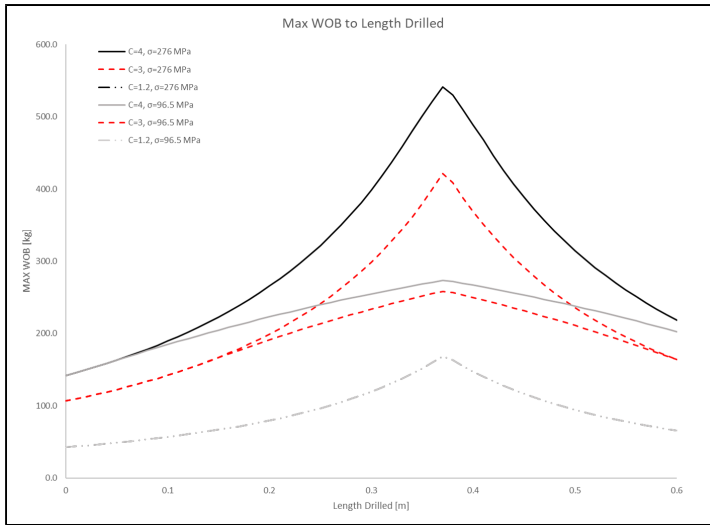
Figure 7.4: Maximum applicable WOB as a function of drilled length. For 3/8" 6061-T6 aluminum with 0.049" wall thickness.

WOB that can be applied will vary with rock height, total drill pipe length, riser position, BHA and bit length, and total depth drilled. **Fig. 7.4** shows an example of the maximum applicable WOB as a function of drilled length, in this case with a 3' drill pipe, 65 cm rock sample, riser centralizer 17 cm below kelly bushing and a total BHA and bit length of 13 cm. Note that using yield strength or fatigue strength yields the same result when applying the recommended end condition constant C = 1.2. This is a result of the maximum unsupported drill pipe length staying above the critical slenderness ratio.

7.1.1 Effect of Internal Pressure

Olsen, et. al. (2017) discussed the effects of internal pressure on buckling limits based on static conditions [28]. They argued that the internal pressure of the pipe increased the buckling limit and subsequently increased the maximum applicable WOB given by **Eq. 7.9** where ID is the inner diameter of the pipe (m), g is the gravitational acceleration (m/s^2) and p is the net pressure differential across the pipe wall (Pa).

$$\Delta WOB = \frac{\pi ID^2}{4g}p \tag{7.9}$$

It is an important statement to investigate as buckling of the pipe is one of the major limitation on the drilling process for the miniature rig. Palmer & Baldry (1974) [47] were able to show that an axially constrained pipe would buckle in the lateral direction when subjected to sufficiently high internal pressure. The internal over pressure of the pipe induces a tension in the pipe. However, Palmer & Baldry included the compression of the liquid resulting in a positive net compression. The critical pressure in which an axially

constrained pipe buckles is given in **Eq. 7.10**, where p_{crit} is the critical buckling pressure (MPa), t is wall thickness (m), E is the Young's modulus (MPa), ν is Poisson's ratio, D is the pipe diameter and L is the pipe length (m) [47].

$$p_{crit} = \frac{2\pi^2 E D t}{(1 - 2\nu)L^2} \tag{7.10}$$

Palmer & Baldry (1974) were able to match the predicted buckling pressures with experimental data. Catinaccio (2009) describes the governing equation yielding the critical buckling limit given in **Eq. 7.10** [48]. The tensile stress induced on a thin walled axially constrained pipe is given in **Eq. 7.11**, in which σ_z is the tensile stress (MPa) and p the internal over pressure (MPa).

$$\sigma_z = \frac{\nu p D}{2t} \tag{7.11}$$

Consider the net axial compressive force as the compressional load from the fluid acting on the inner cross-sectional area minus the induced tension in the pipe. The total compressive force is then given by **Eq. 7.12**.

$$F_{net,comp} = p\frac{\pi D^2}{4} - \frac{\nu p D}{2t} \cdot \pi D t = \frac{p(1 - 2\nu)\pi D^2}{4} \tag{7.12}$$

The second moment of area for a thin walled pipe is given in **Eq. 7.13**. Inserting the expression for the second moment of area into Euler's buckling equation, **Eq. 7.1**, the critical buckling force is given by **Eq. 7.14**.

$$I = \frac{\pi E D^3 t}{8} \tag{7.13}$$

$$F_{cr} = \frac{4\pi^2(\pi E D^3 t/8)}{L^2} \tag{7.14}$$

Equating **Eq. 7.12** and **Eq. 7.14** and solving with respect to pressure yields the critical pressure given by **Eq. 7.10**. For a thin walled pipe which is not axially constrained, the induced axial tension is given by **Eq. 7.15**, thus the net compression in the pipe, accounting for the compression of the fluid, equals zero. Applying Palmer & and Baldry's theory on the buckling limits of the drill pipe suggests that the pipe is in compression due to WOB and that the perceived extra WOB due to induced tension in the pipe from pressure, given by **Eq. 7.9** is incorrect.

$$\sigma_z = \frac{p D}{4t} \tag{7.15}$$

7.2 Burst

Pressure loss across the bit nozzles determine the maximum limit for flow rate. It is restricted by the aluminum pipe's burst rating determined by Barlow's equation for thin walled pipes [31]. In **Eq. 7.16**, σ_{ys} is the material yield strength, t is wall thickness and OD is the pipe's outer diameter.

$$p_b = 0.875 \frac{2\sigma_{ys}t}{OD} \tag{7.16}$$

Burst of the drill pipe might occur under too high flow rates or if loss of circulation occurs during drilling. The team experienced small cutting particles lodged in the nozzles during drilling which increases the pressure loss across the system. Using the alloy yield strength of 276 MPa and a safety factor of 3, the burst limit is calculated to be 210.4 bar, well below expected operating conditions. An additional safe guard is implemented should total loss of circulation occur simultaneously as the pump runs. A pop-off valve at the pump is activated at 100 bar.

7.3 Twist-off

Maximum torque on the drill string before twist-off failure is given by **Eq. 7.17** where τ_{max} is the maximum shear stress the pipe allows for and a, b are the pipe inner and outer radius respectively.

$$T_{DP,max} = \tau_{max} \frac{\pi}{2} \left(b^2 - a^2\right)(b + a) \tag{7.17}$$

Static Twist-off

6061-T6 Aluminum has a shear strength of 207 MPa. **Eq. 7.17** yields a maximum static torque of 27.8 Nm before pipe failure for a 3/8" pipe with wall thickness of 0.049". However, drilling is a dynamic process with induced stresses that affect the torque limit.

Dynamic Twist-off

Stuck pipe or highly heterogeneous formation types can lead to high torque values on the drill string during drilling. The maximum torque provided by the top drive motor before the pipe fails is governed by the von-Mises failure criterion given in **Eq. 7.18**.

$$\sigma_{ys}^2 = \frac{1}{2}\left[(\sigma_{11} - \sigma_{22})^2 + (\sigma_{22} - \sigma_{33})^2 + (\sigma_{33} - \sigma_{11})^2 + 6(\sigma_{12}^2 + \sigma_{23}^2 + \sigma_{31}^2)\right] \tag{7.18}$$

$\sigma_{11}, \sigma_{22}, \sigma_{33}$ are the three normal components of the stress acting on the drill pipe, and $\sigma_{12}, \sigma_{23}, \sigma_{31}$ are the shear stresses. The stress components acting on the pipe due to WOB,
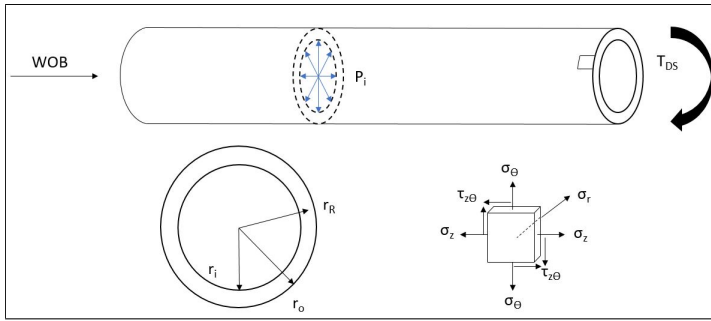
Figure 7.5: Stress components on the drill pipe induced by WOB, internal pressure and drill string torque.

internal pressure and applied drill string torque are illustrated in **Fig. 7.5**. The stress components for a thick walled pipe is given by **Eq. 7.19** through **Eq. 7.21** [49].

$$\sigma_r(R) = \frac{\left(\frac{a}{b}\right)^2 - \left(\frac{a}{R}\right)^2}{1 - \left(\frac{a}{b}\right)^2} \cdot p_i \tag{7.19}$$

$$\sigma_\theta(R) = \frac{\left(\frac{a}{b}\right)^2 + \left(\frac{a}{R}\right)^2}{1 - \left(\frac{a}{b}\right)^2} \cdot p_i \tag{7.20}$$

$$\sigma_z^p = \frac{\left(\frac{a}{b}\right)^2}{1 - \left(\frac{a}{b}\right)^2} \cdot p_i \tag{7.21}$$

$$\tag{7.22}$$

Where a equals the inner radius of the pipe, and b equals the outer radius. Evaluating **Eq. 7.19** through **Eq. 7.21** at the inner diameter (i.e. $R = a$) yields simplified expression given in **Eq. 7.23** through **Eq. 7.25**. The induced stresses are correlated with the stress components of the von-Mises criterion in **Eq. 7.26** through **Eq. 7.29**.

$$\sigma_r = -p_i \tag{7.23}$$

$$\sigma_\theta = \left(\frac{a^2 + b^2}{b^2 - a^2} \right) \cdot p_i \tag{7.24}$$

$$\sigma_z^p = \left(\frac{a^2}{b^2 - a^2} \right) \cdot p_i \tag{7.25}$$

$$\sigma_{11} = \sigma_z, \quad \sigma_{22} = \sigma_\theta \tag{7.26}$$

$$\sigma_{33} = \sigma_r, \quad \sigma_{12} = \tau_{max} \tag{7.27}$$

$$\sigma_z = \sigma_z^p + \frac{WOB - W_B}{A} \tag{7.28}$$

$$A = \pi \left(b^2 - a^2 \right) \tag{7.29}$$

In **Eq. 7.26** through **Eq. 7.29**, σ_z^p is the axial tension in the pipe induced by the flowing drilling fluid through the nozzle in the bit threads W_B (N) is the buoyed weight of the drill string and is in further analysis neglected as it is a order of magnitude smaller than the expected WOB. It is also assumed that the pressure loss across the nozzle is approximately the same as the internal pressure of the pipe. Pressure loss in the circulation system is described in chapter 6.3.5. The maximum shear stress is given by **Eq. 7.30** which is found by evaluating the von-Mises criterion with the induced stresses.

$$\tau_{max} = \sqrt{\frac{2\sigma_{ys}^2 - [(\sigma_z - \sigma_\theta)^2 + (\sigma_\theta - \sigma_r)^2 + (\sigma_r - \sigma_z)^2]}{6}} \tag{7.30}$$

Fig. 7.6 shows the maximum torque on the drill string as a function of pressure and WOB. The difference in maximum torque is minimal in the expected operating conditions of the rig. It is also evident that the pipe tolerates less torque after fatigue, and that the pressure and WOB have more effect on the maximum torque after fatigue.

Note that the calculations above assume an aligned drill string and forces induces solely from WOB and pressure, in addition, $\sigma_{23} = \sigma_{31} = 0$. Realistically the torque limit will be lower due to vibrations during drilling, misalignment of the drill string components, bending moments and fatigue. These factors make design factors essential when operating the rig.
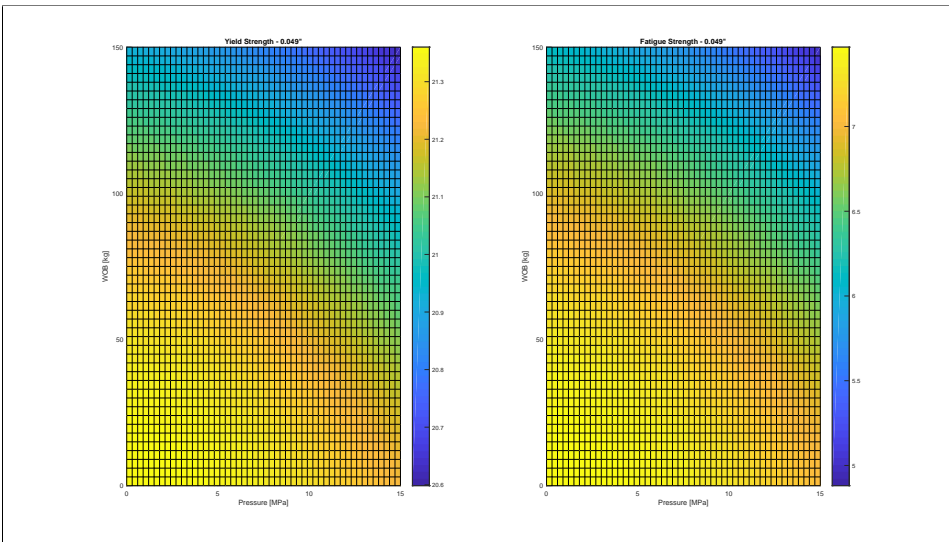
Figure 7.6: Maximum torque as a function of WOB and pressure. Pressure given in MPa.

Table 7.3: Top Drive Power Consumption. An efficiency factor of 0.9 is applied.

Rotational speed [RPM]	Top drive torque [Nm]					
	1	3	5	7	9	11
	Power Consumption [W]					
400	47	140	233	326	419	512
600	70	209	349	489	628	768
800	93	279	465	652	838	1024
1000	116	349	582	814	1047	1280
1200	140	419	698	977	1257	1536
1400	163	489	814	1140	1466	1792
1600	186	559	931	1303	1676	2048
1800	209	628	1047	1466	1885	2304

7.4 Power Consumption

The power consumption in the competition is limited to 25 hp equivalent to 18.64 kW. The motors which provide torque and rotation to the drill string, ball screw and pump are the main components in the rig that consume power. In addition to the motors, the computer consume power. This section will give an overview of the expected power consumed during drilling and if the competition guidelines are honored with respect to the limits stipulated.

7.4.1 Top Drive Motor

Given a rotating shaft with an efficiency factor ϵ, motor torque T (Nm), and angular velocity of w (rad/sec), the power provided by the motor and angular velocity are given by **Eq. 7.31** and **Eq. 7.32**, where N is the number of revolutions per minute (RPM). When drilling, the operational window of the top drive is limited to 1800 RPM and a torque of 14.4 Nm. Testing showed that normal operating conditions resulted in torques at or below 5 Nm. At 5 Nm torque and 1800 RPM, the motor consumes 1.05 Kw. **Table 7.3** summarizes the power consumption at different combinations of rotational speed and motor torque.

$$P = \frac{Tw}{\epsilon} \tag{7.31}$$

$$w = \frac{2\pi N}{60} \tag{7.32}$$

7.4.2 Hoisting Motor

The torque generated from the hoisting motor is given by **Eq. 7.33**, where F (N) is the force acting on the ball screw, l (m) is the ball screw lead, and ϵ_{BS} is the ball screw and

hoisting motor system efficiency factor. The ball screw lead is 5 mm leading to an inherent low torque and power consumption for the hoisting motor. The gear ratio between the hoisting motor RPM and ball screw RPM is 8.935. The instantaneous ROP in cm/min is thus given by **Eq. 7.34**, where γ is the gear ratio, RPM_h is the hoisting motor RPM and l is the ball screw lead. Assuming a maximum ROP of 30 cm/min, and motor torque of 1 Nm, the hoisting motor rotational velocity is 536 RPM, and the power consumption is only 62 W.

$$T_h = \frac{Fl}{2\pi\epsilon_{BS}} \tag{7.33}$$

$$ROP = \frac{RPM_h\gamma l}{100} \tag{7.34}$$

7.4.3   Pump

Circulation of the drilling fluid provides sufficient hole cleaning, cooling of the bit and lubrication. As explained in section 6.1.1, a triplex pump provides the drilling system with sufficient flow rate and pressure. The requirements for pressure and flow rate in the system is described in section 6.3. The power consumed by the pump is dependent on the increased pressure head, flow rate an pump efficiency given in **Eq. 7.35**. The added pressure is the difference in pressure directly downstream the pump and the inlet pressure to the pump, which is 5.3 bar.

$$P_P = \frac{\Delta Pq}{\epsilon} = \frac{(P_{gauge} - 5.3 \cdot 10^5)q}{\epsilon} \tag{7.35}$$

In **Eq. 7.35**, P_P is the power consumption in W, P_{gauge} is the pressure directly downstream the pump, recorded with a pressure gauge, q is the flow rate in m^3/s and ϵ is the pump efficiency factor. **Table 7.4** gives a list of the power consumed at different flow rates and drill pipe pressure. Note that the drill pipe pressure is assumed equal to the pressure gauge readings due to negligible pressure loss from pump to BHA. The flow rate and pump pressure is not expected to exceed 20 bar and 14 l/m yielding an expected power consumption of 0.381 kW.

7.4.4   Other Factors

The computer model used during the competition is a DELL OptiPlex 7440 AIO which has a rated maximum power consumption of 720 W. However, it is not expected to draw more than 200 W. In addition, the second monitor consumes approximately 100 W. The down hole sensors, pressure gauge and load cell consume negligible power relative to the motors.

7.4.5   Total Consumption

Table 7.5 gives a summary of the power consumption during expected operating levels and the maximum power consumption based on their capacity or safety limits. The expected

Table 7.4: Power consumption of the pump for a set of drill pipe pressures and flow rates. The calculations assume an efficiency factor of 0.9.

	Flow rate [l/min]				
	2	4	8	14	20
Pressure [bar]	Power Consumption [W]				
10	17	35	70	122	174
20	54	109	218	381	544
30	91	183	366	640	915
50	166	331	662	1159	1656
100	351	701	1403	2455	3507

Table 7.5: Summary of expected and maximum power consumption and comparison of competition restriction.

	Power Consumption [W]	
Component	Expected	Maximum
Top Drive	760	3020
Hoisting Motor	20	210
Pump	381	3400
Computer	200	720
Monitor	100	360
Total	1380	7710
% of Limit	7.8%	41.4%

power consumption is not expected to exceed 7.8% of the competition limit. At maximum capacity the rig will consume 41.4% of the limit. It is therefore reasonable to conclude that the power limitation is not a bottleneck to the rig design.

7.5 Economics

The Drillbotics guidelines have a limited budget of $10,000 USD. The budget includes all parts of the rig that will be used during the competition day. The student team can receive donations which will not be included in the total expenses. The guidelines indicate that the $10,000 USD is meant to cover hardware, software and labour to construct and operate the rig. Thereafter, the guidelines mention that "other in-kind contributions" and "paraphernalia usually associated with university laboratory projects" will not be included in the total cost. What this includes is a somewhat vague, as the normal standard may vary between universities. The NTNU team has therefore decided to list all new parts added to the rig this year as expenses.

Consumables are not included in the total cost. In Phase II, a considerable amount of material has been used to run tests similar to the challenge that will appear in the competition.

The test samples that has been used were made in wooden boxes. The cost of the wooden boxes are not counted as expenses. The rock samples were all leftovers donated to the NTNU Team from different vendors and are also not included.

The cost estimate only includes material used for the project. When doing a cost estimate of a real project, a large percentage goes to paying salary. The Guidelines specify that labour should not be included in the total cost. However, it is still a requirement to have an estimate on time spent completing the rig and the corresponding cost.

The team consists of five students, four supervising professors and a support crew of four. The students have this as their full time project. It is estimated that students have spent on average 37.5 working hours a week. This includes project management, team meetings, testing and report writing. The professors have mostly been giving advice and guidance during the status meetings every second week. The support team assists on an everyday basis. The amount of hours spent varies from week to week, depending on the overall status on the rig.

Table 7.6 shows the cost estimate for the labour done in Phase II of Drillbotics. It is clear that the total budget of $10,000 USD is not possible to keep if labour is included. Since Drillbotics is a student competition, most of the labour is done by students working for free. Still it is good to have some knowledge of what cost range a project like Drillbotics costs as this is something a company always needs to take into account in the planning phase.

Table 7.6: Shows an overview of the labour expenses from Phase II for the NTNU Drillbotics team 2018.

	Hours per week	Weeks	Hourly Wage [USD]	Total Cost [USD]
Students	37.5	18.0	18.3	58,437.5
Supervisors	1.0	14.0	59.5	3,333.3
Support crew	8.0	18.0	41.7	22,666.7
Total				84,437.5

As mentioned in the Design Report, the team worked on getting sponsors to fund the $10,000 USD expenses. The team contacted several oil companies and also went to NFiPs yearly conference in Stavanger, to establish contact with potential sponsors. Unfortunately, non of the requests got positive response. Funding has therefore been covered by the institute of Geoscience and Petroleum.

Drillbotics is an international competition and the restrictions in the budget are given in USD. The NTNU team is stationed in Norway and most of the purchases are made using NOK. An exchange rate is therefore needed to make the cost estimate in USD. It was stated in the Guidelines for Phase I that the cost estimate was to be included in the Design

Table 7.7: Equipment budget for the NTNU team in the Drillbotics competition 2018. Despite some changes made since the estimate made in the Design Report, the summary shows that the limits has been held with a great margin.

Unit	Cost per Unit NOK	Amount #	Total Cost NOK
Acrylic safety glass	1,500	1	1,500
Connections	1,700	2	3,400
Hoisting motor + drive	15,000	1	15,000
Ball Screw	5,000	1	5,000
Computer screen	0	1	0
Pressure gauge	1,500	1	1,500
Load cell	4,250	1	4,250
Accelerometer	500	1	500
Gyroscope	500	1	500
Hilseher Modbus Ethernet Ip Gateway	6,456	1	6,456
Sum [NOK]			38,106
Sum [USD]			4,536

Report. The exchange rate used is 8.4 NOK/USD from 19th December 2017.

Table 7.7 includes all the equipment bought by the NTNU team in the Drillbotics competition 2018. Total cost estimate is set to $6,982.1 USD. Compared to the cost estimate in Phase I of $9,594 UDS, the planned expenses have decreased drastically. Some equipment have been added to the list. These changes are mostly to compensate for equipment that didn't work according to previous plans. The torque sensor and the DAQ from National Instrument have also been removed from the list and is what makes the largest difference in the estimates. For the Design Report it was important to make a budget which could be fulfilled in Phase II. The budget proposal was therefore made with a large safety margin using the highest prices on the market for the different items.

8

Control System and Optimization

8.1 Hardware Setup and Instrumentation

It is imperative for a robust control system and overall design of the autonomous rig to have all electronics correctly and safely wired to enable digital and analog communication throughout the system. A large part of the team's new design included a new control system and change from Simulink to LabVIEW. Components that are better integrated into the LabVIEW programming environment were purchased. Therefore the electrical hardware and instrumentation have also been altered this semester.

8.1.1 Setup of Last Year

The previous setup was developed for integration with Simulink using an ABB programmable logic controller (PLC). **Fig. 8.1** depicts the original setup of motors, drives and sensors. Rotation of the drillstring is provided by the top drive motor, while the weight on bit is provided by the hoisting motor. Both motors were connected with the PC through respective motor drives and via the Open Platform Communications (OPC) server. In addition, the hoisting motor drive was connected to the OPC via the ABB AC500 PLC. The load cell provided weight measurements to Simulink via a National Instruments (NI) multifunction I/O device, the USB-6002. Note that the pump was not connected to the PC and had to be manually operated.

The original setup and control system enabled for WOB measurements at 50 Hz, while the data from the motors, such as torque and rotational speed were transmitted at a maximum of 10 Hz due to a bottleneck in the OPC server.

8.1.2 Planned Setup

It was early on decided that the software used for the graphic user interface and programming of the control system had to be replaced with a more robust and reliable system. The
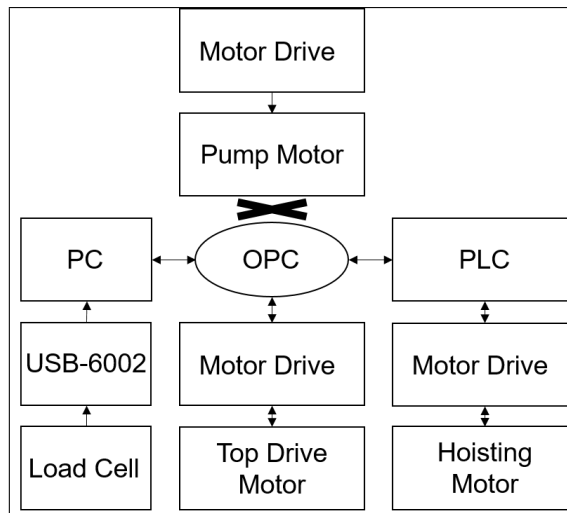
Figure 8.1: Old setup of hardware, motors and sensors

Simulink model was suited for easy manual control of the motors and controlling drilling using simple PID controllers. However, a state machine with more advanced features, such as rock interface detection, was difficult to program in Simulink. In addition, the program was not robust as it occasionally took time from pressing stop until the program executed the command and all actuators were turned off. Replacing Simulink with LabVIEW had also the extra benefit of omitting the need for an OPC server, resulting in higher sampling rates and reaction speed than 10 Hz.

The planned setup included hardware that is more streamlined for use in the LabVIEW programming environment. LabVIEW is a National Instruments software designed to work smoothly with NI hardware, therefore, it was decided to replace the PLC (and OPC server) with a data acquisition system from NI. Initially the planned acquisition system consisted solely of a new NI USB device. The USB-6218 has a maximum sampling rate of 250 kS/s per channel and includes 32 analog input channels, 2 analog output channels, and 8 digital input and output channels respectively. It would have enough channels to serve the purpose of this year's design which would include reading data from a new load cell, a pressure gauge, an acoustic sensor from ClampOn and controlling the pump. However, it was decided that a NI compactDAQ would be better as it allows for a modular setup of the desired data acquisition system. If future teams wish to add functionality to the control system such as external torque sensors, the corresponding module can easily be fitted to the DAQ as an extra module. **Fig. 8.2** shows the components of the cDAQ configuration. The NI cDAQ-9174 is a four-slot chassis connecting the C-series I/O modules to LabVIEW via USB.

The modules purchased and planed for use in the control system included a NI-9207 analog input device with 8 channels for current and 8 channels for voltage with a capacity of
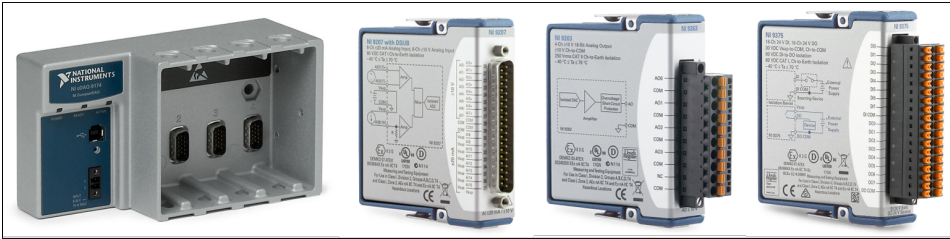
Figure 8.2: NI cDAQ configuration. From left to right: cDAQ-91774 chassis, NI-9207, NI-9263 and NI-9375.
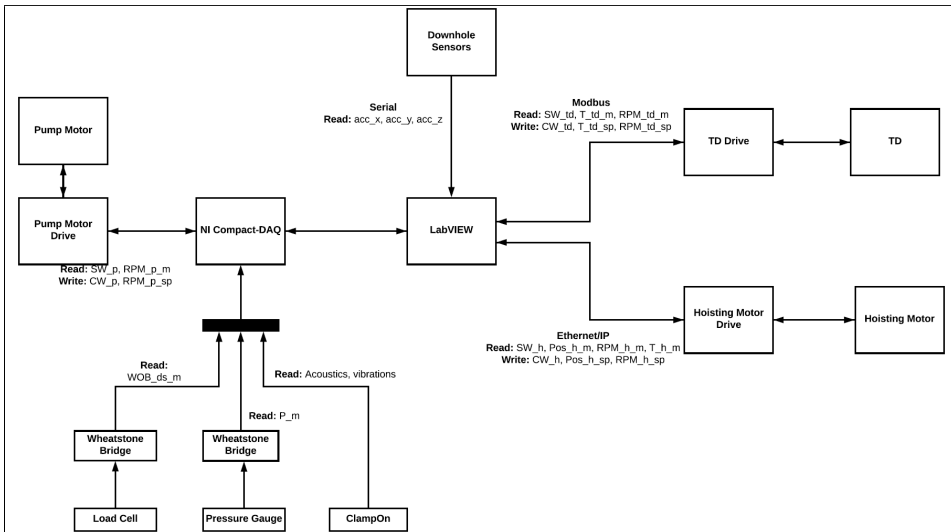
Figure 8.3: Schematic of planned data communication from sensors.

500 S/s, a NI-9263 4-channel voltage output module with 100 kS/s/ch and a NI-9375 32-channel digital I/O module. The plan was to connect the load cell, pressure gauge and pump drive to the cDAQ, while the top drive motor frequency converter and hoisting motor drive was planned to connect through Ethernet cables. The down hole sensors would be connected using serial communication directly to the computer. **Fig. 8.3** depicts the planned communication with LabVIEW.

8.1.3 Setup During Early Testing Phase

Due to many changes to the existing rig design and control system, the setup during testing changed throughout the semester. The LabVIEW script was developed alongside the evolving hardware and had to be adjusted whenever there were changes to sensors, motors, drives or anything that altered the analog/digital communication with the control system and hardware.
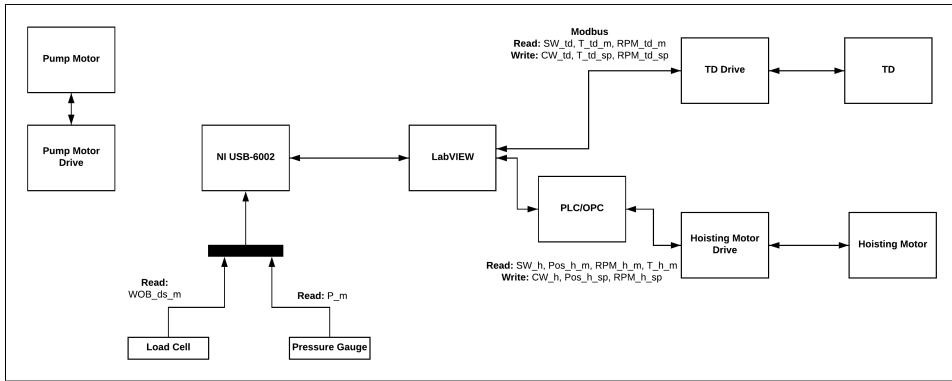
Figure 8.4: Schematic of data communication during early testing.

Much of the initial testing was conducted with the previous control system set up in Simulink. A majority of the tests were conducted with the intent of understanding the effects of drilling parameters and alignment alterations on hole quality. As the LabVIEW script evolved so did the setup with instrumentation and how communication was achieved.

In the start of the semester, the rotation of the drillstring had to be manually controlled directly from the top drive motor drive, i.e. a team member had to physically stand by the electrical cabinet, start the motor, set the rotational speed and stand ready to stop the motor. The first major change in the motor communication occurred when communication with the top drive motor was established through LabVIEW. At that point the top drive was controlled in LabVIEW through Modbus communication while the hoisting motor was controlled by shared network variables with the OPC. That is, the PLC was still installed in the electrical cabinet and used within the LabVIEW program. The pump was still not in use, and the only external sensors in place were the load cell and pressure gauge. **Fig. 8.4** shows the setup during early testing. The pump is not connected to the computer, only the pressure gauge and load cell is connected and to the NI USB-6002, the down hole sensors were not yet constructed and the top drive motor was communicating through an Ethernet cable via Modbus while the hoisting motor was controlled through the PLC and OPC server.

Connecting Hoisting Motor to cDAQ

The new frequency converter (drive) controlling the hoisting motor was equipped with an Ethernet/IP module enabling transfer of I/O data through an Ethernet cable. Issues with the built in TCP and UDP packages in LabVIEW resulted in the need for a Modbus to Ethernet/IP converter. While waiting for the converter, communication with the hoisting motor and LabVIEW was established using the cDAQ. In addition, the USB-6002 device was damaged resulting in low frequent, high amplitude noise in the load cell reading. The device was replaced with a USB-6009 device. The schematic is the same as in **Fig 8.4**, however, the USB device is replaced and the PLC/OPC block is replaced with the cDAQ

chassis.

Issues using cDAQ to Control the Hoisting Motor Drive

Connecting the cDAQ C-series modules to the hoisting motor drive and setting up communication in Lenze Engineering was achieved. This enabled the team to communicate with the drive using LabVIEWs built in packages. However, the control system architecture already in place relied on all I/O data for the hoisting motor drive being processed in a single while loop. The built in LabVIEW block DAQ Assistant is designed for easy setup of hardware communication. The user selects the module, analog or digital signal, generating or acquiring signal, the relevant channel or port on the hardware and sampling frequency. The DAQ Assistant generates the subVI and the hardware is ready for execution. Complications with synchronization resulted in issues when using several DAQ Assitants in a single while loop.

8.1.4   Final Setup

After a meeting with two National Instruments representatives, it was decided that implementation of the cDAQ to control the hoisting motor would need a different base architecture in the main VI. Due to time constraints, it was decided to keep the current solution in which the top drive motor is controlled through Modbus and attempt to set up the communication with the hoisting motor drive and LabVIEW through a Modbus - Ethernet/IP gateway. A schematic of the final setup is given in **Fig. 8.5**. Due to limited time and issues getting the communication with the hoisting motor up and running, the pump was not incorporated into the control system. It was run with a constant rotational speed on the pump motor which was manually set in the drive. The load cell and pressure gauge were connected a NI USB-6009 device which transmitted the data to LabVIEW. Down hole data were transmitted via serial communication connected via a standard USB-cable. ClampOn was not integrated into the control system nor into LabVIEW and was run in a separate application. The top drive motor and hoisting motor were both physically connected with the computer with an Ethernet-cable and communicating with LabVIEW via Modbus TCP.

The following motors and sensor comprised the final instrumentation of the rig.

- Top drive motor: ABB 3GAA091520-ASJ AC motor

- Top drive frequency converter: ABB ACS880-01-05A6-3

- Hoisting motor: Lenze GST03-2M VBR 063C42

- Hoisting motor inverter drive: Lenze 8400 TopLine C

- Pump: HAWK HC980A

- Pump motor: VEM motors Thurm GmbH K21R 112 M-6

- Pump motor drive: SEW Movitrac MC07B0040-5A3-4-00
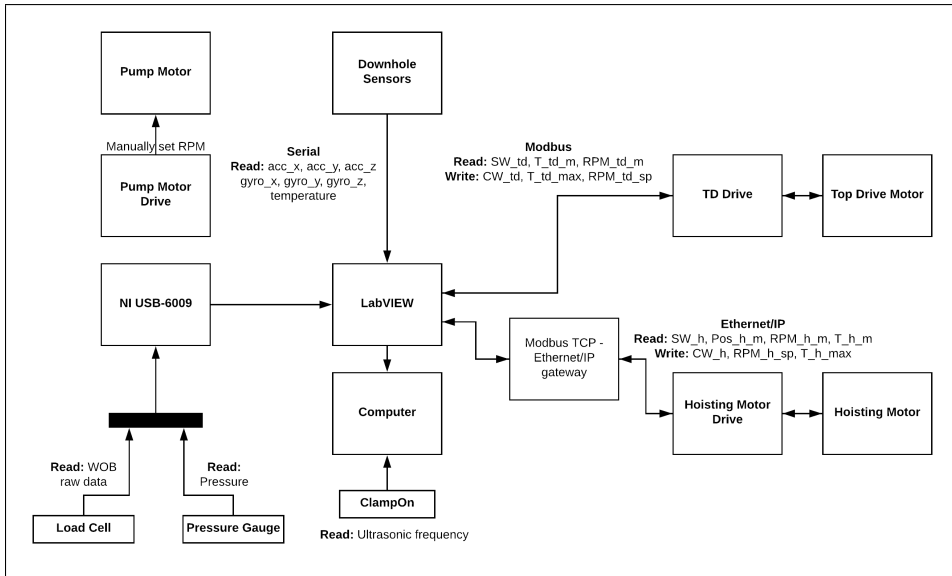
Figure 8.5: Schematic of the final setup in hardware.

- Accelerometer and gyroscope: Invensense 6-axis MPU-6050

- Pressure gauge: Aplisens PCE-28 4m-20m Ampere

- Load cell: AEP TC4-AMP +-5kN

- ClampOn SandQ

- Data communication

    - NI USB-6009 for load cell and pressure gauge data acquisition
    - Modbus TCP - Ethernet/IP gateway: Hilscher NT 100-RE-EN

8.1.5   Calibration and Scaling Data

The load cell and pressure gauge were linked to the USB-6009 and output +-10 V and 4mV - 20mV respectively. The maximum measurable load for the load cell is 5kN, thus the load cell scaling from analog data to kg is given by **Eq. 8.1** where V_{LC} is the load cell voltage output from the NI USB-6009 and C is the offset weight caused by the weight of the traveling block. The scaling is negative due to the configuration of the load cell.

$$WOB = -\frac{5000N}{10V}\frac{1}{9.81m/s^2}V_{LC} + C \qquad (8.1)$$

The load cell arrived pre-calibrated. However, to verify the data a test was conducted where the conversion from **Eq. 8.1** was compared to a scale. The traveling block was

Figure 8.6: Motors and drives. Top row from left to right: Top drive motor, hoisting motor, pump and pump motor. Bottom row from left to right: top drive frequency converter, hoisting motor drive, pump motor drive.

Figure 8.7: Sensors and IO modules. Top row from left to right: Load cell, Modbus TCP - Ethernet/IP gateway, NI USB-6009. Bottom row from left to right: ClampOn SandQ, pressure gauge, down hole sensor.
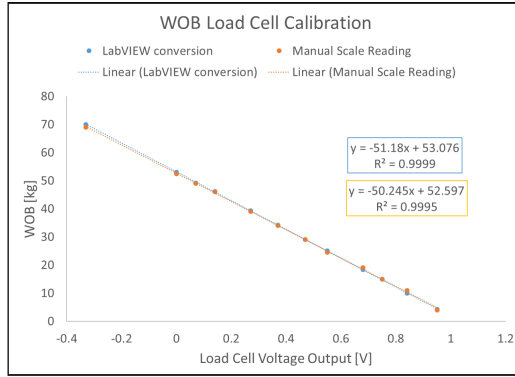
Figure 8.8: Comparison of **Eq. 8.1** and manual scale readings

hoisted down on the weight and both loads were noted. The results are given in **Fig. 8.8**. The manual readings have a higher uncertainty than the load cell readings. It is therefore concluded that the load cell is correctly calibrated.

The pressure gauge has a range of 0-100 bar and outputs 4mA-20mA. Thus, the scaling from current to bar is given by **Eq. 8.2**, where I_{PG} is the pressure gauge current in mA. The pressure gauge conversion was checked with a calibration tool and confirmed the scaling was correct.

$$P = 6250\frac{bar}{mA}I_{PG} - 25bar \tag{8.2}$$

For the Modbus communication with the top drive frequency converter, the following conversions were used to convert RPM and torque to actual holding register values. The torque value is a percentage of the nominal torque value of the motor which is 7.2 Nm. RPM_{TD} and T_{TD} are the actual rotational speed and torque of the top drive motor, while RPM_{HR} and T_{HR} are the value sent from the drive holding register.

$$RPM_{TD} = 0.075RPM_{HR} \tag{8.3}$$

$$T_{TD} = \frac{7.2}{10,000}T_{HR} \tag{8.4}$$

The hoisting motor values sent from the drive are converted from 16 bit words to sensible values. The torque conversion is given in **Eq. 8.5**. Note that the nominal torque limit of the hoisting motor is 4.68 Nm. T_{HM} is the actual hoisting motor torque, while T_{HR} is the 16 bit word from the holding register. Conversion of the holding register value for position to position in mm is given in **Eq. 8.6**, while conversion of RPM is given in **Eq. 8.7**.

$$T_{HM} = 100\frac{T_{HR} - 16384}{\frac{2\cdot4.68}{32768}} \tag{8.5}$$

$$Position_{HM} = \frac{Position_{HR} + 0.48152962}{17.87103511} \tag{8.6}$$

$$RPM_{HM} = 100\frac{RPM_{HR} - 16383.5}{4.81867} \tag{8.7}$$

8.2 PID Control

A PID controller is a mathematical construct used in a suite of industry processes, that through a feedback-loop ensures that parameters follow a desired set point. They require a measurement of the parameter in control, and use the *error* between set point and measurement, $e(t)$, as basis to calculate the control output $u(t)$. The output of the controller will be the input to a mechanical actuator, used to force the control parameter towards the desired set point. In Drillbotics, the PID controller is used to control the drilling process. A set point of WOB is constructed, and compared to actual measurements given by a load cell. The mechanical actuator is an electric motor that rotates a ball screw, which hoists up and down the guide frame to produce weight on the drill bit.

8.2.1 Theory

The name PID is built up of the three controller components P, I and D. These parameters are initials of what they represent, namely the proportional, integral and derivative term of the controller. These terms are simply added to each other to generate the controller. In theory, each element can be used as a controller on its own, however combinations such as PI, PD or PID are popular, depending on the nature of the system to be controlled.

The proportional element is a single constant in the controller. This can be visualized as a spring, where size of P relates to stiffness in the spring. For the sake of argument, the spring's neutral position can be defined as set point. Extending the spring creates an error between measured extension and set point. The spring force will always force the spring towards neutral position, comparable to how a controller always will force the parameter towards its set point. The spring force will further increase linearly with distance, or in control terms, the control output will increase linearly with $e(t)$. Mathematically, the proportional element of the controller can be described as follows:

$$u(t) = K_p e(t), \tag{8.8}$$

where K_p is the *proportional gain* in the controller. Notice that the governing PID-equation appears in different forms. For simplicity, standard PID nomenclature will be applied, identical to that used in LabVIEW, the rig's control software.

The integral term of the controller generates an addition to the control output based on the integrated area between measurement and set point. This is particularly useful for eliminating constant offset issues. Adjusting the integral contribution in LabVIEW is done by varying the integral time t_i, appearing in the equation for the integral term as following:

$$u(t) = \frac{K_p}{t_i} \int_0^t e(\tau)d\tau. \tag{8.9}$$

The integral time is input in LabVIEW in minutes, and will determine the magnitude of the integral control element. The smaller the value of t_i, the higher the control output sent to the hoisting motor. The last element in the PID controller is the derivative action, which acts on the time derivative of the error. The quicker $e(t)$ is changing, the larger the control output sent to the motor is. Should the controlled parameter decrease, its time derivative will be negative, changing direction of the control output. Adding a derivative term is used to counteract or *dampen* oscillations of the parameter to be controlled. Evidently, the derivative term cancels out for a parameter that doesn't oscillate, as the value of the derivative for a straight horizontal line is zero. Mathematically, the term appears like

$$u(t) = K_p t_d \frac{d}{dt} e(t), \tag{8.10}$$

where t_d is the derivative time, adjusted in LabVIEW. Notice all three control parameters are affected by the proportional gain. Thus, should this be increased, it will raise the effect of both the integral and the derivative term of the controller. Summing up the three control terms yields the final equation for the PID controller:

$$u(t) = K_p \left[e(t) + \frac{1}{t_i} \int_0^t e(\tau)d\tau + t_d \frac{d}{dt} e(t) \right]. \tag{8.11}$$

8.2.2 PID Control Variants

The team discussed three PID control variants to use for the miniature rig, namely:

- **PID Option 1**: Torque control through WOB change

- **PID Option 2**: Torque control through RPM change

- **PID Option 2**: Direct WOB control

Even though these PID controls are different, they all serve to the purpose of controlling the drilling process. This is important to avoid reaching the mechanical limits of the drill pipe. Further, they allow the use of a dynamic set of rock-specific drilling parameters such as WOB and RPM. This ensures maximum ROP through the entirety of the rock sample, even through formation change.

PID Option 1: Torque Control Through WOB Change

Torque is a detrimental parameter to have under control, as it directly leads to drill pipe twist-off should it surpass the twist-off limit. Using this controller would imply drilling with a torque set point, sending control output to the hoisting motor to add or slack off weight to indirectly alter torque in the drill pipe towards its set point. This is possible, because adding more weight to the string results in higher drill bit torque, and vice versa for less weight. Torque is estimated from a conversion of current through the top drive

motor. However, the rig is run with a rock estimating algorithm, that based on statistics and a set of equations detects rock type, as described in section 8.5. This estimator requires the controlled parameter to be an independent variable. As torque is dependent on both WOB and RPM, two parameters that also appear in the equation, this controller is not a viable option.

PID Option 2: Torque control through RPM change

It was discussed to implement a controller that adjusts the RPM of the top drive to control drill string torque. However, the top drive motor and drive assembly has a built in PID controller, which controls how fast RPM can be adjusted. For instance, sending a step input to the top drive results in it ramping up towards the set point instead, allowing for a gentle increase preventing wear on the motor. Adjusting RPM is because of this a slow process, and not something that can be done quickly enough to react on spikes in torque. Furthermore, the issue regarding rock estimator and independent variables also comes into play here, ultimately ruling out this control option.

PID Option 3: Direct WOB control

Finally, the last PID variant - and possibly the simplest - is to control WOB directly by sending control output to the hoisting motor. The response in weight change from hoisting motor adjustments is almost instant, traveling at the speed of sound through the material of the guide frame and down the aluminum drill pipe. The quick nature of this response makes this option well suited for drilling, especially in scenarios with sharp changes in formation drillability, where reaction time is critical. Furthermore, WOB is an independent variable in the rock estimator equation, not affected by changes in torque or rotation in the drill pipe. The aforementioned points leave PID option 3 well suited, and the one that is implemented to control the rig.

8.2.3 PID Tuning

Tuning a PID controller is the art of determining values for the parameters K_p, t_i and t_d, to allow the system to follow its set point in best possible manner. The specific values of these parameters strongly depend on the mechanical setup of the system, for instance which drill bit is put to use. If the system is well described by a mathematical model, this can be used to simulate a step response to decide PID-values. Such a model was not made for the Drillbotics rig, and two experimental techniques for tuning the PID controller have been used instead. These are explained below, specifically in conjunction to tuning the miniature rig.

Ziegler Nichols

This PID tuning technique requires the operator to increase proportional gain without the other control terms active, all the way until the rig gives a standing wave response to a step input in WOB. This critical gain is denoted K_{cr}. Further, the period of the standing wave response should be recorded graphically, here denoted T_{cr}. After receiving the step

Table 8.1: Relationships between PID parameters for Ziegler Nichols control tuning.

Control Type	K_p	t_i	t_d
P	$0.5K_{cr}$	-	-
PI	$0.45K_{cr}$	$T_{cr}/1.2$	-
PID	$0.6K_{cr}$	$T_{cr}/2$	$T_{cr}/8$

response, values for t_i and t_d are calculated as described by **Table 8.1**. The detailed Ziegler Nichols tuning run with the rig is fully described in section 9.2.3.

Cohen Coon

As a second alternative is the Cohen Coon tuning procedure. This method is based on a step increase in drilling ROP, done by manually setting a rotational speed of the hoisting motor. The hoisting motor steps are carefully chosen, where experience is critical to predict if the selected ROP is reached with a comfortable WOB. A sufficient step is still necessary, making sure that the actual change in WOB overcomes noise and disturbances. A WOB limit is applied in LabVIEW to avoid buckling of pipe. An idealized step response is shown in **Fig. 8.9**, indicating how τ and θ in **Table 8.2** are found. To calculate K from the same table, the ratio of WOB baseline change to WOB range is divided by this same ratio of the hoisting motor speed. Defining

$$M = \frac{WOB_{Max} - WOB_{Min}}{WOB_{Range}},\tag{8.12}$$

where WOB_{Max} and WOB_{Min} respectively denote the maximum and minimum WOB baseline during the Cohen Coon step response, and WOB_{Range} is the difference between maximum and minimum weight expected to see during drilling. Further, define

$$\omega = \frac{RPM_{Max} - RPM_{Min}}{RPM_{Range}},\tag{8.13}$$

where RPM_{Max} and RPM_{Min} respectively denote the maximum and minimum hoisting motor RPM baseline during the Cohen Coon step response, and RPM_{Range} is the difference between maximum and minimum control output possible in the hoisting motor. K from the Cohen Coon equation in **Eq. 8.2** is now found as the ratio between the two:

$$K = \frac{M}{\omega}\tag{8.14}$$

The Cohen Coon method was used to tune the PID controller. This test was also performed and compared with the Ziegler Nichols method, as discussed in section 9.2.2.
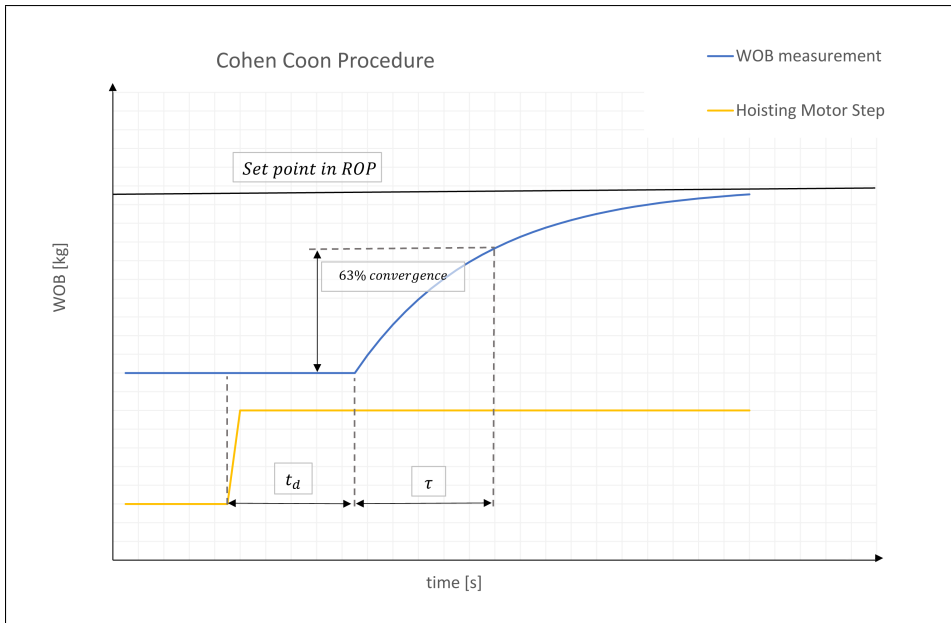
Figure 8.9: How to find the central Cohen Coon parameters from WOB response to a step increase in ROP.

Table 8.2: Equations to calculate PID parameters for Cohen Coon tuning. Only final row is used.

Control Type	K_p	t_i	t_d
P Controller	$K_p = \frac{1.03}{K}(\frac{\tau}{\theta} + 0.34)$	-	-
PI Controller	$K_p = \frac{0.9}{K}(\frac{\tau}{\theta} + 0.092)$	$t_i = 3.33\theta\frac{\tau + 0.092\theta}{\tau + 2.22\theta}$	-
PD Controller	$K_p = \frac{1.24}{K}(\frac{\tau}{\theta} + 0.129)$	-	$t_d = 0.27\theta\frac{\tau - 0.324\theta}{\tau + 0.129\theta}$
PID Controller	$K_p = \frac{1.35}{K}(\frac{\tau}{\theta} + 0.185)$	$t_i = 2.50\theta\frac{\tau + 0.185\theta}{\tau + 0.611\theta}$	$t_d = 0.37\theta\frac{\tau}{\tau + 0.185\theta}$

8.2.4 Control Issues

For the most part, drilling is a slow and steady process. Rapid changes in WOB cause drill string vibrations and other dysfunctions that are unwanted. Because of this, it is natural to prioritize stability and smoothness during drilling as opposed to control speed and short time converging to set point. This has been an underlying mantra for the NTNU Drillbotics team when tuning the PID controller. The characteristics of the rock being drilled will further affect what values are optimal for tuning the PID controller. For instance, less gain is in general found to be required to reach a set point in hard formations, whereas a soft formation requires a higher control output for WOB to converge. However, while this works well for a homogeneous layer of rock, introducing formation boundaries complicates the process. The team found that a faster controller was necessary to tackle the abrupt change in drillability found when facing a formation boundary, where slower control settings often resulted in massive overshoots in WOB going from soft to hard rock.

A solution to such a problem has been found by utilizing a *reinitialize block* in LabVIEW, which essentially clears out values that have been stored in the controller, for instance the integrator term. This reinitialization effectively gives a sharp drop in control output, pulling WOB down from the overshoot allowing the controller to converge towards set point from below. As an interesting side note, this reinitialization block was initially misinterpreted by the team. It's a boolean block, with its state set to either TRUE or FALSE. The block was wrongly left in TRUE state, meaning the PID controller was resetting at the sample rate of the control loop in LabVIEW of 100 Hz. This effectively cut off the integral and derivative action of the controller, only leaving the proportional gain. After reassigning the block to FALSE, control tuning became easier.

Reinitializing the controller is only recommended if WOB surpasses set point by a considerable threshold, for instance due to sharp changes in drillability found in formation boundaries. This is also a useful technique after periods of integral wind-up, which happen after staying for an extended period of time below set point, for instance while tripping in hole. Other countermeasures against integral wind-up are implemented in the control system. Firstly, an upper limit is set to the control output, or the rotational speed of the hoisting motor. This ensures that even after long periods below set point, the motor will not spin up faster than some value. Furthermore, LabVIEW has built in anti wind-up that ensures the integrator term stops integrating once maximum control output is reached. This assures there is no hidden integral being built up when reaching control output that could be detrimental when hitting abrupt changes in formation.

8.3 Optimization Function

During drilling, the factors that can be controlled and continuously adapted are the rotational velocities of the hoisting motor and the top drive motor. These control signals generate the torque and energy required to apply WOB and drill through the rock. The output variables of the system are ROP, MSE, torque and WOB. Optimizing the drilling
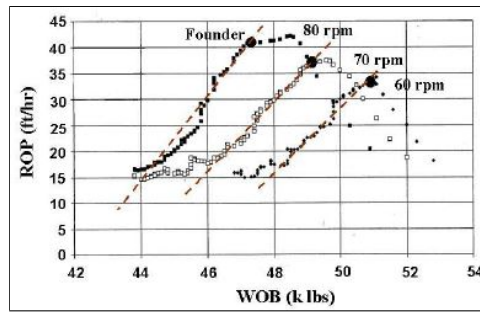
Figure 8.10: ROP response as a function of WOB and RPM from a passive drill of test. Figure from Dupriest & Koederitz (2005) [53].

process can be considered as maximizing the ROP, simultaneously as minimizing the energy wasted on drilling dysfunctions and poor hole quality. In the drilling industry, drill off tests (DOT) are performed to evaluate the drilling efficiency [50]. In a DOT, different combinations of drill string RPM and WOB are tested to determine the set which optimizes the ROP. DOTs can be performed in two ways: active or passive. In an active DOT the WOB is incrementally increased at a constant RPM. At each WOB increment the average ROP value is calculated and plotted against WOB. The process is repeated with different steps in RPM until an optimal ROP value can be determined, or the ROP results in cuttings production exceeding the cleaning capacity of the rig pump system. In a passive DOT, the bit is lowered onto the formation until the WOB reaches a given threshold. The draw works are locked in place such that all drilling progress is a result of drill string decompression. A constant RPM is chosen and drilling commences until ROP reaches zero and the entire drill string is in tension. The passive DOT is repeated for different sets of RPM.

8.3.1 Founder Point

The drill off tests described in chapter 8.3 are closely linked to the founder point. For a fixed RPM, plotting ROP as a function of WOB yields three distinct regions of drilling efficiency. An ROP response to a passive DOT is given in **Fig. 8.10**. The first region is a dead response to an increase in WOB. At too low WOB there is a limited depth of cut which results in grinding of already sheared rock fragments [51], [52]. High frictional forces are also a result of insufficient depth of cut. The insufficient depth of cut yields a marginal or no increase in ROP. The second region is the efficient zone in which ROP is a linear function of WOB, that is, increasing WOB increases the drilling progress. Sufficient depth of cut is achieved and an increase in the energy input, WOB and RPM, yields proportional increase in ROP. The final region begins when the WOB is increased past the founder point. In this region, the transfer of energy to the rock is constrained by foundering and an increase in energy input results in a decrease in ROP. Foundering is often caused by bit balling, bottom hole balling and vibrations.

8.3.2 Mechanical Specific Energy

Mechanical specific energy quantifies the energy input and rate of penetration. Its ability to predict efficient drilling was first given by Teale in 1965, and its definition is given in section 5.4.1. Teale's definition is valid in atmospheric conditions which suits the Drillbotics competition well [54]. Pessier (1992) [55] presented an MSE model when torque readings are unavailable, while Dupriest, F. & Koederitz, W. (2005), Hammoutene, C. (2012) [56] and Amadi, W. (2012) [57] introduced MSE models in which bit efficiency is included. Chen et. al (2014) proposed a model which includes calculations of actual bottom hole WOB based on the surface WOB reading for a more accurate real time surveillance of MSE [54].

MSE and foundering are closely related as both are a measure of drilling efficiency. In the flat region of **Fig. 8.10**, already chipped off rock fragments are excessively ground, thus energy input is wasted on friction and not actually doing work toward shearing new rock formation. Since MSE is defined as the specific energy of work done per unit volume of rock excavated, the MSE will be high in the first region and decrease until it reaches the efficient second zone [51], [53]. In the efficient region, the MSE response flattens out and reaches a minimum. Foundering will result in higher MSE as vibration is wasted on drilling dysfunctions. Therefore, the goal of the drilling rig is to minimize MSE at highest possible ROP.

8.4 Control Algorithm

8.4.1 Autonomous Drilling

This section aims to describe the control algorithm which is designed to optimize drilling efficiency through innovative state conditioning and testing. In essence, the control algorithm can be summarized as follows: Identify the current formation type, choose optimal drilling parameters suited for the identified formation, react to drilling dysfunctions and detect new formation interfaces. A flow chart of the different stages of the algorithm is given in **Fig. 8.11**. The autonomous drilling algorithm is programmed as a state machine compromised of the following states:

1. Initialize

2. Hoist up

3. Ramp to rotation set point

4. Identification

5. Drilling

6. Trip out

Note that the identification and drilling process are governed by a PID controller where WOB is the process variable and hoisting motor rotational speed is the control variable.

The algorithm is programmed to reinitialize the PID gains whenever it transits to a new state to avoid "perceived" integral wind-up and massive overshooting in WOB resulting in an unstable process variable or buckling of the drill string. Discussions on the PID controller and re-initialization of the PID gains are found in section 8.2 and 9.2.

Initialization State

The initialization state of the state machine is immediately set in action when the driller starts the VI. The state hoists down the drill string until the measured WOB exceeds a threshold (5 kg) which indicates the bit tagging the top of the virgin formation. The initialization state is only called once during a drilling run. When bit landing is indicated, the state machine changes state from initialization to the hoist up state.

Hoist Up State

In the hoisting up state, the hoisting motor will hoist up the drill string at slow velocity for 7 seconds, then hoist down at the same velocity for 2 seconds. This is to prevent starting rotation of the drill string with a landed bit as this results in high torque and excessive vibrations. Hoisting down is done to equalize the measured WOB to 0 kg because the measured WOB is negative when hoisting up. The state machine will transit to the hoist up state in one of three ways:

1. From initialization state: Bit has tagged top of rock sample.

2. From identification state: Torque or WOB has exceeded a maximum allowable limit. Proceed to hoist up and redo identification test.

3. From drilling state: Torque or WOB has exceeded a maximum allowable limit. Proceed to hoist up and continues drilling

The transition from the hoist up state to another depends on the previous state encountered. The state machine will transit to the ramp rotation state if the last state was initialize or the identification state. If the previous state was drilling, the state machine will transit from hoist up directly to drilling in order to save time in ramping up or down the drill string rotation to its optimal set point.

Ramp Rotation State

Ramp rotation is a state in which the drill string rotation is either increased or decreased towards 700 RPM, depending on the previous state. The ramp rotation will always transit to the identification state where the first rotation set point is 700 RPM and WOB set point equals 10 kg. The state machine will move on to the identification stage when the measured rotational speed is within 690 and 710 RPM.

Identification State

The identification state is based on the rock response estimator, which will be discussed in section 8.5. The total duration of the identification state is approximately 35 seconds in which RPM and WOB are ramped up. If the torque or WOB exceed a maximum limit, then the identification process is restarted after hoisting up and reducing rotational speed to
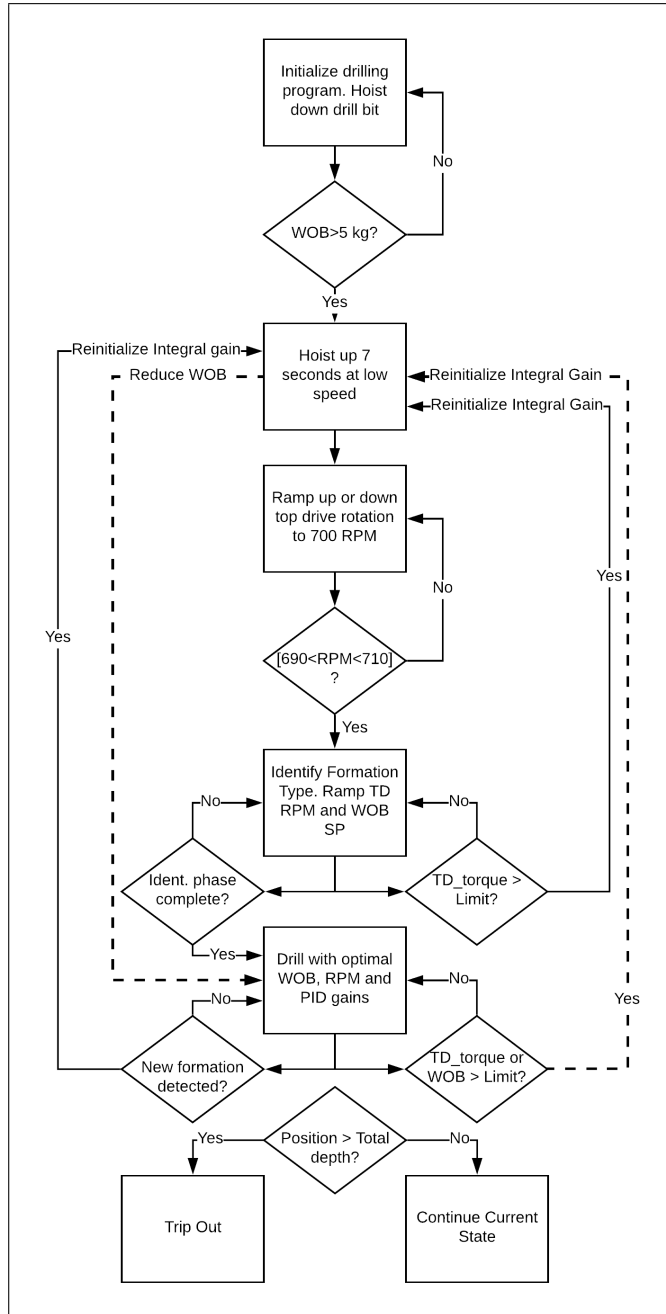
Figure 8.11: Flow chart of the different states during autonomous drilling.

700 RPM. Once identification is complete, the state machine continues to the drilling state.

Drilling State

The drilling state is entered either from the identification state or the hoist up state if the hoist up state was activated due to unwarranted drilling parameters. In the drilling state, there is a predefined library of optimal drilling parameters such as WOB and RPM set point, and proportional, integral and derivative gain. These parameters are based on testing in manual mode. The optimal parameters are then polled from the library during the drilling state based on the response from the identification phase. If the torque or the measured WOB are above their respective limits, the state machine will hoist up the bit. Since no new formation has been identified, the state machine transits directly from the hoist up state to the drilling state while using the retained WOB and RPM set points. If a new formation is detected, the bit is hoisted up and a new identification phase is initialized.

Trip Out State

The trip out phase is activated when the measured position is above a predetermined depth. Independent on the current state, if the measured position exceeds the limit, the bit is hoisted up until it reaches the original tagging depth and the operation is concluded.

8.4.2   Competition Drilling

Discussions on rock response test are given in section 9.6. In summary, tests were conducted where RPM was ramped from 700-1800 RPM and WOB incrementally stepped up during the RPM ramps, effectively mapping out ROP as a function of both RPM and WOB. For the expected operating range of WOB and RPM, the tests showed that no founder point was reached, thus there was no need to detect the formation type as maximum efficiency translates to maximum rotational speed and WOB. The operating limitations are then given by the set of RPM and WOB which drills fastest without risking buckling, twist-off or resulting in poor borehole quality. Testing showed that too high rotational speed and WOB resulted in torque spikes, twist-off and poor borehole quality, thus it was decided to drill with constant 1300 RPM and 50 kg WOB. The control algorithm is a simplified version of the autonomous algorithm described in section 8.4.1, however with the added focus on torque handling for stuck pipe situations. **Fig. 8.12** describes the control system used during the competition.

PID Controller

Last year, the team designed the control system around a cascaded PID controller where the goal was to maintain a constant torque. The torque controller output a WOB reference which was then controlled by a WOB PID controller outputting a hoisting motor rotational speed set point. In addition to the cascaded PID controller, non-linear gain was implemented. The old controller design is given in **Fig 8.13**. The control design made it difficult to tune. It was therefore decided to implement a simplified WOB controller with torque management. The new PID controller design is given in **Fig 8.14**. The cascaded controller has been replaced by a single WOB PID controller.
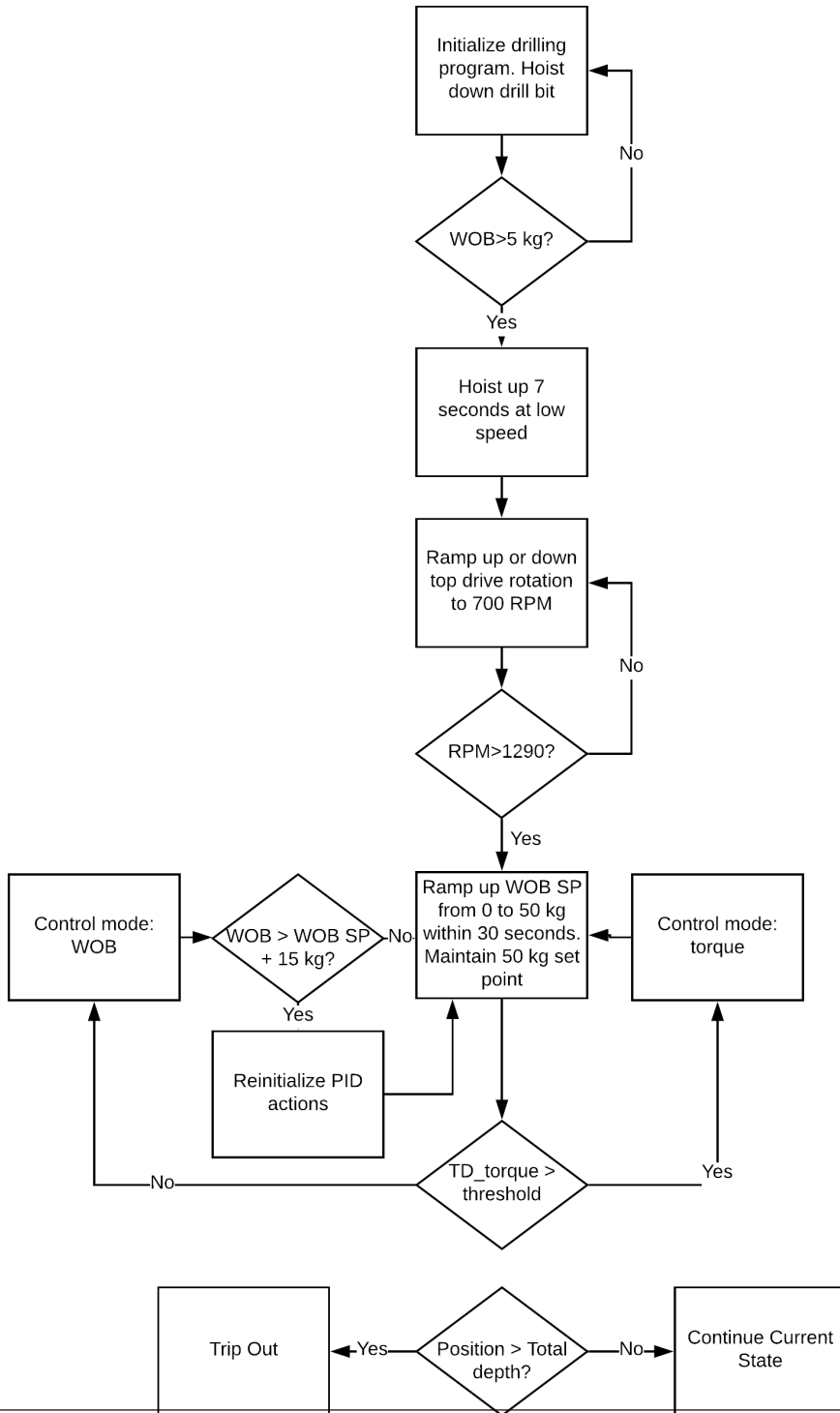
Figure 8.12: Flow chart of competition algorithm.
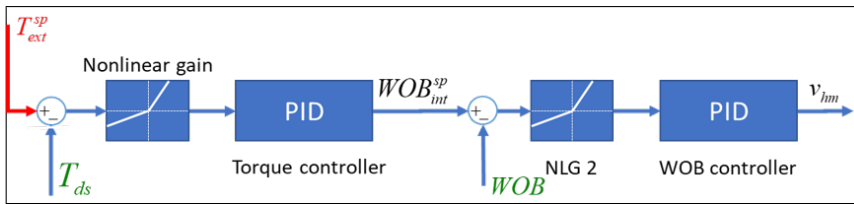
Figure 8.13: Old PID controller design using cascaded PID blocks with non-linear variable gain

The single WOB PID controller is easier to tune. In addition, a logics block is implemented for torque handling. The driller sets an operating threshold for the drill string torque. When the torque is below the threshold level, the WOB error is fed into the PID block, thus acting as a pure WOB PID controller. If the torque exceeds the threshold, the WOB set point is too high for the given formation. A scaled error between the threshold and drill string torque is fed into the PID block. Since the torque error is by definition negative in this state, the controller responds to high torque by decreasing the control variable. The control output is decreased until the measured torque is below the threshold and a true WOB PID block is used again. The PID actions are re-initialized every time there is a transition from the pure WOB control to the torque control, or whenever WOB exceeds 15 kg above set point. The simplified PID controller makes it easier to tune, enables the rig to operate at a desired WOB, rather than a constant torque in which the WOB will fluctuate uncontrollably, It also handles over-torqueing of the drill string and automatic handling of stuck pipe. Massive overshoots generally happen in two ways when drilling in homogeneous rock formations:

1. Transitioning from soft to hard rock: Maintaining a given WOB in a soft rock requires a higher output on the hoisting motor RPM, which translates to higher ROP, while a hard rock requires significantly lower hoisting motor RPM to achieve the same WOB. Drilling trough a soft rock into a hard rock will therefore result in a rapid increase of WOB.

2. Transitioning from hard rock to soft rock. Following the same line of logic as the case above, drilling through a hard rock into a soft rock results in the WOB rapidly decreasing. This results in a large offset between WOB set point and measured WOB, thus the proportional action kicks in and results in massive overshoot.

Implementing a re-initializing feature to the PID block alleviates the issues with massive overshoot caused by layer transition, thus mitigating the risk for buckling and improving the hole quality.

8.5 Recursive Least-squares Estimator

The recursive least-squares estimator in the control algorithm is an adapted version of the proposed estimator given by Arnø (2017). The purpose of the estimator is to classify drilled formation in order to choose optimal drilling parameters. Given the linear regression model in **Eq. 8.15**, where at time $t = t_i$, $y(t_i)$ is the model regressand, $\phi_1 \cdots \phi_n$
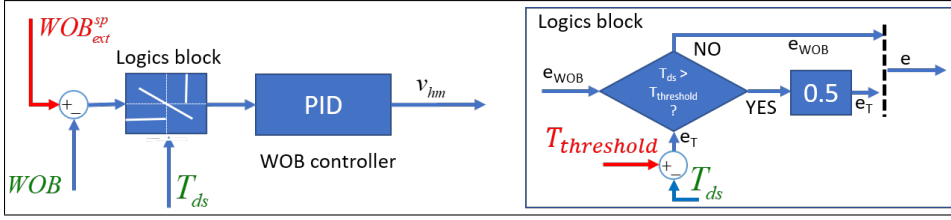
Figure 8.14: New PID controller design with torque management.

are the model regressors and $\theta_1 \cdots \theta_n$ are the regression parameters to be determined, the least squares method minimizes the cost function given by **Eq. 8.16**. Defining $Y(t)$, $\Phi(t)$ and $P(t)$ as in **Eq. 8.17**, **8.18** and **8.19**, the regression parameters are given by **Eq. 8.20** [58].

$$y(t_i) = \phi_1(t_i)\theta_1 + \phi_2(t_i)\theta_2 + \ldots + \phi_1(t_n)\theta_n = \phi^T(t_i)\theta \tag{8.15}$$

$$V(\theta, t) = \frac{1}{2}\sum_{i=1}^{t}\left(y(i) - \phi^T(i)\theta\right)^2 \tag{8.16}$$

$$Y(t) = \begin{bmatrix} y(1) & \cdots & y(t) \end{bmatrix}^T \tag{8.17}$$

$$\Phi(t) = \begin{bmatrix} \phi^T(1) \\ \vdots \\ \phi^T(t) \end{bmatrix} \tag{8.18}$$

$$P(t) = \left(\Phi^T(t)\Phi(t)\right)^{-1} \tag{8.19}$$

$$\hat{\Theta}(t) = \left(\Phi^T(t)\Phi(t)\right)^{-1}\Phi^T(t)Y(t) = P(t)\left(\sum_{i=1}^{t}\phi(i)y(i)\right) \tag{8.20}$$

For real time incremental estimation, the recursive least squares equation with exponential forgetting, λ are given by **Eq. 8.21**, **8.22** and **8.23** where $0 < \lambda \le 1$ [58].

$$\hat{\Theta}(t) = \hat{\Theta}(t-1) + K(t)\left(y(t) - \phi^T(t)\hat{\Theta}(t-1)\right) \tag{8.21}$$

$$K(t) = P(t-1)\Phi(t)\left(\lambda I + \phi^T(t)P(t-1)\phi(t)\right)^{-1} \tag{8.22}$$

$$P(t) = \left(I - K(t)\phi^T(t)\right)P(t-1)/\lambda \tag{8.23}$$

The initial conditions of the recursive least squares model are given in **Eq. 8.24** and **Eq. 8.25**, where the initial time is chosen such that $\Phi^T(t_0)\Phi(t_0)$ is invertible.

$$P(t_0) = \left(\Phi^T(t_0)\Phi(t_0)\right)^{-1} \tag{8.24}$$

$$\hat{\Theta}(t_0) = P(t_0)\Phi^T(t_0)Y(t_0) \tag{8.25}$$

ROP Regression Model

As discussed in section 8.4.1, the control algorithm relies heavily on identifying the formation type in order to apply relevant set points for the process variables. To do so, a model based on RPM and WOB measurements to calculate ROP was chosen. Bourgoyne & Young (1974) introduced a multiple regression model of ROP based on eight effects derived from:

1. Formation strength

2. Formation depth

3. Formation compaction

4. Pressure differential across the hole bottom

5. Bit diameter and bit weight

6. Rotational speed of the drill string

7. Bit wear

8. Bit hydraulics

The multiple regression model is given in **Eq. 8.26** [59].

$$ROP = e^{\left(a_1 + \sum_{i=2}^{8} a_i x_i\right)} \tag{8.26}$$

In **Eq. 8.26**, the model parameters $a_1 \cdots a_8$ represent the effects of the eight parameters listed above. The model regressors $x_2 \cdots x_8$ are defined in **Eq. 8.27** through **Eq. 8.33**, where D is the well depth (ft), g_p is the pore pressure gradient of the formation (ppg), ρ_c is the mud equivalent circulating density at the bottom of the hole (ppg), WOB is the weight on bit (1,000s lb), d is bit diameter (in), $(WOB/d)_t$ is the threshold bit weight at which the bit begins to drill (1,000 lb/in), N is the rotational speed of the bit (RPM), h is fractional tooth height worn away, ρ is mud density (ppg), q is flow rate (gal/min), μ is the mud apparent viscosity (cp), and d_n is bit nozzle diameter (in).

$$x_2 = 10,000 - D \tag{8.27}$$

$$x_3 = D^{0.69}(g_p - 9.0) \tag{8.28}$$

$$x_4 = D(g_p - \rho_c) \tag{8.29}$$

$$x_5 = \ln\left[\frac{\frac{WOB}{d} - \left(\frac{WOB}{d}\right)_t}{4 - \left(\frac{WOB}{d}\right)_t}\right] \tag{8.30}$$

$$x_6 = \ln\left(\frac{N}{100}\right) \tag{8.31}$$

$$x_7 = -h \tag{8.32}$$

$$x_8 = \frac{\rho q}{350\mu d_n} \tag{8.33}$$

The recursive least squares method is used to estimate the rock drillability based on a multiple regression model from Bourgoyne & Young (1974) with applied simplifications. The rock sample during the competition and during testing is small, between 30 and 60 cm in height. In addition, there is no pore pressure in the sample. Thus, the effects of compaction, pore pressure and frictional pressure loss can be neglected. Furthermore, Bourgoyne & Young's (1974) model was developed with the use of roller-cone bits, while the Drillbotics team utilizes a PDC bit. In addition, the flow rate will remain constant throughout the estimator phase. The model is then reduced to the one given by **Eq. 8.34**.

$$\ln ROP = a_1 + a_5 \ln\left[\frac{\frac{WOB}{d} - \left(\frac{WOB}{d}\right)_t}{4 - \left(\frac{WOB}{d}\right)_t}\right] + a_6 \ln N \tag{8.34}$$

It is evident that the model assumes a ROP which is proportional to $(WOB/d)^{a_5}$ and N^{a_6}. Due to inherent low penetration rate with the miniature drilling, the simplified model given by **Eq. 8.34** might give erroneous estimates as ROP goes towards zero. Arnø (2017) further simplified the model by assuming a linear dependency between ROP and WOB, and between ROP and RPM, yielding the model described in **Eq. 8.35** [58].

$$ROP = \theta_1 + \theta_2 N + \theta_3 WOB \tag{8.35}$$

The identification run is based on running the recursive least-squares algorithm on the ROP model with a specific change in drill string rotation and WOB. It is assumed that the ROP is linearly dependent on the drill string rotation and applied WOB in the given RPM and WOB interval. The total duration of the identification process is 35 seconds and consist of ramping up the WOB set point from 10 kg to 30 kg at a constant 700 RPM within 15 seconds, then ramping up the rotational speed from 700 RPM to 1200 RPM at a constant 30 kg WOB set point. The process is shown in **Fig. 8.15**.

Estimating more parameters than available regressors tend to create issues in determining the unpaired parameter, in this case θ_1 which gives an indication on rock hardness. The ROP model proposed by Arnø (2017) has therefore been altered to better estimate θ_1. Normalizing the effects of RPM and WOB around their starting values gives a quicker estimate of θ_1. Since the identification process begins at 700 RPM and 10 kg set point, the adjusted model used in the fully autonomous algorithm is given in **Eq. 8.36**.

$$ROP = \theta_1 + \theta_2(N - 700) + \theta_3(WOB - 10) \tag{8.36}$$

The first five seconds of the identification process is run with a constant 700 RPM and 10 kg WOB set point. The estimated θ_1 parameter is then the average ROP for that rock type,
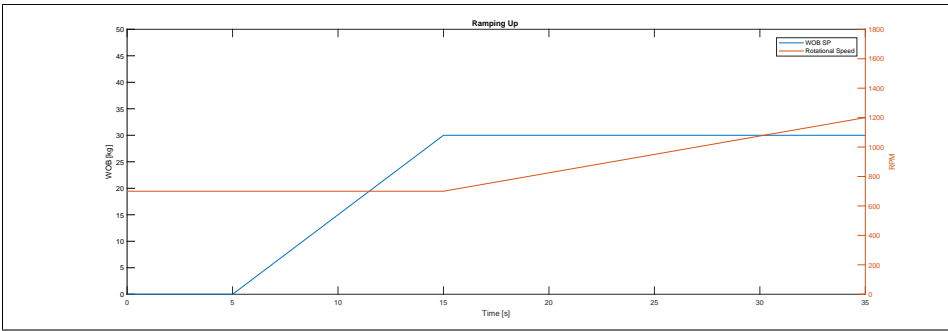
Figure 8.15: Ramp up sequence of WOB and RPM during the identification state.

or drillability, at 700 RPM and 10 kg set point. The test results in section 9.5 show that the parameters converge within 35 seconds. During the testing phase, a library of θ_1, θ_2 and θ_3 values are determined for a set of different rock types, e.g. shale, concrete and sandstone. Based on the estimator parameters obtained during the identification state of the state machine, the theta values are compared to those defined during the testing phase. The following pseudo code is used when the identification phase is complete:

1. Ramp sequence complete $\rightarrow$ Store latest θ_1, θ_2 and θ_3

2. Calculate Euclidean distance from latest $\theta_1, \theta_2, \theta_3$ and θ values in predefined library

3. Identify the current formation as the one in the library with the shortest Euclidean distance

4. Choose optimal WOB set point and RPM set point defined from previous tests in the identified rock type

5. Choose appropriate PID parameters defined from previous tuning tests in the identified rock type

The Euclidean distance is defined as the straight line distance between two points, in this case in $\mathbb{R}$, where the two points are $(\theta_1, \theta_2, \theta_3)$ and $(\theta_{1,x}, \theta_{2,x}, \theta_{3,x})$, where θ_1, θ_2 and θ_3 are the latest estimator parameters from the recursive least squares algorithm, and $\theta_{1,x}, \theta_{2,x}$ and $, \theta_{3,x}$ are the predetermined estimator parameters fitted for rock type x. The Euclidean distance, d_x is therefore given by **Eq. 8.37**.

$$d_x = \sqrt{(\theta_1 - \theta_{1,x})^2 + (\theta_2 - \theta_{2,x})^2 + (\theta_3 - \theta_{3,x})^2} \tag{8.37}$$

8.6 Formation Change Detection

In an autonomous drilling process, being able to detect changes in formation is essential for optimal drilling. There are two main reasons for why detecting formation changes were deemed important for the Drillbotics competition:

1. It was expected that different rock types would be present in the rock sample given for the competition. The drillability of different rock types varies significantly, ranging from very high ROP in cement to low progress in shale and tile. Due to bit-rock interaction, optimal drilling parameters such as WOB set point and drill string rotation speed differ from rock to rock. To ensure optimal drilling parameters, it is therefore important to detect new formations.

2. Tuning of the WOB PID controller showed that the optimal PID parameters differ from one rock type to another, such as cement and shale (see section 9.2). Inability to detect changes in the formation would in worst case result in detrimental unstable oscillations in WOB as the rig drills with non-optimal PID parameters in the new layer.

Quickly determining when a new layer is encountered is therefore important for safety and the drilling progress. Several methods for detecting a new layer have been considered, all of which relied on the measured ROP.

8.6.1 Comparing Measured ROP and Regrassand

Prior to drilling with a set point in WOB and set point in drill string rotation, an identification phase has been performed in which the model determines three parameters; θ_1, θ_2 and θ_3, as discussed in section 8.5. As drilling commences, measured ROP can be compared to the model regrassand given by **Eq. 8.36**. A new layer is indicated when the error between the ROP regrassand and measured ROP is above a given threshold. It was decided not to use this method because ROP varies naturally due to the inherent resolution of the position measurement (see section 8.7.4). In addition, the model regressors are valid in the linearized area of the estimator ramps: 700-1200 RPM and 10-30 kg WOB set point. This is not necessarily the case, as can be seen in section 9.6. Given that the optimal set points for WOB and RPM are outside the estimator range, the ROP regrassand and measurement might be different even in a homogeneous rock.

8.6.2 Comparing Standard Deviation

Another approach to formation change detection is taking advantage of the bit-rock interaction at a constant WOB and rotational speed. In a homogeneous rock, ROP should stay fairly constant when using constant drilling parameters. At a given set point there will be natural variations in the measured ROP. **Fig. 8.16a** displays a test run when drilling with a constant WOB set point of 30 kg and drill string rotation of 1000 RPM. The bit tagged the first formation, cement, at 17 seconds. It is evident that a new formation was hit at 62 seconds, indicated by the drop in ROP. The drop in ROP at 66 seconds is the operator terminating the drilling operation. The proposed solution in detecting the new layer is based on the variance in ROP data within a given interval, specifically the standard deviation defined by **Eq. 8.38**.
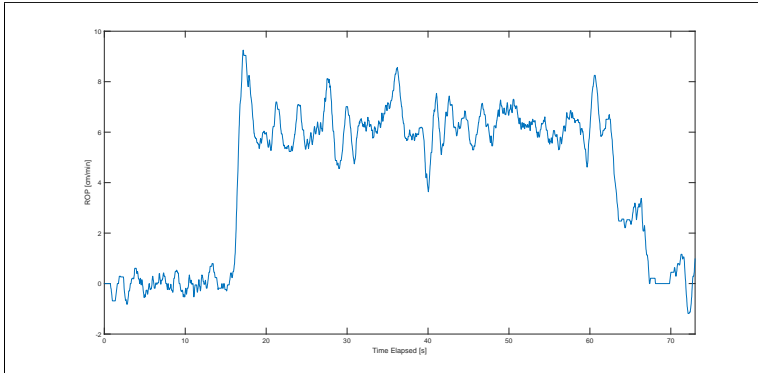
(a) ROP data when drilling through cement and hitting shale at 62 seconds. Drilling was terminated at 67 seconds.
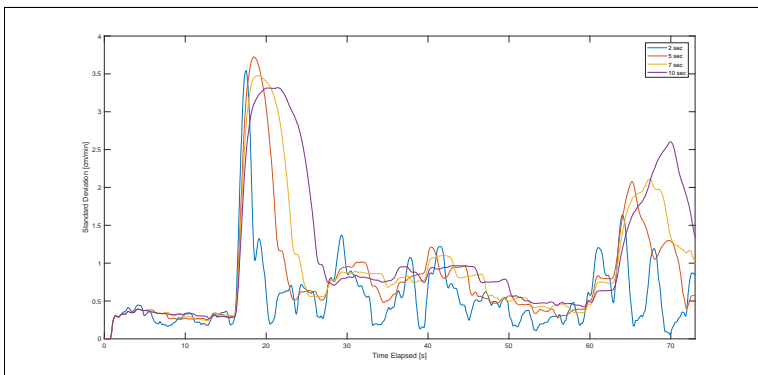
(b) Standard deviation plotted for different running time intervals for the from the ROP data in **Fig. 8.16a**.

$$\sigma = \sqrt{\frac{\Sigma_{i=1}^{N} \left(ROP_i - \overline{ROP} \right)^2}{N-1}} \tag{8.38}$$

In **Eq. 8.38**, σ is the standard deviation of the ROP, N is the number of samples in a given time interval and $\overline{ROP}$ is the sample mean. Given a tuned PID controller and a fixed set point in WOB and RPM, the standard deviation is expected to be small and fairly constant. **Fig. 8.16b** depicts the standard deviation as a function of time and sample size. At time t, the standard deviation of the past x seconds is calculated. Increasing the sample size results in smoother data and higher standard deviation when a new layer is encountered. The state machine detects new layers when the following criteria is met: The measured standard deviation has been above a certain threshold the past T seconds. Trial and error would determine the optimal sample duration and threshold values. **Fig. 8.16b** shows that a new layer is easier to detect when sampling over a longer time period. However, it is evident that requiring a high threshold and duration of drilling above the threshold yields an increase in the time it takes for the new layer to be detected. **Fig. 8.17** depicts a schematic of the identification process when comparing the standard deviation.
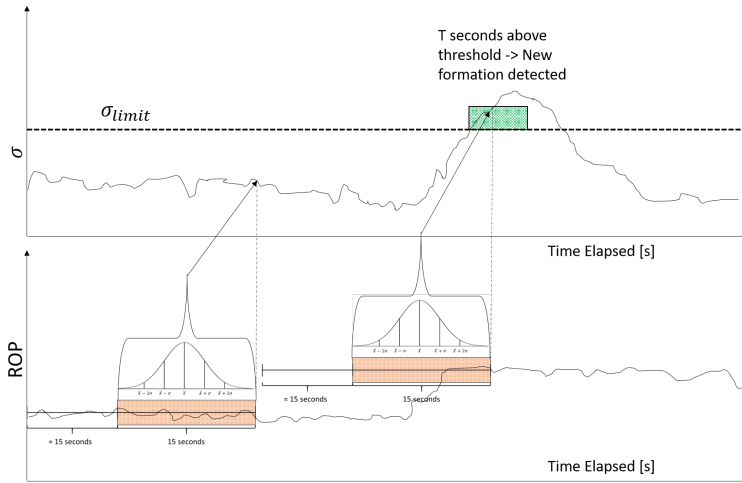
Figure 8.17: Schematic of detecting a formation change based on a standard deviation above a threshold lasting more than T seconds.

8.6.3 Comparing a Sample Mean to a Sample Distribution

A frequency distribution of the measured ROP data from **Fig. 8.16a** is given in **Fig. 8.18**. The distribution is based on the ROP data measured from 20 to 60 seconds, i.e. within the shale. The WOB set point and drill string RPM were held constant in this run. **Fig. 8.18** shows that the distribution follows a Gaussian distribution. In this case, the mean ROP

value is 6.2 cm/min with a standard deviation of 0.73 cm/min.

In a Gaussian distribution, 68% of the data points are withing one standard deviation of the mean, 95% within two standard deviations and 99% within three. In **Fig. 8.16a**, the ROP mean in the interval 63 to 65 seconds is close to 3 cm/min, approximately four standard deviations from the longer sample mean. A schematic of the identification process is given in **Fig. 8.19**. An array of 3,000 elements is implemented in the method and acts as a buffer. At each iteration, the most recent ROP value is appended to the buffer and the oldest value is deleted from the array. This maintains the buffer size and reduces memory allocation, mitigating issues when running over a long time. The following process describes the identification given in **Fig. 8.19**:

1. Append and delete element in the buffer

2. Calculate mean ROP, ROP_1, for past T_2 seconds

3. Calculate mean ROP, ROP_2, and standard deviation, σ, for interval T_1 seconds ago to T_2 seconds ago

4. Is the following true: $ROP_1 > ROP_2 + N\sigma$ or $ROP_1 < ROP_2 - N\sigma$?

   - Yes: New formation detected, go to identification state
   - No: Still in same formation, repeat process

The number of seconds to generate the distribution and number of seconds of new measurements to compare with the distribution determines the sensitivity of the detector. When formation estimation was still planned for the competition drilling run, it was concluded that detecting a new layer that has almost the same drillability is disadvantageous. The state machine would reinitialize the rock estimator phase, increasing the total drilling time. It is more important that the detector never falsely detects new layers. It is possible to implement hypotheses testing in LabVIEW, however, due to lack of time, the team did not implement change detection based on hypotheses testing.

8.6.4 Possible Caveats

Purely basing change detection on the probability distribution or the standard deviation might prove dysfunctional if the rig operates in certain conditions. Misidentification of a new layer is a possibility if, for some reason, ROP has remained fairly constant within a time interval. This will yield a very small deviation in which slight changes in ROP might falsely indicate a new formation. On the other hand, if the rig encounters a formation in which maintaining a constant WOB proves difficult, ROP will fluctuate accordingly and the standard deviation will remain high. If the deviation threshold is set too low, the machine risks misidentifying the same formation as a new rock. A possible solution would be to have several criterion that must be met in order to conclude that a new layer has been met. An additional criteria is e.g. to compare the numerical value of the mean of the new time interval with the numerical value of the mean of the old time interval. This way, if
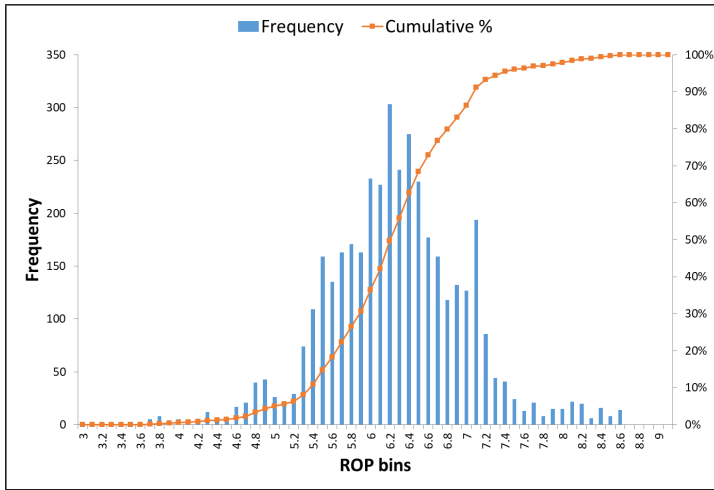
Figure 8.18: Frequency distribution of the measured ROP from **Fig. 8.16a**, from 20 to 60 seconds.
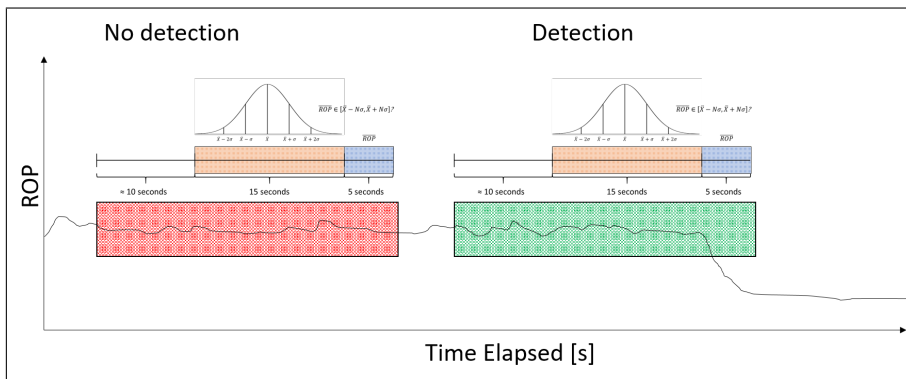
Figure 8.19: Schematic of detecting formation change.

ROP data has been fairly constant for a while and changes by a relatively small value, which is still statistically significant when comparing it to the probability distribution, the change is not considered a new formation, since the change in mean value is small.

8.7 Control System Software

This section aims to introduce the reader to the software in which the control system is programmed. A short introduction of LabVIEW is given before a description of the autonomous script and the competition script is given. The section also gives a brief description of why the NTNU team decided to replace SimuLink with LabVIEW.

8.7.1 Introduction to LabVIEW

LabVIEW is short for Laboratory Visual Instrument Engineering Workbench and is a graphical programming language developed by National Instruments. It is commonly used for research and in the industry for data acquisition and for designing control systems in the automation industry. The interface and data flow makes it intuitive to program and debug complex algorithms and makes it an ideal software for testing, measuring, visualizing and logging data, and controlling machinery.

Building applications in LabVIEW consists of editing two panels, the front panel and the block diagram. The graphical programming itself is done in the block diagram where controls and indicators are connected to nodes via wires. The user interface is updated simultaneously as the block diagram is edited and is built with controls and indicators. Controls and indicators can be compared to input and output, respectively, and can be represented (visualized) in the front panel in many different ways. For instance, a numeric control can be visualized as a single digital input, a thermometer or sliding bars. Dragging a control from the controls palette to the front panel automatically creates a corresponding node in the block diagram. An example of the controls palette is shown in **Fig. 8.20**. When working in the block diagram, built in functions can be dragged from the functions palette. The functions are not shown graphically in the front pane, but are performing actions based on the controller input and outputs to an indicator or another function as input. **Fig. 8.21** shows a sample of the available functions in the functions palette. The given example shows string manipulation functions such as conversion of a numeric to a decimal string.

LabVIEW subroutines are called VI's (virtual instrument) and will always consist of a front panel, block diagram and a connector pane. The connector pane allows the VI to function as a sub-function within another VI. The VI is then referenced as a subVI where the input nodes and output nodes in the subVI are determined based on the chosen connectors in the connector pane. The use of custom subVI's enables for modular design of the main VI when repetitive blocks need to be used and saves space on the main block diagram as large graphical representation of code can be represented as an icon. **Fig. 8.22** shows a basic example of a LabVIEW VI. The VI allows the user to edit a value for velocity in km/h in the front panel. This is done by changing the value of the numeric control, in
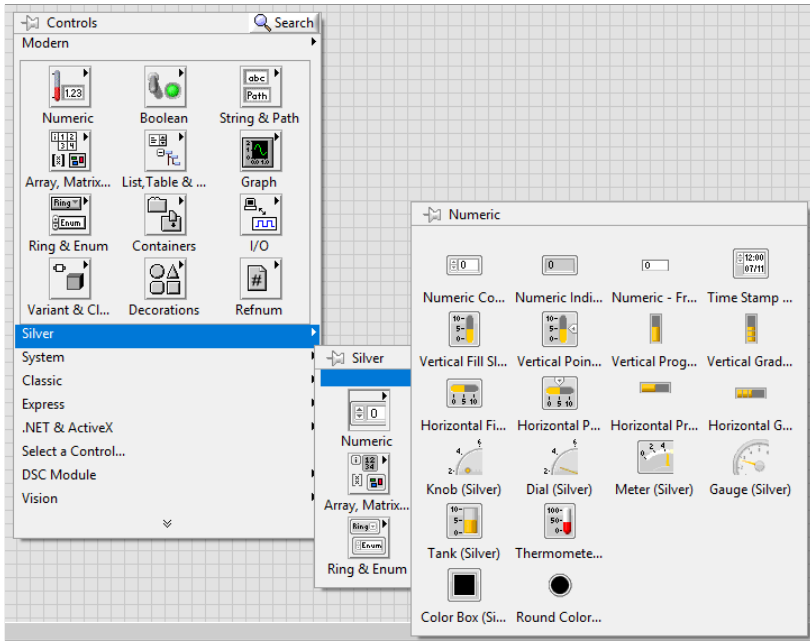
Figure 8.20: Silver numeric controls and its forms of representation.
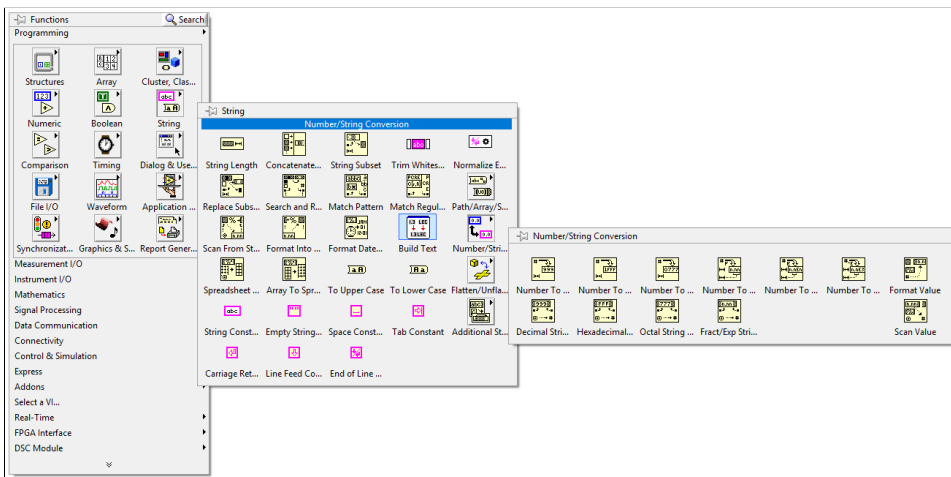
Figure 8.21: Block diagram functions palette showing an example of string manipulation.
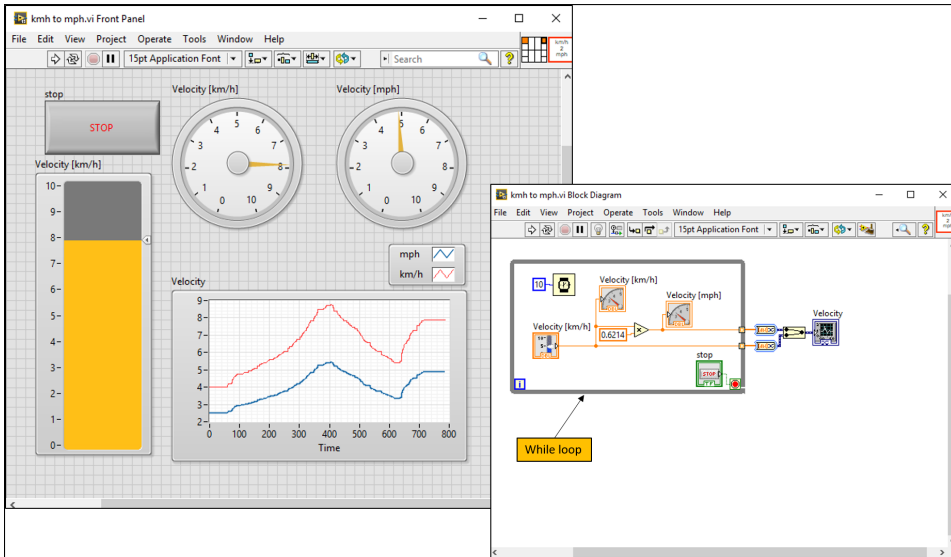
Figure 8.22: Example VI depicting the LabVIEW coding environment with a front panel, block diagram and connector pane.

this case represented by a vertical pointer slide. The VI converts the velocity to mph and displays the value as a numeric gauge indicator. A while-loop has been placed around the code such that the user can change the value in real time rather than executing the code once to obtain one conversion rate. A wait function has been placed inside the while-loop with a constant of 10 wired to the icon. The loop will execute every tenth millisecond and update the indicators on the front panel with the latest conversion until the user presses the stop button and aborts the while-loop. The time series of the velocity in km/h and mph are then plotted on a graph.

Fig. 8.23 shows the same code with the same controls and indicators, however the conversion from km/h to mph has been implemented in a subVI called "kmh to mph subVI.vi". The front panel and block diagram to the subVI is shown in **Fig. 8.24**. The block diagram of the subVI is simply the numeric conversion from km/h to mph. The connector pane shows what terminals are connected to the subVI icon, in this case one numeric control and one numeric indicator. Notice that the subVI is placed in the "kmh to mph with subVI.vi" by placing the subVI icon in the block diagram. The control is wired to the icon and the output is wired to the gauge indicator.

Data Flow

Data flow in LabVIEW is determined by what data is available. If a subVI or function requires a set of inputs, the subVI or function will not execute before all necessary data is available. The blocks in the block diagram execute from left to right following the data
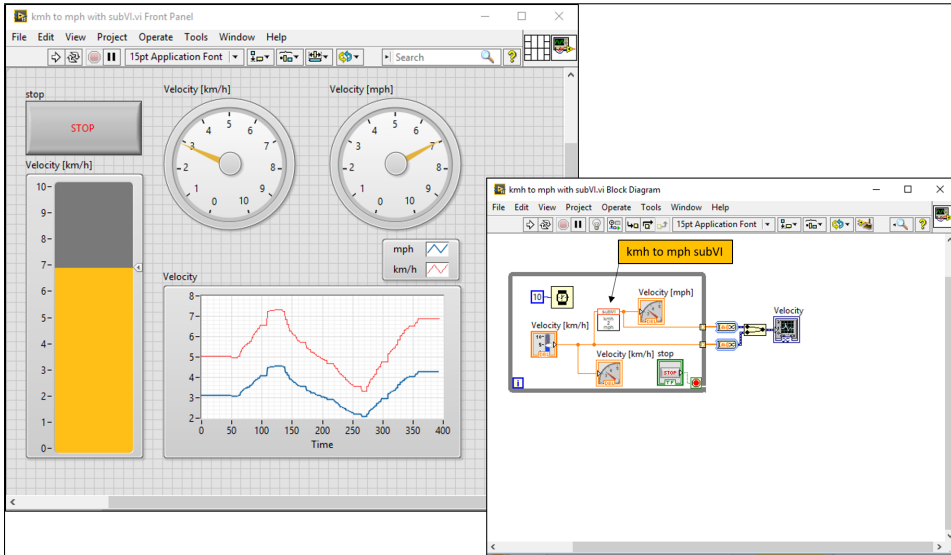
Figure 8.23: Example VI depicting the use of subVI's.
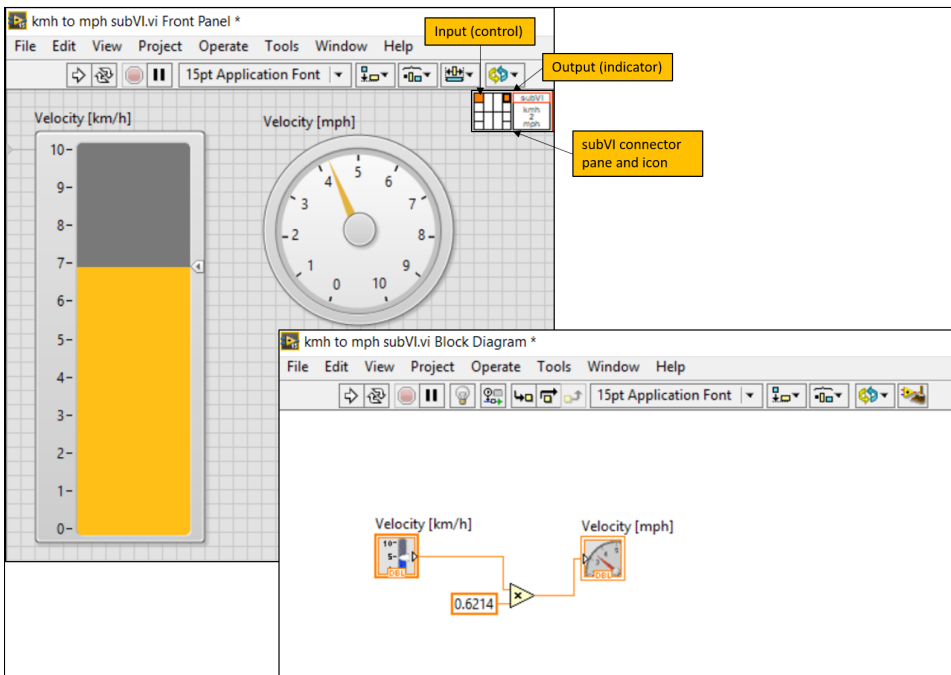
Figure 8.24: Front panel and block diagram of simple subVI.

wires. The wires will propagate all variables throughout the block diagram. In the simple example of **Fig. 8.22**, the leftmost node is the velocity control. The value from the control is propagated by a numeric wire to the multiplication block which performs the operation. The multiplication block will not execute before it receives a value from the controller. When all operations in the while-loop have executed, a new iteration begins and the velocity control sends a new value to the multiplication block. The plot on the rightmost side of the block diagram will not execute before the while-loop has stopped. A real time visualization can be achieved by placing a waveform chart block inside the while-loop. Independent parts of the block diagram will execute "simultaneously", and determining which part is executed first is sometimes impossible. Forcing the execution order is done by wiring the code in series. Since code blocks are executed as soon as all input is available, LabVIEW programming is inherently parallel. An obvious example is placing two while loops besides one-another. The code inside the loops are executed independently of the other and in parallel. This is a major advantage to text based programming, where code is compiled and executed line by line.

8.7.2 Benefits with LabVIEW

This is the second year NTNU has entered the Drillbotics competition. NTNU finished second in the competition last year with a control system developed in SimuLink. However, it was decided early on that the control system should be implemented in LabVIEW instead. The decision was based on the experience the team gathered during the design phase in 2017 when operating the first version of the rig [1]. The main reasons why the team decided to replace SimuLink with LabVIEW are discussed below.

Sampling Frequency

Last year, the motor drives communicated with the computer through an OPC block in the SimuLink model. This block limited the motor write and read sampling frequency to a maximum of 10 Hz, sufficient enough for a WOB PID controlled drilling process. However, the main issue during drilling with a 0.035" thick aluminum drill pipe was torque spikes resulting from drilling through heterogeneous rock formations. High torque would lead to twist-off of the drill string above the BHA. One of the proposed solutions to mitigate the risk of drill string failure was detection of torque spikes, followed by a quick response to cause a torque drop. The proposed solution was dependent on high sampling frequency and better response time, in addition to a system capable of monitoring and reacting to torque spikes.

New Sensors

The new load cell and pressure gauge data are easily acquired in LabVIEW.

Control System Robustness

When using SimuLink, the program would often generate errors or not establish communication with motors. The program would also struggle to keep up with user input, such

as toggling the off-switch. The slow response of the user interface controls was an HSE problem as it could take a second or two for the motors to stop after pressing the stop button. This increased the risk of buckling the drill string and damaging rig components. Since both the top drive motor and hoisting motor stopped immediately if the physical emergency stop button was pressed, a team member was required to stand proximate to it at all times during drilling. This was the means to stop drilling opposed to handling it in the control system. Slow response was especially a problem during longer periods of testing.

Limited Experience in Both SimuLink and LabVIEW

None of the team members had any prior experience with neither SimuLink nor LabVIEW. Hence there were no pre-existing preferences to either of the programming environments. The existing communication lines with the motors used in SimuLink could remain the same, however, the team would most likely begin from scratch in both softwares. Experienced users of both SimuLink and LabVIEW assisted with thorough advice. One advice was that SimuLink is excellent for simulation, however, real time applications and integration with hardware is better in LabVIEW and allows for more customized user interfaces and subroutines. Their advice and recommendations were a key factor as to why this year's team decided to replace the control system with LabVIEW.

Programming Environment

LabVIEW offers an intuitive programming environment where the data flow is determined in the flow chart-like block diagram. Data type representations are also explicitly visualized by data wires in different colors and thickness, e.g. a numeric floating point scalar is represented by a thin orange wire, a vector in a thicker wire, an integer as blue and boolean as green. The ability to create custom subroutines (subVI's) with custom icons enables for use of modularized code. This makes it easier for editing and upscaling of existing VI's.

8.7.3   LabVIEW Script: Autonomous Drilling

In this section, a brief description of the main features of the LabVIEW code are given. As discussed in section 8.7.1, the use of subVI's modularizes the code and keeps it clean and intuitive. Most of the programming is included in these subVI's. The reader can refer to appendix D.2 for a detailed overview of all subVI's in the state machine. The block diagram of the main LabVIEW VI consists of six main modules, as highlighted in red in **Fig. 8.25**. A summary of the modules is given below.

VI Initialization

The first module initializes the VI. Here, the first state of the state machine is given as the initialization state as discussed in section 8.4.1. In VI initialization, the current time is used to calculate loop time of the main while-loop, the notifier used for plotting the data in the GUI is initialized and the NI USB-6009 connection is established in order to acquire and read raw data from the pressure sensor and load cell. Furthermore, the communication
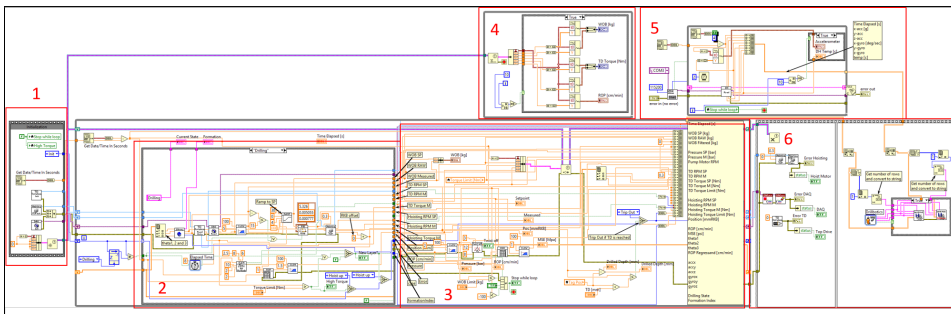
Figure 8.25: Block diagram of the LabVIEW main VI of the autonomous drilling program. The five highlighted parts are: 1 - VI initialization, 2 - State machine, 3 - Preparing data for plotting and saving, 4 - Real time plotting in GUI, 5 - Down hole data acquisition, 6 - Shut down sequence and saving to file.

with the hoisting motor and top drive motor is established.

State Machine

The second module of the main VI includes the state machine with all the logics described in section 8.4.1. The state machine is programmed as a case structure within a while-loop. At each iteration in the while-loop, a single state is executed and data is passed through the case structure for plotting and for saving to file. Each state has a specific execution code and one or several transitioning codes, in which a state transition occurs if a criteria is met. In LabVIEW, the state machine is implemented by including a case structure in which all the case items correspond to one specific case. All the states are declared in an *enumerated type* (enum), which is a list of string labels. Passing the enum into the case selector of the case structure determines the state in each iteration. In each iteration of the while-loop, the enum is passed through a shift register. That is, the enum which is passed out of the case structure is also passed into the case structure during the next iteration of the code. A true/false selector is implemented as a transition code, in which the current state enum is passed through the shift register if the statement is false, and a different enum item is passed if the statement is true. The position is acquired from the hosting motor drive and reports the relative position to its previous *homing* position. The homing is performed such that 0 mm equals the top drive at the top of the derrick. An offset, which will depend on the length of the bit, pipe, BHA and rock, is added in each state to convert the reference point from homing position to RKB. Relevant measurements are passed through tunnels for further actions.

Initialization State
The block diagram of the initialization state is given in **Fig. 8.26**. On the GUI, there are two string indicators that show the current state and formation type. These are updated in all of the states, in this case with the string constants *"Init"* and *"Unknown"*. The hoisting motor receives a constant rotational speed corresponding to a downward translation of
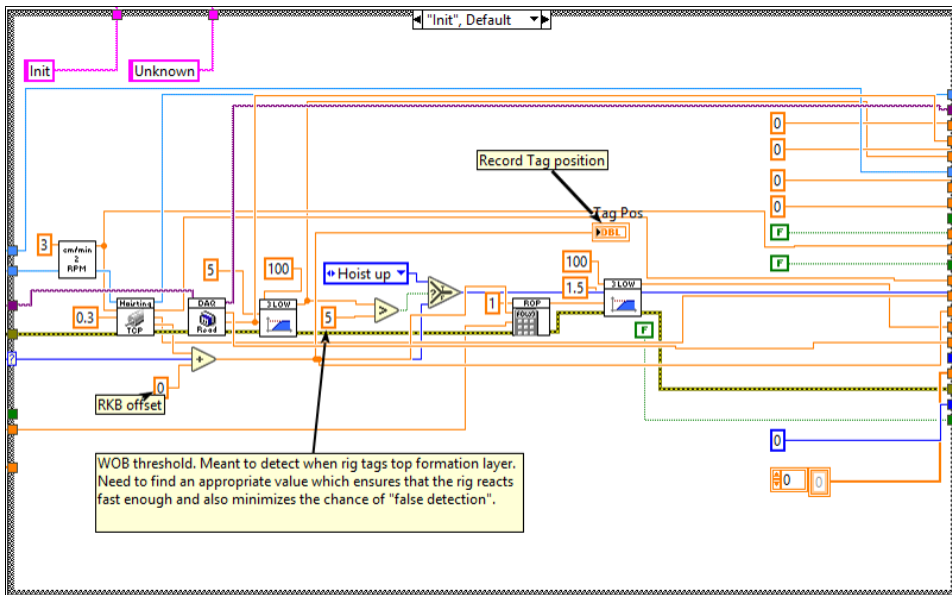
Figure 8.26: Block diagram of the first state in the state machine, the initialization state which hoists down the bit until the formation is tagged.

the drill bit of 5 cm/min until the measured WOB, after passing through a low pass filter, reaches 5 kg. If the criteria is met, the state machine transitions to *"Hoist Up"*. The current position and *"apparent ROP"* are also measured and passed through the case structure tunnels on the right side.

Hoist Up State

Fig. 8.27 depicts the block diagram of the hoist up state. The hoisting motor receives a rotational speed set point corresponding to -1 cm/min (upwards) when the time elapsed is less than 4 seconds (since the state machine first transitioned to the hoist up state). Then the motor hoists down for 2 seconds to equalize the measured WOB. After 6 seconds has passed, the state machine transits to either the *"start rotation"* state or *"drilling"* state if a torque breach was the reason for hoisting up. Note that the internal timer *"Elapsed time: "Hoist Up" "* is reset only when a transition from another state to the hoisting up state occurs. This ensures that the state machine will stay in the hoist up state for 6 seconds, every time the state is called.

Ramp to Rotation Set Point

"Start rotation" is another fairly straight forward state in which rotation is ramped towards 700 RPM to prepare for the identification process. Since there are several state changes leading up to the start rotation case, the duration of this state will vary. The hoisting motor subVI is included with a speed set point of 0 cm/min, ensuring no contact with the formation when rotation is started. The state machine moves on to identification of the rock sample once the rotational speed is within 10 RPM of 700 RPM. The block diagram of
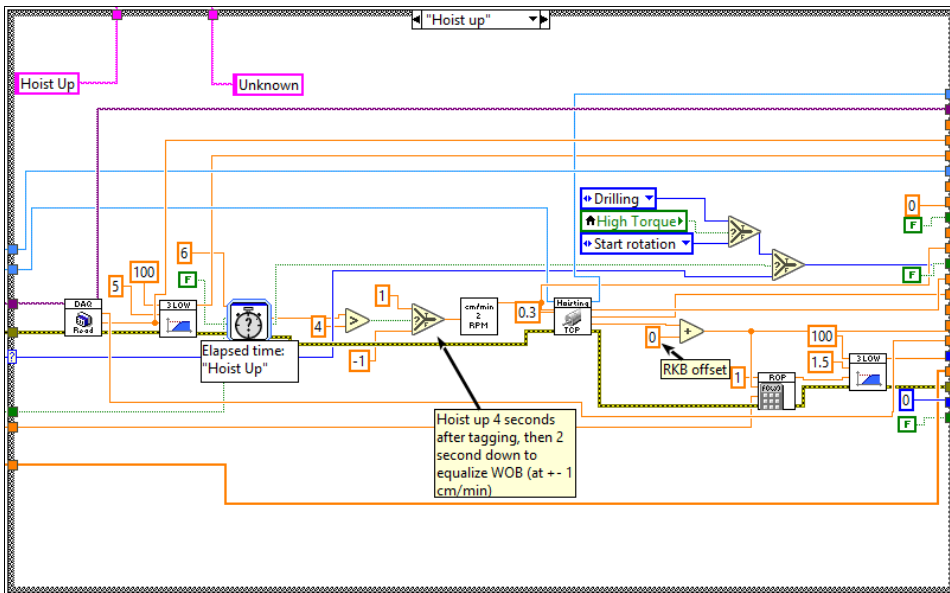
Figure 8.27: Block diagram of the second state in the state machine, the hoist up state which hoists up the bit before drilling is commenced.

this state is given in **Fig. 8.28**.

Identification State

The block diagram of the identification state is given in **Fig. 8.26**. The rotational speed and WOB set points are determined by the ramp functions passed through the *"TD Rotation Read Write"* subVI and the *"WOB PID"* subVI. The recursive least squares estimator is included in the *"EST"* subVI, in which the inputs are measured WOB, rotational speed and ROP. Note that the PID gains are constant for the WOB PID controller in the identification state. The proportional, integral and derivative gains are set equal to that of tuned parameters in shale. The integral action reset feature is also added to the identification state. If the time elapsed in the identification state exceeds 35 seconds, the *"Drilling"* enum is passed through the enum shift register. If the torque limit is reached the state machine will transit to *"Hoist up"*.

Drilling

The block of the drilling state is given in **Fig. 8.30**. θ_1, θ_2 and θ_3 from the identification state are passed to the drilling state where the library of optimal WOB, RPM and PID gains are chosen based on the shortest Euclidean distance. The WOB set point is gradually increased to the library set point to avoid sudden changes in WOB. To avoid integral wind up effects when drilling into a new formation, the PID gains are reset if the measured WOB exceeds the WOB set point plus 15 kg. The drilling state is continued until the detection subVI indicates a new layer or the torque exceeds the chosen maximum limit. In the block diagram given in **Fig. 8.30**, the PID gains are set constant. They can also be polled from
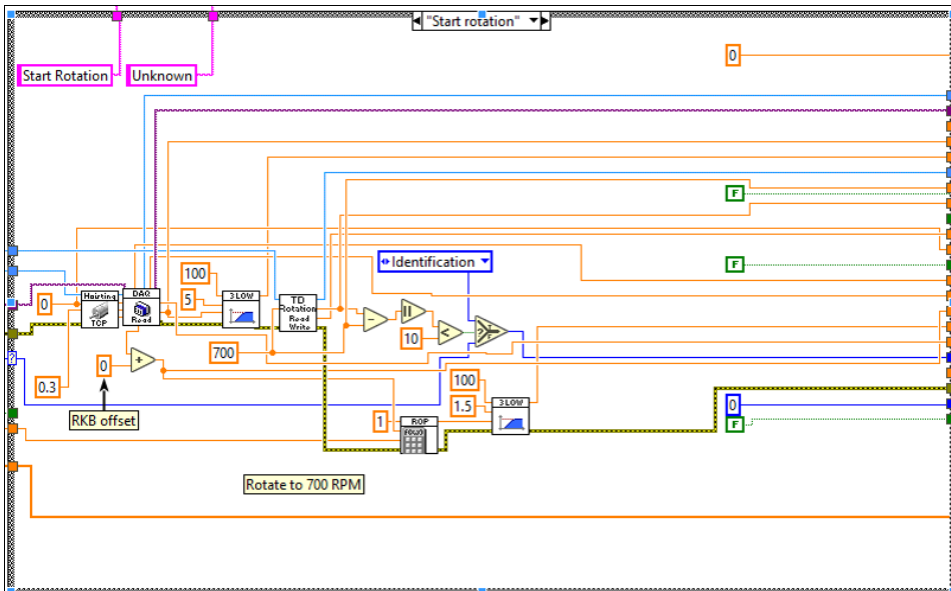
Figure 8.28: Block diagram of the third state in the state machine, the *"Ramp to Rotation SP"* state.
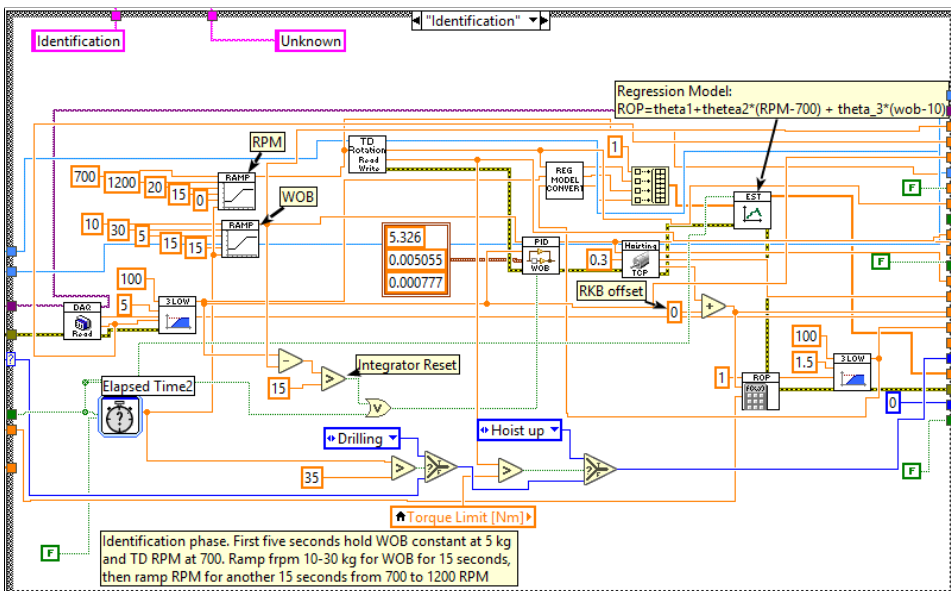
Figure 8.29: Block diagram of the fourth state in the state machine, the *"Identification State"* state.
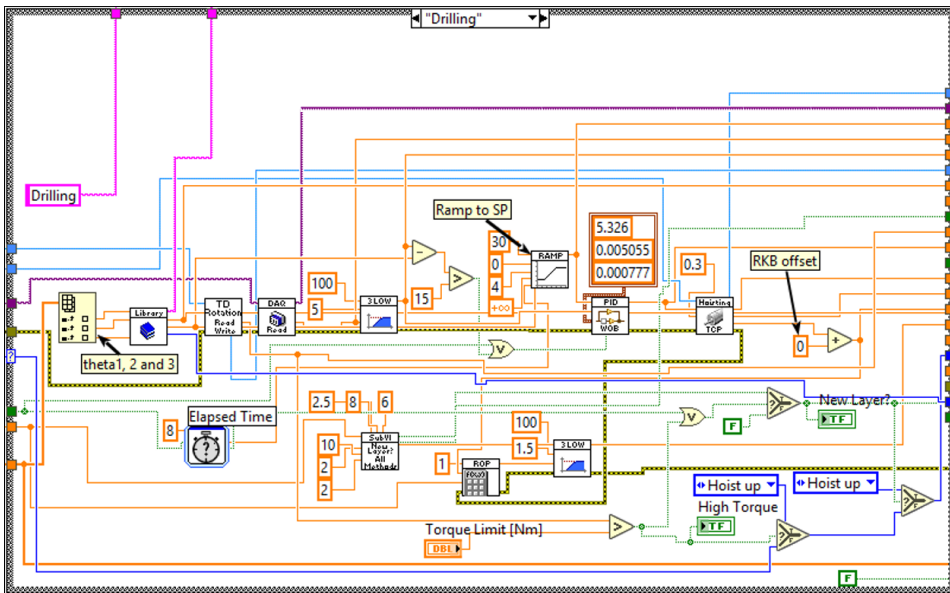
Figure 8.30: Block diagram of the fifth state in the state machine, the *"Drilling State"* state.

the library based on the identified rock type.

Trip Out

In the trip out state, rotational speed is set to 50 RPM while the bit trips out of the bore hole with a constant speed of 10 cm/min. The rotation is set to mitigate the risk of getting stuck when tripping out. The maximum overpull is not defined explicitly in the trip out state, however the script is terminated at a overpull of -100 kg.

Prepare Data for Plotting and Saving to File

Data points that are logged at each time increment in the main while-loop are shown in **Table 8.3**. The data points are appended to a 2D array in each iteration and only released for storage once the while-loop is executed. In this module, relevant data points for the GUI are passed through a notifier into a designated plotting loop.

Acquiring Down Hole Data

Down hole data is acquired in a separate while loop which is executed at 500 Hz. The acceleration in axial direction is plotted in the GUI, together with a numeric indicator of the down hole temperature. The code is identical to that of the competition script as discussed in section 8.7.5. The block diagram is given in **Fig. 8.43**.
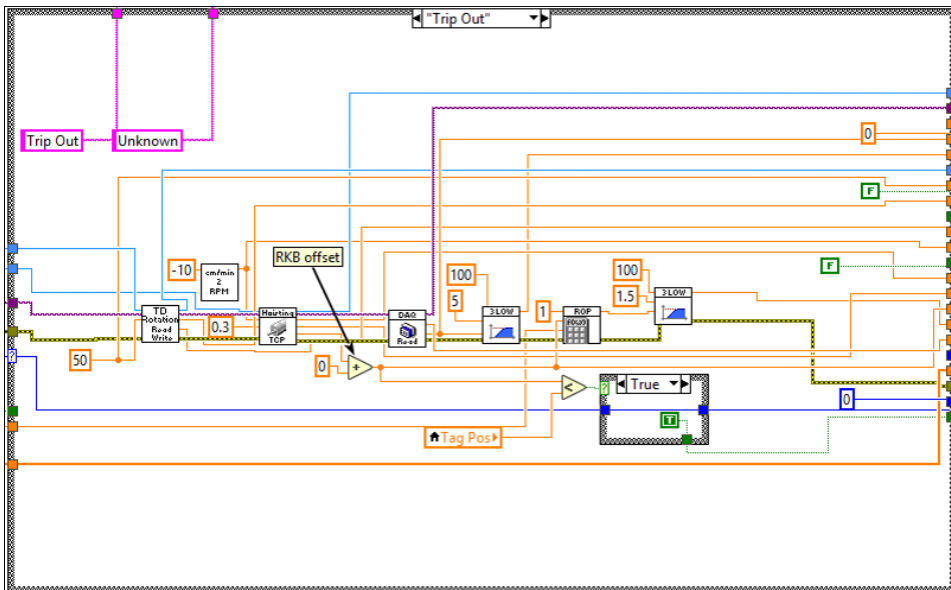
Figure 8.31: Block diagram of the sixth state in the state machine, the *"Trip Out State"* state.

Shut Down Sequence

The shut down sequence includes terminating the load cell connection and notifier, and shutting down the top drive and hoisting motor. The 2D data array is passed through the *"save file"* subVI which saves all data points to a text file. The subVI is explained in detail in appendix D.1.1 and exhibits the benefit of modularized code. The block diagram is identical to that of the competition scrip and is given in **Fig. 8.45**.

Real Time Plotting

The relevant data in the main while-loop is bundled in a cluster and sent to a parallel loop via a notifier. Notifiers are functions that suspend the execution of a block diagram, in this case, the while loop for plotting data, until they receive data from another section. Notifiers do not buffer data, nor are they loss-less. They simply broadcast the latest data. Notifiers are chosen over queues because buffering data points can lead to lag in the GUI charts. In addition, it is not imperative to plot every single data point live on the graph. Note that all data points for each time increment are save, even though they are not always plotted in the GUI.

8.7.4 Digital Filters

Passing data through low pass filters has proven to be an integral part of the control system. The filtered data includes measured WOB, calculated ROP and calculated MSE. Of the three, WOB and ROP are most important to the control system. The new configuration of the cylindrical load cell gives a very stiff setup in which most of the vibrations are

Table 8.3: Parameters appended to the 2D array in the main while loop.

Parameter	Unit	Parameter	Unit
Time Elapsed	s	Hoisting Motor Torque M	Nm
WOB SP	Kg	Hoisting Motor Torque Limit	Nm
WOB RAW	Kg	Position	mmRKB
WOB Filtered	kg	ROP	cm/min
Pressure	Bar	MSE	MPa
Top Drive ROP SP	RPM	θ_1	
Top Drive RPM M	RPM	θ_2	
Top Drive Torque M	Nm	θ_3	
Top Drive Torque Limit	Nm	Drilling State	
Hoisting Motor RPM SP	RPM	Formation Index	
Hoisting Motor RPM M	RPM		
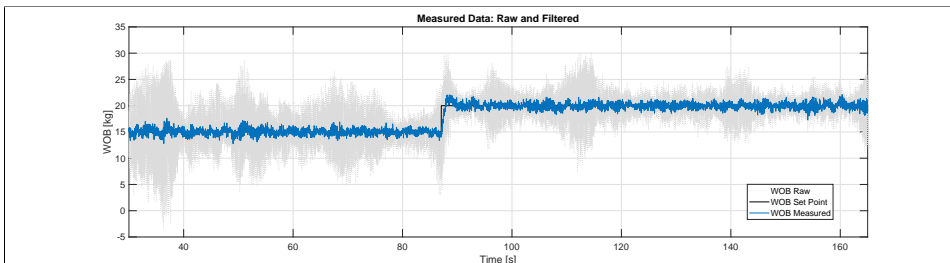
Figure 8.32: Drilling yields vibrations which are caught by the load cell, resulting in noisy raw data.

transferred to the load cell. This is contrary to the original design where much of the load was damped by the flexible structure. The load cell is rated to 5 kN and outputs a $\pm$ 10 V signal, based on the strain caused by the deformation in the strain gauges. The combination of a stiff setup and high load rating results in noisy data when drilling. Essentially, high-frequency vibrations caused by drilling propagates to the load cell. It is difficult to regulate the WOB PID controller on high frequent and high amplitude measurements.

To enable better control of the drilling process, the load cell raw data is passed through a third order low pass filter with a cut-off frequency of 5 Hz. A plot of measured raw WOB data and filtered data is given **Fig. 8.32**. It is apparent that vibrations during drilling yield noise in the measurements. Low pass filters will always result in time delay between raw data and filtered signal. In general, lowering the cut-off frequency yields a smoother signal as lower frequencies are damped. However, a reduction of the cut-off frequency also results in more time delay. This may cause unstable response in the PID controller. A cut-off frequency of 5 Hz has worked well in the PID controller.

Low pass filters are also implemented on the calculated ROP. The instantaneous ROP is readily calculated from the ball screw lead and hoisting motor rotational speed. However,
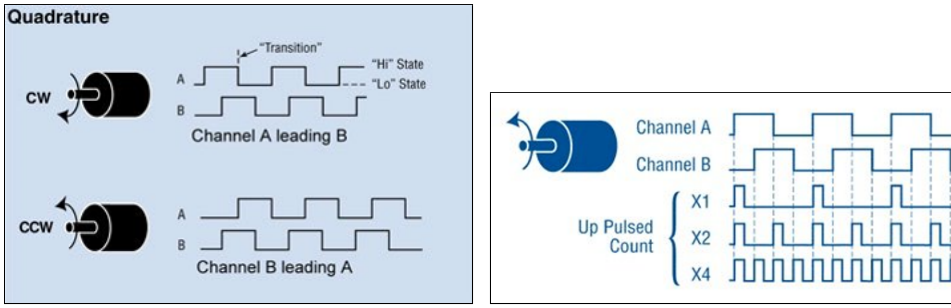
(a) Channels used to determine rotational speed and direction of the rotation in the motor. Figure from Dynapar [60].

(b) Increased resolution is achieved by counting leading and trailing edges. Figure from Dynapar [60].

Figure 8.33: Schematic of a quadrature encoder.

the PLC was limited to two analogue channels from the hoisting motor drive. These two were configured to output position and motor torque. Thus, the ROP was calculated based on measured position. However, there are a few challenges related to the derived ROP based on position change. The main issues regard resolution of the calculated ROP and inherent time delay when calculating ROP based on the equation given in **Eq. 8.39**, where ΔD and Δt are the change in depth and time increment.

$$ROP = \frac{\Delta D}{\Delta t} \tag{8.39}$$

The position is measured by an incremental encoder in the motor and motor drive. Three lines of pulses are produced by the quadrature encoder, with each line containing a given number of pulses per revolution. The pulses enable the encoder to calculate both direction of the rotation and the rotational speed of the motor. Counting the leading and trailing edges of the pulses can increase the resolution of the encoder, as seen in **Fig. 8.33**.

The incremental encoder used on the rig yields a position resolution of 0.2641 mm. Thus, the minimum increment in calculated ROP in cm/min is given by **Eq. 8.40**, where ΔROP_{min} is the ROP resolution determined by the time increment Δt used. It is evident that there is a trade-off between ROP resolution and time delay of the measurement when ROP is a derived measurement from position.

$$\Delta ROP_{min} = \frac{0.2641mm}{\Delta t} \cdot 6\frac{s \cdot cm}{min \cdot mm} = \frac{1.5846}{\Delta t}\frac{s \cdot cm}{min} \tag{8.40}$$

The ROP data is an integral component of the control system and overall parameter when looking at drilling performance. It is therefore important to consider the consequences of the aforementioned trade-off. The identification process is concluded within 35 seconds, where the ramp sequences have a duration of 15 seconds. The state is therefore sensitive to how many seconds are used to calculate ROP. Because ROP is low in harder formations, calculated data is much smoother if a 10 second interval is used to calculate the ROP. However, 10 seconds is too long for the identification phase. On the other side, reducing
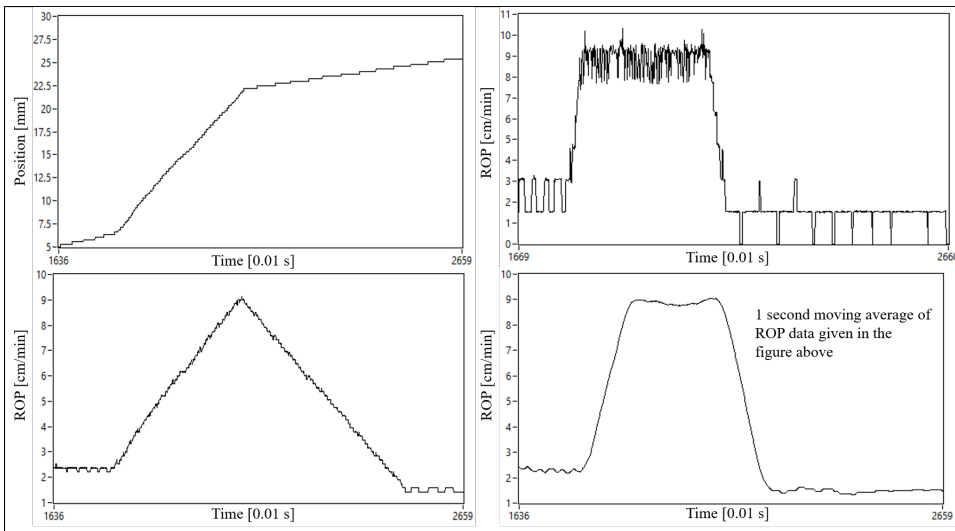
Figure 8.34: Simulated data showing how ROP is affected by the sample time when calculating ROP based on a change in measured position.

the sample time results in discrete ROP values. It is also important to quickly identify a formation change. Smoothing out ROP data by increasing the sample time would increase the time it takes to detect new formations. **Fig. 8.34** shows how ROP is measured in discrete intervals when using a small time duration, and how increasing the time smooths out, disperses and results in time delay. Applying a moving average with a half length of 0.5 seconds yields a much smoother ROP graph and reduced time delay. Running the ROP data through a low pass filter produces the same response.

Arnø (2018) discretized a third-order Buttorworth filter and implemented it as a stand alone LabVIEW VI [61]. **Eq. 8.41** through **Eq. 8.48** define the implemented low pass filter, where $y[n]$ and $x[n]$ are the filtered and unfiltered data at time step n, τ is filter time constant (inverse of cut-off frequency) and T is the sampling time. The LabVIEW block diagram of the digital filter is given in **Fig. 8.35**.

$$y[n] = -a_1 y[n-1] - a_2 y[n-2] - a_3 y[n-3] + b_0 x[n] + b_1 x[n-1] + b_2 x[n-2] + b_3 x[n-3]$$
$$(8.41)$$

where:

131
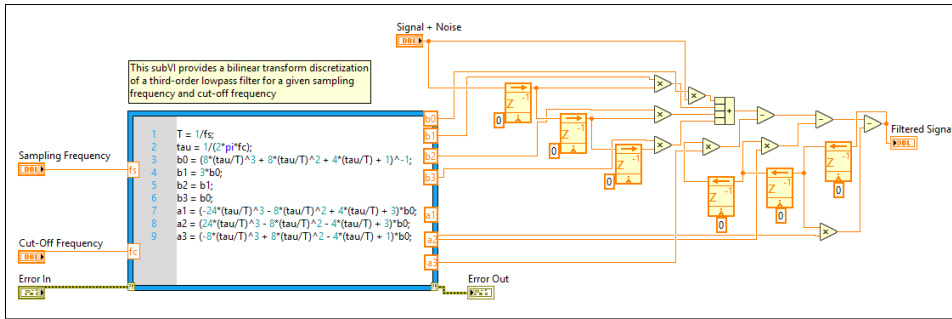
Figure 8.35: LabVIEW block diagram of a discretized third-order Butterworth filter.

$$b_0 = \left(8\frac{\tau^3}{T^3} + 8\frac{\tau^2}{T^2} + 4\frac{\tau}{T} + 1 \right)^{-1} \tag{8.42}$$

$$b_1 = 3b_0 \tag{8.43}$$

$$b_2 = b1 \tag{8.44}$$

$$b_3 = b0 \tag{8.45}$$

$$a_1 = \left(-24\frac{\tau^3}{T^3} - 8\frac{\tau^2}{T^2} + 4\frac{\tau}{T} + 3 \right) b_0 \tag{8.46}$$

$$a_2 = \left(24\frac{\tau^3}{T^3} - 8\frac{\tau^2}{T^2} - 4\frac{\tau}{T} + 3 \right) b_0 \tag{8.47}$$

$$a_3 = \left(-8\frac{\tau^3}{T^3} + 8\frac{\tau^2}{T^2} - 4\frac{\tau}{T} + 1 \right) b_0 \tag{8.48}$$

8.7.5 LabVIEW Script: Competition Drilling

The LabVIEW script used for the competition is similar to that of the fully autonomous program. The overall structure of the VI is given in **Fig. 8.36** and comprises of the following modules:

Initializing Script

The initialization of the script is seen on the top of **Fig. 8.36**. Time stamps for logging time elapsed are based on the difference in two time references, where one is constant. This is initialized in the first flat sequence structure. The state enum is also initialized to start in the *"Init"* state. Plotting of data is done separately by using a notifier. The notifier is initialized with the correct data type. Two Modbus master instances are opened for motor drive I/O communication as well as creating the DAQmx task for reading data from the load cell and pressure gauge. Warnings for high torque and stopped script are forced to false in the first iteration of the loop.
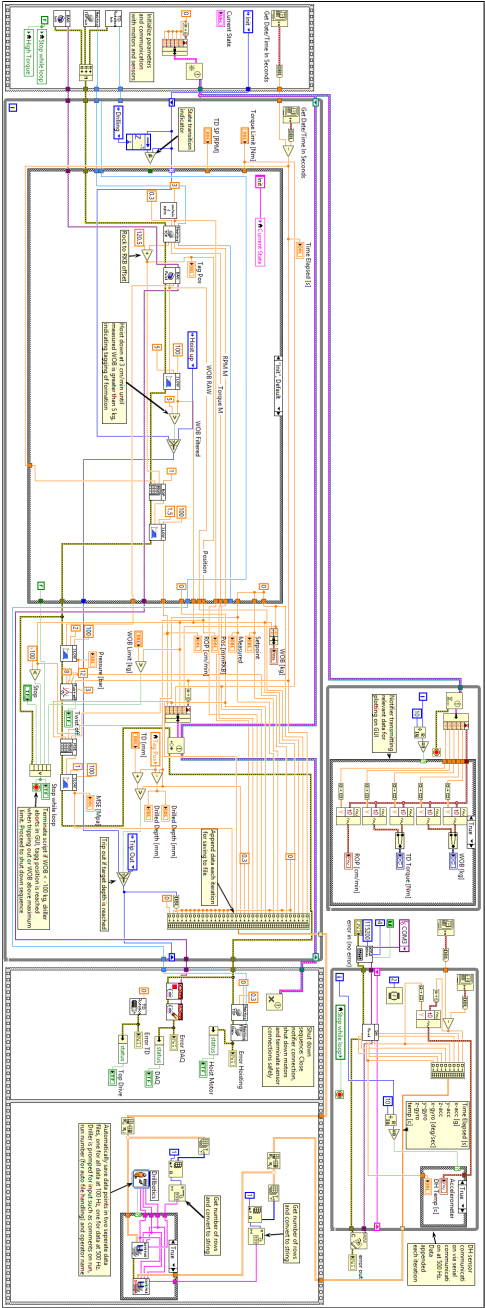
Figure 8.36: LabVIEW competition script. Script is initiated from the top.

Main While-Loop

The majority of the code resides within the main while-loop that runs at 100 Hz. The state machine is run in the loop together with most of the GUI indicators and controls. The measurements are sent to a parallel loop for plotting through a notifier and the data appended to a 2D-array. The while-loop is terminated if one of several criteria are met:

1. WOB > maximum limit. Indicates fault in script. The drill string will buckle if more weight is applied.

2. WOB < minimum limit. Stuck pipe is handled in the state machine by reducing WOB until torque falls below a certain threshold. If necessary, the hoisting motor will pull the drill string. Maximum overpull is set to 100 kg.

3. Driller stops VI. If the driller manually presses the stop button, the while-loop stops.

4. Tag position reached. If the target depth is reached, drilling is stopped and the bit is pulled out of the hole until the the bit is back at the registered tag depth.

The states in the competition script are similar to that of the fully autonomous script, with the exception of the identification state. The execution codes of the initialize, hoist up, start rotation and tripping out remain the same. These were discussed in section 8.7.3. The execution code of the drilling state includes torque control. The states are briefly summarized below. The block diagrams of the main while loop are given in **Fig. 8.37** through **Fig. 8.42**.

- **_"Init"_**: Initializes drilling by tagging the formation and recording the tagging position. Proceeds to _"Hoist up"_ when WOB reaches 5 kg.

- **_"Hoist up"_**: After tagging the rock formation, the bit is hoisted up at 1 cm/min for 4 seconds, before being lowered down for 2 seconds at the same speed, ensuring no contact of the bit. After 6 seconds, the state transits to _"Start rotation"_.

- **_"Start rotation"_**: Rotational speed of the drill string is increased until the measured value is within 10 RPM of the top drive RPM set point set in the GUI. Then, it proceeds to the _"Drilling"_ state.

- **_"Drilling"_**: The RPM set point is constant throughout the drilling state. Initially, WOB is ramped from 0 to the WOB set point over 30 seconds. The hoisting motor is controlled with a PID controller _tuned for shale_ with proportional gain, integral time, and derivative time of 5.326, 0.005055 minutes and 0.000777 minutes respectively. I.e., PID gains remain constant throughout the run, contrary to in the autonomous script. The PID actions were programmed to reinitialize if WOB surpasses 15 kg above its set point.

- **_"Trip out"_**: When target depth is reached, the bit is tripped out at 10 cm/min until recorded position reaches tag depth.
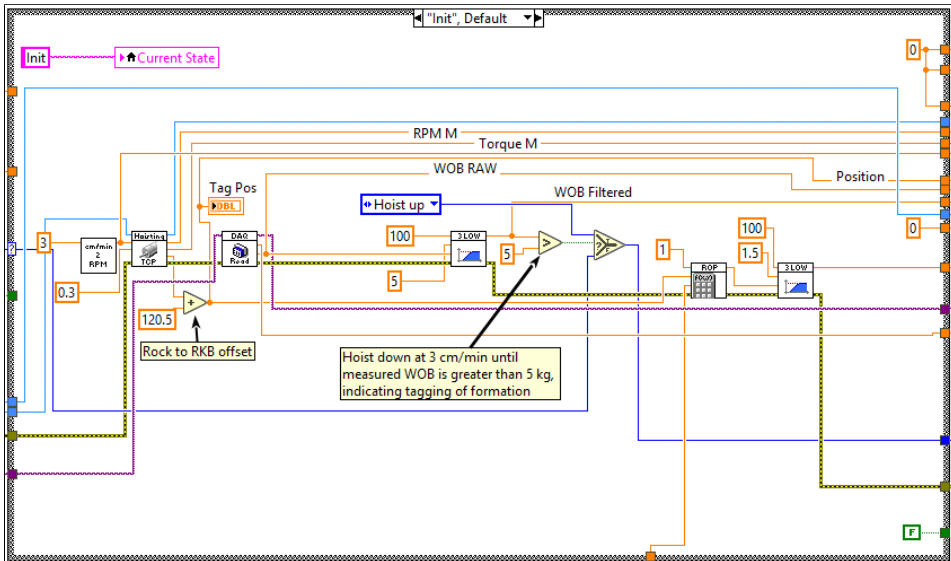
Figure 8.37: LabVIEW block diagram for the *"Init"* state of the competition script.
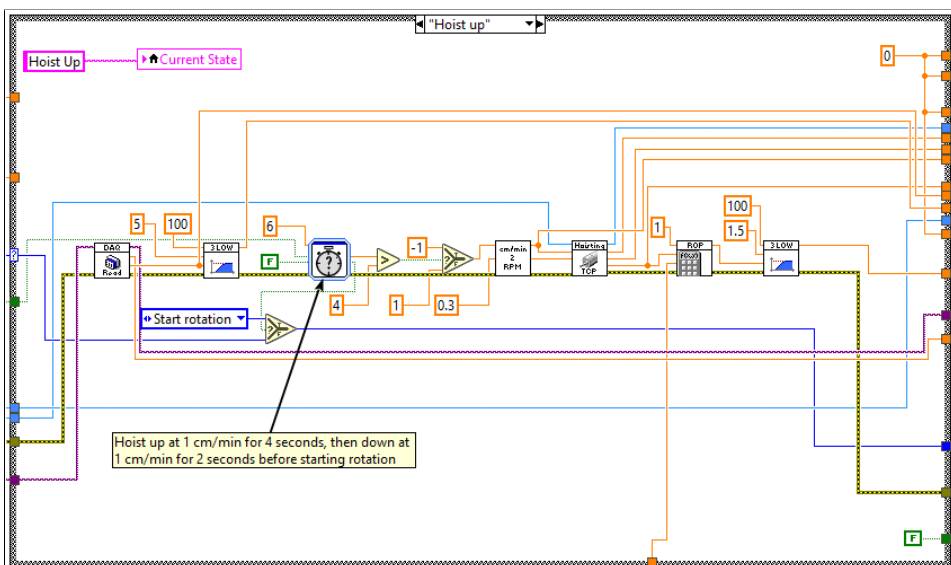
Figure 8.38: LabVIEW block diagram for the *"Hoist up"* state of the competition script.
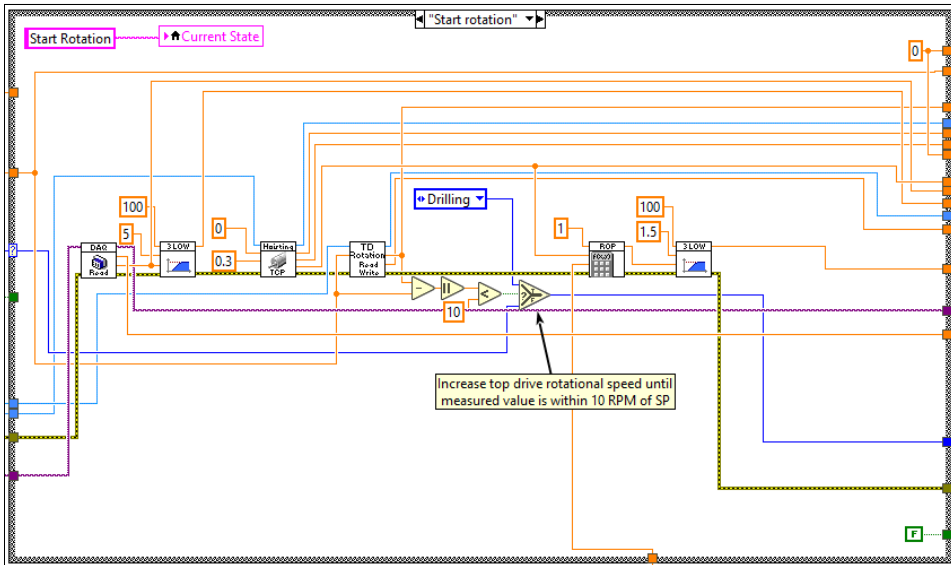
Figure 8.39: LabVIEW block diagram for the *"Start rotation"* state of the competition script.
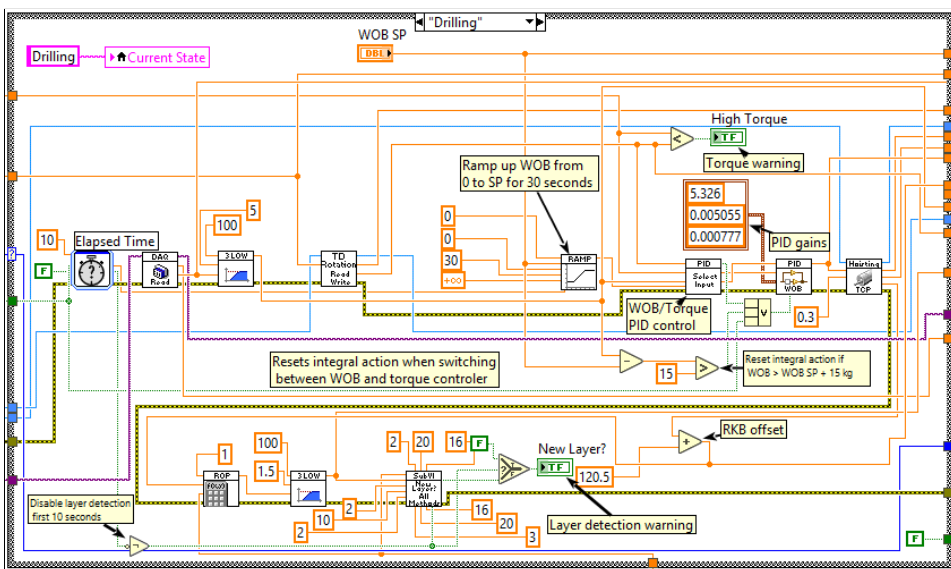
Figure 8.40: LabVIEW block diagram for the *"Drilling"* state of the competition script.
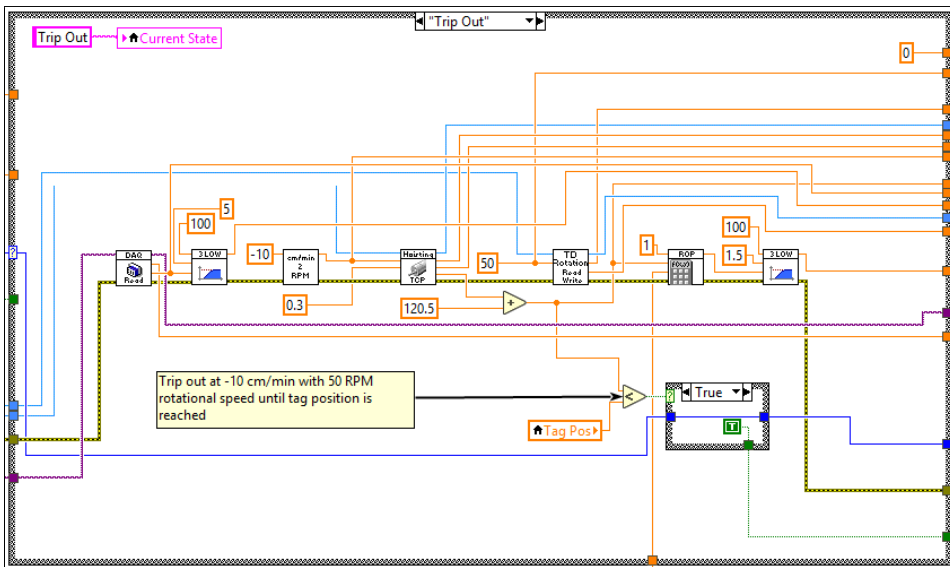
Figure 8.41: LabVIEW block diagram for the *"Trip out"* state of the competition script.

Down Hole Data Acquisition

Down hole sensor data is transmitted from the down hole card to LabVIEW via a USB cable. The data is acquired using the VISA serial VI's. Data is acquired at 500 Hz in a parallel while-loop and plotted at 50 Hz in the GUI. The temperature, acceleration and gyroscope data are appended in the same way as the other parameters in the main while-loop for data storage. The block diagram of down hole data acquisition and plotting is shown in **Fig. 8.43**.

Plotting Data

Numeric indicators such as down hole temperature and drilled depth are placed inside the main while-loop. The charts that are placed in the GUI are placed in a parallel loop which executes when the notifier sends the latest data points. Every tenth point is plotted in the GUI. This gives the driller enough information and saves resources and memory on the computer. WOB, WOB set point, top drive torque, top drive torque threshold and ROP are plotted in the parallel loop. The block diagram for plotting data is shown in **Fig. 8.44**.

Shut Down Sequence and Saving to File

The final action of the competition script is similar to that of the fully autonomous script: a shut down phase and logging data to file are placed in a stacked sequence structure. In the shut down sequence, the notifier connection is closed as well as the DAQmx connection for the load cell and pressure gauge. The hoisting motor and top drive motor are shut down. Data from the main while-loop, which is logged at 100 Hz, is saved to one text file.
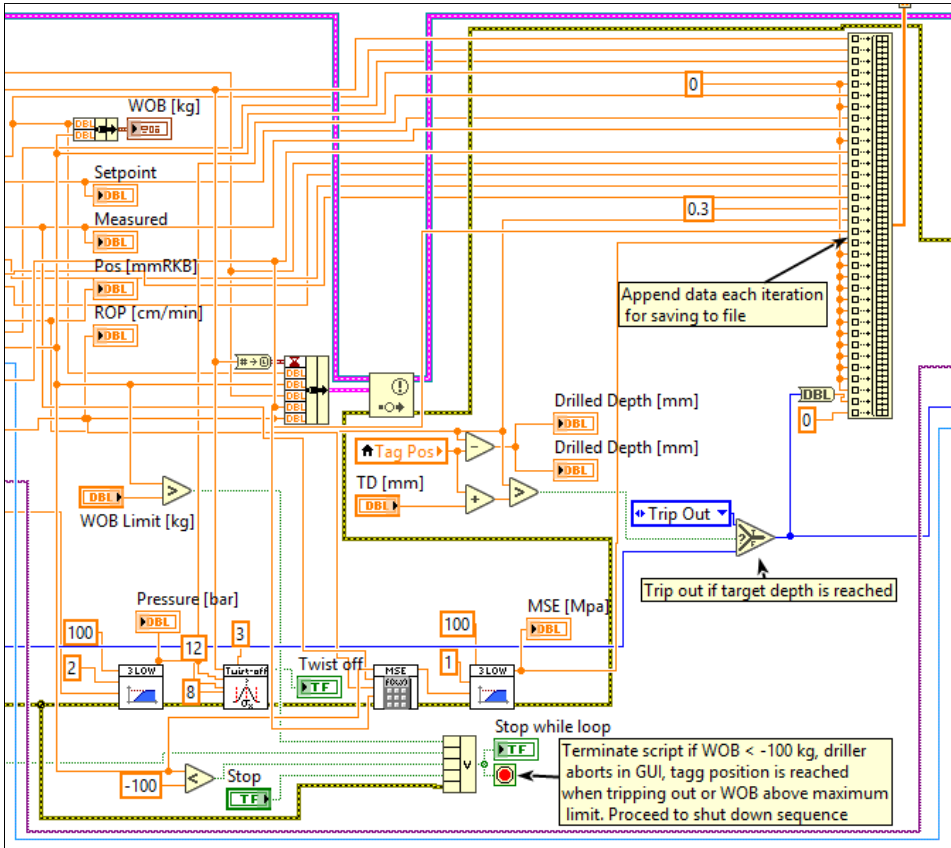
Figure 8.42: LabVIEW block diagram for the remainder of main while loop of the competition script, as seen in **Fig. 8.36**
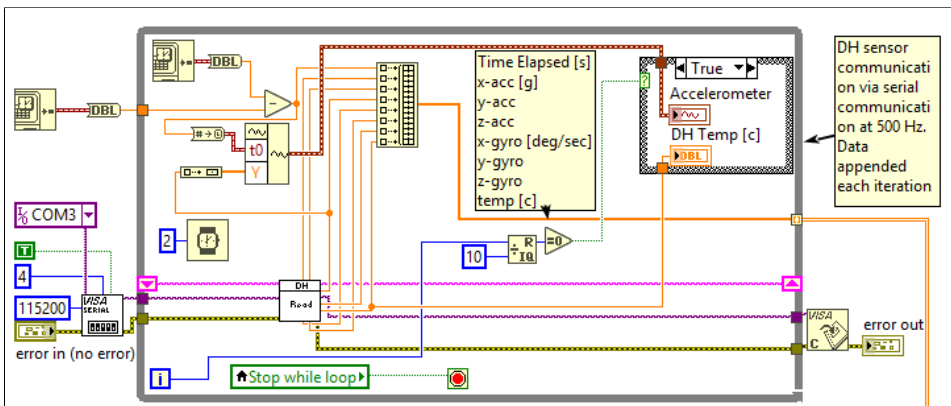
Figure 8.43: LabVIEW block diagram for acquiring down hole data.
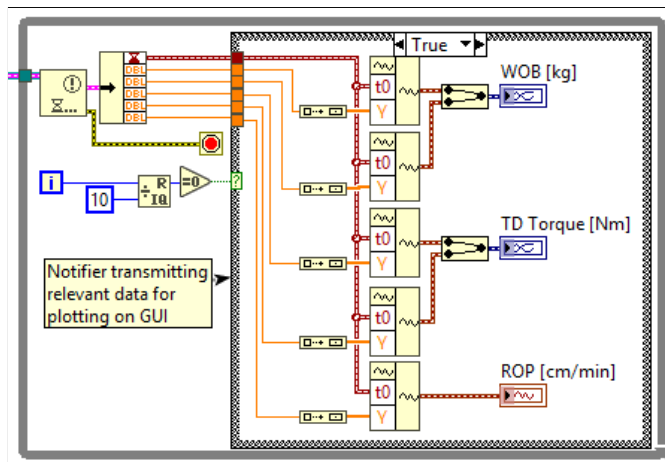
Figure 8.44: LabVIEW block diagram for plotting data.

Down hole data, which is logged at 500 Hz, is saved to a separate file. The block diagram of the shut down and saving to file sequence is given in **Fig. 8.45**.

8.8 Automated File Handling

Logging all drilling data is paramount to the project. It allows for comparison of drilling response and performance to changes in drilling parameters, quality control of the control algorithm state machine, PID control tuning and many more advantages. It was decided that all important parameters used in the control system should be saved. Even if a parameter seems irrelevant at one point, it might become relevant at a later time. Saving more parameters is therefore a better practice if it doesn't lead to memory issues, manifested in large saved files or increased buffer size in the internal memory of the computer. Such issues may result in poor performance or increased computer execution time.

Saving files is automated in the developed LabVIEW script. The data file is stored in a specified folder with an auto-generated file name. At a later point, all data can be loaded, plotted and published to a PDF by running a MATLAB-script. During drilling or any mode in which the LabVIEW main VI is active, data is continuously appended to a data array after each iteration in the while loop. When the program is ended, either by the user pressing stop in the front panel, or if an error occurs, the motors are turned off and the auto-indexed array is released from the while loop and enters the file storage module of the VI. The user is prompted for input, including comments describing the run, operator and the run number. The input and the data stored internally in the VI are processed and merged into a text file.

The structure of the text file is shown in **Table 8.4**. In addition to user input, date and time are automatically stored in the header information. **Fig. 8.46** shows a flow chart of the file
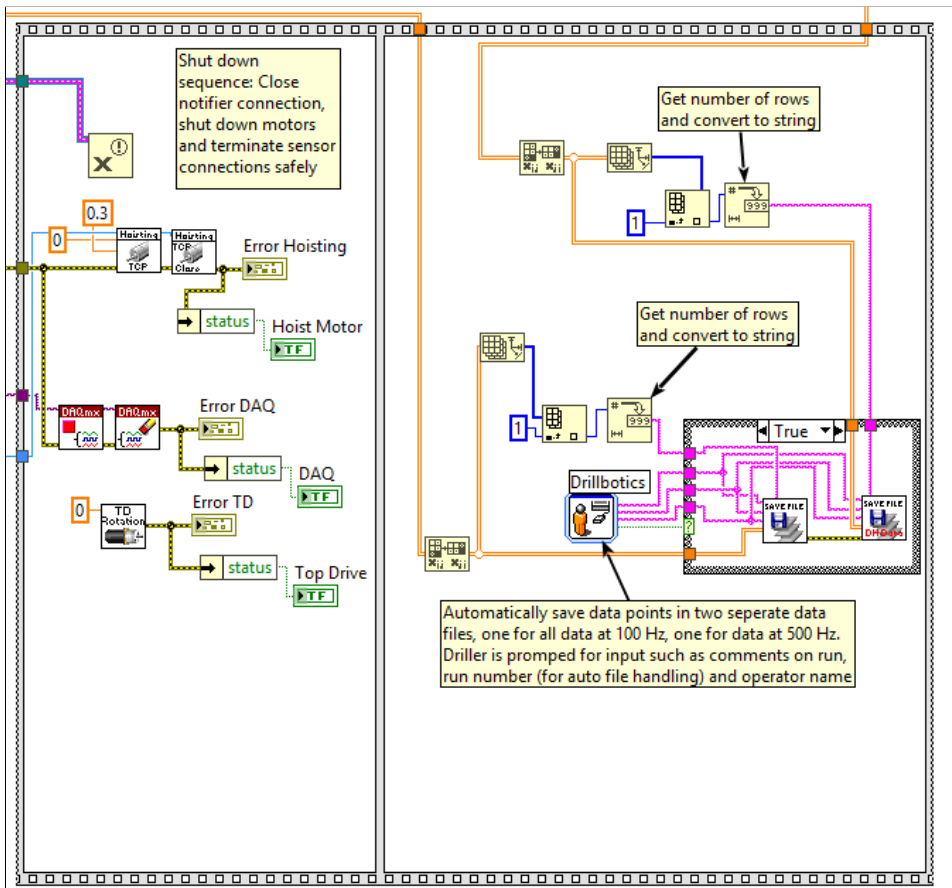
Figure 8.45: LabVIEW block diagram for shutting down the motors, terminating sensor communication, and saving data to file

Table 8.4: Data text file structure.

Date	23.04.18			
Time	14.49			
Operator Name	Andreas			
Comment	Example			
Row Numbers	23155			

Time Elapsed [s]	WOB SP [kg]	WOB Raw [kg]	WOB Filtered [kg]	$\cdots$
0.0000	20.0000	18.2426	18.2420	$\cdots$
0.0100	20.0000	19.6353	19.4231	$\cdots$
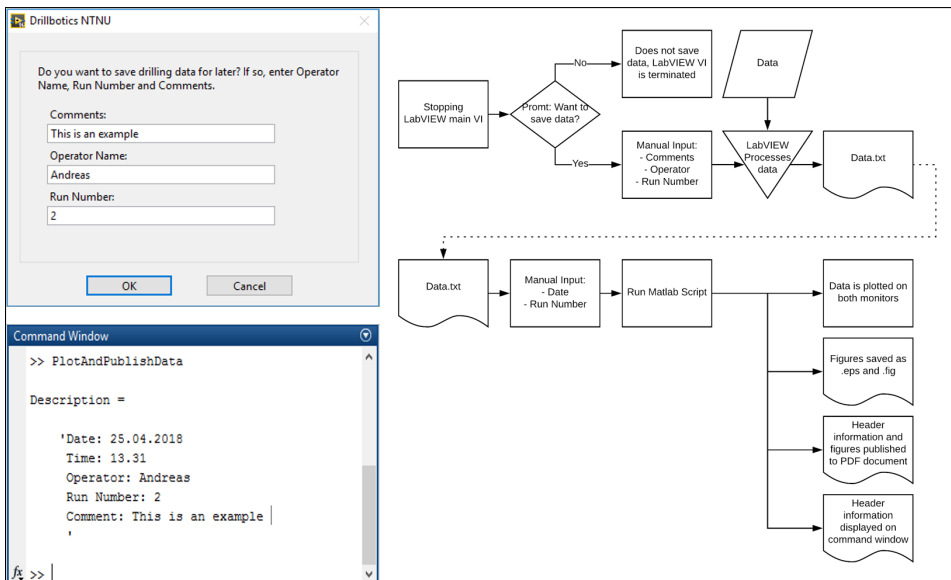
Figure 8.46: LabVIEW prompt, MATLAB command window output and flow chart of file handling.

handling system, from ending a drilling run in LabVIEW to executing the MATLAB script for publishing the data to a pdf-report. It also shows how users are prompted at the end of drilling, and how the run is summarized in MATLAB. An in depth description of the developed file saving system in LabVIEW is found in appendix D.1.1. It also displays an excellent example of the opportunity for modular design in LabVIEW. MATLAB codes for the system are found in appendix D.1.3. An example of the auto-generated drilling report is given in appendix D.1.6.

8.8.1 Choice of Method

Two methods for saving data to a file were considered. These are:

1. Append all data to a 2D array in every iteration of the code and save all once the
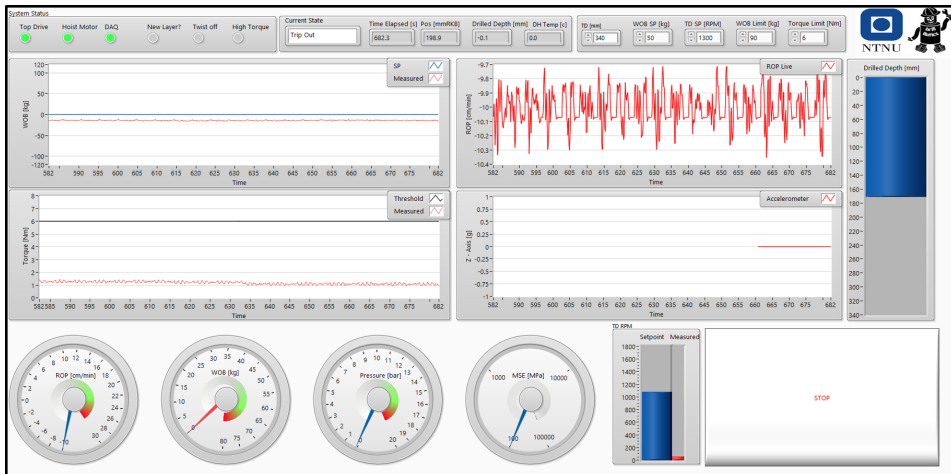
Figure 8.47: Final layout of the GUI.

script terminates.

2. Stream data to a file in real time through queued data streams in parallel with the control system

It was easier to implement the first method. The biggest concern with the method is that data is stored in internal memory when running the script. If too many data points are appended, memory issues might occur. However, no issues with memory allocation has been experienced with this method. The script ran at 100 Hz, even when running the script for longer than an hour.

8.9 Data Visualization and Control: GUI

The GUI of the autonomous script and the competition script are identical except for an added indicator for identified formation with the autonomous script. The design of the GUI is tied to one of the four main design focuses of the rig: simplicity. Toggles for switching between control modes, manual mode and auto mode are removed to mitigate any confusion for the driller. There is only a start button and a stop button. The number of controls have been reduced to the minimum and include only: target depth (mm), WOB set point (kg), top drive rotational speed set point (RPM), WOB limit (kg) and torque threshold (Nm). One of the most important indicators is the display of the current state. The system status is readily available on the top left. The LED lights for twist-off and high torque light up in red if there is an indication of twist-off or the torque is above the torque threshold. Progress of the drilling run is easily monitored by the drilled depth indicator. Only the most important parameters are plotted real-time on the GUI. These include WOB, torque, ROP and axial acceleration. The GUI is shown in **Fig. 8.47**.

Chapter 9

Testing and Results

The purpose of the testing is optimizing the drilling process with the scope of performing as well as possible 4th June on the Drillbotics competition. This chapter will describe the findings gathered in the testing phase of the project. Almost 400 drilling tests have been performed in the standardized rock samples resulting in 54 wells.

One of the main priorities for the team has been to make the rock estimator work properly. Ultimately this would allow for higher performance using gentler parameters. Making a robust system is essential to avoiding failures during tests. The operational limits of the drill pipe and the hydraulics has been tested before going more into detailed PID tuning. This year the team has designed their own drill bit to use on the competition. Drill bit is an essential part of efficient drilling and thorough testing has been done comparing different models. The testing is original as the instrument, the rig, is built from scratch by the student team supported by the team from the workshop. A lot of work has therefore been done related to making the programming and the mechanics work properly to conduct valid results.

9.1 Pipe Limits

The drill pipe can only operate within its mechanical limits. Should it be exposed to too much compressional load it will buckle, whereas twist-off happens under high torques or as a result of fatigue due to bending moments and stress cycling in the pipe. Also, the pipe will burst if exposed to too high internal pressure. This section will discuss and show results found after testing said limits.

9.1.1 Buckling

Static Buckling
Six static buckling test were performed with a 3/8" drill pipe with a wall thickness of

Table 9.1: Results from static buckling tests of 3/8" drill pipe with wall thickness of 0.016".

L [m]	P [bar]	C=4 [kg]	C=1.2 [kg]	Buckling Force [kg]	Fitted C
0.68	0	72.7	21.8	55	3.03
0.68	30	#N/A	#N/A	58	#N/A
0.58	0	99.9	30	72	2.88
0.58	20	#N/A	#N/A	75.5	#N/A
0.68	0	84.7	25.4	66.7	3.15
0.68	0	72.7	21.8	60	3.3

0.016". **Fig. 9.1** depicts the WOB profile for one of the tests. The buckling force and calculated end condition constant C are given in **Table 9.1**, along with the calculated buckling force when using an end condition constant of 4 and 1.2. The thin pipe is aluminum 3003 H14, a different alloy than the pipe with 0.049" wall thickness, which has a yield strength of 130 MPa, fatigue strength of 60 MPa and Young's modulus of 70 GPa. **Table 9.1** indicates that 3 is a fitting value for the end condition constant.

A more interesting result is the effect of internal pressure on the buckling limit. Given a 3/8" pipe with wall thickness of 0.016", **Eq. 7.9** estimates an increase in buckling limit of 18.2 kg for an internal pressure of 30 bar. **Fig. 9.1** shows a slight increase in the buckling limit, however, it is far below the estimated 18.2 kg. It is difficult to determine why a slight increase in the buckling limit occurs or if it is an increase at all. The drill pipes might not be of equal length, or, since these test were conducted with the old load cell set up, the reading might be erroneous. Furthermore, two identical pipes were buckled without internal pressure resulting in both higher and lower buckling limit compared to the test run with pressure, suggesting the inaccuracy of the test is larger than the potential geometrical stiffening effect. In chapter 7.1.1 the effect of internal pressure on buckling limit was discussed. The results from the static buckling test indicate that Palmer & Baldry's (1974) hypothesis on buckling limit is applicable for the Drillbotics set up, and that increased internal pressure does not increase the static buckling limit.

The results from the static buckling tests for the thicker drill pipe used in the competition are given in **Table 9.2**. No tests with internal pressure were conducted. Note that the end-condition constant C which corresponds to the measured buckling forces are close to the values measured in the thin pipe. Critical buckling force as a function of unsupported pipe length for an end-condition constant of 3.0 is plotted in **Fig. 7.3**.

Dynamic Buckling
Only two dynamic buckling test were performed due to limited time in combination with buckling tests straining the system. The first test was conducted in cement, the second in granite. The WOB response for the two test are given in **Fig. 9.2**. The buckling force as well as the unsupported drill pipe length are given in **Table 9.3**. Euler and Johnson's equations assume no eccentricity of the load and are thus applicable for static tests. In a dynamic drilling process with rotation and vibrations, it is expected that the pipe will
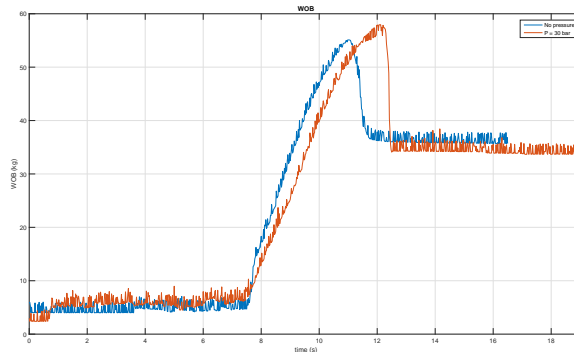
Figure 9.1: Buckling test of 0.016" drill pipe with and without internal pressure.

Table 9.2: Results from static buckling tests of 3/8" drill pipe with wall thickness of 0.049".

L [m]	P [bar]	C=4 [kg]	C=1.2 [kg]	Buckling Force [kg]	Fitted C
0.76	0	138	41.4	109	3.2
0.65	0	186.2	55.9	135	2.9
0.62	00	204.7	61.4	159	3.1

buckle at less weight than in static conditions. Attempts to quantify the effect of dynamic processes have been made by applying the equations governing static buckling prediction on the test results. The fitted end condition constant for the dynamic tests are three times lower than for the static tests, indeed confirming that the drill string buckles at less load during drilling. It should also be noted that the end-condition constants for the dynamic test are close to one-another suggesting that the equations for static buckling can be applied to dynamic buckling as well. Practical use of these results on the miniature drilling rig include automatically changing the maximum allowable WOB as a function of drilled depth.

9.1.2 Burst

No dedicated test was performed to reach the burst limit of the pipe. The operating pressure was far below the calculated burst rating, and thus only operating limits plus a safety margin was tested. The system was pressure tested to 30 bar with no damage to the pipe

Table 9.3: Results from dynamic buckling tests of 3/8" drill pipe with wall thickness of 0.049".

L [m]	P [bar]	Buckling Force [kg]	Fitted C
0.571	4	69	1.14
0.405	5	130	1.11
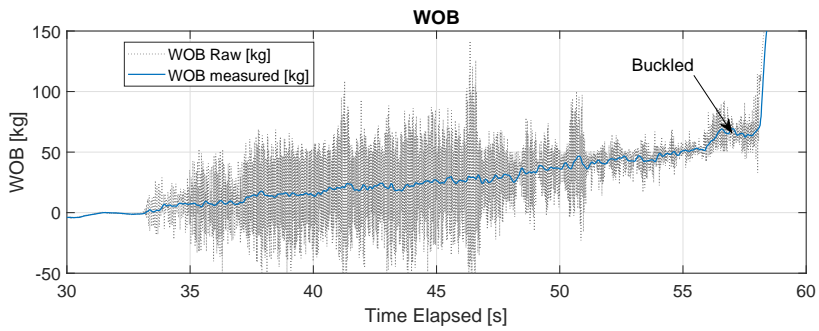
(a) Buckling test in cement.
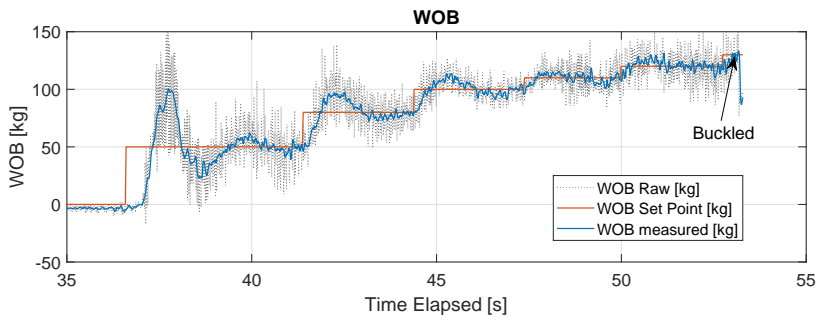
(b) Buckling test in granite.

Figure 9.2: Dynamic buckling tests.

or hydraulic swivel.

9.1.3 Twist-off

Static Twist-off
A static twist-off test of the 0.035" thick pipe was attempted. 6061-T6 aluminum alloy has a shear strength og 207 MPa. This is equivalent to twisting off at 21.6 Nm for the a 3/8" pipe with wall thickness of 0.035" and 27.8 Nm for a pipe with wall thickness of 0.049". However, no static twist off test was completed as the pipe started to slip in the lathe at 17 Nm.

Dynamic Twist-off
No explicit tests were conducted for dynamic twist-off. However, twist-offs did occur several times during testing of the LabVIEW script. Based on the expected operating conditions in pressure and WOB, dynamic twist-off are calculated to occur at roughly 20 Nm if one bases the calculations on the yield strength (see section 7.3). However, it was experienced that twist-off would always occur at lower torque levels. **Fig. 9.3** show three data sets for three different drilling runs. The three scenarios summarize the experience during drilling with the 0.049" drill pipe. It was generally experienced that twist-off would occur at varying levels of torque. In **Fig. 9.3a** and **Fig. 9.3b** the drill string twisted off at 3.2 Nm and 6.9 Nm respectively, however, no twist-off occurred in the run depicted in **Fig. 9.3c** where the torque reached 12.2 Nm. The torque at which the pipe twists off is close to what is expected when calculating torque limits using the fatigue strength of the drill string (96.5 MPa), rather than the yield strength (276 MPa). It should also be noted that the majority of all twist-offs occurred at the end of the mechanical connection where most of the fatigue is expected to occur due to bending moments and stress cycling resulting from down hole vibrations. Only once did the connection twist off at the upper connection in the hydraulic swivel. A twist-off in the bottom connection is depicted in **Fig. 9.4**. Experience gained from numerous drilling runs indicate that alignment of the drill string to the two stabilizing bearings is the most important parameter with regards to twisting off. Minor misalignment in any of the components results in vibrations, poor hole quality and high torque. Misalignment also causes the BHA to hit the inner wall of the riser. Once the BHA is in contact with the metal of the riser and it starts to resonate the torque jumps up. It is difficult to stop the process and more often than not, the misalignment will cause the drill string to twist off. Such an example is given in **Fig. 9.5** where the BHA starts to uncontrollably resonate in the riser at 21 seconds. The torque responds immediately by increasing from 1.7 Nm to 6 Nm before twisting off at 7.3 Nm.

Twist-off also occurred with stuck pipe, or at the interface between two rock layers, such as cement and shale. The transition between a hard and soft layer would often lead to poor hole quality in the vicinity of the interface. The transition is often visible in the form of a ledge. The same metal scraping sound could be heard when the BHA is passing through the layer interface often causing unstable torque spikes. **Fig. 9.6** shows the typical response of stuck pipe in torque and WOB. Since the drill bit is no longer rotating, the raw data of the load cell dissipates. It was also experienced that increasing the rotational speed towards 2000 RPM was detrimental to the hole quality and thus also increased the torque.
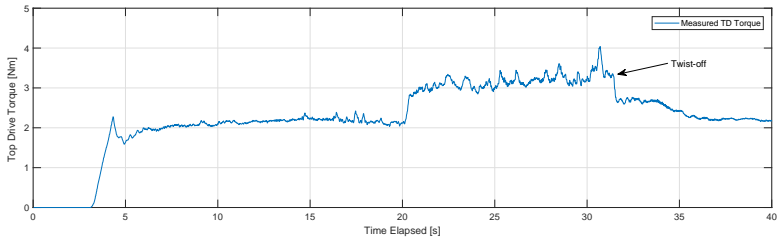
(a) Twist-off at 3.3 Nm while drilling.
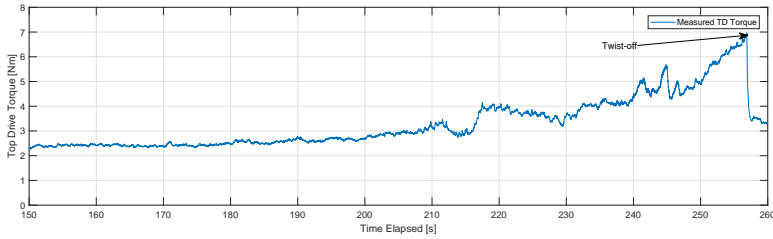
(b) Twist-off at 6.9 Nm while drilling.
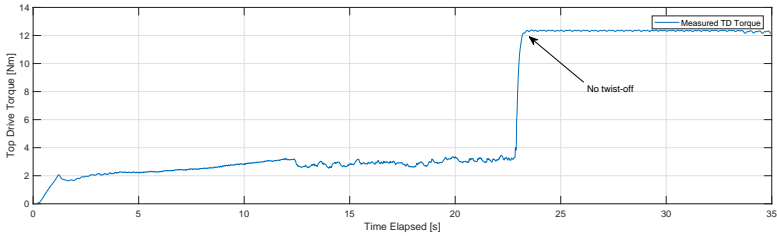
(c) Getting stuck at 12 Nm and not twisting off.

Figure 9.3: Top Drive torque measurements for three different runs, two of which resulted in twist-off.

Figure 9.4: Twist-off occurred mainly at the bottom connection, always in the transition from pipe to connection.
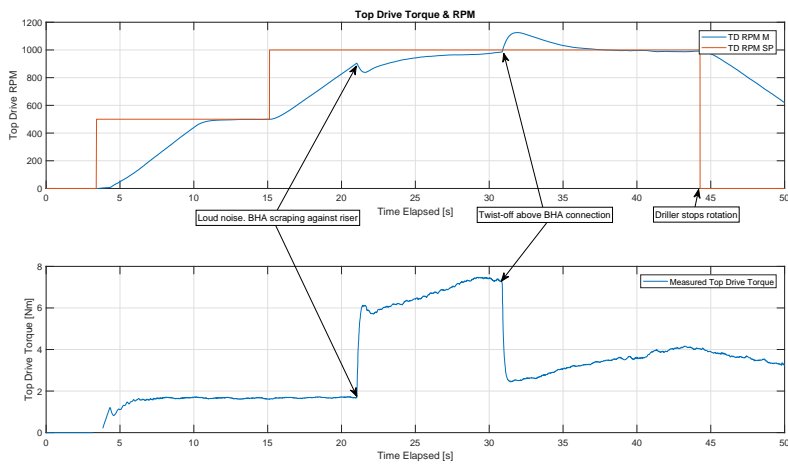
Figure 9.5: BHA hitting the riser wall causing excessive vibrations and high torque. Eventually the pipe twists off.
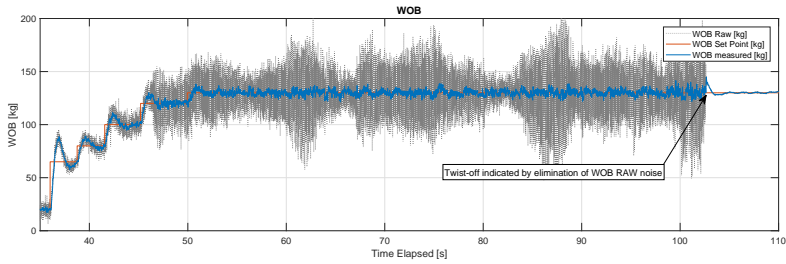
(a) Typical response in WOB when twisting off. The raw data noise dissipates.
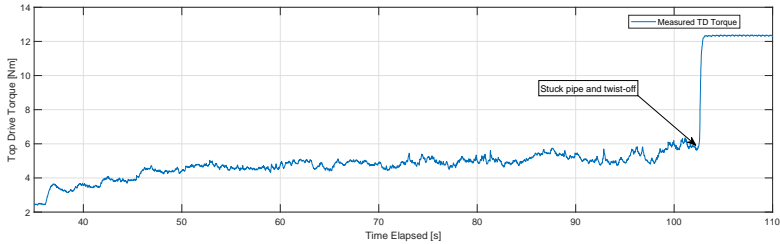
(b) Torque jumping up close to the motor drive limit indicates stuck pipe.

Figure 9.6: Stuck pipe resulting in twist off.

Fig. 9.7 shows an example of how drilling through an interface at high RPM can cause torque spikes. These "shark fin" torque spikes were a clear indicator that the pipe might twist off in the near future. The spikes correspond to a high sound when drilling and are easily detected by the driller. The section enclosed in the black ellipsis is given in more detail in **Fig. 9.8**. The torque spikes are easily identified by the driller since the y-scale is auto-scaled in the control system GUI.

9.2   PID Control Tuning

Tuning the PID controller of the rig has proven to be of critical importance, necessary for stable drilling performance. An example run with poorly tuned controller is for reference shown in **Fig. 9.9**, where the test is terminated at 170 seconds due to unstable and growing oscillations.

The WOB-based PID controller of the Drillbotics rig was tuned using three different methods:

1. Trial and Error

2. Ziegler Nichols

3. Cohen Coon
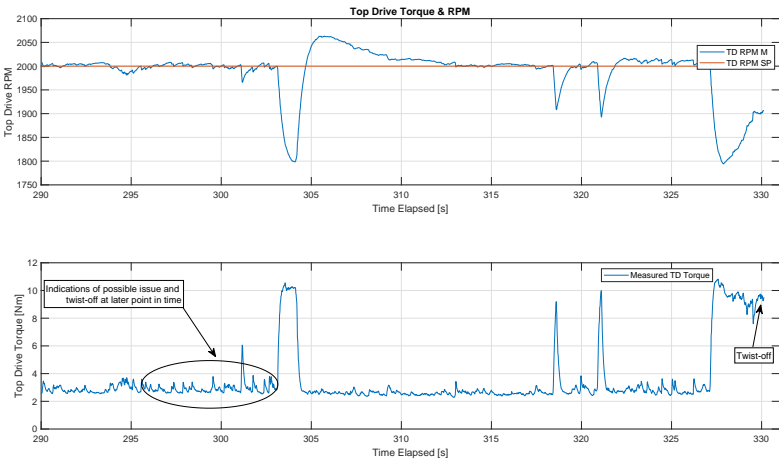
Figure 9.7: Twist-off when BHA is in contact with a formation interface. In this example the BHA passed an interface between two granite blocks.
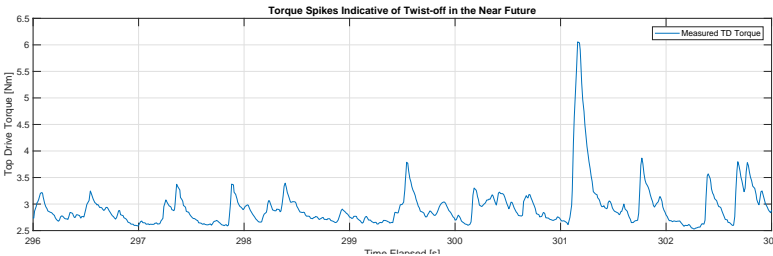
Figure 9.8: Torque response of the highlighted section in **Fig. 9.7**. This is what the driller would see since the y-scale is auto-scaled.
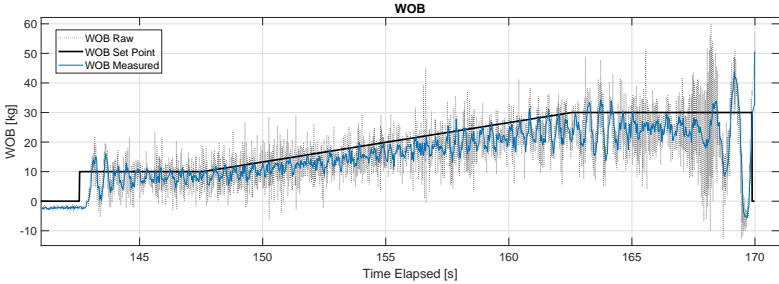
Figure 9.9: This is an example of how a drilling run may look with a poorly tuned PID controller. Drilling is unstable, where growing oscillations cause the test to terminate upon reaching a user-input safety limit of 50 kg.

Table 9.4: Tuned PID control parameters for soft and medium hard rock using trial and error.

Formation	K_p	t_i	t_d
Cement	27	0.02	5
Shale	23	0.0001	4

As discussed in 8.2.4, the team by accident left a reinitialize block in LabVIEW to reset at every sample. Effectively the controller was reduced to a simple proportional term. The rig had difficulties reaching WOB set points, and both the Ziegler Nichols and Cohen Coon tuning methods did not leave satisfactory performance. Also, it was found that the rig required quite different PID parameters depending on the formation it was drilling through. For instance, more control output was necessary to reach set point in softer formation, most likely due to not having integral effect. After resolving the reinitialize mistake, Cohen Coon tuning method was utilized with much better performance. Furthermore, it was found that tuned PID parameters for one formation works substantially better in other formations. Due to limited time, neither Ziegler Nichols or full manual tuning were re-tested after fixing the reinitialize block, but this was not prioritized due to the already well performing controller with Cohen Coon.

9.2.1 Manual Tuning

Trial and error tuning was done by setting a step in WOB, running the rig at constant RPM of 1000. Different weights were tested, from 10 to 50 kg. Tests were run for a short period of time, just long enough to evaluate steady state performance in the formation. Example of a step response is shown in **Fig. 9.14**. In this example, it is evident that 25 to 30 seconds would be sufficient to evaluate the performance in the formation. When evaluating the run, the team considered several aspects of the step response. Firstly: Does the graph reach the desired set point, or is there a steady state error? If weight reaches set point - does it do so with or without an overshoot? And lastly - are there any major oscillations in weight on bit? As a rule of thumb, the team increased proportional gain all the way until weight reached its steady state baseline sufficiently quick. Further, if encountering steady state error, the integral term was reduced (meaning more integral effect) until set point was reached. And finally, on seeing oscillations, the dampening term t_d was increased step wise by trial and error in small increments. It was found that increasing the effect of each control term should not be done after reaching desired performance. For instance: adding more integral term after already reaching set point resulted in oscillations and poor performance. Similarly, too much proportional gain leaves the rig behaving with large overshoots, and drilling with a standing wave behaviour, with the hoisting motor rotating back and forth instead of smoothly going downwards. Best-attempt results after tuning the PID controller manually can be found in **Table 9.4**.
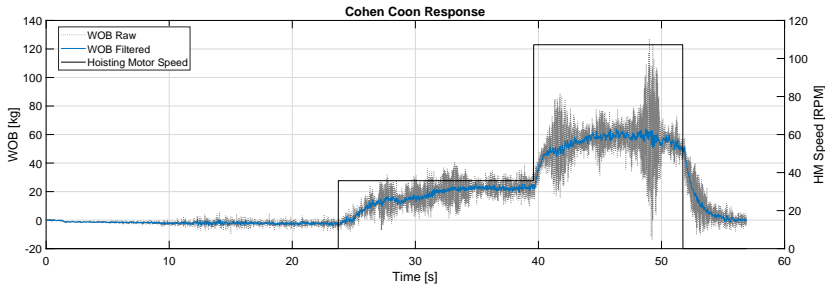
Figure 9.10: Cohen Coon test in Shale, with an ROP step of 2-6 cm/min. WOB baseline increases from 22.5 to 60 kg.

Table 9.5: After using the theory from **Fig. 8.9** on the actual test in **Fig. 9.10**, the following parameters were found. Range in WOB and Hoisting Motor RPM are listed based off experience, while the max/min values for Hoisting Motor RPM and WOB are registered from the drilling data. These parameters are used to calculate the Cohen Coon tuning for shale in **Table 9.6**.

Parameter	Value
$\Delta WOB_{max/min}$	60 - 22.50
ΔWOB_{Range}	80 - 10
$\Delta RPM_{max/min}$	107.22 - 35.74
ΔRPM_{Range}	200 - 0
M	0.54
ω	0.36
K	1.50
τ	0.0125
θ	0.002167

9.2.2 Cohen Coon

This method was implemented after solving the reinitialize block mistake, having a fully functional PID controller. The initial tuning run for Cohen Coon is shown in **Fig. 9.10**, where a step in ROP is run with the top drive at a constant 1000 RPM. The step response was evaluated graphically as discussed in section 8.2.3, finding PID parameters as shown by **Fig. 8.9**. After calculating parameters for K_p, t_i and t_d, further fine tuning was done using trial and error. The final Cohen Coon tuning parameters are summarized in **Table 8.2**, and support parameters τ, t_d and K from the test in shale are shown in **Table 9.5**.

Test in Cement

A test run at 1000 RPM of the tuned Cohen Coon parameters in cement is shown in **Fig. 9.11**. Also, two different sets of Cohen Coon parameters are compared in **Fig. 9.12** and

Table 9.6: Tuned PID control parameters for different rocks using Cohen Coon method.

Formation	K_p	t_i	t_d
Cement	2.8	0.0064	0.00112
Shale	5.362	0.005055	0.000777
Granite	4	0.005055	0.000777
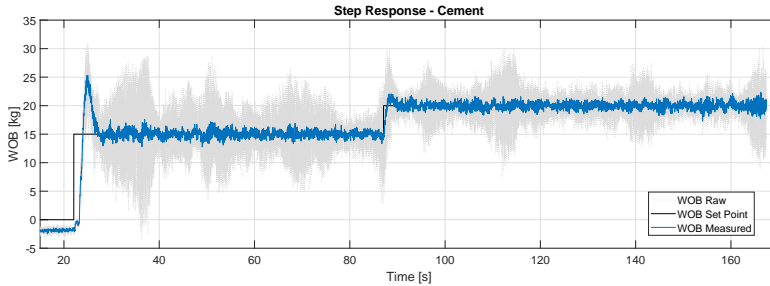
Figure 9.11: Step response in cement after specifically tuning PID controller for that formation. Overshoot in the beginning is a result of integrator build-up during tagging, and should not be taken into account when evaluating steady state performance. A specific tagging-sequence is run to achieve critical damping in autonomous mode. Control parameters are $K_p = 2.8, t_i = 0.0064$ and $t_d = 0.00112$.

Fig. 9.13. The runs are identical apart from PID tuning, where the latter is run with considerably higher proportional gain. Notice how this results in a quicker response, at he cost of more axial oscillations.

Test in Shale

The Cohen Coon parameters were tested in shale, with pure shale response shown in the first minute of **Fig. 9.14**. The team found shale to be a medium hard rock, placing itself in the middle in the range of drillability, with cement and granite on the far edges. As such, the PID tuning parameters for shale are thought to be well-rounded and a good compromise to be used in unknown formations. This is demonstrated in **Fig. 9.14** hitting both shale and cement, and further in **Fig. 9.17** drilling granite, suggesting the controller has the ability to tackle different drilling environments.

Test in Granite

A test of the PID controller was lastly done in granite, with parameters as shown in **Table 9.6**. The run was done with the top drive at a constant 1000 RPM, increasing WOB in steps from 20 to 50 kg, at 10 kg increments, as shown in **Fig. 9.15**. This step procedure is done twice for good measure, before testing the controllers ability to follow a ramping WOB
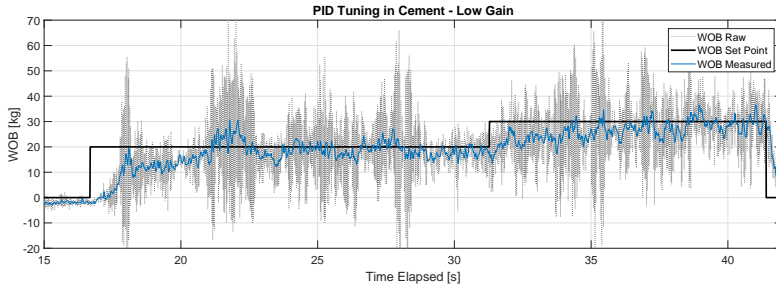
Figure 9.12: Step response in cement after fine tuning a set of Cohen Coon parameters, with $K_p = 2.8, t_i = 0.0064$ and $t_d = 0.00112$. The performance is preferred over that in **Fig. 9.13**, where the NTNU Drillbotics team value stability and less oscillations over speed and time reaching set point.
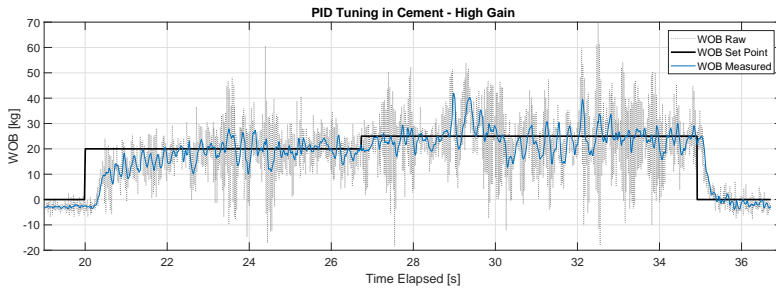
Figure 9.13: Step response in cement after tuning with Cohen Coon, with $K_p = 30, t_i = 0.02$ and $t_d = 0.0005$. Even though this response is quicker than that in **Fig. 9.12**, the axial vibrations observed are not desirable. Notice especially peaks in WOB Measured at 29 and 32 seconds, and a standing-wave-behaviour.
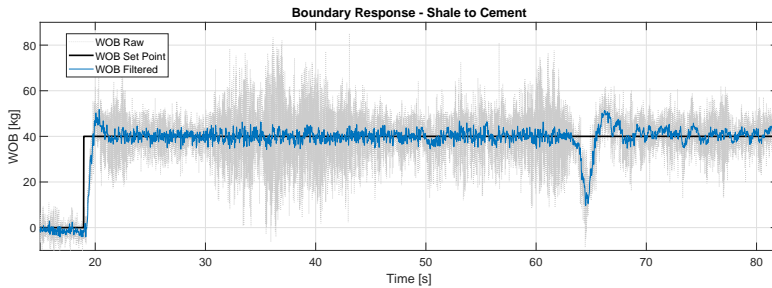
Figure 9.14: Cohen Coon PID response in shale, and rig behaviour when encountering boundary from shale to the softer cement. PID values of $K_p = 5.362, t_i = 0.005055$ and $t_d = 0.000777$. Notice sharp drop in WOB as the boundary is hit, before the PID controller responds to bring WOB back up to set point.
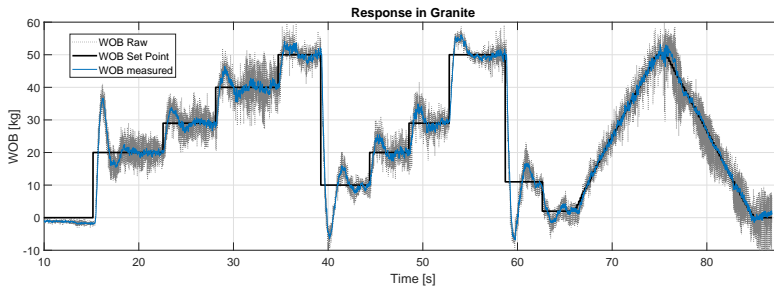
Figure 9.15: Rig response in granite, from both step and ramp set points. Notice how increasing WOB in a ramp allows for no overshoot and good consistency between measurement and set point. Initial overshoot at 15 seconds is a result of integrator wind-up during tagging, and should be disregarded in evaluating the PID performance. PID values of $K_p = 4, t_i = 0.005055$ and $t_d = 0.000777$.

Table 9.7: Tuned Ziegler Nichols PID control parameters after standing wave response in cement, with $K_{cr} = 50$ and period $T_{cr} = 1/3$ seconds. Calculated as depicted by **Table 8.1**.

Formation	K_p	t_i	t_d
Cement	25	0.17	0.042

set point. Notice especially how well the controller is following a ramping sequence as opposed to stepwise increase, suggesting that increasing weight should be done gradually in the estimator to allow for a more gentle transition in WOB.

9.2.3   Ziegler Nichols

The Ziegler Nichols method was done before fixing the reinitialize block. However, this should not have an effect on the tuning procedure itself. After setting all control parameters to zero (and t_i to infinity, corresponding to zero integral effect), proportional gain was increased gradually, running a WOB step response each increment. As the proportional gain was increased, the resulting step response got progressively more chaotic. Finally, a full standing wave response was achieved at $K_p = K_{cr} = 50$. This is shown in **Fig. 9.16**. The frequency was graphically noted to 3 Hz, used alongside the critical gain K_{cr} to calculate the PID parameters in **Table 9.7**. Notice that upon testing these PID parameters the performance was sub-par, likely due to the issue with the reinitialize block. Ziegler Nichols control parameters are not used, as the team is satisfied with Cohen Coon performance.

9.2.4   Handling Boundaries: Integral Reset vs High Gain

The NTNU Drillbotics team wishes to prioritize a slow but steady PID tuning as opposed to quick with oscillating behaviour. However, when facing formation boundaries, this has
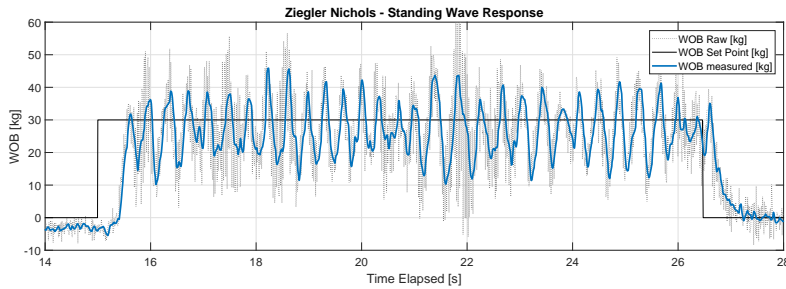
Figure 9.16: After incrementally increasing proportional gain, this standing wave response was achieved as part of the Ziegler Nichols tuning method. Frequency is graphically noted to 3 Hz, and amplitude is recorded at 13 kg, with a baseline average at 28 kg. Calculated PID values are shown in **Table 9.7**.
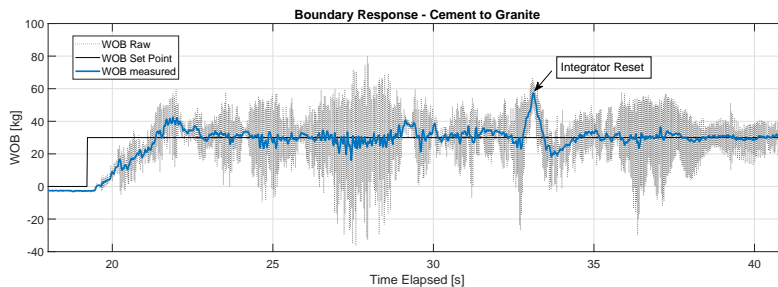
Figure 9.17: Run 1, 210518. Showing WOB behaviour when hitting boundary from soft cement to hard granite. Integrator reset is used as a technique to bring down WOB after the boundary. PID values of $K_p = 5.362, t_i = 0.005055$ and $t_d = 0.000777$.

proven to be difficult, especially for large changes in drillability. WOB has a tendency to increase substantially going from soft to hard rock, and a slow controller is not able to pull WOB down after a big overshoot quickly enough. As a countermeasure against overshoot, but still receiving the benefits of a low gain controller, integral reset is used. The effect of this is shown in **Fig. 9.17**, and possibly more evident through hoisting motor RPM response in **Fig. 9.18**. Additional information about the same run is shown in **Fig. 9.19** and **Fig. 9.20**, showing respectively torque and ROP.

As an alternative to integral reset, a high gain controller can have the ability to deal with formation boundaries and change in drillability. The team found that overshoots can be handled by the quick high-gain controller, however, this comes at the cost of more oscillations during drilling. Morevover, integral reset gives the user an exact WOB threshold to stop the overshoot, not possible with just high gain. As the high gain controller does not offer significant benefits over integral reset, it is not being put to use in the autonomous drilling rig.

Hitting an opposite formation boundary - that is, going from hard to soft rock, is a also
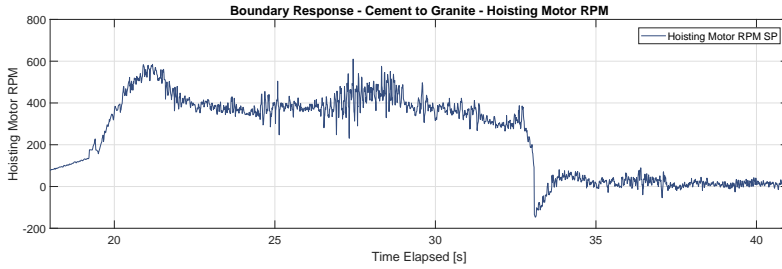
Figure 9.18: Run 1, 210518. Showing HM RPM behaviour when hitting boundary from soft cement to hard granite. Integrator reset is used as a technique to bring down WOB after the boundary. PID values of $K_p = 5.362, t_i = 0.005055$ and $t_d = 0.000777$.
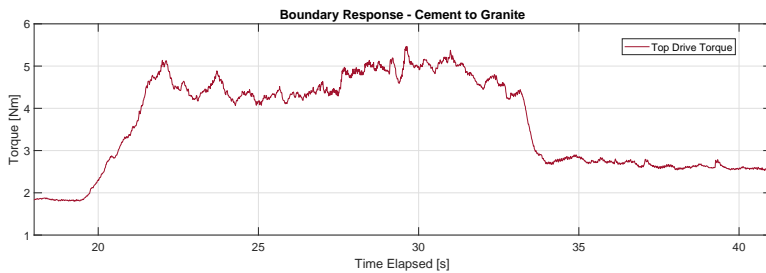
Figure 9.19: Run 1, 210518. Showing torque behaviour when hitting boundary from soft cement to hard granite. Torque is dropping considerably in the granite, due to shallow depth of cut, resulting in the bit meerely scratching the surface of the rock.
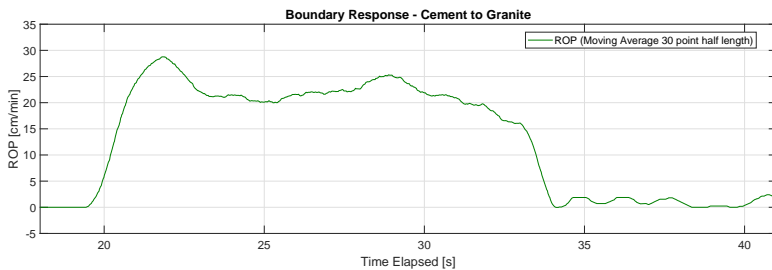
Figure 9.20: Run 1, 210518. Showing ROP behaviour when hitting boundary from soft cement to hard granite. Notice sharp drop in ROP entering granite.

a challenge. An example of this is shown in **Fig. 9.14**, where the softer cement is hit at around 63 seconds. The sharp drop in WOB is happening because the rock ahead gives in more easily, and that the motor at the very instant of the boundary still pushes with the same rotation as in the formation above. As time goes, the controller detects the measurement is beneath set point, and the proportional gain as well as the integrator delivers more control output to bring weight back up. Should the difference in drillability be more extreme, the more difficult such a boundary would be to handle. This is because weight would drop even further, resulting in a large gap between measurement and set point. Should the controller be tuned too aggressively with either gain or integral effect, this weight drop will result in an overshoot. Again, this could be handled by integral reset, which could be applied at a certain weight threshold above set point - for instance 15 kg.

9.3 Bottom Hole Assembly

One of the purposes of the new custom miniature BHA is to reduce frequency of twist-off. It attempts to do so by being light, reducing the mass discrepancy between the drill pipe and BHA. The BHA is light because the primary stabilizing sub is short. Consequently, the light BHA provides less stability downhole. The custom BHA is modular. Additional stabilizing subs may be assembled below the main sub to increase overall stabilizing length at the cost of more weight.

The team intended to investigate the trade-off between a light and short BHA to a long and heavy one by drilling with different BHA configurations. A key question is how short the downhole stabilizers can be before compromising hole quality. Unfortunately, the additional stabilizing subs used to increase length broke during other testing before BHA configuration was properly investigated. The subs broke because one of the threaded pins was too thin and weak. A redesigned stronger sub would have been manufactured and tested had there been more available time. The broken subs are depicted in **Fig. 9.21**.

9.3.1 Dynamic Stabilizer

The stabilizing subs that broke allowed freely moving masses to counteract lateral vibrations in the drill string. The term *dynamic stabilizer* was used for the concept. Unfortunately, no designated testing of the effect of a dynamic stabilizer was done before the sub broke. Perhaps a similar but more robust solution may work.

9.4 Drill Bit

Testing and comparison of bits are motivated by several aspects. The Drillbotics competition allows for use of any bit, as long as it has been designed by the team. The ultimate goal of the bit testing session is to select a single bit for use in the competition, a bit that is deemed to be *best*. Determining which bit is better impacts further tuning of drilling parameters and competition performance. Secondly, it is of educational interest to investigate which bit parameters primarily affect drilling on such a small scale. Hopefully, next

Figure 9.21: Broken pin with threads on the dynamic stabilizer subs. The broken male part is stuck inside the corresponding female part.

year's team can learn from this year's bit design and further improve it. The research may also be applied outside of Drillbotics.

Three bits have been tested: the bit provided by DSATS for the on-site test, the custom bit described in section 6.4 and a bit purchased on Alibaba Express for testing last year. For ease of reading, the bits will be referred to as the DSATS, NTNU and Alibaba bit, respectively. The bits are depicted in **Fig. 9.22**. Neither the DSATS bit nor the NTNU bit had been used prior to these tests, while the Alibaba bit had been used regularly for some time. The bits are compared based on tests in two different rocks: shale and granite.

Optimal drilling parameters may vary for different bits in different formations. To map performance over the operational range of drilling parameters, all tests are run with a sequence of change in both WOB and RPM. The former is increased step-wise, while simultaneously ramping up and down the latter. Hopefully, an overall best-performing bit may be identified. While WOB and drill string rotation *set points* are equal for all compared tests, *measured* parameters may vary due to differences in bit-rock interaction or other factors. Consequently, data may be unrepresentative and affected by variance or error on a small scale, however the *trends* over time are indicative. All tests are run with PID controller gains tuned with the Alibaba bit. Thus, the rig should have more issues maintaining set points with the other bits. A small selection of test results are available due to considerable bit wear and damage to cutters during the tests.

When analysing bit performance, it is important to fully define which bit qualities are relevant when drilling with a miniature rig and the environment it drills in. For instance, there is a well-known trade-off between ROP and bit aggressiveness at the cost of vulnerability

Figure 9.22: Drill bits involved in performance testing. From left to right: DSATS, NTNU and Alibaba bit. The bits are not to scale.

to vibrations, stability and bit damage. An autonomous drilling rig benefits from reliable and consistent bit-rock response and a bit that provides operational integrity. Since the primary goal is to perform well in the competition, bit evaluation is closely related to how performance in the competition is judged. In a somewhat successive order, the bits are evaluated by ROP, torque, hole quality, bit wear and ease of use.

9.4.1 Rate of Penetration

ROP measured while drilling is filtered data, as described in section 8.7.4. These tests mainly use ROP based on a 5 seconds interval. **Fig. 9.23** shows ROP as a function of time for the three bits drilling with 30 kg WOB set point in shale. For 28 seconds, drill string rotation is ramped down from 1800 to 700 RPM with a constant WOB set point. By studying the presented graph, one may observe that initially, at the highest drill string RPM, all three bits drill relatively fast. As rotational velocity is reduced, ROP decreases for all bits. The Alibaba bit performs worst, generally drilling at speeds around 0.5 cm/min, never reaching more than 2.2 cm/min. The DSATS and NTNU bits drill faster. Although ROP varies a lot over the course of the test, they drill at average speeds of 2.1 and 2.0 cm/min over the course of the test, respectively. At lower RPMs, the NTNU bit performs slightly worse than the DSATS bit. ROP of the NTNU bit appears to oscillate more than the others. This is not the case, but rather a result of basing ROP on the position 1 second ago rather than 5.

Equivalent results from drilling with 40 kg WOB set point and drill string rotation ramping up from 700 to 1800 RPM is shown in **Fig 9.24**. The trend is somewhat similar to that of 30 kg WOB set point: the DSATS and NTNU bits drill significantly faster than the Alibaba bit, penetrating the shale at average speeds of 3.7 and 4.4 cm/min, respectively. They alternate at drilling fastest, making it difficult to conclude if one is faster than the
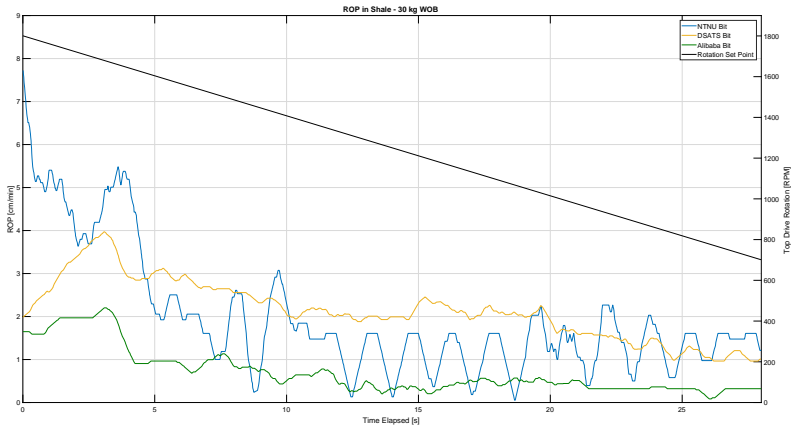
Figure 9.23: ROP in shale with 30 kg WOB and rotation decreasing from 1800 to 700 RPM.

other. The ROP peak between 15 and 20 seconds for the NTNU bit is possibly explained by a short burst of higher measured WOB. The Alibaba bit struggles to make any decent progress over the course of the test, drilling at speeds of less than 1 cm/min.
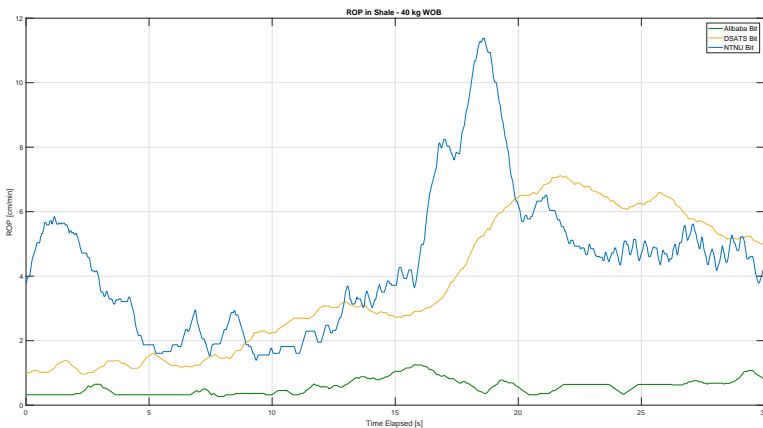
Figure 9.24: ROP in shale with 40 kg WOB and rotation increasing from 700 to 1800 RPM.

Fig. 9.25 shows ROP when drilling in granite. The test runs a sequence of WOB set points from 15 to 40 kg, incrementing 5 kg every 30 seconds. For each WOB set point, drill string rotation is gradually ramped either up or down between 700 and 1800 RPM. Due to a mistake when running the DSATS bit test, its rotation cycle is opposite of that of the other bits. This is evident by ROP cycles (increasing and decreasing trend) that are out

of sync and alternate between each other. Since WOB is increased for every half cycle, the next peak always outperforms the previous. Regardless, the plot provides valuable information. All bits drill considerably slower in the hard granite compared to in shale. At 40 kg WOB, both the DSATS and NTNU bits are able to drill around 2 cm/min. Recall that at 40 kg in shale, they show tendencies of drilling consistently at 4-6 cm/min. Again, the Alibaba bit lags behind the others with an average ROP around 0.25 cm/min and a somewhat consistent gap of 0.5-1 cm/min.

Based on ROP, the data presented clearly indicates that the DSATS and NTNU bits are faster than the Alibaba bit. However, it cannot, with certainty, be concluded that either of the two drill faster than the other.
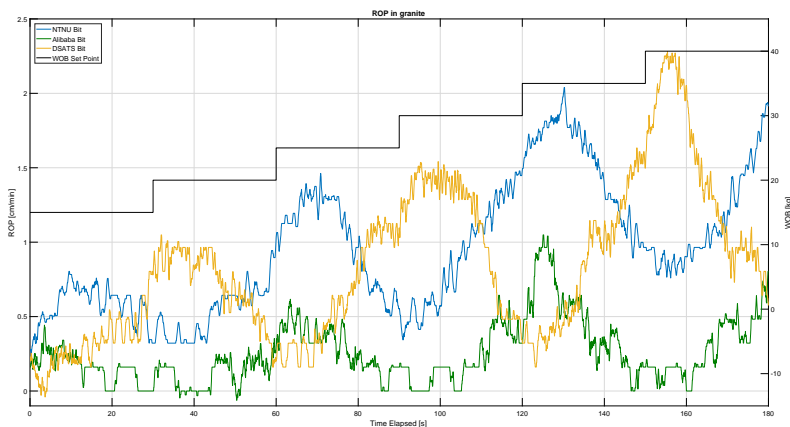
Figure 9.25: ROP in granite with WOB increaseing from 15 to 40 kg with 5 kg increments. Drill string rotation alternates between ramping up to 1800 RPM and down to 700 RPM for each WOB set point.

9.4.2 Torque

Torque measured in the top drive motor reflects aggressiveness of a bit. Based on ROP results, the DSATS and NTNU bits appear more aggressive than the Alibaba bit. Torque is an important measure due to the amount of twist-offs that is experienced with the miniature rig. Avoiding drill string failure and drilling autonomously depends on reliable and consistent parameters. Preferably, torque variation should be limited. Torque relative to ROP is indicative of bit efficiency.

Fig. 9.26 shows drill string torque measured by the top drive motor for all bits drilling in shale with 40 kg WOB set point. The data is collected from the same test as in **Fig 9.24** (i.e. drill string rotation is steadily increased from 700 to 1800 RPM). The slower Alibaba

bit generates low torque. Over the course of the test, it drills with rather consistent torque between 2.5 and 3 Nm. The Alibaba bit is the only bit with bevelled cutters, which may explain why it is non-aggressive with a short depth of cut. Likewise, the relatively fast and aggressive DSATS bit generates relatively high torque in the range 7 to 8 Nm. The NTNU bit drills at considerably lower torque. It generally drills with 3 Nm less torque than the DSATS bit, which is only around 1 Nm more than the Alibaba bit. This may possibly be a result of higher cutter density. Torque variation is larger for the NTNU bit, with two periods of increased torque levels, both lasting for several seconds. There is no apparent relationship between drill string rotational speed and torque for any of the bits. Comparisons at other WOB set points, for instance at 30 kg WOB, show similar results.
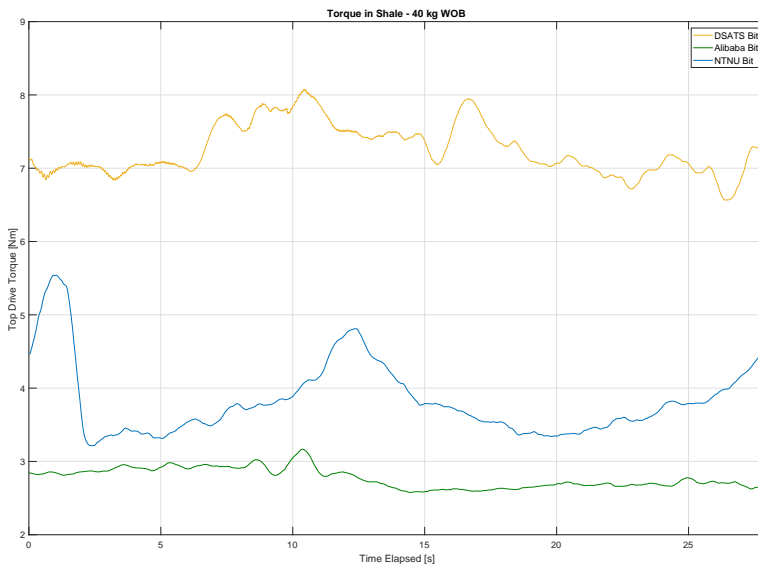
Figure 9.26: Torque in shale with 40 kg WOB and rotation increasing from 700 to 1800 RPM.

More context is provided by relating torque to ROP. **Fig 9.27** shows a scatter plot of torque and ROP in the same shale experiment with 40 kg WOB (i.e. a combination of **Fig 9.24** and **Fig. 9.26**). On this graph, a *good* bit is one that plots close to the upper left corner: such a bit yields high ROP and low torque. At the other end of the scale are bits that generate low ROP with high torque. Such bits plot in the lower right corner. Considering by the graph, it is evident that, in shale, the DSATS bit generates excessive torque without outperforming the NTNU bit in terms of ROP. The NTNU bit is more efficient. Torque variations are larger with the NTNU bit, ranging from 3.2 to 5.5 Nm as opposed to between 6.5 and 8 Nm with the DSATS bit. The Alibaba bit presents itself as reliable, gentle and consistent with the least variation in torque.
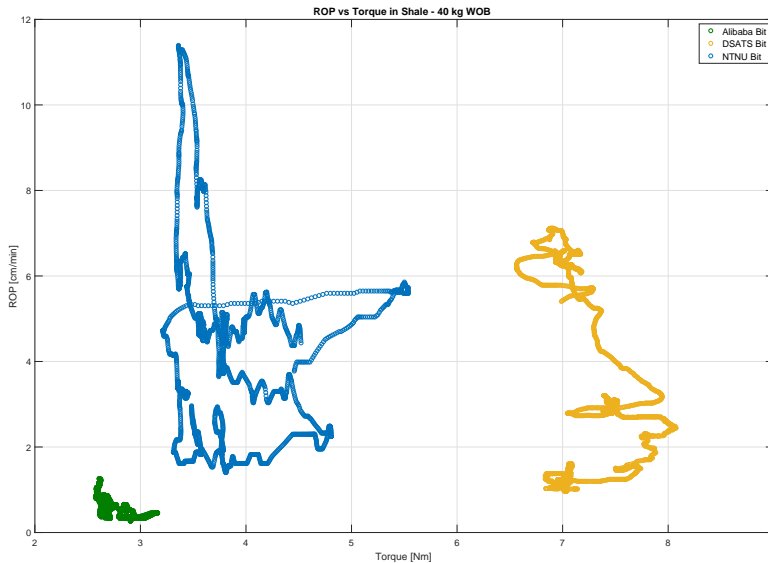
Figure 9.27: Relationship between torque and ROP in shale with 40 kg WOB and rotation increasing from 700 to 1800 RPM.

Fig 9.28 shows a scatter plot of torque and ROP in granite. The data is from the tests where WOB is increased in steps from 15 to 40 kg with increasing and decreasing drill string rotation (as shown in **Fig. 9.25**). The plot indicates similar trends as the one in shale, although at generally lower torque and ROP for all bits. This suggests a reduction in depth of cut in the hard granite. Again, the NTNU bit drills at similar speeds as the DSATS bit with lower torque. However, the discrepancy between the two is smaller. Torque variation trends are different than in shale: variation in torque for the DSATS bit is significantly greater, ranging from around 2.2 to 5.5 Nm. The NTNU bit torque ranges from 1.6 to 3.5 Nm. The Alibaba bit operates around 2-2.8 Nm in granite, which is less than in shale. It continues to produce the most reliable results.

9.4.3 Bit Damage

After running the tests in shale and granite, substantial bit damage and abrasion were evident on the NTNU and DSATS bits. When retrieving the DSATS bit after the granite test, one of the cutters was chipped. The chipped cutter is shown in **Fig. 9.29**. At that time, the bit had gone through approximately 15 cm cement and 13 cm shale preceding the test in granite. No damage was evident after these tests. It is difficult to tell when it broke during the granite test.
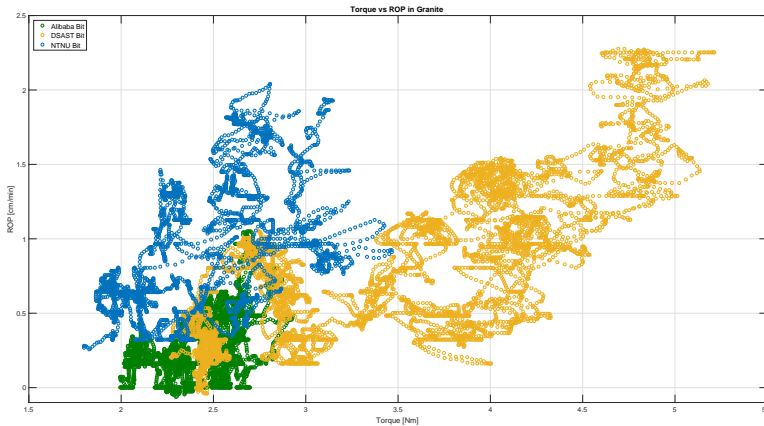
Figure 9.28: Relationship between torque and ROP in granite. WOB set points range from 15 to 40 kg with 5 kg increments. Drill string rotation alternates between ramping up to 1800 RPM and down to 700 RPM for each WOB set point. Every fifth sample from the test is shown (20 Hz).

The NTNU bit drilled 9 cm through cement before commencing tests in shale. During the first attempt to drill shale, one of the cutters got chipped and the drill string twisted off. Consequently, all tests with the NTNU bit in shale and granite were done with at least one chipped cutter. When the bit was retrieved after finishing the tests in granite, severe cutter damage was evident. Four of six cutters on the bit face were chipped. Furthermore, the cutters at the gauge were relatively mildly damaged. Cutter damage on the NTNU bit is shown in **Fig. 9.30**. The Alibaba bit, which had been used in many other tests prior to the bit comparison session, remained intact.

The chipped cutters suggest that bit damage is more significant than first anticipated when drilling on a minor scale. Reasons for this may be that - although the miniature rig operates with low WOB - weight is distributed over very few cutters. Also, it operates at very high rotational speeds. As would be expected, bit wear is a greater issue for bits that generate high torque.

9.4.4   Drilling Stability and Hole Quality

Fast and efficient drilling is of little relevance if the hole quality is poor and operation integrity is at risk. Drilling with the different bits caused different quality-reducing issues, such as vibrations, difficulties to maintain controller set points, grooves on the borehole wall and over-gauge wells. Vibrations in the drill string and rig structure are complex. Amongst several other factors, they depend on the bit-rock interaction. The bit comparison tests were run without accelerometers, neither topside nor downhole. Nonetheless, vibrations are indicated by oscillating WOB-measurements.

Figure 9.29: Chipped cutter on the DSATS bit.

Figure 9.30: Chipped cutters on the NTNU bit. Cutters at the gauge are less damaged than those close to the center.

Helical patterned grooves sometimes form on the internal borehole wall. No correlation between bit and borehole wall quality can be determined from the small selection of drilled holes. The grooves rather seem to be related to alignment, hardness of the rock and drilling parameters when drilling the pilot hole.

The nominal diameter of the holes drilled in shale measure approximately 3.15", 3.05" and 2.90" for the DSATS, NTNU and Alibaba bits, respectively. A hole drilled with the NTNU bit is shown in **Fig. 9.31**. The large hole diameter drilled with the DSATS bit is possibly

explained by the long distance from the bit face to the lower stabilizer. Upon inspection, it was discovered that the Alibaba bit measures 1.1" in OD, which is smaller than the requirement of 1.125". This explains the low gauge of holes drilled with the Alibaba bit, and disqualifies it from being used in the competition.

Figure 9.31: Measured OD of a hole drilled in granite with the NTNU bit.

Fig. 9.32 shows a plot of drill string rotational speed in shale for the DSATS, NTNU and Alibaba bits. The figure shows a run with WOB set point increased from 30 to 40 kg in a single step, halfway through the experiment. The plot compares drill string rotational velocity set points to measured rotational velocities for all three bits. After 28 seconds, the drill string rotates at 700 RPM and begins to ramp up. As evident by the graph, the top drive struggles to maintain its RPM set point when drilling with the DSATS bit. This is a result of stalling in the top drive motor, possibly due to high drill string torque. As evident by the graph, this is not an issue for the Alibaba and NTNU bits. Results when incrementing at higher WOB set points are similar. This suggests smoother drilling with the NTNU and Alibaba bit, which in light of the torque evaluation earlier is reasonable.

9.4.5 Ease of Use

Convenience when handling the bits is relevant because of the limited space on the miniature rig. Ease of use refers to practical issues of assembling and handling the bit when drilling. For day-to-day testing, setup time and consistency when testing impact quality and quantity of results. Setup time is less relevant for the on-site test. The team is allowed to assemble the drill string and drill a short pilot hole before commencing the competition run. During the competition, bit handling is only relevant in the case of dysfunctions that require reassembly.
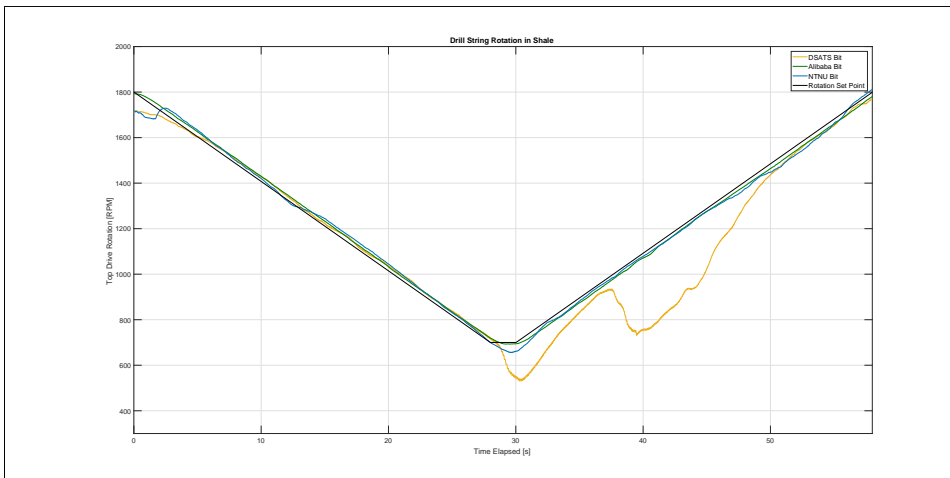
Figure 9.32: Drill string rotation measured in the top drive motor.

In terms of bits, the primary factor affecting ease of use is bit length. There is limited space between the surface of rock samples and the rig floor. Handling of the drill string is more convenient with shorter bits. The DSATS, NTNU and Alibaba bits are 139.7, 44.6 and 23.7 mm long, respectively. The DSATS bit is more difficult to handle, and cannot drill rock samples taller than 65 cm. It requires a longer riser than the one originally designed for the lower bearing to land inside it before drilling.

9.4.6   Overall Performance

Based on the data presented, the NTNU bit is selected for use in the competition run. It is selected primarily due to its efficiency of drilling with relatively high ROP at relatively low torque. The low torque allows use of higher operational parameters in the competition run while reducing the risk of twist-off. Bit integrity and stability is jeopardized by continued drilling with the damaged bit, as it is vulnerable to more cutter damage and eventually bit matrix damage. Therefore, the Alibaba bit should be used for further testing and development of the autonomous system. However, the NTNU bit performance in granite, where it drilled with at least one chipped cutter, is still considerably better than the Alibaba bit. The competition rock is 35 cm tall, and the bit is expected to remain functional throughout the rock. Future teams are encouraged to coordinate with Lyng Drilling for repair of the NTNU bit before further testing.

9.5   Estimator

The estimation algorithm was tested in different formations. An example run in basalt is shown in **Fig. 9.33**, where the formation was successfully identified. This is evident from
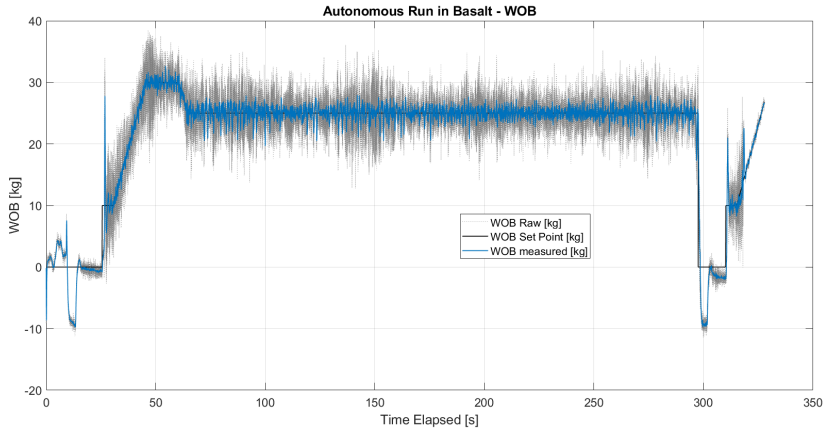
Figure 9.33: WOB for the autonomous estimator run in basalt. Notice spike at 25 seconds, correlating with the chaotic behaviour in **Fig. 9.36**.

change in formation index as seen in **Fig. 9.35**. The autonomous run starts with a tagging sequence, before running through the states as described in **Fig. 9.34**, eventually reaching steady state drilling in the identified formation. A new boundary layer was detected slightly before 300 seconds, which in this case was a gap between two basalt plates. The script was aborted due to an unexpected twist-off. The estimator parameters are shown in **Fig. 9.36**, describing the convergence of the three thetas. The beginning is coloured by sharp changes, before reaching convergence.

However, running the formation estimator in autonomous mode has not been consistently successful. Typical symptoms include discrepancy between theta-sets in the same formation, and misinterpreting one rock for another. Interestingly, there seems to be difference in rock-detecting performance when comparing autonomous estimator runs to those run non-autonomously in a standalone script.

Two autonomous runs were done in seemingly identical cement, converging to estimator parameters as listed in **Table 9.9**. Notice the big discrepancy from run to run, especially noticable for θ_1. Further testing in autonomous mode has proven that the estimator has difficulties correctly identifying rock type, due to inconsistent convergences between runs. Running the estimator sequence in a standalone script, done before implementing it in fully autonomous mode, gave different results. Listed in **Table 9.8** are eight runs done in cement running a non-autonomous standalone script. Despite certain outliers, a clear trend can still be seen. The cement cannot be expected to be perfectly homogeneous, and response will vary from run to run. **Fig. 9.37** gives the convergence of estimator parameters for a non-autonomous run. Comparing convergence rate with that of the autonomous run in **Fig. 9.36**, it is evident that the non-autonomous parameters are much more well-behaved and quick to settle. This behaviour is likely to be the cause of the inconsistent performance achieved running the estimator in autonomous mode. It is possible that something
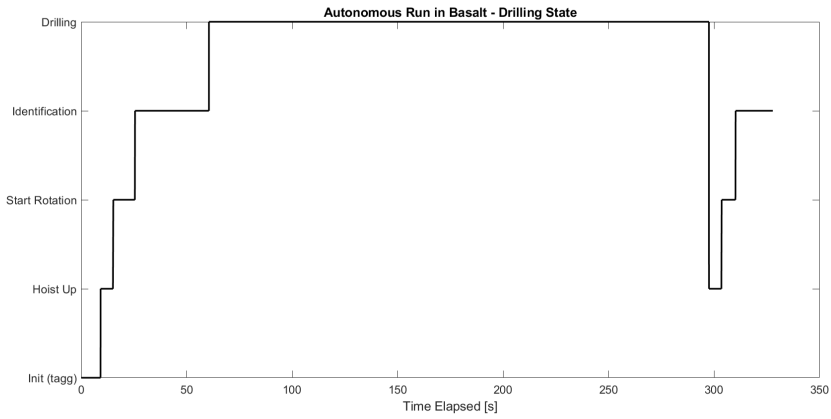
Figure 9.34: Driling states for the autonomous estimator run in basalt.
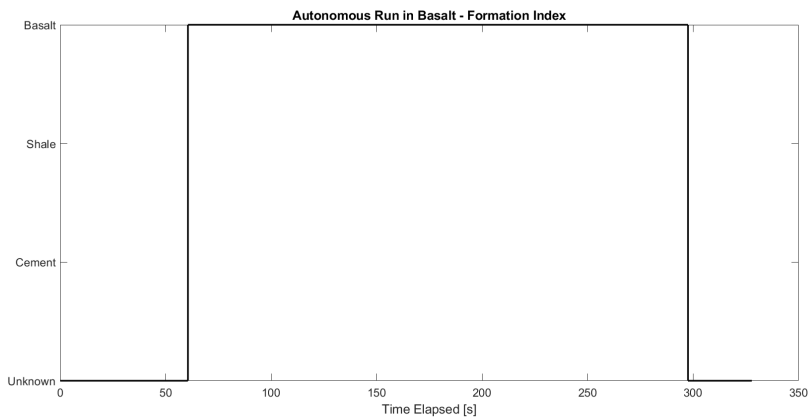
Figure 9.35: Formation index for the autonomous estimator run in basalt.
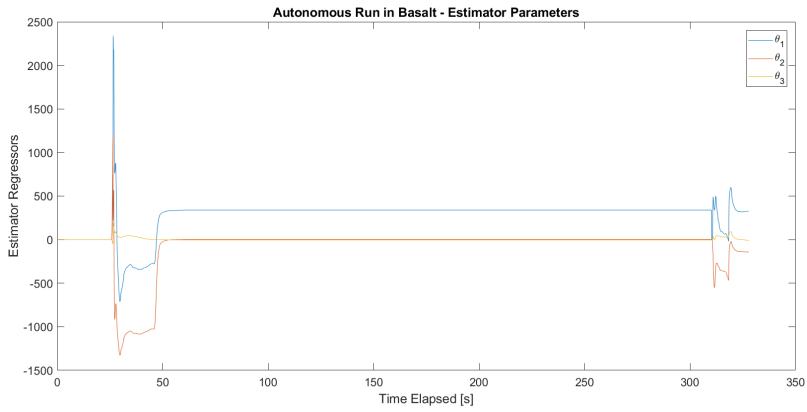
Figure 9.36: Estimator parameters for the autonomous run in basalt. Chaotic behaviour can be seen before reaching convergence.
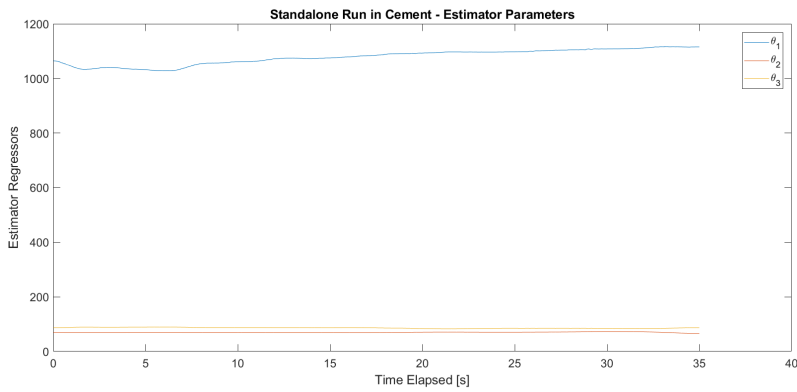
Figure 9.37: Estimator parameters for non-autonomous run in cement. Notice quick convergence and small discrepancy between initial and final values.

Table 9.8: Comparing eight sets of estimator parameters from non-autonomous runs. Despite some outliers, a clear trend can be seen between runs, allowing for more robust formation identification.

Run	θ_1	θ_2	θ_3
1	1062	81	138
2	794	73	99
3	919	69	98
4	1064	70	87
5	1115	66	87
6	1196	62	95
7	1143	50	120
8	1245	41	121

Table 9.9: Estimator parameters for autonomous runs in seemingly identical cement. A large difference between the runs is evident.

Run	θ_1	θ_2	θ_3
1	1775	41	81
2	820	21	77

was done wrong when implementing the estimator in the autonomous script. A theory of the team is that the tagging sequence is interfering with the estimation sequence. Waiting a few seconds after tagging before initiating the estimation state might be worth investigating, to let important parameters such as WOB and ROP stabilize before being used in calculations.

Due to limited time, the team has not been able to get to the bottom of this issue. The concept of the rock estimator has still been proved to be working, in particular when run non-autonomously. Future teams are encouraged to investigate and develop this further, hopefully evolving it into a more robust solution.

9.6 Rock Response

The drilling machine algorithm attempts to detect and estimate rock formations to select optimal drilling parameters. Optimal drilling parameters assumes a founder point that yields the most efficient drilling, as discussed in section ref. Essentially, at a certain set of WOB and drill string rotational speed, an increase in any of the two gives a non-linear increase in ROP. That set of parameters is known as the founder point, and is unique for different types of rock. To optimize the drilling algorithm, tests were run in different rocks to determine the founder point, or to investigate if the miniature rig is capable of reaching the point of foundering. These tests are referred to as rock response tests.

To quickly identify if the miniature rig reaches the founder point with normal operating parameters, a method to efficiently map a broad spectrum of WOB and drill string rotation set points is used. The method is as follows: for one WOB set point, rotational speed is ramped up from 700 to 1800 RPM. Then, the WOB set point is incremented by a discrete value, e.g. 5 kg, before ramping rotation down from 1800 to 700 RPM. Then, the WOB set point is incremented yet again before ramping back up to 1800 RPM. The cycle is repeated until a desired interval of WOB and rotating speed is covered. ROP is computed as described in section 8.7.4 and plotted together with corresponding drilling parameters.

Fig. 9.38 shows results of a rock response test in granite. The 3D plot relates WOB and drill string rotation (given as rotation in the top drive motor) on the x- and y-axis to ROP on the z-axis. Due to large vibrations and risk of drill string failure when drilling with a combination of high WOB and low RPM, the test ramps between 1400 and 1800 RPM at higher WOB. As indicated in the figure, data is plotted yellow for higher ROP and purple for lower ROP. The trend is generally that higher WOB and drill string rotation generate higher ROP. **Fig. 9.39** shows the same graph plotted from above as a 2D plot. Again, ROP is reflected by the colour of the data points. Lower WOB and rotational speed give lower ROP. This is seen clearly by purple and blue colours dominating the lower left corner of the graph. At higher drilling parameters, ROP is higher. The plot shows no indication of foundering. If a founder point was reached, at some point, higher WOB or drill string rotation would cause less of an increase in ROP. This would be visible as a larger area of yellow-like colours.
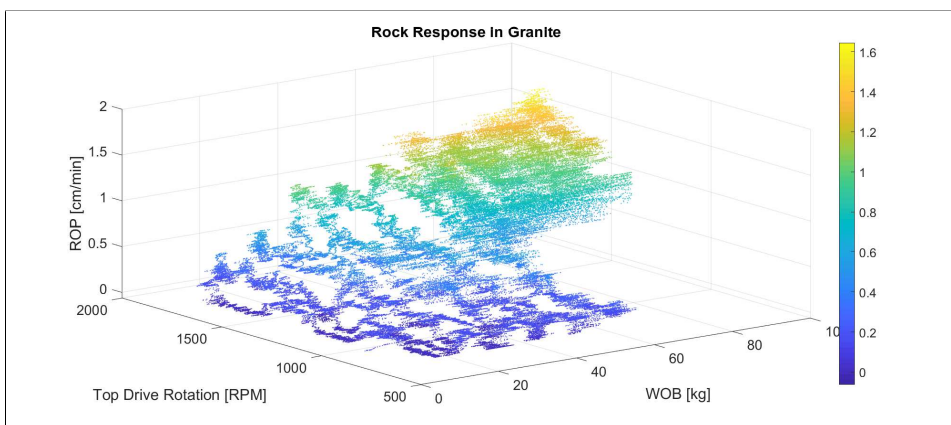
Figure 9.38: Isometric plot of rock response in granite. ROP is indicated to the colour of the data points, and is plotted for a variety of WOB and drill string rotation parameters.

Fig. 9.40 shows the same data set with ROP plotted against WOB. Now, colours are used to indicate drill string rotation. The absence of a founder point becomes more evident by this graph. Yellow colours dominate the top of the graph, and ROP increases somewhat linearly with WOB. If the miniature rig in fact managed to reach a founder point, at some
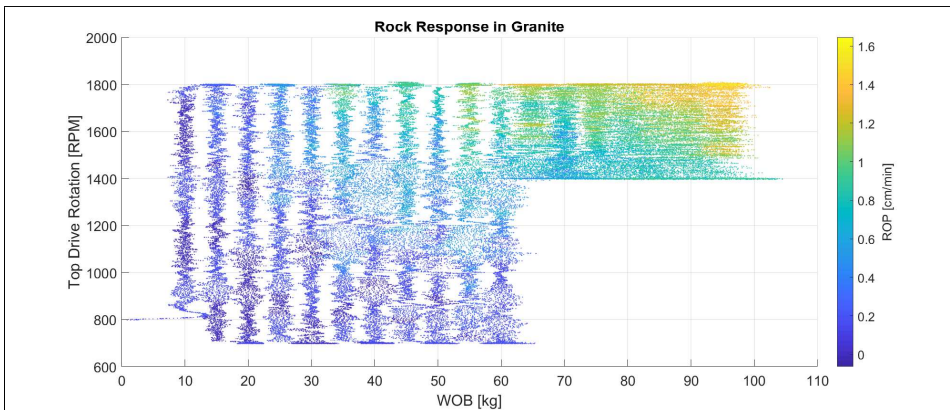
Figure 9.39: RPM vs WOB plot of rock response in granite.

WOB for some RPM, the graph would be concave. Essentially, the plots presented reveal that higher WOB and drill string rotation always give higher ROP in granite when drilling with parameters within the operational window of the miniature rig.
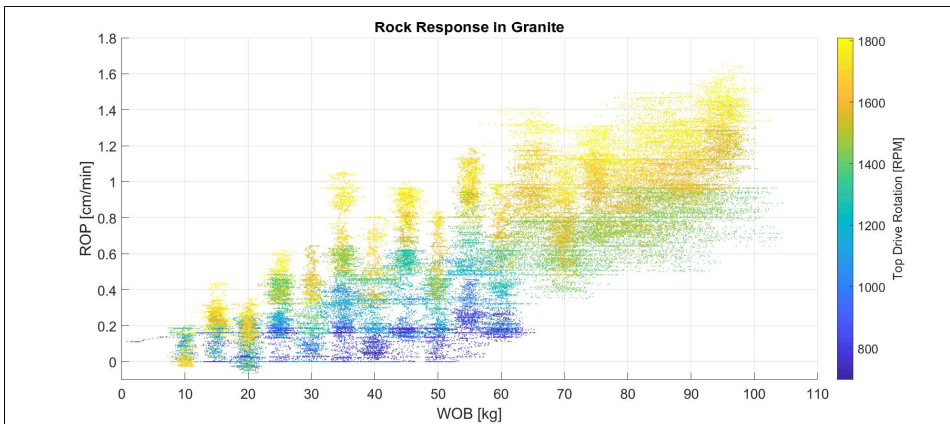
Figure 9.40: ROP vs WOB plot of rock response in granite.

Similar results are found for shale. **Fig. 9.41** shows an isometric plot of ROP as a function of WOB for 30, 40 and 50 kg set points and drill string rotation ramping between 700 and 1800 RPM. Again, higher WOB and RPM give higher ROP.

Fig. 9.42 shows ROP plotted against WOB for the same shale data. Rotational speed is indicated by the colour of the data points. Higher RPM is yellow and lower RPM is purple. As seen by the plot, the relationship between ROP and WOB is linear also for shale. More interestingly, at higher WOB, it seems as if the highest rotational speeds give lower ROP than intermediate speeds. This is seen as yellow data points gathering close to the mean
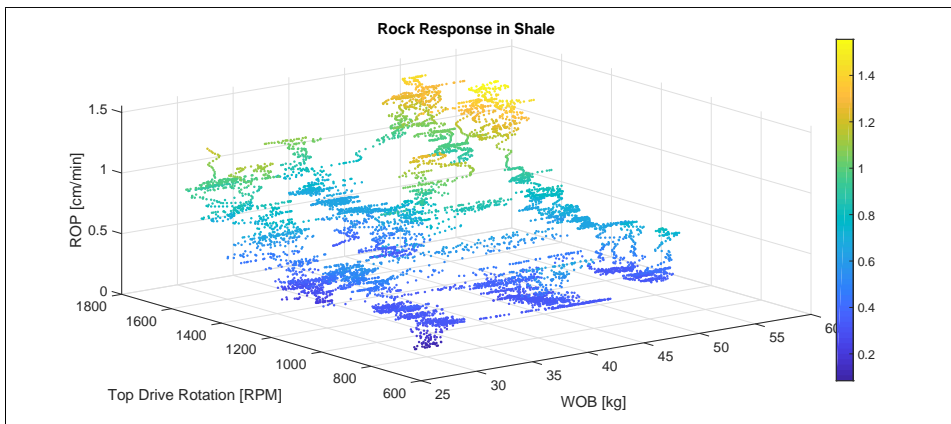
Figure 9.41: Isometric plot of rock response in shale. ROP is plotted for a variety of WOB and drill string rotation parameters.

of the ROP for each WOB set point column. It is important to note that this test was run with the non-aggressive Alibaba bit. The bit has a low depth of cut, and ROP is generally very low. Such conditions won't necessarily benefit from higher rotational speed. Similar plots for the more aggressive DSATS and NTNU bits don't show this trend, but rather that higher RPM gives higher ROP. Data from drilling with the DSATS or NTNU bit is not presented for the following reason: the shale formation used for testing consists of several layers of thin shale rocks stacked on top of each other. When the rig drills through one of the interfaces between two shale layers, there is an instantaneous burst in ROP. The DSATS and NTNU bits drill through the shale too quickly. Their rock response plots are greatly affected by these bursts of ROP, and are difficult to present without filtering away too much data. Nonetheless, there is no indication of a founder point when drilling with these bits.

As a consequence of not finding a founder point, there is no benefit from detecting and determining which layer is being drilled in the competition. The miniature rig will not drill more efficiently nor faster by knowing which rock it drills in. The algorithm would always tell the control system to drill with the highest possible parameters that don't compromise drill string integrity. As discussed in section 8.7.4, rock estimation runs a sequence of drilling parameters to determine rock layers. The estimation sequence takes more time than regular drilling. If a founder point is never reached, rock estimation is wasted time. Based on these results, it was decided not to run rock estimation in the competition run. Nonetheless, layer detection remains an integral part of the evolution of automatic drilling, and is perhaps the most interesting aspect of this project that can be brought to full scale.
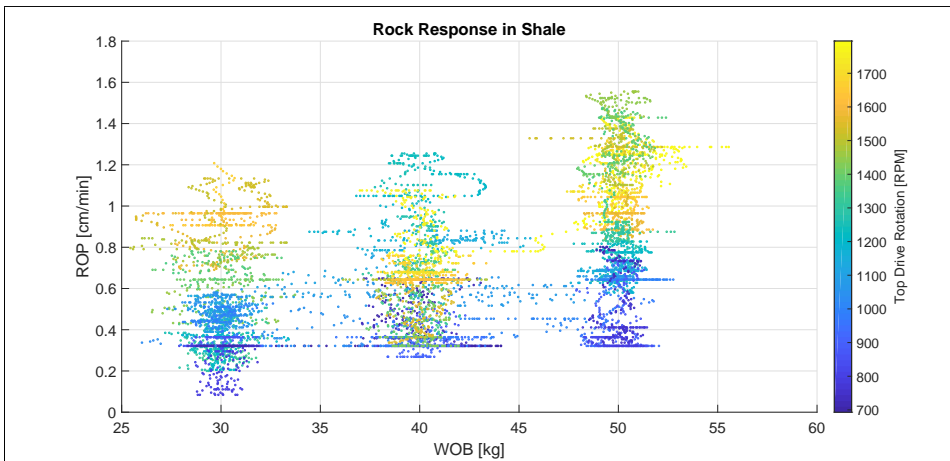
Figure 9.42: ROP vs WOB plot of rock response in granite.

9.7   Hydraulics

Increasing the flow rate is necessary for transporting larger cuttings out of the wellbore. As expected, the pressure increases more rapidly for higher flow rates through the smaller nozzles. To verify the theory of pressure drop in the system, a flow test was executed. The results of the flow test are presented in **Table 9.10**.

Table 9.10: Shows the results from the flow test. The test was run with 0, 300, 600 and 900 RPM on the pump for nozzle sizes of 1.1 mm, 1.5 mm and 5 mm.

Nozzle size [mm]	1.1		1.5		5.0	
Pump rate	q [l/min]	Pressure [bar]	q [l/min]	Pressure [bar]	q [l/min]	Pressure [bar]
0	6.5	5.3	7.0	5.3	9.0	5.0
300	6.6	5.3	7.3	5.3	9.3	5.3
600	11.9	13.4	11.4	12.0	11.7	7.0
900	17.0	25.2	16.6	21.8	18.2	12.8

The results in **Table 9.10** are graphically presented in **Fig. 9.43**. The trend line fits well to the second order trend line. The figure also includes numerical formulas for the pressure as a function of flow rate for the different nozzle sizes.

To calculate the minimum flow velocity in the annulus, **Eq. 6.1**, **6.2** and **6.3** are used. The result is presented in **Fig. 9.44**. The calculations include a safety factor of 20% as sufficient hole cleaning is crucial to prevent stuck pipe.

As discussed in section 6.3, the cutting size depends on which formation is being drilled. Since the flow rate is set to a constant value throughout the whole run, the set point should
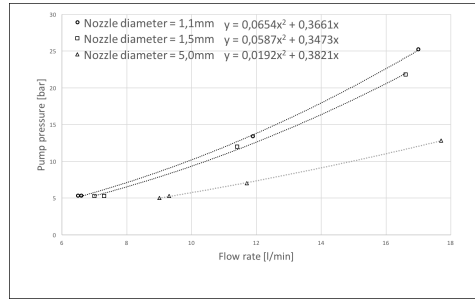
Figure 9.43: Showing the relationship between flow rate and the pressure required from the pump obtained from the flow test. A regression model in Excel has been used to obtain the formula for each nozzle size.
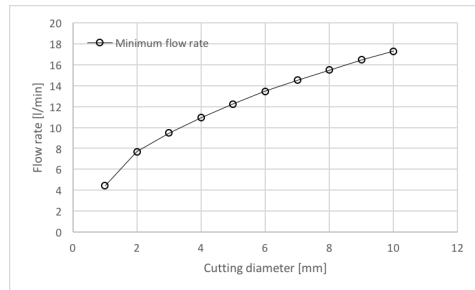
Figure 9.44: The graph shows the required flow rate for transporting cuttings out of the wellbore. The flow rate is conservative and calculated for spherical cuttings with a density of 2,640 kg/m^3.
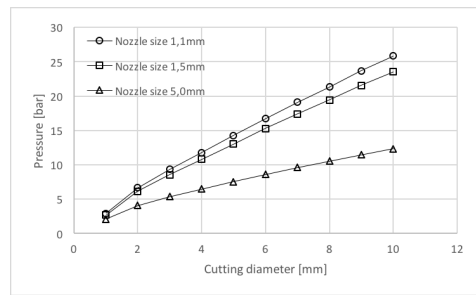
Figure 9.45: The graph shows the pump pressure as a function of cutting size for the different nozzle sizes.

Table 9.11: The table shows the pressure drop in the different components and the total pressure drop. The total pressure drop does not include the pressure drop over the nozzle.

q [l/min]	Δp_{tube}	Δp_{swivel}	Δp_{pipe}	Δp_{BHA}	p^*_{system}
10.0	0.1	0.2	0.3	0.0	0.6
13.4	0.1	0.3	0.5	0.0	0.9
18.0	0.1	0.6	0.8	0.1	1.6

be designed to transport even the largest expected cuttings. For the driller to be able to choose suitable flow rate based on pressure readings, pump pressure is plotted as a function of cutting size based on combining **Fig. 9.44** and the regression model made from **Fig. 9.43**. The result can be seen in **Fig. 9.45**.

Having a high internal pressure is no longer considered to be beneficial, based on the discussion in section 7.1.1. The nozzle size is therefore chosen to be 5 mm. By inspecting the graph in **Fig. 9.45**, the required pump pressure for removing the largest expected cuttings set to 6 mm is 8.6 bar yielding a flow rate of 13.4 l/min.

9.7.1 Pressure Drop in the System

The pressure drop in the system is dependent on the flow rate. The pressure drop in the system is calculated using **Eq. 6.5** and **Eq. 6.6** and is summarized in **Table 9.11**.

The pressure drop over the nozzle is 7.7 bar and is calculated using **Eq. 6.10**. The weakest point concerning twist-offs is at the end of the pipe in the transition with the mechanical connection. When the pipe twists, the pressure in the system will drop as the water does not need to go through the nozzle any more. For twist-off detection, the pressure reduction after twisting the pipe needs to be noticeable for the driller. When twist-offs occur, the pressure drops to 6.2 bar as it still needs to exceed the pressure drop from pump through the pipe. During normal drilling the pressure will be constant, and a pressure drop of 2.2 bar when twisting off should be more than sufficient for the program and the driller to
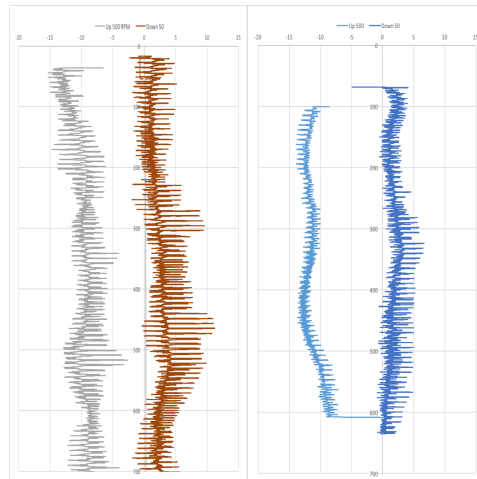
Figure 9.46: The graphs shows the WOB measurements as a function of position of the ball screw. The graph to the left shows the results before reassembling the roller guide and the graph to the right shows the results after.

react.

9.8   Ball Screw

When hoisting at a constant velocity, the measured WOB should be constant both when going up and down. During testing, oscillations in the WOB measurement were experienced. The amplitudes of the oscillations were nearly 9 kg at the most which makes using a PID controller on WOB hard. This also makes it difficult knowing how much weight the rock is actually exposed to and how much is lost in friction. The first attempt to solve the problem was to reassemble the roller guide and the guide frame to resolve any restrained forces in the system. The result can be seen in **Fig. 9.46**. From the results it is evident that considerable tension in the system was been relieved after reassembling the roller guide. The amplitude of the oscillations is halved, going from 10 kg to a little less than 5 kg.

9.8.1   New Ball Screw

Fig. 9.46 shows a huge improvement in the WOB measurement. Still there was an unexplained pattern in the measurement permeated through the whole test. When reassembling the rig in Phase I, it was discovered that the ball screw was bent. The bending of the ball screw was caused by the old setup of the load cell which allowed for movement in horizontal directions. The new load cell straightens out the screw causing some friction. A new ball screw was bought and implemented on the rig. A similar hoisting test was run to verify the improvement. The result can be seen in **Fig. 9.47**.
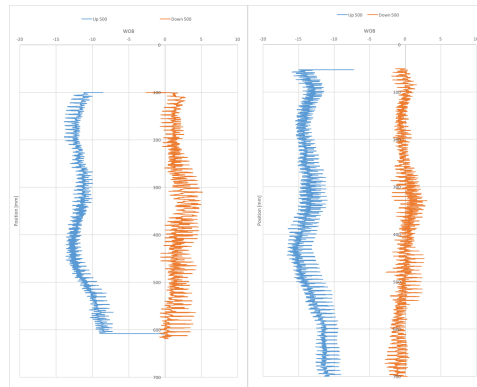
Figure 9.47: The graphs shows the WOB measurements as a function of position with the old (left) and the new ball screw (right).

After changing the ball screw the variations in WOB for hoisting up and down decreased even further. The trend line of the WOB measurements also became straighter with the new screw, especially when hoisting down. This confirmed that some of the irregular pattern was caused by the bent ball screw. There is still an almost constant gap of 15 kg between hoisting up and down. This gap is most likely caused by friction in the system which could be induced if the derrick is slightly shifted with an angle. When it comes to operating the rig, a gap between WOB when hoisting up and down can easily be handled it the offset value is constant and taken into account in the system. By studying the graph carefully, one can detect a pattern in the more rapid oscillations in WOB. Further inspection has shown that the period does not fit with one rotation of the ball screw which was first believed to be the case. The period may be equivalent to one rotation of the balls inside the ball screw, but this has not yet been verified.

Chapter 10

Competition

Ahead of the competition day, the miniature rig was moved to the center of the lab hall. This allowed for better visibility for the spectators, and improved floor leveling. Considerable time was spent to find the best spot in terms of where the floor was closest to being horizontal. The top layer of the competition rock was slightly tilted, most likely due to inaccuracies during construction, and not intended as a competition feature. The rig setup is intended to mount against a horizontal surface. Because of this, a mount was made for the competition rock, orienting it so that the drill bit would tag perpendicular to the formation surface. Further, four hooks were bolted to the floor, surrounding the test sample. This allowed the team to strap the formation firmly, preventing any movement and vibrations in the competition rock. A picture of the rig on the competition day is shown i **Fig. 10.1**, and a close-up on the formation is given in **Fig. 10.2**. The competition rock was drilled with the NTNU bit, and the full BHA configuration is shown in **Fig. 10.3**.

Figure 10.1: Showing the rig setup on the test day, accompanied by judges and team members.

Figure 10.2: Showing the formation located underneath the miniature rig on the competition day. Two straps are used to secure the formation, connecting to four floor-mounted hooks.

Figure 10.3: The final BHA configuration used in the competition run, featuring the NTNU bit, stabilizer housing DH sensors and pipe connection.

Figure 10.4: Showing the NTNU bit in its condition after drilling through the competition rock. Significant damage is evident on all but the gauge cutters.

10.1 Pilot Hole

Prior to the actual drilling run, a pilot hole of 0.5" was drilled in advance, as explained by the competition guidelines [20]. Based on experience, the team selected gentle parameters for the pilot hole, drilling with a constant 700 RPM, ramping WOB up to 15 kg. The weight on bit-graph for the run is shown in **Fig. 10.5**. The competition script worked as intended, where top drive rotation started after the initial tag and a slight hoist-up. Both RPM and top drive torque can be seen in **Fig. 10.6**. As shown in the figure, the top drive and consequently also drill string torque is well below the control limit. This is expected due to the low weight applied. All the different drilling states are shown in **Fig. 10.8**. To accomplish the slow drilling, the pilot was drilled at a low circulation rate, with no pump and pressure drive solely from the water supply network. The resulting pressure measurements are shown in **Fig. 10.7**, with the pressure running steadily at 5.4 bar as expected. Downhole sensor data can be seen in **Fig. 10.9** and **Fig. 10.10**. The pilot was drilled exclusively through homogeneous sandstone, reaching TD after 37.69 seconds.

10.2 Main Run

Following the pilot, the miniature rig was set to drill the main part of the hole. The same script was used to drill both this and the pilot, only adjusting input parameters. For the main run, a WOB set point of 50 kg was applied, alongside top drive rotation of 1300 RPM. **Fig. 10.11** shows the WOB plot for the main run, while top drive RPM and torque are given in **Fig. 10.12**. Notice that the torque lies just below the control limit of 6 Nm for the majority of the run, indicating good correspondence between drilling parameters and torque limit. By studying **Fig. 10.11**, it is evident that there is one major incident in the run, taking place at around 125 seconds. A large drop in WOB can be observed,
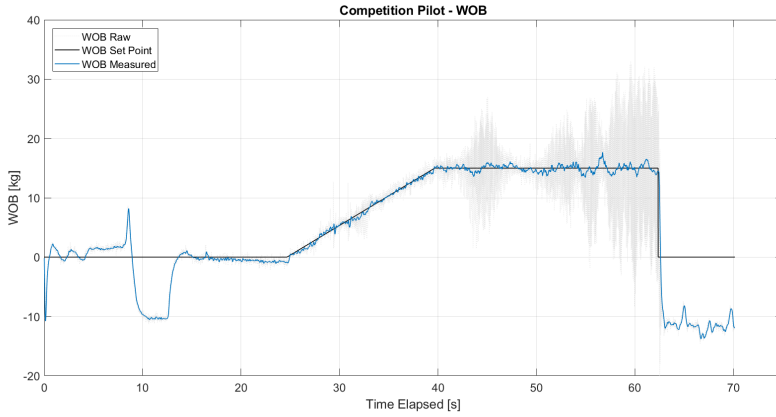
Figure 10.5: Showing the WOB graph from the competition pilot. The bit can be seen tagging for the first time slightly before 10 seconds, before hoisting up and starting rotation. Spudding the pilot commences at 25 seconds.
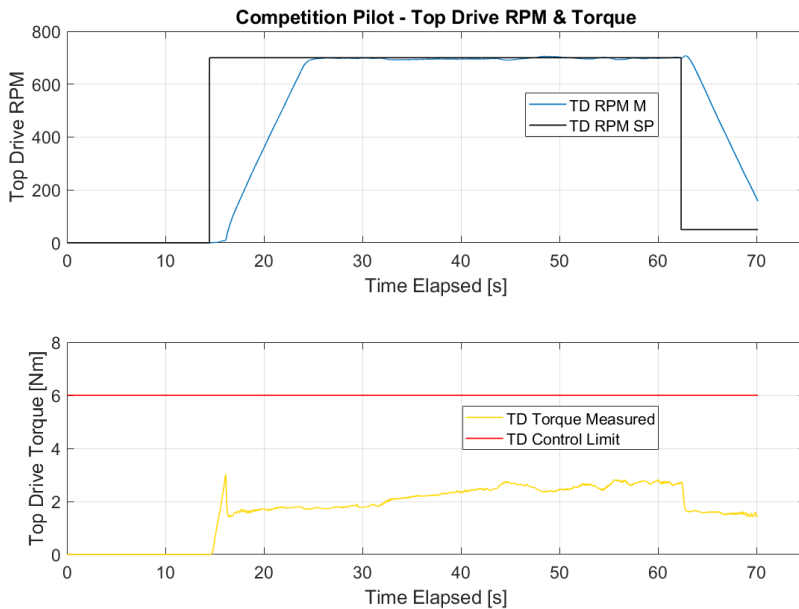
Figure 10.6: Showing the top drive RPM and torque for the competition pilot. Drilling commences first after the top drive has ramped all the way up to the intended set point of 700 RPM.
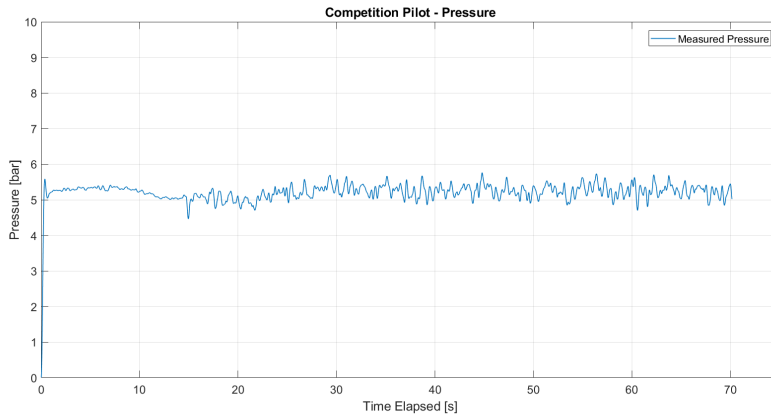
Figure 10.7: Showing pressure plot of the pilot run.
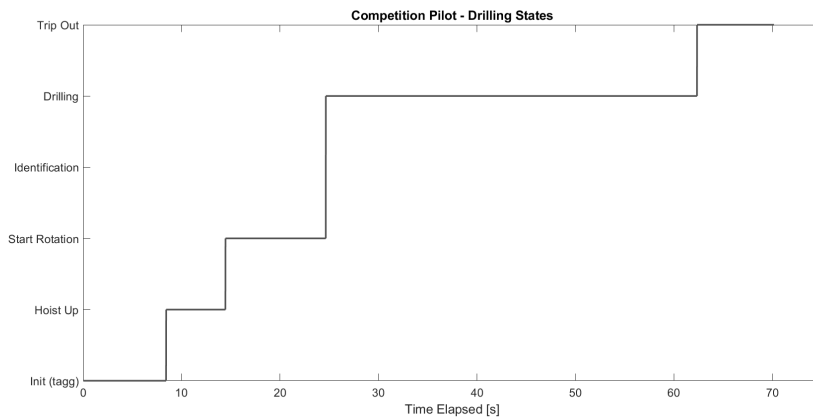
Figure 10.8: The different states of the miniature rig during drilling of the pilot hole.
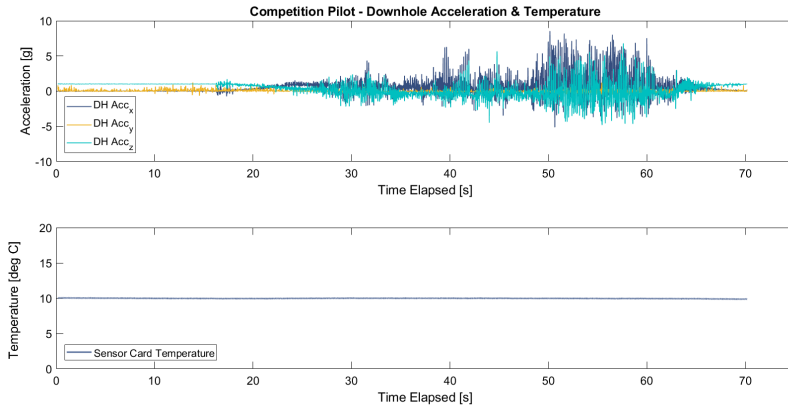
Figure 10.9: Showing the downhole accelerometer and temperature data for the competition pilot.
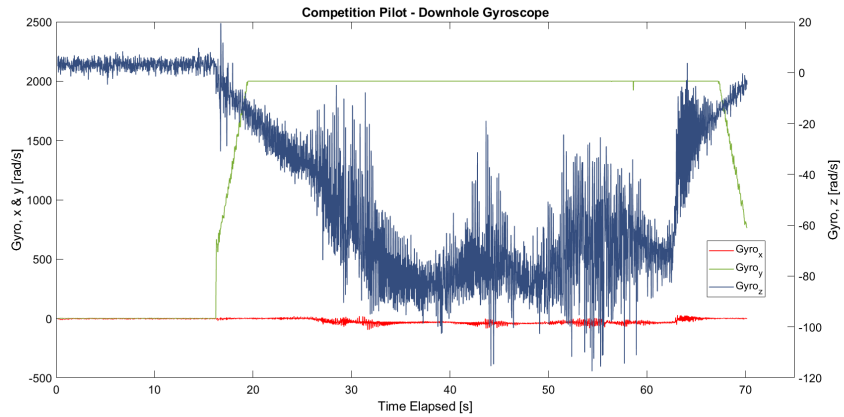
Figure 10.10: Showing downhole gyro data from the competition pilot. Connection was lost after drilling the pilot, making downhole data unavailable for the remaining section of the hole.
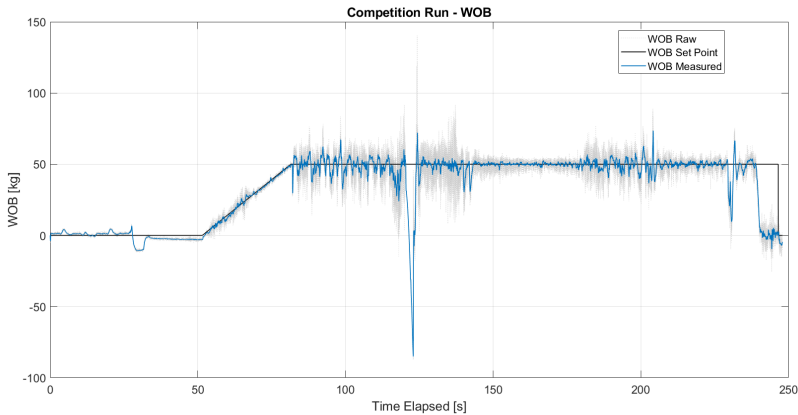
Figure 10.11: Showing the WOB graph for the main competition run, ramping to set point to avoid overshoot. The first section at constant weight reveals the controllers sub-optimal ability to run in soft rocks. A large overpull of 85 kg is noticeable at 125 seconds, followed by a smooth section hard rock drilling between 145 and 180 seconds. The dip at 229 seconds is investigated in **Fig. 10.16**.

hoisting up with an overpull of 85 kg. This comes as a result of torque build-up, evident in **Fig. 10.12**. The torque increase occurred when hitting a 45 degree inclined tile in the competition rock, after leaving a section of pebbled cement, where a peak ROP of 27.66 cm/min was reached. The team believes the inclined tile got shifted slightly downwards due to the massive impact load of the bit, causing the drill string to lock up entirely. The rig reacted as it should when torque surpassed the control limit of 6 Nm by pulling off bottom, causing the torque to drop. Rotation stopped due to the *internal* torque limit in the drive being reached, but commenced again as soon as the bit was free and the torque dropped. Interestingly, the circulation pressure increased at the very moment of the impact with the inclined tile, as seen in **Fig. 10.14**. The team cannot be certain of why this happened. A possible explanation can be that the internal sensor wire was slightly twisted due to a slip between connection and BHA during the high torque load. The twisted wire may have added an additional pressure restriction inside the pipe. The drilling dysfunction lasted around three seconds, and is not believed to have a major impact in the overall drilling speed or hole quality.

Further analysis of the drilling parameters reveals a smooth section of drilling between 145 and 180 seconds. This is evident in the WOB graph, but also from the top drive torque. Investigating the corresponding ROP graph shown in **Fig. 10.15** reveals this to be a somewhat hard layer, with slower drilling progress compared to previous layers - not considering the torque incident and hoist-up. Remembering the PID tuning described in section 8.2, the rig uses PID parameters for shale as a best-fit compromise between hard and soft rock performance. The smooth steady state performance in this section can be explained by the PID tuning chosen, where this rock seems to match closely in character-istics the one the controller initially was tuned for.
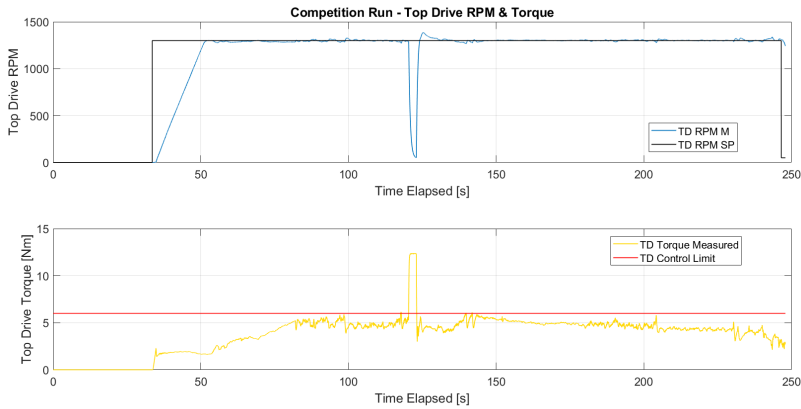
Figure 10.12: Showing the RPM and torque of the top drive for the competition run. RPM is ramped up by the internal drive controller to set point of 1300 RPM. Notice the sharp dip in RPM as the torque surpasses the internal drive limit at 125 seconds. When the string is lifted free off bottom the torque drops, automatically reinitiating rotation.
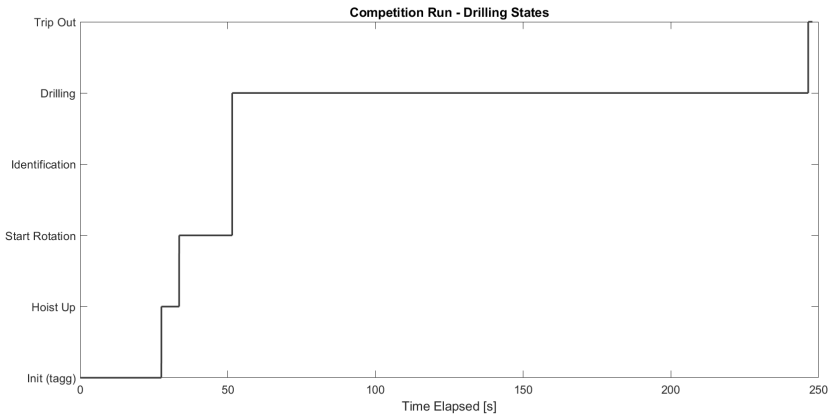
Figure 10.13: Overview of the different drilling states throughout the competition run. This reveals actual drilling time of 195 seconds. Furthermore it is evident that the Trip Out phase indeed was reached by the autonomous script, unfortunately user-terminated by mistake.
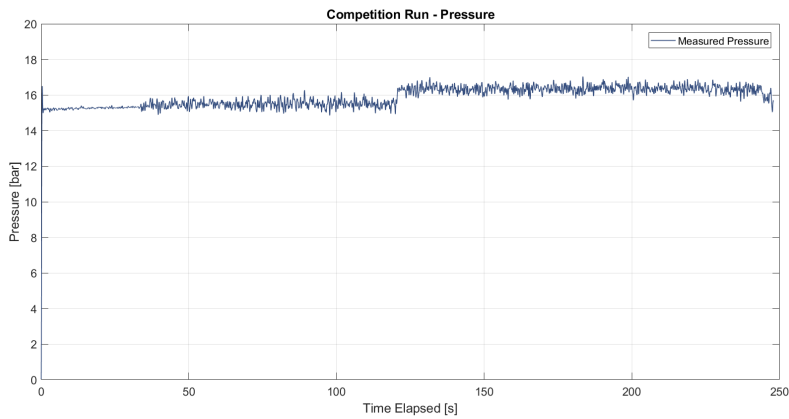
Figure 10.14: Showing the competition circulation pressure. A sharp increase can be seen just as the bit hit an inclined tile, possibly explained by a twist in the sensor wire causing additional flow restriction.
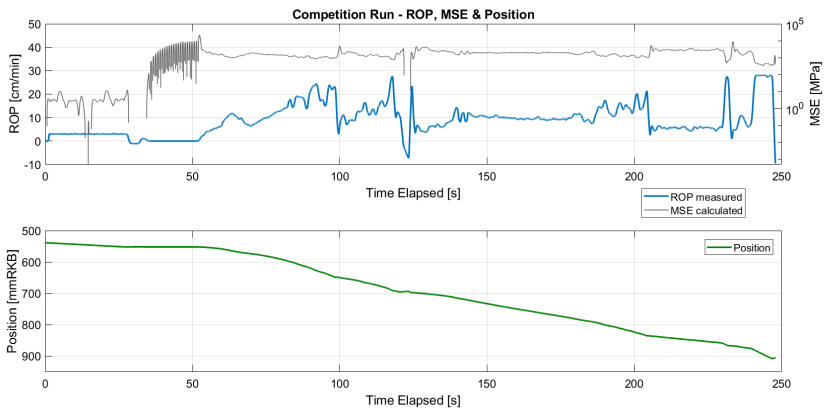
Figure 10.15: Showing the ROP, MSE and positional plot of the competition run. An average ROP of 10 cm/min was obtained, peaking at 27.66 cm/min. Minimum ROP was actually negative, and occurred when lifting off bottom due to drill pipe over-torque.
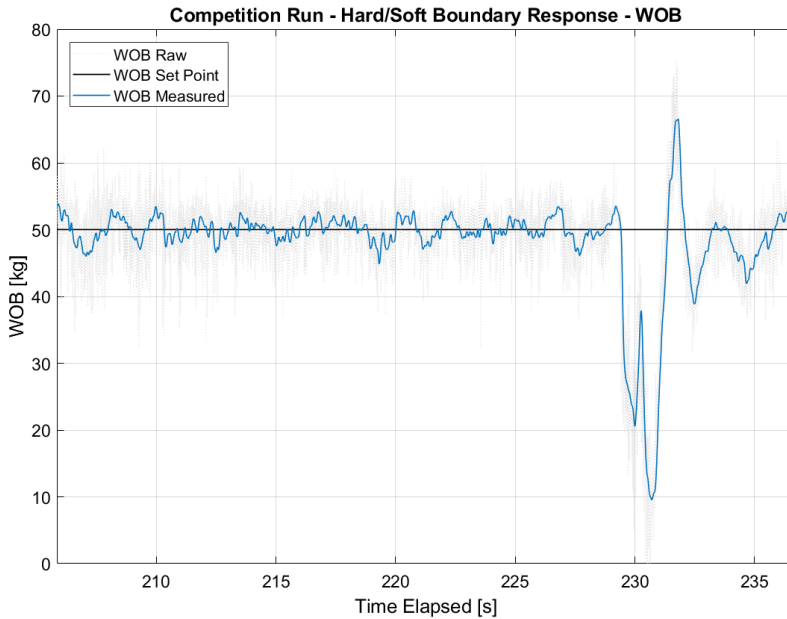
Figure 10.16: Highlighting the inverse heartbeat-like WOB response, revealing a transition from hard to soft rock. Study this in correlation with the hoisting motor RPM for the same time interval in **Fig. 10.17**. Integrator reset occuring at 15 kg above set point.

Another interesting event in the competition run can be found close to the end at 229 seconds, evident in the zoomed-in WOB graph in **Fig. 10.16**. This characteristic inverse heartbeat response has been encountered during testing with the rig, and is well-understood. A sharp boundary from a hard to softer rock is happening, causing a sudden drop in WOB as the same control output as earlier is sustained just breaching into the soft rock. The hoisting motor responds by sending the control output sky-high, to counteract for the lost weight. This results in an overshoot in weight, which is eliminated at 15 kg above set point by integrator reset, all according to plan. It can be seen in **Fig. 10.17** that the RPM of the hoisting motor drops vertically at 232 seconds, just as the integrator is reset. The weight is brought down towards set point, and drilling continues steadily in the new layer. As shown by **Fig. 10.13**, the rig managed to successfully enter the trip-out state after drilling to TD. However, due to a user error, the script was terminated after the tripping out-phase had begun, and the string was pulled out manually. TD was further set a few millimeters deep by mistake, and the bit ended up drilling through the wooden base of the competition rock. This should not affect the hole quality by any means, and only acts as a minor disadvantage to the team, drilling slightly deeper than necessary. Still - the drilling phase ended lasting nothing more than 3 minutes 15 seconds, netting a satisfactory 10 cm/min average ROP excluding the pilot hole. A post run close-up of the bit is given in **Fig. 10.4**, showing cutter damage and overall condition, while the borehole is shown in **Fig. 10.18**.
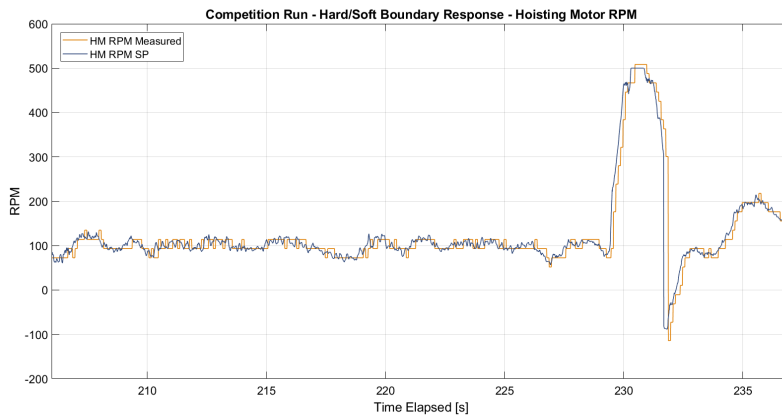
Figure 10.17: Hoisting motor response to hard/soft formation boundary in the end of the competition run. Sharp increase in control output as the new formation is reached due to drop in weight, before integrator reset pulls the output down again.

Figure 10.18: Showing the competition borehole, ready for completions. The boundary between sandstone and pebbled cement can be seen a few centimeters down. A smooth surface was obtained, with some imperfections noticeable especially in formation transitions. The hole was drilled through the entire competition rock, and the very last layer is actually the outline of the wooden crate's floor.

Chapter 11

Challenges and Solutions

Every technical project experiences unexpected events and challenges which need to be acted upon and Drillbotics is no exception. Some challenges have been quick fixes, whereas others have been significant and had impact on the progress of the overall project. Most challenges which have been discovered have gotten permanently fixes while others, due to time limiting factors, still only have temporary solutions. This chapter will discuss the most essential challenges and solution to the project divided into the three main categories: project management, hardware- and software issues.

11.1 Project Management

The team consists of four petroleum students and one studying cybernetics. This has lead to some difficulties on the electrical aspect and communication between different components where the team has been fully dependant on the support team.

To construct a functional drilling rig, loads of parts had to be ordered. The team has dedicated team members to be the contact person for specific vendors to ensure information flow and follow-up in the progress. Despite large effort in ordering parts as early a possible, the project has experienced long downtime on the rig as a consequence of delayed orders. The team has also experienced delays due to deliveries missing parts and ordered parts which do not work as first assumed.

Alone, most delays have not caused the project too long down time, but the sum of the delayed deliveries combined with hardware and software issues have caused severe downtime, preventing the team from proceeding as planned.

11.2 Hardware

Practical projects are new to all the team members and have lead to several unpredicted events due to inconsistency between theory and reality. Regarding hardware, the main challenges have been due to alignment and vibrations. Having a perfectly straight setup is important, but also extremely difficult to achieve. When drilling with high RPM, vibrations are expected. It is important to mitigate these vibrations as they will damage and weaken the aluminum pipe, causing failure due to fatigue.

11.2.1 Alignment

The alignment has been challenging and considerable time has been spent on clever solutions to make the system perfectly straight. The alignment starts with the top drive motor. The top drive was connected to the electrical swivel and the water swivel before connecting to the drill pipe and BHA. There are two topside stabilizing elements on the drill pipe.

Universal Coupling

The alignment starts with the top drive providing rotation and torque to the drill string. Misalignment was experienced through the whole section from the top drive and all the way down to the BHA causing extra stress onto the drill string and making the wells larger in diameter. A new universal coupling has been implemented between the top drive and the electrical swivel. With the new system misalignment between the top drive and the water swivel does not cause wobbling of the drill string.

Bent Guide Frame

Before installing the cylindrical load cell, the team had spent time aligning the swivel towards the kelly bushing and the riser guide. After the installation, the whole system was misaligned. After some investigation, the team concluded that the guide frame was bent after welding on the new load cell setup. Luckily, it was an easy fix when realizing the situation, and the support team was able to straighten out the bent guide frame.

Wear on Pipe

The axial bearings in the kelly bushing and inside the riser were made of metal. During drilling, lateral vibrations made the pipe hit against the metal balls causing severe pipe damage. To shield the pipes, the bearings were changed to teflon sleeves. Teflon is a self-lubricating material which drastically reduces the friction against the drill pipe, but also causes the bearings to wear. The team still decided to go for this solution as the wear time of the teflon sleeve was much higher than on the pipe with the previous bearing, which was completely ruined after one run.

Levelling of Rock Sample

The new riser guide allows for quicker setup time with higher accuracy. Still, the riser is mounted onto the rock sample to reduce play. The alignment regarding this process depends on the levelling of the rock sample. To make it levelled, tiles and thin metal plates have been added underneath the wooden box. This solution helps for levelling, but the rock formation has a tendency to move due to low friction on small contact area between the metal plates and the box. On the competition day, the rig was moved to a levelled section in the lab. This solution proved to be much better. Finding a better spot for placing the rig is recommended for future drilling.

11.2.2 Vibrations

Vibrations in the system can cause severe damage as they induce unwanted stress to the drill pipe. During test runs, both lateral and axial vibrations have been experienced. During last year's competition, the vibrations almost made the driller terminate the drilling operation due to safety reasons. Reducing vibrations have been one of the main challenges for the team this year.

Support Beams

During the first test of the rig in Phase I, lateral vibrations were a huge problem as the derrick moved violently during drilling. Two support beams were installed connecting the derrick to the drill floor, in order to counteract these vibrations. The team experienced less movement in the derrick during drilling afterwards. The positive effect of the support beams was further supported by research done by Wildemanns (2017).

Load Cell

The previous load cell design caused movement in the load cell mounting arm before weight could be transferred to the string. The flexibility of the setup caused vibrations and trouble during drilling. Further, part of the actual WOB changes disappeared in the load cell measurements, being used to physically displace the load cell arm. The setup was switched out to include a cylindrical load cell with stiffer mounting. Results showed that more of the WOB data was detected by the load cell, and to regulate and control weight became easier due to the improved responsiveness.

Loud Noise Due to Vibrations

After fixing all the changes mentioned above, still the team experienced loud metal noises during drilling. The noises were first assumed to be caused by fluctuations in the drill string when the bearing moved out of the riser guide. After more testing the noise started to occur without fluctuations in the pipe and with the bearing placed in the riser. More testing showed that the noise correlated with increase in torque and it was concluded that the issue could be related to the downhole stabilizer hitting against a layer interface. The stabilizer was rounded off slightly which seemed to help, but too little testing has been done to verify this theory and should be investigated more carefully next year.

11.2.3   Dimensioning Issues: Length of Bit and Riser

The team has been drilling with a variety of different subs and bits in the BHA. An important component for good hole quality is having support from the riser guide while making the pilot hole. The change in length of the BHA has not been taken into account when making the new riser guide and has especially been a challenge when drilling with the longer DSATS bit. The solution has been to drill the pilot hole a couple of centimetres before guiding the bearing into the riser and then tighten the stop screws before drilling further.

11.2.4   Hydraulic Integrity

The new hydraulic system controls return flow and transports it to the drain. The system includes a neoprene layer which is compressed against the rock, sealing the flow loop. The system fits rock samples where the mounting plate is placed 5 cm above the rock. This has become a problem as the rock samples are custom made and not all are designed for hydraulic sealing. Some of the rock samples have cracks where flow can escape as well. The rig is placed close to the drain and since the return flow is not used for analysis, leaks have not been of high priority stopping.

11.2.5   Installing Downhole Sensor Card

The solution for the wiring system of the sensor card does not have a robust design. The new design of the BHA includes a track fitting the downhole sensor card perfectly. The end of the wire is placed inside the quick pipe connection. When making up the drill string, there is high risk of damaging the wire connection if not being careful. The sensor card was ready for use only days before the competition, granting little time for the team to come up with a good solution to the problem. The current solution has been to take precautions and act with high precision when making up the drill string. Also, the wire tends to unplug itself during drilling operations. The reason has not yet been discovered, but the team believes that the quick connection may slip due to torque spikes, twisting and shortening the wire until it eventually gets pulled off.

11.2.6   Drill Bit Wear

During drilling operations the cutters on the drill bit were chipped and damaged. Three bits were mainly tested: Alibaba, DSATS and the NTNU bit manufactured by Lyng Drilling. In Phase I, another bit from Lyng was tested with low performance both regarding ROP and durability. In Phase I, the team only possessed the bit from Alibaba. This bit did not see any wear despite several hours of drilling. Due to this, and the low operational limits of the pipe, the team believed that bit wear was not a challenge to take into account. Closer to the competition, both the DSATS and the NTNU bit were ready for testing. These bits are much more aggressive which may be the reason why both were exposed to severe damage only after a few test runs. Due to the high performance in ROP and low torque the NTNU bit was still used in the competition. The solution was not optimal, but the choice was justified with tests which did not show lack in performance due to the damages.

Chapter 12

Future Work

Downhole sensoring was a competition requirement this year. On the competition day, the team got the impression through discussions with the jury that this will be put to even more focus in the coming years. The team this year did not believe in using downhole sensors actively in the control system, and conducting tests with the sensors were not prioritized. The sensor package failed after drilling the competition pilot, suggesting that the current design is lacking in terms of reliability. The complexity of installing the downhole sensor card to the wiring should also be reduced as it is both cumbersome and tricky to set up. Regarding areas of use, this year's team has discussed logging the wellpath while tripping out of the hole after the well is finished. The gyroscope does not work while drilling, where its functionality fails under high rotational speeds.

The team has had large focus on handling vibrations during drilling. This has mainly been dealt with through hardware stiffening and optimization of load cell setup. The stiffness of the load cell setup enables it to become very sensitive towards downhole vibrations. However, having a backup sensor to detect vibrations is highly recommended. Redundancy is important in all aspects of rig instrumentation. As a backup for vibration sensing, the Clamp On SandQ unit has been installed. The team has been able to correlate vibrational data from the SandQ unit to WOB measurements from the load cell, allowing for more reliable boundary layer detection. Combining measurements from all the vibrational units, including downhole, SandQ and load cell, will enable a robust system that still is operational should one of the components fail, and is something future teams could pursue.

The NTNU team spent considerable time designing a custom PDC drill bit in cooperation with Lyng Drilling. This was one of the major focus points this semester, as the team believed great performance benefits could be gathered from it. Three bits were tested against each other, where the winning NTNU bit was selected to be used in the competition. It was superior in terms of torque/ROP to the other bits, but unfortunately saw issues with bit wear. The team initially believed bit wear would not become a problem, due to the small scale drilling and short well sections. We had been using an Alibaba bit for the

entire previous semester, which did have problems with wear, giving a contribution to our beliefs. However, both the NTNU and the DSATS bit had problems with bit wear. This is likely because of their aggressive design. For future work, we would recommend teams to buy several bits of different designs, and test them against each other. Hopefully these test results will generate a pattern on bit wear and performance. With this in mind a new and more resilient bit can be designed, while still hopefully achieving desired performance.

The team wanted to test different downhole BHA configurations. One of the major issues this year has been drill pipe twist-off. The NTNU team believes this is related to the sharp change in torsional inertia transitioning from drill pipe to BHA. Both weight and length of the stabilizer in the BHA should be tested and optimized. Length of the BHA will also have an impact on stabilizing effect and probably hole quality. The length of the BHA might especially be of importance when hitting an inclined layer while drilling. Unfortunately, this year's team did not have enough time to test optimal weight and length of the BHA, and were forced to use a shorter stabilizer when the threads of the ABU sub broke. We believe that the hole quality is largely dependent on BHA assembly and would recommend systematic testing of this matter.

The team designed and manufactured an automatic balancing unit as part of the stabilizer design. This was briefly put to use during drilling, but unfortunately broke due to under-dimensioning. The team did not gather any vibrational data using the sub. We believe this could be an interesting feature to incorporate in the next year's design, but recommend the team to put effort in making the design more robust.

The Drillbotics juries put large focus to digitalization, including convenient and easy access of information. We believe third party access to the control system is something worth implementing as a response to this focus area. Control software was changed this year from SimuLink to LabVIEW. This allows for a plug and play app named Data Dashboard, which is compatible with LabVIEW. The team looked into this and had it working for private networks, but did not implement it due to lack of time and restrictions on the university network.

Drilling performance has been of highest importance this year. The team wanted to drill as efficient as possible, starting the search for a Founder's point. Formation response tests were run in multiple rocks, including granite, shale, basalt and cement, mapping ROP vs WOB and RPM. The team did not find any tendency to foundering in any of the formations, neither for WOB nor RPM, suggesting highest possible WOB and RPM to maximize ROP. We believe this can be related to the weak mechanical limits of the drill pipe. However, more thorough testing should be done to investigate this. The technology behind a rock estimator can be transferred to a full scale drilling operation, where it can be beneficial regarding optimal drilling and geological mapping of the subsurface. Further developing the rock estimator and expanding the library to include more rocks is highly recommended. The Drillbotics competition is not all about ROP, and having a robust rock estimation algorithm will count positive in the overall evaluation of the rig. Ways of reducing estimation time should further be investigated, to allow for better use in thin layered formations.

Investigating buckling of drill pipe is crucial to understand the operational limits of the drilling rig. Both static and dynamic buckling tests were conducted by this year's team, with good correlation between Euler's buckling criterion and test results. The buckling limit will change as function of free drill pipe length. The theoretical equation has been matched with two dynamic buckling tests, for different free pipe lengths. To be fully able to predict buckling as function of depth drilled, this should be expanded with more testing data. The dynamic buckling tests should also be run both with and without internal pressure in the drill pipe. This would be the final step in falsifying the theory about geometric stiffness and believed increase in buckling limit due to high internal drill pipe pressure.

Chapter 13

Summary

This theses has outlined the design considerations and implementation of a control system for use in a miniature autonomous drilling rig. The rig was designed for the fourth consecutive Drillbotics competition hosted by DSATS, which aims to promote the adoption of automatic techniques in the drilling industry.

Safety, performance & reliability, simplicity and digitalization have been the four key focus areas in this project when implementing the design features discussed in the first phase of the competition.

Acrylic glass has been added to the rig frame, shielding the drill pipe and pump shaft from their surroundings. Additional HSE improvements like a semi closed flow loop have been implemented.

Twist-off has been the dominant drill pipe failure during this project. A drill bit was therefore designed in a 3D CAD software with focus on reducing torque. Tests have shown that the bit performed as designed, drilling at a higher ROP for the same torque compared to the bit provided by DSATS.

Olsen, M. A, et al. (2017) based much of their design on using high internal pressure in the drill string, thus allowing higher WOB [28]. Experiments have shown that the critical buckling load does not increase with an increase in internal pressure for static buckling. It has also been shown that dynamic buckling with the miniature rig can be modelled using a curve fitted adoption of Euler's buckling equation and Johnson's parabolic buckling equation, allowing for adaptive limits in WOB with drilled depth.

The cascaded control system from last year has been replaced with a single WOB PID controller with anti-wind up and an automatic use of PID action reset. Furthermore, a torque control feature was implemented to the competition control system for better control of stuck pipe situations. This proved to work as intended during the competition, success-

fully backing off when getting stuck in an inclined formation. Optimal PID parameters have been found for a set of rock, including shale, granite and cement.

A fully autonomous control system was developed which aimed to automatically detect formation boundaries and identify the rock formation, thus allowing to poll optimal drilling parameters from a predefined library. However, no founder point was identified in the tested formations with the designed drill bit. Thus, the estimator was not run during the competition.

The sampling rate of the control system has been increased from 10 Hz to 100 Hz. This is achieved by replacing the OPC and PLC setup from the previous year with Ethernet/IP and modbus communication directly with the motor drives.

Testing have proved that alignment of the drill string components are of utmost importance for bore hole quality and mitigating vibrations. A universal coupling has been included in the top drive to mitigate misalignment of the drill string. In addition, stiffness of the rig is improved with the new load cell configuration.

A framework for digitalization has been established. Drilling parameters are automatically saved to a text file and published in an auto-generated drilling report, readily available to any from the data lake.

The 2018 competition was held June 4th. The rig was able to drill through the rock, without buckling or twisting off, within 195 seconds. The control system was able to handle formation boundaries using the automatic integrator reset, and react to torque spikes indicating stuck pipe.

Bibliography

[1] Alexander S. Handeland, Sebastian Knoop, Andreas Thuve, and Per Øystein Turøy. Design considerations for a miniature autonomous drilling rig, 2017.

[2] Energy - crude oil production - oecd data. `https://data.oecd.org/energy/crude-oil-production.htm`. (Accessed on 06/09/2018).

[3] Daily global crude oil demand 2006-2018 | statistic. `https://www.statista.com/statistics/271823/daily-global-crude-oil-demand-since-2006/`. (Accessed on 06/09/2018).

[4] Fields on the norwegian continental shelf - norwegianpetroleum.no. `https://www.norskpetroleum.no/en/facts/field/`. (Accessed on 06/09/2018).

[5] Oil and gas production - norwegianpetroleum.no. `https://www.norskpetroleum.no/en/production-and-exports/oil-and-gas-production/`. (Accessed on 06/09/2018).

[6] Investments and operating costs - norwegianpetroleum.no. `https://www.norskpetroleum.no/en/economy/investments-operating-costs/#overall-costs`. (Accessed on 06/09/2018).

[7] Home - drilling systems automation technical section. `http://connect.spe.org/dsats/home`. (Accessed on 06/09/2018).

[8] Sandy Smith. Safety in oil and gas industry | ppe safety. `http://www.ehstoday.com/safety/safety-practices-oil-and-gas-industry-infographic`. (Accessed on 05/28/2018).

[9] Hazard prevention and control occupational safety and health administration. `https://www.osha.gov/shpguidelines/hazard-prevention.html`. (Accessed on 05/28/2018).

[10] Cambridge dictionary - automation. `https://dictionary.cambridge. org/dictionary/english/automation`, 2018. (Accessed on 05/10/2018).

[11] Jeremy Rifkin. The end of work: The decline of the global labor force and the dawn of the post-market era. Putnam Publishing Group, ISBN 0-87477-779-8, 1995. (Accessed on 05/5/2018).

[12] John D Macpherson, John P de Wardt, Fred Florence, Clinton Chapman, Mario Zamora, Moray Laing, Fionn Iversen, et al. Drilling-systems automation: Current state, initiatives, and potential impact. *SPE Drilling & Completion*, 28(04):296–308, 2013.

[13] John P de Wardt, Michael Behounek, Clinton Chapman, Devi Putra, et al. Drilling systems automation-preparing for the big jump forward. In *SPE/IADC Drilling Conference*. Society of Petroleum Engineers, 2013.

[14] National Oilwell Varco. Novos - reflexive drilling system. `http://www.nov. com/NOVOS.aspx#`, 05 2018. (Accessed on 05/27/2018).

[15] FB Poletto and Francesco Miranda. *Seismic while drilling: Fundamentals of drill-bit seismic for exploration*, volume 35. Elsevier, 2004.

[16] K. Solem. The impact of wired drill pipe on the martin linge field. Master's Thesis: University of Stavanger, 06 2015. (Accessed on 05/14/2018).

[17] Elon Musk. Critical tweet on automation. `https://twitter.com/ elonmusk/status/984882630947753984`, 04 2018. (Accessed on 05/27/2018).

[18] Josh Kaufman. The paradox of automation. `https://personalmba.com/ paradox-of-automation/`, 2018. (Accessed on 05/27/2018).

[19] Chenevert M.E. Bourgoyne A.T., Millheim K.K. and Young F.S. Applied drilling engineering. Society of Petroleum Engineers, 1986. (Accessed on 05/27/2018).

[20] Drillbotics guidelines version 2018. `https://drillbotics.com/ download/guidelines/Drillbotics-Guidelines-2018.pdf`, 2018. (Accessed on 05/22/2018).

[21] Odfjell Drilling. Drill pipe specifitaions. `https://www. odfjellwellservices.com/rental-services/tubulars/ drillpipe-specs/`, 05 2018. (Accessed on 05/27/2018).

[22] Make it From. Strength of aluminum and steel. `https://www. makeitfrom.com/compare/6061-T6-Aluminum/AISI-304-1. 4301-S30400-Stainless-Steel`, 05 2018. (Accessed on 05/27/2018).

[23] Constantijn Raap, Andrew David Craig, Daniel Perez Garcia, et al. Understanding and eliminating drill string twist-offs by the collection of high frequency dynamics data. In *SPE/IADC Middle East Drilling Technology Conference and Exhibition*. Society of Petroleum Engineers, 2011.

[24] R Teale. The concept of specific energy in rock drilling. In *International Journal of Rock Mechanics and Mining Sciences & Geomechanics Abstracts*, volume 2, pages 57–73. Elsevier, 1965.

[25] Fred E Dupriest, William L Koederitz, et al. Maximizing drill rates with real-time surveillance of mechanical specific energy. In *SPE/IADC Drilling Conference*. Society of Petroleum Engineers, 2005.

[26] Xiangchao Shi, Yingfeng Meng, Gao Li, Jiaxue Li, Zuwen Tao, and Shandong Wei. Confined compressive strength model of rock for drilling optimization. *Petroleum*, 1(1):40–45, 2015.

[27] Pavement Interactive. Portland cement compressive strength. `http://www.pavementinteractive.org/portland-cement-compressive-strength/`, 2018. (Accessed on 05/27/2018).

[28] Martin Aagaard Olsen, Runa Linn Egeland, Mayuran Vasantharajan, and Astrid Lescoeur. Design and construction of an autonomous, miniature drilling rig, contribution to the drillbotics competition, 2017. Master's thesis, NTNU, 2017.

[29] R. Wildemanns. Vibration analysis and control of a miniature rig, 2017.

[30] Rate of penetration optimization using moving horizon estimation. `http://www.mic-journal.no/PDF/2016/MIC-2016-3-1.pdf`. (Accessed on 05/29/2018).

[31] Adam T. Bourgoyne Jr., Keith K. Milheim, Martin E. Chenevert, and F.S. Young Jr. *Applied Drilling Engineering*. Society of Petroleum Engineers, USA, 1st edition, 1986.

[32] Robert F. Mitchell and Stefan Z. Miska. *Fundamentals Of Drilling Engineering*. Society of Petroleum Engineers, USA, 12rd edition, 2014.

[33] Pdc drill bits. `http://petrowiki.org/PDC_drill_bits`. (Accessed on 05/22/2018).

[34] Pdc bit design. `http://petrowiki.org/PDC_bit_design`, 2018. (Accessed on 05/22/2018).

[35] Double row 6-blade - rockpecker | pdc drill bits and accessories. `http://rockpecker.com/2r-6b-bit`. (Accessed on 05/24/2018).

[36] Runar Nygaard, Geir Hareland, et al. How to select pdc bit for optimal drilling performance. In *Rocky Mountain Oil & Gas Technology Symposium*. Society of Petroleum Engineers, 2007.

[37] Miska Rajabov et al. The effects of back rake and side rake angles on mechanical specific energy of single pdc cutters with selected rocks at varying depth of cuts and confining pressures. *SPE Journal*, pages 1–17, 2012.

[38] Hsin I Huang, Robert E Iversen, et al. The positive effects of side rake in oilfield bits using polycrystalline diamond compact cutters. In *SPE Annual Technical Conference and Exhibition*. Society of Petroleum Engineers, 1981.

[39] DDEF Melo, SAB Fontoura, AMB Braga, et al. Analytical solution for rock cutting taking into account backrake, siderake, confining pressure and cutter bluntness. In *48th US Rock Mechanics/Geomechanics Symposium*. American Rock Mechanics Association, 2014.

[40] Pdc bit profile. `http://petrowiki.org/PDC_bit_profile`. (Accessed on 05/23/2018).

[41] Sinor Warren, Brett. Development of a whirl resistant bit. *SPE Journal*, pages 1–8, 1990.

[42] Bottom hole assembly (bha) design for directional control -. `http://petrowiki.org/Bottom_hole_assembly_(BHA)_design_for_directional_control`. (Accessed on 05/24/2018).

[43] Column buckling | mechanicalc. `https://mechanicalc.com/reference/column-buckling`. (Accessed on 06/11/2018).

[44] Rapier Dawson et al. Drill pipe buckling in inclined holes. *Journal of Petroleum Technology*, 36(10):1–734, 1984.

[45] Scott W Long, Donald W Bennett, et al. Euler loads and measured sucker rod/sinker-bar buckling. In *Permian basin oil and gas recovery conference*. Society of Petroleum Engineers, 1996.

[46] Richard G. Budynas and J.K. Nisbett. *SHIGLEY'S MECHANICAL ENGINEERING DESIGN*. McGraw-Hill, New York, NY, 9th edition, 2011.

[47] AC Palmer, JAS Baldry, et al. Lateral buckling of axially constrained pipelines. *Journal of Petroleum Technology*, 26(11):1–283, 1974.

[48] Andrea Catinaccio. Pipes under internal pressure and bending. Technical report, 2009.

[49] Fridtjof Irgrens. *Fasthetslære*. Tapir Akademisk Forlag, Trondheim, 7th edition, 2006.

[50] Paal Vegar Berg and Øving Sæter Tveit. Model for evaluating drilling efficiency based on the concept of mechanical specific energy. Master's thesis, NTNU, 2016.

[51] Todd Robert Hamrick. *Optimization of Operating Parameters for Minimum Mechanical Specific Energy in Drilling*. West Virginia University, 2011.

[52] R Teale. The concept of specific energy in rock drilling. In *International Journal of Rock Mechanics and Mining Sciences & Geomechanics Abstracts*, volume 2, pages 57–73. Elsevier, 1965.

[53] Fred E Dupriest, William L Koederitz, et al. Maximizing drill rates with real-time surveillance of mechanical specific energy. In *SPE/IADC Drilling Conference*. Society of Petroleum Engineers, 2005.

[54] Xuyue Chen, Honghai Fan, Boyun Guo, Deli Gao, Hongshu Wei, and Zhi Ye. Real-time prediction and optimization of drilling performance based on a new mechanical specific energy model. *Arabian Journal for Science and Engineering*, 39(11):8221–8231, 2014.

[55] RC Pessier, MJ Fear, et al. Quantifying common drilling problems with mechanical specific energy and a bit-specific coefficient of sliding friction. In *SPE Annual Technical Conference and Exhibition*. Society of Petroleum Engineers, 1992.

[56] Cherif Hammoutene et al. Fea modeled mse/ucs values optimize pdc design for entire hole section. In *North Africa Technical Conference and Exhibition*. Society of Petroleum Engineers, 2012.

[57] Williams Kingsley Amadi, Ibiye Iyalla, et al. Application of mechanical specific energy techniques in reducing drilling cost in deepwater development. In *SPE Deepwater Drilling and Completions Conference*. Society of Petroleum Engineers, 2012.

[58] Mikkel Leite Arnø. Recursive least-squares estimator to classify drilled formation for autonomous miniature drilling rig. 2017.

[59] Adam T Bourgoyne Jr, FS Young Jr, et al. A multiple regression approach to optimal drilling and abnormal pressure detection. *Society of Petroleum Engineers Journal*, 14(04):371–384, 1974.

[60] Quadrature encoder - dynapar. `https://www.dynapar.com/technology/encoder_basics/quadrature_encoder/`. (Accessed on 06/10/2018).

[61] M. Arnø. The design and implementation of a control system for an autonomous miniature drilling rig. Master's thesis, NTNU, 2018.

[62] Ballscrew-(e).pdf. `http://www.hiwin.tw/download/tech_doc/bs/Ballscrew-(E).pdf`. (Accessed on 12/18/2017).

[63] www.hiwin.com/pdf/linear_guideways.pdf. `http://www.hiwin.com/pdf/linear_guideways.pdf`. (Accessed on 12/18/2017).

[64] https://www.lenze.com/fileadmin/lenze/documents/en/catalogue/cat_gst_gfl_mf_15593808_en_gb.pdf `https://www.lenze.com/fileadmin/lenze/documents/en/catalogue/CAT_GST_GFL_MF_15593808_en_GB.pdf`. (Accessed on 12/18/2017).

[65] Abb 3gaa091520-jsj436. `http://new.abb.com/products/ABB3GAA091520-JSJ436`. (Accessed on 12/18/2017).

[66] S2m high-precision s-type load cell at a low price | hbm. `https://www.hbm.com/en/3364/s2m-reliable-high-precision-s-type-force-load-cell/`. (Accessed on 12/18/2017).

Appendix A

Drillbotics Guidelines 2018
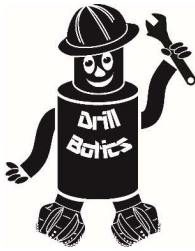
Society of Petroleum Engineers
Drilling Systems Automation
Technical Section (DSATS)

Revised 7 November 2017

Drillbotics™ Guidelines

International University Competition
2017 - 2018

1. Introduction

This year marks the fourth competition for the title of Drillbotics champion and a chance for sponsored travel to present a paper at the next SPE/IADC Drilling Conference and at an event organized by DSATS. The past years involved undergraduates, masters and doctoral students from a variety of disciplines who built innovative drilling machines and downhole tools while developing a deeper understanding of automating the drilling process. The university teams freely shared lessons learned, which more rapidly advances the science of drilling automation. Everyone involved claims to have had a lot of fun while learning things that are not in the textbooks. Students also participated in related events at conferences and workshops meeting and networking with industry leaders in drilling automation. This year's contest promises to be just as challenging and hopefully more fun.

How did the competition first come about? The origins began in 2008 when a number of SPE members established the Drilling Systems Automation Technical Section (DSATS) to help accelerate the uptake of automation in the drilling industry. DSATS' goal was to link the surface machines with downhole machines, tools and measurements in drilling systems automation (DSA), thereby improving drilling safety and efficiency. Later, at an SPE Forum in Paris, the idea of a student competition began to take shape. A DSATS sub-committee was formed to further develop the competition format and guidelines. Several universities were polled to find out the ability of academic institutions to create and manage multi-disciplinary teams. The Drillbotics committee began small in 2014-2015 to see if the format could succeed. With fine tuning, we continue along those lines as we start the 2018 process.

Version	Date	Section	Description
2018.01	15 Sept 2017	All	Initial Release
2018.02	7 Nov 2017	4.5	Attaching bell nipple
		4.6	Bit design
		4.7	Aluminum tubing specs
		4.18.4 &.5	File naming conventions

212

The 2018 competition has a few changes worth highlighting here:

- The 2018 rock sample may have new surprises, but it will be similar to 2017 material
- The drillpipe will still be 0.035" wall aluminum tubing, but it could be changed prior to Phase II if we cannot find a more suitable connection/tool joint.
- A safety case must be presented in Phase I and updated in Phase II. See section 4.3.5.12.
- The engineering section of the Phase I report needs to include formulae and calculations even if the team is using a previous design. See section 4.3.5. These should be summarized in a table within the engineering section of the design report.
- To attain a higher rating by the judges, the Phase I report should include a summary paragraph or table in the design report containing details of the control algorithm proposed. See section 4.3.5.2.3. This should be updated for the Phase II presentation to judges at the on-site test.
- The 2018 design should allow for third-party plug and play interface. See section 4.14.4. This is optional for 2018, but it will likely be mandatory in 2019.

The DSATS technical section believes that this challenge benefits students in several ways. Petroleum, mechanical, electrical and control engineers, gain hands-on experience in each person's area of expertise that forms a solid foundation for post-graduate careers. They also develop experience working in multi-disciplinary teams, which is so important in today's technology driven industries. Winning teams must possess a variety of skills. The mechanical and electrical engineers need to build a stable, reliable and functional drilling rig. Control engineers need to architect a system for real-time control, including selection of sensors, data handling and fast-acting control algorithms. The petroleum engineers need an understanding of drilling dysfunctions and mitigation techniques. Everyone must work collectively to establish system functional requirements understood by each team member, properly model the drilling issues, and then to create a complete package working seamlessly together.

The oil and gas industry today seeks lower costs through efficiency and innovation. Many of the student competitors may discover innovative tools and control processes that will assist drillers to speed the time to drill and complete a well. This includes more than faster ROP, such as problem avoidance for dysfunctions like excessive vibrations, stuck pipe, and wellbore stability issues. Student teams built new downhole tools using 3D printing

techniques of designs that would be difficult, if not impossible to machine. They used creative hoisting and lowering systems. Teams modeled drilling performance in particular formations and adjusted the drilling parameters accordingly for changing downhole conditions. While they have a lot to learn yet about our business, we have a lot to learn about their fresh approach to today's problems. Good Luck!

From the DSATS Drillbotics Committee

Fred Florence   (Chairperson)
Aaron Logan   (Co-Chair)
Mark Anderson
David Blacklaw
Frode Efteland
Mark Hutchinson
Jayesh Jain
Hege Kverneland
Raul Lema
John Macpherson
Nii Nunoo
Ovie Oghor
Veronica Simonds
John Shriver
Suresh Venugopal
Kurt West

3

Contents

2. Objectives for the 2018 Competition

2.1. During the school year beginning in the fall of 2017, a team of students will organize themselves to solve a drilling related problem outlined in item 4 below. The team should preferably be a multi-disciplinary team that will bring unique skills to the group to allow them to design and construct hardware and software to demonstrate that they understand the underlying physics, the drilling issues and the usual means to mitigate the issues. We cannot stress enough the need to involve students with different technical training and backgrounds. They will need to develop skills to understand drilling dysfunctions and mitigation strategies, but they must also have the mechanical engineering capabilities to design the rig/drilling package. In past years, some entrants have not adequately considered the control network and algorithms needed for autonomous drilling. They have often misunderstood the need for calibrated sensors and fast, accurate data handling. All of this and more is needed to build and operate a complete automated drilling system.

2.2. The students could produce novel ideas leading to new drilling models, improved drilling machines and sensors, and the ability to integrate the data, models and machines that will hopefully create new, more efficient ways to drill wells in the future. Any such innovation will belong to the students and their university in accordance with the university's written policies. DSATS and SPE waive any claims to students' intellectual property.

2.3. The students, working as a multi-disciplinary team, will gain hands-on experience that will be directly applicable to a career in the upstream drilling industry.

3. Background

3.1. What is DSATS?

3.1.1. DSATS is a technical section of the Society of Petroleum Engineers (SPE) organized to promote the adoption of automation techniques using surface and downhole machines and instrumentation to improve the safety and efficiency of the drilling process. More information is available about DSATS at the DSATS homepage (http://connect.spe.org/DSATS/Home/).

3.1.2. The Drillbotics website at www.Drillbotics.com includes official updates to the competition guidelines and schedule, as well as FAQs, photos, and previous entrants' submittals and reports. Questions and suggestions can be posted here, or teams can email the sub-committee at 2018@Drillbotics.com.

3.2. Why an international competition?

3.2.1. DSATS, as part of the SPE, is a group of volunteers from many nations, connected by their belief that drilling automation will have a long-term, positive influence on the

5

drilling industry. This diversity helped to shape the direction of the organization. The group feels that the industry needs to attract young professionals from all cultures and disciplines to advance drilling practices in all areas of the world. The winners of the competition will receive a grant for economy class transportation and accommodations to attend the next SPE Drilling Conference and will present an SPE paper that will be added to the SPE archives of One Petro[1]. Additional teams may have an opportunity to present their work at the DSATS automation symposium preceding the conference, and may receive a grant for economy class transportation and accommodations[2]. DSATS believes recognition at one of the industry's leading technical conferences will help encourage student participation. Also, the practical experience with drilling automation systems increases the students' visibility to the companies that are leading automation activities.

4. Competition Guidelines

4.1. Problem statement for the 2017-2018 competition:

Design a rig and related equipment to autonomously drill a vertical well as quickly as possible while maintaining borehole quality and integrity of the drilling rig and drillstring.

4.2. Two Project Phases

Fall Semester 2017

The first phase of the project is to organize a team to design an automatic drilling machine to solve the project problem. It is not necessary to build any equipment in this phase, but it is okay to do so. Design considerations should include current industry practices and the team should evaluate the advantages and shortcomings of today's devices. The design effort may be assisted by university faculty, but the students are encouraged to introduce novel designs for consideration. The level of student, faculty and technical staff involvement shall be reported when submitting the design. For returning teams, the Phase I Design should include an analysis of data and learnings from previous ("offset") wells drilled.

Spring Semester 2018

During the second phase, the finalist teams selected by DSATS proceed to the construction and drilling operation will use the previous semester's design to build an

---

[1] Publication is subject to the SPE program committee's acceptance of the abstract/paper. If the abstract is not accepted, DSATS will solicit other SPE events try to get the paper into OnePetro.
[2] Subject to approval of the DSATS Board of Directors and organizers of the symposium.

automated drilling machine. As per industry practices, it is common during construction and initial operations to run into problems that require a re-design. The team may change the design as needed in order to solve the problem subject to section 4.3.4.

4.2.1. Teams may use all or part of a previous year's rig.

4.3. Phase I – Design Competition

Design an automated drilling machine in accordance with the rules below.

4.3.1. DSATS envisions a small (perhaps 2 meters high) drilling machine that can physically imitate the functionality of full-scale rig machinery. The machine will be the property of the university and can be used in future research and competitions. New and novel approaches that improve on existing industry designs are preferred. While innovative designs are welcome, they should have a practical application to drilling for oil and gas.

4.3.2. The drilling machine will use electrical power from the local grid not to exceed 25 horsepower. Lower power consumption resulting from energy efficient designs will receive additional consideration.

4.3.3. The design must provide an accurate and continuous measurement of Weight-On-Bit (WOB) and other drilling parameters, as well as a digital record across the period of the test. Measurements should be made at frequencies appropriate to the dynamics of the drilling system both at surface and downhole. Discussion of such choices should be included in the design report.

4.3.4. The proposed design must be offered in Phase I of the project, but changes are allowed in Phase II, as long as they are reported to the Committee via students' monthly reports. A summary of all significant changes, including the reason modifications were necessary, must be included in the students' final report.

4.3.5. Design submittal by the students shall include:

4.3.5.1. Engineering drawings of the rig concept, mechanical and electrical and auxiliary systems, if any

4.3.5.2. Design notes and calculations

4.3.5.2.1. All engineering calculations shall be included in the Phase I report, even if the rig is built using previous years' designs. This ensures that the 2018 team reviewed and understood the previous design assumptions and calculations.

4.3.5.2.2. Calculations should include each formula considered in the design, a reference that shows the origins of the formula, why is was chosen, what

engineering assumptions were made, a definition of all variables and the values used in the calculation.

Example

Buckling limit   Euler's Equation   (1) cite a reference here or in the reference section of your design report

The critical buckling load, bcr, is calculated:

$$Pbcr = \pi 2 * E * I / (K * L)^2$$

$Pbcr$:   Critical buckling load

E: Modulus elasticity of the aluminum drill pipe

I: Area moment of inertia

L: Length of the column

K: Column effective length factor (explain how you chose the appropriate k or n factor)

4.3.5.2.3.   The report should include a table that summarizes ALL calculations.

Example

Calculations	Formula	Reference	Results
Moment of Inertia	$I = \pi / 64 \, (dp\,4 - idp\,4)$	Thin wall approx. or ID/OD calc separately or other? List your reference	0.000546 $in4$
Buckling Limit	$Pbcr = \pi 2 * E * I / (K * L)^2$	Euler's Eq	18.9 kg

4.3.5.3.   Control system architecture. (The response time of measurements, data aggregation and control algorithms should be estimated.)

4.3.5.4.   Key features for any models and control software.

4.3.5.5.   Proposed data handling and display.

4.3.5.6.   Specification for sensors and instrumentation, (verifying their precision, frequency response and environmental stability), including the methods planned for calibration before and after the Phase II testing.

4.3.5.7. Plan for instrumentation of sensors in the BHA, as well as a method to synchronize all measurements and utilize both the surface and downhole sensors for real-time control of the drilling process.

4.3.5.8. An explanation of the implementation of the output of the BHA sensors to improve the trajectory of the wellbore, drilling efficiency and other drilling concerns.

4.3.5.9. Cost estimate and funding plan

4.3.5.10. A design summary video used to outline the design submittal not to exceed five (5) minutes in length. Videos shall be the property of the university, but DSATS shall have the rights to use the videos on its websites and in its meetings or events.

4.3.5.11. All design, construction and operation of the project are subject to the terms and conditions of section 11.

4.3.5.12. A safety case shall be part of the Phase I design. Include a review of potential hazards during the planned construction and operation of the rig, and for the unloading and handling of any rock samples or other heavy items. An example of a safety case will be posted on the Drillbotics.com website.

4.3.6. A committee of DSATS members (the Committee) will review the Phase I designs and select the top five (5) teams[3] who will progress to Phase II of the competition.

4.3.7. DSATS shall also award a certificate of recognition and publication on its website for the most innovative design. The design video will also be shown at the DSATS automation symposium at SPE conferences.

4.3.8. DSATS will not fund any equipment, tools, software or other material, including labor, for the construction of the rig. Student teams are encouraged to find external funding from industry participants and suppliers.

4.4. Phase II – Drilling Competition

4.4.1. In the spring term of 2018, qualifying teams will build the rig and use it to drill rock samples provided by DSATS. Drilling a vertical well efficiently though the sample while controlling drilling dysfunctions is the primary technical objective of the competition. The use of both surface and downhole measurements to control the drilling process in real-time is mandatory. To avoid disqualification due to a downhole sensor failure,

---

[3] The number of finalists could be increased or decreased by the DSATS Board of Directors subject to available funding.

redundant or immediately replaceable items should be part of the design and implementation. Time to replace a sensor will be added to the drilling time for calculation of ROP.

4.4.2. Once drilling commences, the test will continue until the depth reaches the bottom or the rock sample or two (2) hours, whichever comes first.

4.4.3. Drilling performance will be observed and measured by DSATS members invited to attend and witness the test.

4.4.4. DSATS will survey the completed wellbore and compare their survey with that of the students' downhole measurements.

4.4.5. The final test will be scheduled late in the school year or soon after graduation. The test will occur at the participating university in accordance with the timeline per section 8 below.

4.5. Rock Samples

4.5.1.1. DSATS will prepare a set of nearly identical samples (appx. 12"W x 12"L x 24"H (30 x 30 x 60 cm) that will be packaged in a crate and shipped to each of the teams that qualified for the actual drilling test. The crates shall not be opened or tampered with, as the rock and formations shall remain unknown until after the test.

4.5.1.2. The rock sample will be a manufactured using cement, varying soil samples and perhaps some materials that are not typically encountered during regular drilling, but will imitate unusual downhole conditions experienced in some drilling programs. All simulated formations may not be parallel to each other (e.g. formation dip).

4.5.1.3. The university and/or students may acquire or produce rock samples as needed to verify the design and allow students to practice using their machine prior to the test. Drilling of the samples provided by DSATS prior to Phase II testing is not allowed and could lead to disqualification.

4.5.1.4. Teams may use glue or use a mechanical fastener to attach a bell nipple or diverter housing to the top of the rock to allow connection of a flowline for return mud flow. If you use a fastener, be careful not to break the rock.

4.6. Bits

4.6.1. Upon request, DSATS will send a drillstring and bit to the finalist teams for use in Phase II. It is expected that the BHA and pipe will cause some difficulty, both for causing drilling dysfunction and for sensor integration and data telemetry. The judges will look

for creative concepts supported by sound reasoning showing an understanding of how the BHA, bit and drillstring function together, and how the downhole system measures, samples and transmits the drilling data.

4.6.2. Upon request, the bit shall be returned to the Committee following Phase II testing for reconditioning for use in future competitions.

4.6.3. One (1) bit, roller cone or PDC, will be provided by DSATS to be used during the Phase II tests. For 2017-2018 the bit will be:

4.6.3.1. A PDC micro-bit 1.125" in (28.6 mm) diameter, with brazed cutters and two nozzles. The drill bit is 5.5" long with 1 1/8" OD (i.e. hole size). It weighs 280g.

4.6.3.2. A bit sub will be provided with the bit. It is 1" OD, 0.5" ID, 3" long, and weighs 220 g. Some students modify the sub ID, in which case it will change accordingly. Teams may decide whether or not to use this bit sub.

4.6.3.3. Cutter backrake is 20 degrees; Cutter diameter is 0.529 inches

4.6.3.4. Nozzles are 2.35mm diameter, two each at approximately 180 degrees.

4.6.4. Students are encouraged to consider bit wear prior to the final test and its impact on drilling performance during the onsite testing. Based on prior competitions, bit wear should be minimal but some cutter damage is always possible.

4.6.5. Student teams may build or buy similar drill bits to test their design with the rock samples they sourced.

4.6.6. Students are also allowed to design and use their own bits for the Phase II on-site test, within the dimensional limits of 4.6.3.1 above.
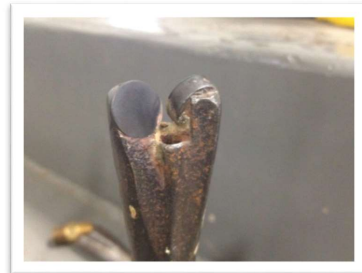
4.7. Drillpipe

    4.7.1. The drill string provided by DSATS, if requested by the student teams, will be chosen to ensure drilling dysfunctions will be encountered. How these dysfunctions are mitigated is a key objective of the competition. Final details of the construction of this drill string will be furnished in late fall of 2017 to all entrants upon request. Preliminary specifications are listed below to assist with the mechanical and electrical design of the rig.

    4.7.2. The drill pipe specifications for the 2017-2018 competition are subject to change, but should be:

        4.7.2.1. Round Aluminum Tube 3/8 inch diameter x 36 inches long; 0.049 inch wall or equivalent (previous years 0.035" wall)

        4.7.2.2. The material from KS Precision Metals is a typical low alloy material: "Our Aluminum tubing with wall thickness of .035 or .049 is 6061 T6"

        4.7.2.3.

        4.7.2.4. DSATS will provide, upon request, the finalists four (4) joints of pipe. Any additional pipe needed can be purchased by the student teams or university if needed.

        4.7.2.5. The use of a metric equivalent of the tubing is permitted.

        4.7.2.6. Tubing is usually available from various hobby shops such as K-S Hobby and Craft Metal Tubing and via Amazon and other suppliers. http://www.hobbylinc.com/htm/k+s/k+s9409.htm

ROUND ALUMINUM TUBING		
OUTSIDE DIAMETER INCHES	WALL THICKNESS	ID
3/64 (.047)	.014	.019
1/16 (.0625)	.014	.035
5/64 (.078)	.014	.050
3/32 (.094)	.014	.066
	.016	.062
7/64 (.109)	.014	.081
1/8 (.125)	.014	.097
9/64 (.141)	.014	.113
5/32 (.156)	.014	.128
11/64 (.172)	.014	.144
3/16 (.187)	.014	.159
	.022	.143
	.035	.117
	.049	.089
13/64 (.203)	.014	.175
7/32 (.219)	.014	.191
	.022	.175
	.035	.149
15/64 (.235)	.014	.207
1/4 (.250)	.014	.222
	.016	.218
	.022	.206
	.035	.180
	.049	.152
9/32 (.281)	.014	.253
	.016	.249
5/16 (.312)	.014	.284
	.016	.280
	.035	.242
	.049	.214
11/32 (.344)	.016	.312
3/8 (.375)	.016	.343
	.035	.305
	.049	.277
13/32 (.406)	.016	.374
7/16 (.437)	.016	.405
	.035	.367
15/32 (.468)	.016	.436
1/2 (.500)	.016	.468
	.035	.430
17/32 (.531)	.016	.499
9/16 (.562)	.016	.530
5/8 (.625)	.016	.593

4.8. Tool joints

4.8.1. Students may design their own tooljoints as long as the design concept is included in the Phase I proposal.

4.8.2. Alternately, students may use commercially available connectors/fittings attached to the drillpipe using threads, epoxy cement or other material, and/or may use retaining screws if desired, as long as the design concept is included in the Phase I proposal.

    4.8.2.1. A fitting used successfully in 2017 is available from Swagelock.

    4.8.2.2. A fitting used successfully in 2016, but which did not work well in 2017, is available from Lenz (http://lenzinc.com/products/o-ring-seal-hydraulic-tube-fitting/hydraulic-straight-connectors) uses a split-ring to allow a torque transfer across the fitting.

4.8.3. Students must state WHY they choose a tooljoint design in the Phase I proposal.

4.9. Bit sub/drill collar/stabilizers

4.9.1. Upon request, DSATS will provide a bit sub 3/8" NPT box down by ¼" NPT box up by 3"long. However, it is expected that each team will design and build their own bit sub.

4.9.2. Additional weight may be added to the bit sub provided by DSATS, or surface weight/force (above the rock sample) may be applied to provide weight on bit and drillpipe tension. However, the additional weight shall not directly impose lateral forces to stabilize the drillstring. This weight is meant to add to string tension/compression but shall not improve steering through interaction with the rock.

4.9.3. The student team will be evaluated on how the weight is designed and how it attaches to the drill string. Advise the committee of your choice and why and include this in the Phase I design.

4.9.4. Stabilizers are permitted, but excessive stabilization to stiffen the drillstring to avoid buckling or torsional failure is disallowed. The maximum combined length of stabilizers is 3.5" (8.9 cm). This year's shorter stabilizers should make steering more of a challenge than in previous years. The student team will be evaluated on how the stabilizers are designed and how they attach to the bit sub. Advise the committee of your choice and why and include this in the Phase I design.

4.9.5. Students must add sensors to the drillstring, but are not permitted to instrument the rock samples. The sensors cannot appreciably increase the stiffness of the drillstring or add significant weight (see 4.9.2). They must have a smaller diameter than the stabilizers and bit by at least 10%. Please include design concepts in the Phase I design.

4.9.6. The addition of along-string sensors to measure vibrations, verticality and/or tortuosity or other parameters will receive extra consideration. They must have a smaller diameter than the stabilizers and bit by at least 10%.

4.10. Automated Drilling

4.10.1. Drilling automation should be considered a combination of data, control AND dynamic modeling so that the control algorithm can determine how to respond to differences between the expected and actual performance. Process state detection can often enhance automation performance. Refer to documents posted on the DSATS website for more information.

4.10.2. Once drilling of the sample commences, the machine should operate autonomously. Remote operation and/or intervention is not allowed.

4.11. Sensors

4.11.1. The team may elect to use existing oilfield sensors or may look to other industries for alternate sensors.

4.11.2. The team may develop its own sensors if so desired.

4.11.3. Sensor quality differs from data quality. Both are important considerations in this competition.

4.11.4. The final report shall address which sensors were selected and why. The sensor calibration process shall also be explained.

4.12. Data collection and handling

4.12.1. The team may elect to use standard data collection and recording techniques or may develop their own. Data handling techniques and why they were chosen should be described in the Phase I submittal.

4.12.2. The final report shall address which data systems were selected and why.

4.12.3. The observed response time of measurements, data aggregation and control algorithms should be compared to the Phase I estimates.

4.13. Data visualization

4.13.1. Novel ways of presenting the data and progress of drilling in real time while drilling will receive particular attention from the judges.

4.13.2. Visualization of the processes (automation, optimization, drilling state, etc. should be intuitive and easily understood by the judges, who will view this from the perspective of the driller operating a rig equipped with automated controls.

4.13.3. Data must be presented in a format that allows the judges to easily determine bit depth, elapsed drilling time, ROP, MSE, verticality/inclination, vibration, and any other calculated or measured variable used to outline the drilling rigs performance to the judges. Lack of an appealing and usable Graphic User Interface (GUI) will be noted to the detriment of the team.

4.13.4. All depths shall use the industry-standard datum of rotary/kelly bushing interface (RKB), which should be the top of the rig's "drill floor."

4.14. Measure and analyze the performance

4.14.1. The drilling machine should react to changing "downhole" conditions to select the optimal drilling parameters for improved performance, as measured by the rate of penetration (ROP), mechanical specific energy (MSE), verticality, cost per foot or meter, and other standard drilling measures or key performance indicators. Adding parameters such as MSE, or similar features, to the control algorithms will receive special attention from the judges.

4.14.2. Design limits of the drilling machine shall be determined and shall be incorporated in the programming of the controls during the construction phase.

4.14.3. The final report (see Clause 4.19) shall outline drilling performance and efficiency criteria and measured results.

4.14.4. One of DSATS' goals is to promote plug and play capability to accelerate the implementation of drilling automation. A DSATS committee is preparing definitions and examples of proposed data communication protocols and interfaces. Once this is available, the Drillbotics competition will require the use of these standard protocols. This will not be a requirement for 2018 but it will be included in future competitions. Links to these standards will be added to the Drillbotics.com website when they are published.

4.15. The test well:

4.15.1. Will be drilled as a vertical well. Verticality and drift will be measured by the judges and compared with the students' measurements, so calibration issues should be carefully considered

4.15.2. Should be drilled with a maximum allowable Weight-On-Bit dependent on the rig and dynamic drillstring integrity.

4.15.3. Will not require a closed-loop fluid circulation system, but the bit and machinery should be cooled with air or fluid/water if needed. The design of the fluid system, if any, should be included in the Phase I design.

4.15.4. The rock sample may simulate the drilling of hydraulic hazards such as lost circulation, surge, swab and other effects, but no well control equipment for over-pressure considerations will be necessary. Note that the rock samples may leak at the junctions between the simulated formations, so a rig design that includes a containment system is strongly suggested.

4.15.5. Will not require casing or cement

4.15.6. Will not be drilled with a mud motor or turbine.

4.15.7. Will not require a rig move, walking or skidding, but the mobility of the rig will be considered in the design phase.

4.16. Not included in the 2017-2018 competition

4.16.1. The drilling will not include automating the making or breaking of connections. If connections are necessary due to the rig and drillstring design, connections should be made manually, and the time involved with the connections will be included with respect to its effect on drilling performance (rate of penetration reduction).

4.17. Presentation to judges at Phase II Testing

4.17.1. The judges will arrive at the university to meet with the student teams and advisors immediately prior to the Phase II testing. The university should provide a suitable meeting room for discussion lasting about two hours.

4.17.2. The students will present a BRIEF summary of their final design, highlighting changes from their Phase I design, if any. Include an explanation of why any changes were necessary, as this indicates to the judges how much students learned during the design and construction process. Explain what measurement and control features have been deployed. Describe novel developments or just something learned that was worthwhile. Also include how actual expenses compared with the initial estimate. (Previous teams used a short PowerPoint presentation of about ten slides or so. Use any format you like.) Be sure to include all your team members as presenters, not just one spokesperson. At some time during your talk, let us know who the team members are and what background they have that pertains to the project.

4.17.3. Judges will ask questions to ascertain additional details about the design and construction process and to see if all team members have a reasonable understanding how all the various disciplines used for the rig design and construction fit together.

4.18.   Project report

4.18.1. The student team shall submit to DSATS a short monthly project report that is no more than one page in length (additional pages will be ignored) due on or before the last day of each month that will include:

4.18.2. Phase I

- Key project activities over the past month.
- Rig design criteria, constraints, tradeoffs, and how critical decisions were determined
- Cost updates
- Significant new learning, if any

4.18.3. Phase II

- Construction issues and resolution
- Summary of recorded data and key events
- Drilling parameters [such as WOB] and how they impact the test
- Other items of interest
- To teach students that their work involves economic trade-offs, the monthly report should include at a minimum a summary estimate of team member labor hours for each step in the project: design, construction, testing, reporting, and a cost summary for hardware and software related expenditures. Also include labor for non-students that affect the cost of the project. Labor rates are not considered, as to eliminate international currency effects. Labor is not considered in the cost limits of item 6.1, but should be discussed in the report and paper.

4.18.4. Report content

4.18.4.1.   To teach students that their work involves economic trade-offs, the monthly report should include at a minimum a summary estimate of team member labor hours for each step in the project: design, construction, testing, reporting, and a cost summary for hardware and software related expenditures. Also include labor for non-students that affect the cost of the project. Labor rates are not considered, as to eliminate international currency effects. Labor is not considered in the cost limits of item 6.1, but should be discussed in the report and paper.

4.18.5. File naming convention

4.18.5.1.   To avoid extra work by the committee to rename all files, please use this convention for:

       4.18.5.1.1.   Monthly reports

                Year-Month# University Name (abbreviated)

                (note this is the competition year (spring term))

                Example 2018-09 UDC

       4.18.5.1.2.   Design reports

                Year University Name (abbreviated)

                (note this is the competition year (spring term))

                Example 2018 University of Drillbotics Competition

4.19.   Final report and paper

4.19.1. The finalists shall prepare a project report that addresses the items in 4.19.6 below. We suggest you use the format of most SPE papers. For reference, please see http://spe.org/authors/resources/

4.19.2. The winning team shall update the report as needed to comply with SPE paper submittal guidelines to write a technical paper for publication by the SPE at its Annual Drilling Conference. SPE typically requires that the manuscript is due in the fall following the Phase II test. While the Drillbotics committee will make every effort to have the paper presented during the Drilling Conference, the SPE Program Committee has authority over which papers will be accepted by the conference. If the paper is not accepted by the conference, the Drillbotics committee will endeavor to have it presented at the DSATS Symposium and will use its contacts to have the paper published via other related SPE conferences.

4.19.3. The report, paper and all communications with DSATS shall be in the English language. The presentation will be made by at least one member of the student team.

4.19.4. The timing for submittal of the abstract and paper will be the published deadlines per the call for papers and conference guidelines as posted on the SPE's website (www.spe.org).

4.19.5. The abstract must generate sufficient interest with the SPE review committees to warrant publication, although DSATS will help promote acceptance where possible

4.19.6. The paper should address at a minimum

    4.19.6.1.   The technical and economic considerations for the rig design, including why certain features were chosen and why others were rejected.

    4.19.6.2.   The setup of the experimental test, the results and shortcomings.

    4.19.6.3.   Recommendations for improvements to the design and testing procedures.

4.19.6.4.   Recommendations for improvements by DSATS of the competition guidelines, scheduling and provided material.

4.19.6.5.   Areas of learning gained through the competition not covered in the university course material.

4.19.6.6.   A brief bio or CV of the team members and their sponsoring faculty.

5. *Team Members*

5.1. DSATS envisions that the students would be at least senior undergraduate or Masters level, well versed in the disciplines needed for such a project. The maximum number of students per team is five (5) and the minimum shall be three (3). Any team that loses team members during the project can recruit a replacement.

5.2. At least one member of the team must be a Petroleum Engineering candidate with sufficient coursework completed to understand the physics relating to the drilling problems and the normal industry practices used to mitigate the problem.

5.3. Students with a background in mining, applied mathematics, mechanical and electrical engineering, as well as controls, mechatronics and automation or software development, are the most likely candidates, but students with any applicable background is encouraged.

5.4. A multi-disciplinary team simulates the working environment in the drilling industry today, as most products and services are produced with the cooperation of technical personnel from differing backgrounds and cultures.

5.5. A university may sponsor more than one team but must submit only one team/design for Phase II evaluation.

6. *Expenditures*

6.1. Teams selected to advance to the second phase must limit the cost of the rig and materials to US$ 10,000 or its equivalent in other currencies. The students shall find a source of funding and report the source in the Phase I proposal. All funding and procurement should comply with university policy. These funds are intended to cover the majority of expenses for hardware, software and labor to construct and operate the team's equipment. DSATS shall not be liable for any expenditure other than DSATS provided material and specified travel expenses.

6.2. DSATS will assist when possible to obtain free PLCs or similar control devices from suppliers affiliated with the DSATS organization.   Such "in-kind" donations shall not be included in the team's project costs.

6.3. Students and universities may use other "in-kind" contributions which will not be included in the team's project costs. Such contributions may include modeling software, laboratory

equipment and supplies, and similar paraphernalia usually associated with university laboratory projects.

6.4. Any team spending more than US$ 10,000, or its equivalent in other currencies, may be penalized for running over budget.

6.5. DSATS reserves the right to audit the team's and university's expenditures on this project.

6.6. Any devices built for the project will become the property of the university and can be used in future research and competitions. Any maintenance or operating costs incurred after the competition will not be paid by DSATS.

7. *Other Considerations*

7.1. The design concepts shall be developed by the student team under the supervision of the faculty. Faculty and lab assistants should review the designs to ensure student safety.

7.2. Construction of the equipment shall be supervised by the student team, but may use skilled labor such as welders and lab technicians. The use of outside assistance shall be discussed in the reports and the final paper. DSATS encourages the students to gain hands-on experience with the construction of the rig since this experience will be helpful to the career of individuals in the drilling industry.

7.3. University coursework and credit: Each university will decide whether or not this project qualifies as a credit(s) towards any degree program.

8. *Project Timeline*

Phase I - Design:	Fall 2017
Submit monthly reports	On or before the final day of each month
Submit final design to DSATS	31 Dec 2017, midnight UTC
Submit an abstract to DSATS*	31 Dec 2017, midnight UTC
Phase II – Construction and Testing	Spring 2018
DSATS to announce finalists	On or about 15 Jan 2018
Construction	Spring 2018
Monthly reports	On or before the final day of each month
Drilling Test	Specific on-site test dates at each university to be arranged not later than 31 March 2018. The testing will typically occur in late May or early June. All tests must be completed by 15 June.
Prepare and submit paper	Per SPE deadline*

20

Prepare and submit presentation   Per SPE deadline

Present paper at the Drilling Conf   Per SPE and DSATS schedule

*DSATS will submit an abstract to the SPE that will include excerpts from the student abstracts by the conference paper-submittal deadline, typically in mid-summer, for consideration of a paper by the conference program committee.

9. *Evaluation Committee*

9.1. DSATS will select an evaluation committee from its membership

9.2. Criteria/Weighting (see chart):

Criteria	Parameter	Weighting
Phase I:		
a.Safety	Safety: construction and operation	10
b.Mobility of rig	Rig up, move, rig down	5
c.Design considerations and lessons learned		10
d.Mechanical design and functionality, versatility		25
e.Simulation/Model/Algorithm		25
f.Control scheme	Data, controls, response times	25
	Total	100%
Phase II:		
a.Creative Ability	Analysis, concepts, development	10
b.Engineering Skills	Problem/Goal, design criteria, feasibility	10
c.Construction Quality		10
d.Cost Control		10
e.Performance		20
Various parameters such as:	ROP, MSE, Landing Bit, Inclination, and other	
Are these used within the control algorithms		
	Optimal landing of bit	
f.Quality of wellbore		20
	Verticality, tortuosity, caliper, other	
g. Data	Data handling, data visualization, data comparison to judges' wellbore logs, and other	20
	Total	100%
Intangibles	Additional score may be added or subtracted by the judges at their discretion	

10. Prizes

10.1.　　The winning team will be sponsored by DSATS to attend the next SPE/IADC Drilling Conference to present a paper that explains their project in detail.

　　10.1.1. The program committee of the Drilling Conference awarded the Drillbotics subcommittee a permanent slot in one of the drilling sessions at the conference. As per SPE's customary procedures, the paper will be archived in OnePetro. In addition, SPE has agreed to furnish a booth in the exhibition area during the conference where the team can erect their rig and describe its operation to the conference attendees. This is an excellent opportunity for students to network with the industry.

10.2.　　Upon submittal to DSATS of a valid expense statement (typically a spreadsheet supported by written receipts) of covered expenses will be reimbursed by the treasurer of DSATS for the following:

　　10.2.1. Reasonable shipping costs of the Drillbotics rig to and from the conference as long as charges are pre-approved by the chair or co-chair of the Drillbotics subcommittee.

　　10.2.2. Round trip economy airfare for the team and one university sponsor/supervisor to the gateway city of the next SPE/IADC Drilling Conference. Entrants should use the SPE approved carrier where possible to minimize cost. Airfares that exceed the SPE rate must be pre-approved by the committee or the reimbursement will be limited to the SPE rate. Information of reduced fare flights is available on the conference website. Please note that reservations must be made before the SPE published deadline. The departure point will be a city near the university, the student's home, or current place of work, subject to review by the Committee. Alternately, a mileage reimbursement will be made in lieu of airfare should the entrants decide to drive rather than fly to the conference. The reimbursement is based on current allowable mileage rates authorized by the US Internal Revenue Service.

　　10.2.3. One rental car/van at the gateway city for those teams that fly to the conference.

　　10.2.4. Lodging related to one hotel room per team member will be reimbursed at a rate not to exceed the SPE rate. Note that the room reservations are limited, so entrants must book their rooms early. Room and taxes for the night before the DSATS symposium, the night of the symposium and for the nights of the conference are covered. Charges for the room on the last day of the conference need to be pre-approved by the Committee as most conference attendees depart on the last day of the conference unless there are unusual circumstances.

10.2.5. A per diem will be pre-approved by the Committee each year, which will vary with the cost of living in the gateway city. The per diem is intended to cover average meals (breakfast, lunch and dinner) and incidentals.

10.2.6. ATCE registration will be reimbursed. Students should register for the conference at the student rate. Early registration is appreciated.

10.3. Individual award certificates will be presented to all participants upon request, with special certificates given to all finalists.

10.4. DSATS may provide additional awards, at its sole discretion.

10.5. The evaluation and all decisions on any matter in the competition by the DSATS judges and DSATS board are final.

11. Terms and conditions

11.1. In no event will SPE, including its directors, officers, employees and agents, as well as DSATS members and officers, and sponsors of the competition, be liable for any damages whatsoever, including without limitation, direct, indirect, special, incidental, consequential, lost profits, or punitive, whether based on contract, tort or any other legal theory, even if SPE or DSATS has been advised of the possibility of such damages.

11.2. Participants and Universities agree to indemnify and hold harmless SPE, its directors, officers, employees and agents, as well as DSATS members and officers, and sponsors of the competition, from all liability, injuries, loss damages, costs or expenses (including attorneys' fees) which are sustained, incurred or required arising out of participation by any parties involved in the competition.

11.3. Participants and Universities agree and acknowledge that participation in the competition is an agreement to all of the rules, regulations, terms and conditions in this document, including revisions and FAQs posted to the DSATS and Drillbotics websites (see section 3.1).

11.4. Winning teams and finalists must agree to the publication of their names, photographs and final paper on the DSATS web site.

11.5. All entries will be distributed to the Drillbotics Committee for the purpose of judging the competition. Design features will not be published until after all teams have been judged and a winner is announced. Previous years' submittals, reports, photos and similar documentation will be publically available to foster an open exchange of information that will hopefully lead to faster learning for all participants, both new and experienced.

11.6. DSATS and the SPE cannot provide funding to sanctioned individuals and organization per current US law.

11.7.   Participants must comply with all local laws applicable to this contest.

12. Marketing

12.1.   Upon request, DSATS will provide a link on its website to all participating universities.

12.2.   If university policy allows, various industry journals may send a reporter to witness the tests and interview students to publicize the project.

- End -

Appendix B

Risk Assessment

NTNU ⬛ HSE/KS	Risk assessment	Prepared by HSE section	Number HMSRV2603E	Date 05.10.2017	
		Approved by The Rector	Page 1 out of 4	Replaces NA	

Unit: Department of Geoscience and Petroleum   **Last Updated:**   **05.10.17**
Line manager: Noralf Vedvig
Participants in the risk assessment (including their function):

Activity from the identification process form	Potential undesirable incident/strain	Likelihood: Likelihood (1-5)	Consequence: Human (A-E)	Environment (A-E)	Economy/ material (A-E)	Risk value	Comments/status Suggested measures
Handling of rocks	Injury to personnel: • Back injury/strain • Cutting fingers • Crushing fingers, feet etc.	4	B	A	A	4A	• Redesign rock sample/carrier. • Use proper PPE • Use proper lifting technique • Don't lift to much at a time
Tripping accidents	Injury to personnel Damaging equipment	4	B	A	B	4B	• Maintain a clean work environment • Housekeeping • Use proper PPE
Loud noises	Damage to hearing	3	B	A	A	3A	
Rotating Objects	Loose clothing being caught up by rotating parts. Potential injury to personnel.	2	C	A	A	2B	• Keep away from moving objects • Do not use loose clothing
Accidents and injury related to pipe buckling	Injury to personnel from debris and damage to equipment	4	B	A	B	4B	• Design the system with proper safety factors • Follow the drilling procedures • Test buckling limit and implement in control system • Take precautions when setting up the

							pipe • Verify control system safety values prior to starting up
Accidents and injury related to pipe bursting	Injury to personnel from debris/fluids and damage to equipment	1	B	A	B	1B	• Include safety factors to pipe pressure
Spilling of fluids	Slippery floor, or fluids in eye	5	A	A	A	5A	• Include splash guard • Use caution when in the proximity of the rig
Falling objects	When connecting the BHA/drill pipe or tools falling	3	B	A	A	3A	• Use helmet • Place tools properly and keep a clean work environment
Electrical hazards	Electric shocks and damage to equipment	1	C	A	B	1B	• Keep water away from electric sources. • No power will be supplied while connecting wires and components. All electrical connections will be secured and wiring will be insulated. Qualified personnel will be responsible for high voltage setup
Fire	Personnel could suffer from burns and smoke inhalation	1	C	B	C	1C	• Only qualified personnel should modify electrical equipment • Regularly look over the electrical equipment and

239

NTNU	Risk assessment	Prepared by	Number	Date	
◻		HSE section	HMSRV2603E	05.10.2017	
		Approved by	Page	Replaces	
HSE/KS		The Rector	3 out of 4	NA	

									inspect for any damages

Likelihood, e.g.:
1. *Minimal*
2. *Low*
3. *Medium*
4. *High*
5. *Very high*

Consequence, e.g.:
A. *Safe*
B. *Relatively safe*
C. *Dangerous*
D. *Critical*
E. *Very critical*

Risk value (each one to be estimated separately):
Human = Likelihood x Human Consequence
Environmental = Likelihood x Environmental consequence
Financial/material = Likelihood x Consequence for Economy/materiel

Potential undesirable incident/strain
Identify possible incidents and conditions that may lead to situations that pose a hazard to people, the environment and any materiel/equipment involved.

Criteria for the assessment of likelihood and consequence in relation to fieldwork
Each activity is assessed according to a worst-case scenario. Likelihood and consequence are to be assessed separately for each potential undesirable incident. Before starting on the quantification, the participants should agree what they understand by the assessment criteria:

Likelihood

Minimal 1	Low 2	Medium 3	High 4	Very high 5
Once every 50 years or less	Once every 10 years or less	Once a year or less	Once a month or less	Once a week

Consequence

Grading	Human	Environment	Financial/material
E Very critical	May produce fatality/ies	Very prolonged, non-reversible damage	Shutdown of work >1 year.
D Critical	Permanent injury, may produce serious serious health damage/sickness	Prolonged damage. Long recovery time.	Shutdown of work 0.5-1 year.
C Dangerous	Serious personal injury	Minor damage. Long recovery time	Shutdown of work < 1 month
B Relatively safe	Injury that requires medical treatment	Minor damage. Short recovery time	Shutdown of work < 1week
A Safe	Injury that requires first aid	Insignificant damage. Short recovery time	Shutdown of work < 1day

NTNU	Risk assessment	Prepared by	Number	Date	
[logo]		HSE section	HMSRV2603E	05.10.2017	
HSE/KS		Approved by	Page	Replaces	
		The Rector	4 out of 4	NA	

The unit makes its own decision as to whether opting to fill in or not consequences for economy/materiel, for example if the unit is going to use particularly valuable equipment. It is up to the individual unit to choose the assessment criteria for this column.

Risk = Likelihood x Consequence
Please calculate the risk value for "Human", "Environment" and, if chosen, "Economy/materiel", separately.

About the column "Comments/status, suggested preventative and corrective measures":
Measures can impact on both likelihood and consequences. Prioritise measures that can prevent the incident from occurring; in other words, likelihood-reducing measures are to be prioritised above greater emergency preparedness, i.e. consequence-reducing measures.

Appendix C

Hardware

C.1 Cutting Analysis

Cutting Transportation System

When the cuttings come out of the well, it is desired to have them flow through a closed system to be able to analyse the colors for detecting a change in formation. This system starts with a redesign of the riser. The cuttings will then follow the return flow into a separator. From the separator the cuttings moves over a screen, where a camera should analyse the color of the cuttings.

Cutting Separator

The cutting separator is built using a transparent pipe with a inner diameter of 8 cm. Since the cuttings are much more dense than water, the cuttings will settle fast. A vertical separator was preferred over a horizontal one as it would start accumulating cuttings faster. The separator has one inlet and two outlets. The first outlet is places at the top of the separator. This is the water outlet to separate most of the water out without significant losses of cuttings. The second outlet is places at the bottom of the separator and should contain most of the cuttings. The inlet is located between the two outlets. The reason for this is to prevent the cuttings from flowing straight from the inlet to the water outlet in the top of the separator. The cutting separator is picture in **Fig. C.1**.

While testing the prototype of the separator, problems regarding plugging of the cutting outlet was experienced. There are mainly two problems regarding plugging of the system. One related to accumulation of smaller cuttings around the outlet and the second one regarding larger cutting size. Since the force in the outlet flow is low, this lead to accumulation of cuttings and eventually plugging of the system. For the prototype, this was fixed by tilting the separator slightly towards the cutting outlet. In this way the gravity helped prevent cutting accumulation. This was later improved with a smoother approach, inserting a 45° tilted Teflon layer having the same function as tilting the whole separator. The

Figure C.1: The figure shows the cutting separator with the cutting outlet on the bottom left. The floor is tilted 45°, guiding the cuttings towards the outlet.

second problem regarding plugging of the separator is due to large grain size which can't fit through the nipple. It is desirable to have as high concentration of cuttings as possible in the water coming out of the lower outlet in order to determine a change in color. A smaller nipple diameter in the cutting outlet will decrease the flow rate and let more water flow through the upper outlet. The amount of cuttings is only a function of hole size and ROP, thus the lower outlet will have a higher concentration of cuttings. The downside of a smaller nipple size is the increased chance of plugging, as larger diameter cuttings does not fit. The cutting diameters in Drillbotics are expected to be small for most rocks. From the previous year it was noted that asphalt was the rock providing the largest cutting size. This year, tiles have shown to give the largest cutting size. Further testing will be done to choose the optimal nipple size both for separation of water and preventing plugging.

The flow rate through the lower outlet is dependant on the hydrostatic column in the separator. If the height between the inner and the outer outlet is large enough, all the flow will eventually go through the cutting outlet. This is clearly not desirable since the purpose of the separator is to extract the water and have mostly cuttings in the color analysis. The current setup separate out 2/3 or the water while the water outlet contains almost no cuttings.

The flow from the separator has a relatively high velocity when moving over the back plate. To slow the velocity down it has been proposed to use a splash plate for the cuttings to hit and fall onto a slightly tilted plate. The tilting angle is crucial to have the cuttings flow at a speed of which they can be detected by the camera. **Fig. C.2** shows the prototype of angled plate with the camera mounted perpendicular on to it. The angle depend on the roughness of the underlying surface as well as the flow rate of the cutting outlet. For photo analysis, it is important to distinguish cutting samples from the background. The back

Figure C.2: The figure shows the setup of the screen and the camera for picture analysis of the cuttings in the return flow.

plate should be of a color which easily can be identified and extracted from the analyses. The optimal solution would be a green screen with the color code of $R = 0$, $G = 255$ and $B = 0$. This screen can easily be detected and ignored in the color analysis.

The camera used to analyse the colors of the cutting samples is a Logitech C925e webcam. The camera can take photos in full HD at 1080p up to 1920x1080 pixels. It also comes with auto focus and light regulator for increased sharpness and brightness in the photos. The auto focus and the light regulator will change the base of the image making it impossible to compare a sequence of photos and should therefore be held constant. To detect a color change in the cuttings, it is important to have a constant surrounding light.

For now the cutting analysis will be a support system to the estimator. The purpose is to have an extra indicator telling the system it has hit another layer in the test rock. Clearly there is a lot of changing parameters which needs to be taken into account when doing image analysis.

- Reflections from the water surface, as the cuttings are a part of the circulation fluid, the reflection from the water will effect the color of the image.

- The amount of cuttings in the return flow. The pump provides a continuous flow of water, while the amount of cuttings in the return flow will be dependant on the ROP of the drilling process. For harder rock formations the ROP will decrease, thus less cuttings will be retrieved from the well. As sufficient hole cleaning is important to prevent stuck pipe and twist-off, the flow rate can not change as a function of ROP. For harder rocks, problems can be related to having insufficient amount of cuttings to analyse.

- Accumulation of cuttings on the plate may occur for softer rocks as the amount of cuttings will increase. Theoretically the code should be able to tell the difference between cuttings and the background plate, but due to reflections this might not always be the case.

- Intensity and color of the constant surrounding light.

Drillbotics is a competition with focus on drilling performance and efficiency. Cutting analysis for layer detection would be a nice feature in addition to a well functioning rig, but due to lack of time and other priorities, this project has been abandoned and left for future work. When looking into the complexity of color analysis in the return flow, the team highly recommends this project to be an individual master thesis or PhD program which could be implemented in Drillbotics when finished.

C.2   Load Cell Configuration Analysis

Disclaimer: *This section of the appendix is taken from the project report of the thesis.*

The original load cell placement needed to be change. Several possible solutions for load cell configuration have been analysed. According to petroleum literature, torque and WOB should have a near linear relationship when drilling. Based on this, the team wanted to investigate the possibility of excluding WOB sensors from the rig and rely on estimating WOB through torque readings from the hoisting motor. In order to analyse the relationship, the team conducted an experiment where the rig pushed down against a scale without drill pipe and rotation in the top drive. WOB, which was recorded both manually from the scale and digitally by the load cell, was compared to torque readings in the top drive motor. The experiment used PID controller set points ranging from 5 to 45 kg and hoisting motor torque limitations of 0.2, 1 and 2 Nm. **Fig.** (C.3) shows a scatter plot of WOB measured by the load cell versus hoisting motor torque for a WOB set point of 25 kg and maximum torque of 1 Nm.

As evident by the graph, hoisting motor torque generally varies between 0 and 0.4 Nm a set point of 25 kg. There is no clear linear correlation between WOB and torque. It is also worth noting that set points around 25 kg generally resulted in little spread compared to scatter plots of low and high WOB set points. Based on these results, it was concluded that torque measurements in the hoisting motor can not produce reliable measurements of WOB, and that a load cell must be included in the rig design.

The team has considered several rig designs with a load cell in different locations. Initially, the idea was to place a load cell between the top drive motor and swivel. With this solution, the load cell would rotate together with the drill string. Wiring for power and measurements would be connected to the electrical swivel that is already installed on the rig. Upon investigation, the solution proved to be troublesome. Firstly, suppliers did not specify distribution of weight in the available load cells. For instance, wire sockets along the outer wall of the cylinder are usually placed on the edge of load cells. If the mass is not evenly distributed in the load cell, mass imbalance when rotated could impact drilling performance. Secondly, all cylindrical load cells that were investigated were designed for stationary systems. Incorporating a rotating load cell would require investigation whether they would read reliable measurements while rotating, and how to compensate for rotation at varying rotational speeds.

A second solution was proposed to incorporate a stationary load cell between the top drive and swivel. With this design, the load cell would sit between the upper stationary section of the swivel and below a horizontal steel beam connected to the ball screw. In order to stabilize the rig, the design included a second set of vertical steel beams and roller guides, as well as a larger frame surrounding the top drive motor. The principle of the design is shown in **Fig.** C.4. The top drive sits above the load cell to limit the total height of the rig. An implication of this design is that either the cylindrical load cell would have to be hollow, or the design would need two load cells at either side of the rotating parts below the top drive motor. While at first glance the design seems rigid and able to provide
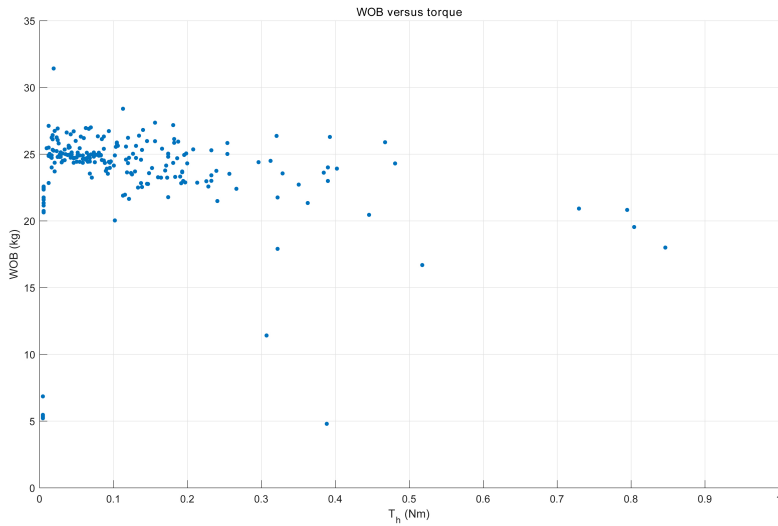
Figure C.3: Scatter plot of WOB versus hoisting motor torque with a maximum hoisting motor torque of 1 Nm and WOB set point of 25 kg.

stable measurements of WOB, it was rejected due to its impact on the overall design, added weight to the rig and the fact it got outperformed by the final, more simple and less intrusive design proposal.
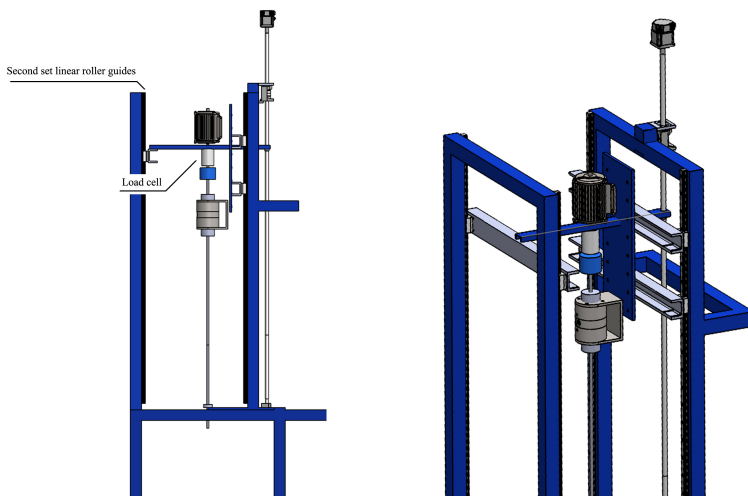
Figure C.4: Principle of design with stationary cylindrical load cell mounted between the top drive motor and swivel. Note that the horizontal steel beam connected to the ball screw is connected to both sets of linear roller guides, as well as the load cell.

C.3 Alignment Analysis

Disclaimer*: This section of the appendix is taken from the project report of the thesis.*

In an effort to locate causes of misalignment and lateral vibrations when drilling, all parts involved in the rotating system have been analysed. These include the top drive motor and all parts mounted around it, the upper pipe connection, the roller bearing at RKB, the roller bearing between RKB and rock samples, and the lower pipe connection. These are shown in **Fig. C.5**. The discussion is shown below:

All components above drill pipe and connection

All components above the upper drill pipe connection are permanently attached to the rig and will normally not be modified between drilling experiments. These components include the top drive motor, electrical and hydraulic swivel and steel pipe connecting the components. Assuming all other sections in the rotating system are aligned, misalignment of these components would cause the drill pipe to extend at an angle from the rig, as can be seen by the illustration in **Fig. C.5a**. As illustrated, this misalignment would cause the drill pipe to extend and rotate around an axis offset from the upper roller bearing and other equipment below RKB. Lateral force must be applied to guide the drill pipe inside the roller bearing.

Upper connection between top drive motor and drill pipe

A second potential cause of misalignment in the rotating system is the upper connection used to attach the drill pipe to the rig. The case is illustrated in **Fig. C.5b**. If the upper connection is misaligned, the drill pipe will extend at an angle to the axis of rotation, causing the pipe to rotate in a circular periodic motion around the upper roller bearing.

Roller bearing at RKB

The upper roller bearing may be misaligned either by being mounted at an incline, or at an offset relative to the axis of rotation of the pipe. The first case has similar consequences as in (b) above, although with the cause of the problem closer to the bit. The latter case is illustrated in **Fig. C.5c**. In this case, lateral force must be applied to the pipe to guide it inside the roller bearing.

Roller bearing in riser below RKB

A second roller bearing is housed in a riser below RKB. It serves as a second stabilizing element between the first stabilizer and the rock sample. If the bearing is displaced from the axis of rotation, similar misalignment issues as those related to the upper roller bearing would arise. This is illustrated in **Fig. C.5d**.
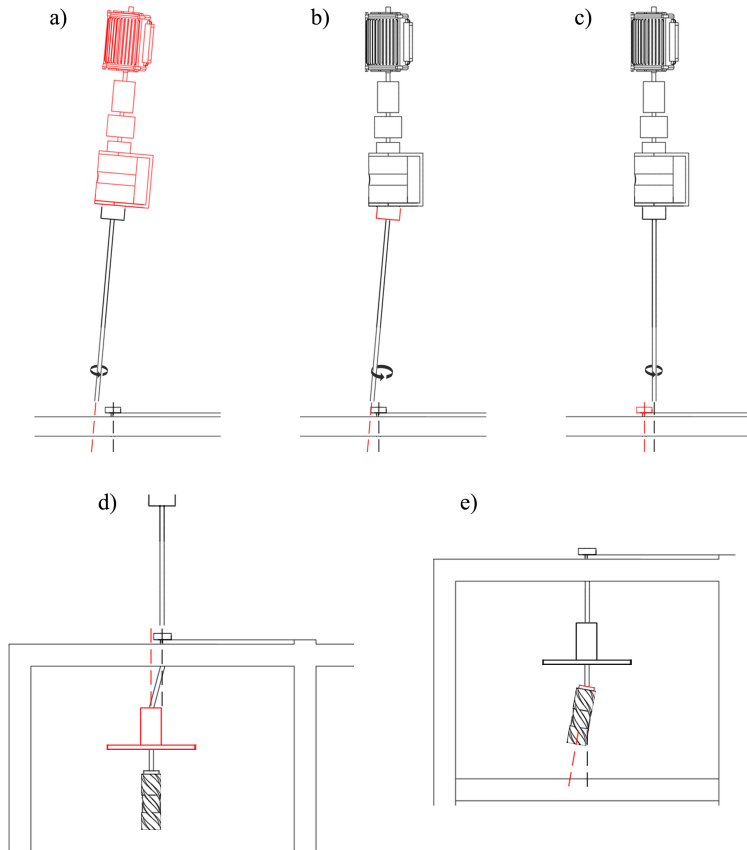
Figure C.5: Illustration of causes with misaligned components in the rotating system. a. Misalignment of all components attached to the guide frame. b. Misalignment of upper connection. c. Misalignment of upper stabilizer at RKB. d. Misalignment of lower stabilizer below RKB. e. Misalignment of lower connection.

Lower connection between drill pipe and BHA

The BHA is connected to the drill pipe by the same type of connection that is used to attach the drill pipe to the rig. Misalignment of the lower connection is illustrated in **Fig. C.5e**. Due to eccentricity, the contact area between the bit and rock samples is be larger than the bit itself, resulting in drilling of over-gauged wells.

C.4 Swivel Challenges

The hydraulic swivel is an integral part of the rig design and was initially designed last year for the first version of NTNU's miniature drilling rig. The hydraulic swivel serves as an inlet for the drilling mud, seals of the fluid and drill shaft and supports pressure build up in the drill string.

Fig. C.6 shows a photo of the actual hydraulic swivel and a schematic of the layout. The Top Drive motor provides power to the drill string shaft and is connected with a variable couple to mitigate vibrations. Cables for the down hole sensors are fitted through the shaft and connected to the BHA. The schematic shows how the rotating shaft is supplied with high pressure drilling mud without it spilling. Two small chambers are filled with hydraulic oil and is kept at a 5.3 bar backpressure to hold the rubber v-seals and metal seals in place. It is evident that faulty seals will result in leakage.

A leak was discovered during the initial testing phase of the rig. Hydraulic oil was spilling from the hydraulic connections highlighted in the red circle of **Fig. C.6**. As a result, the swivel was disassembled and re-threaded. The dissasembled swivel is shown i **Fig. C.7**. More issues arouse after the swivel was reassembled. Pressure testing of the hydraulic swivel was performed whenever it had been altered. A test is successful only if the seals hold for a longer period of time. If the seals are pressure tight, the water and oil filled piston remains stationary as 5.3 bars of backpressure is applied from the water supply. Note that oil inside of the drillpipe indicates a leak in the rubber v-seals and that oil on the outside of the shaft and roller bearings indicate a leak in the rubber/metal seal. During the pressure testing, it was evident that the swivel leaked in one of the rubber v-seals as oil leaked out from the drillpipe. **Fig. C.8** shows the cause of the leakage. During assembly, the shaft had caught metal shavings from re-threading the connectors. The metal shaving had damaged the rubber v-seal and shaft effectively creating a channel for the oil to flow across the rubber v-seal. The upper rubber/metal seal was also damaged and had to be replaced.

Subsequent pressure testing after the shaft had been fixed and seals replaced indicated that the lower v-seal had also been damaged, as well as the the lower rubber/metal seal. **Fig. C.9** shows the result of a pressure test where the rubber v-seals have failed. Again, the swivel had to be taken apart, fixed, reassembled and pressure tested. The final result is a functioning swivel ready for operation. Towards the end of the semester, a new leak in the swivel occurred in the metal seal, and the process of assembling and disassembling the swivel was repeated. The leaks in the hydraulic swivel is one of many examples of mechanical issues that have taken alot of time to fix.
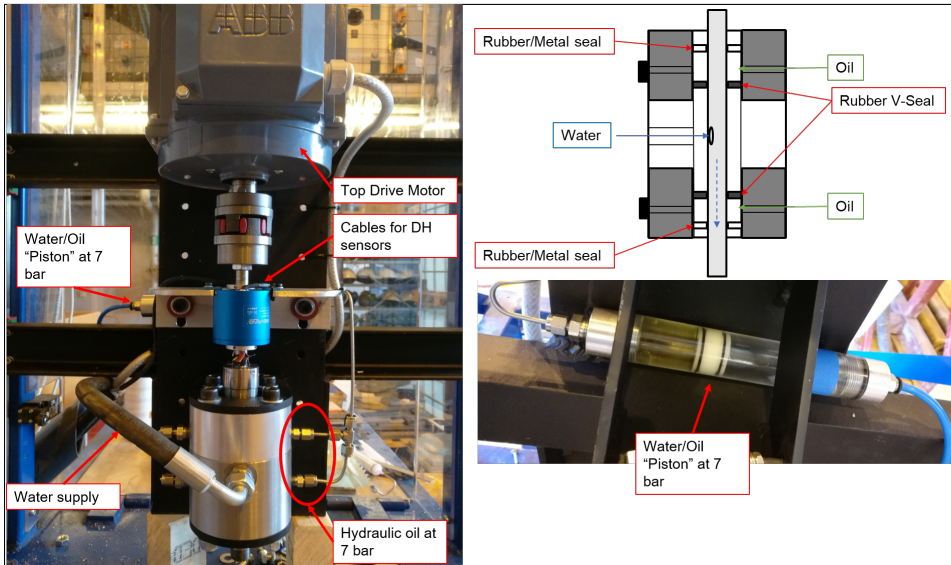
Figure C.6: Photo and schematic of the hydraulic swivel. Note that the back pressure is 5.3 bar, not 7 bar as indicated by the figures.

Figure C.7: Photo of the disassembled swivel.
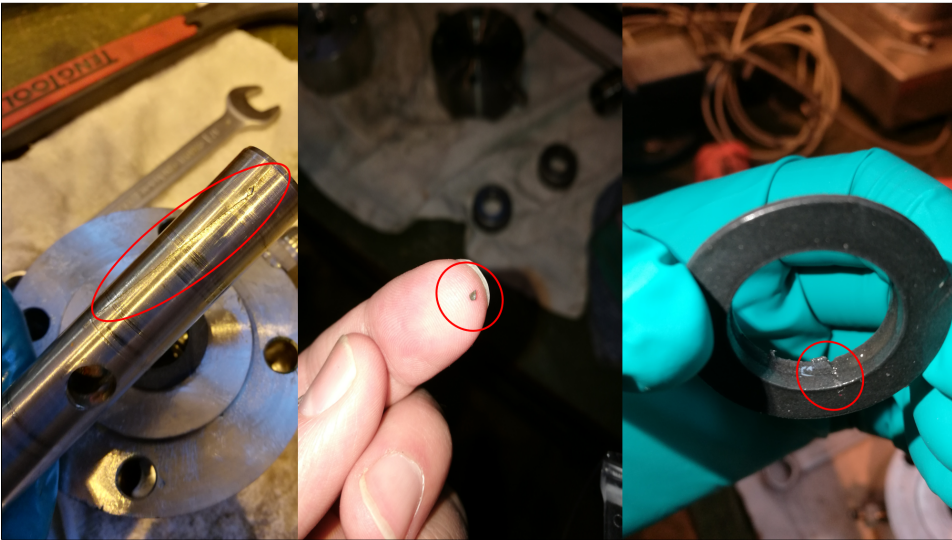
Figure C.8: Damage to upper v-seal and shaft leading to leak in the hydraulic swivel.
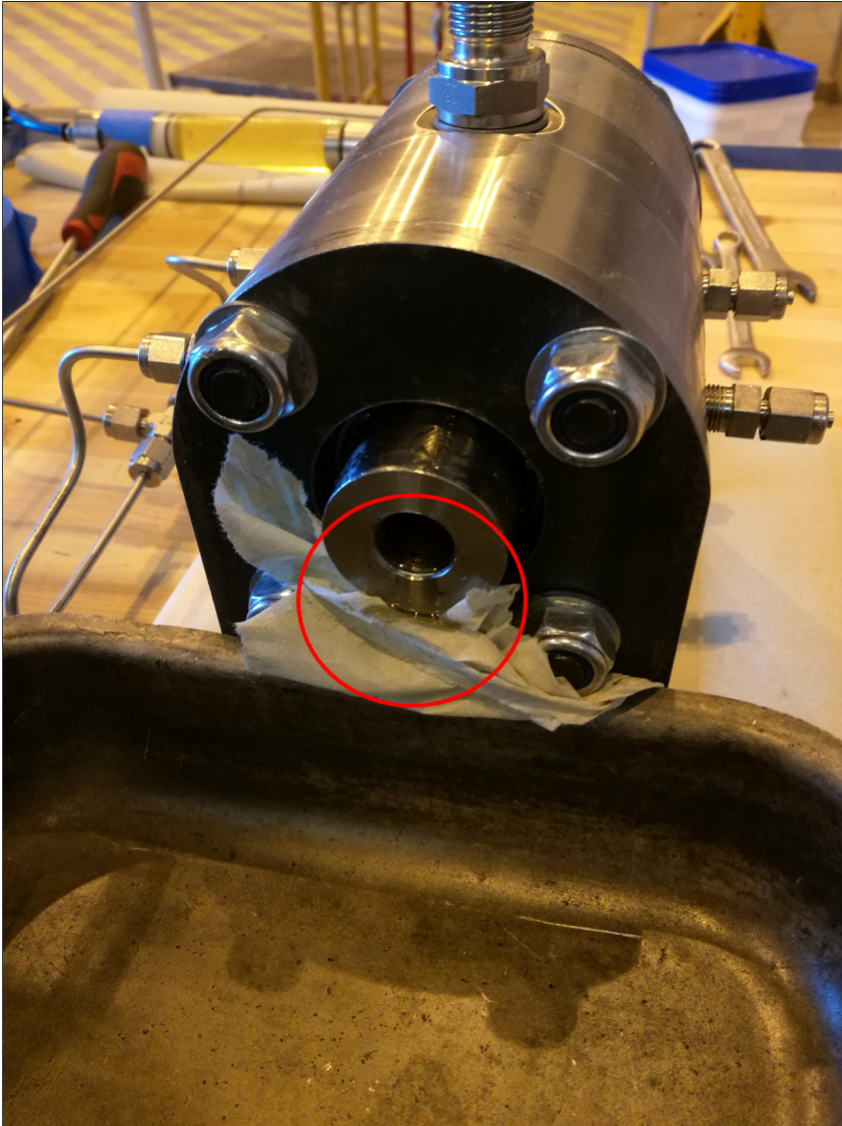
Figure C.9: Pressure test showing a leak in on of the rubber v-seals evident by oil inside the shaft.

C.5 Rig Components and Instrumentation Specifications

C.5.1 Rig Specifications
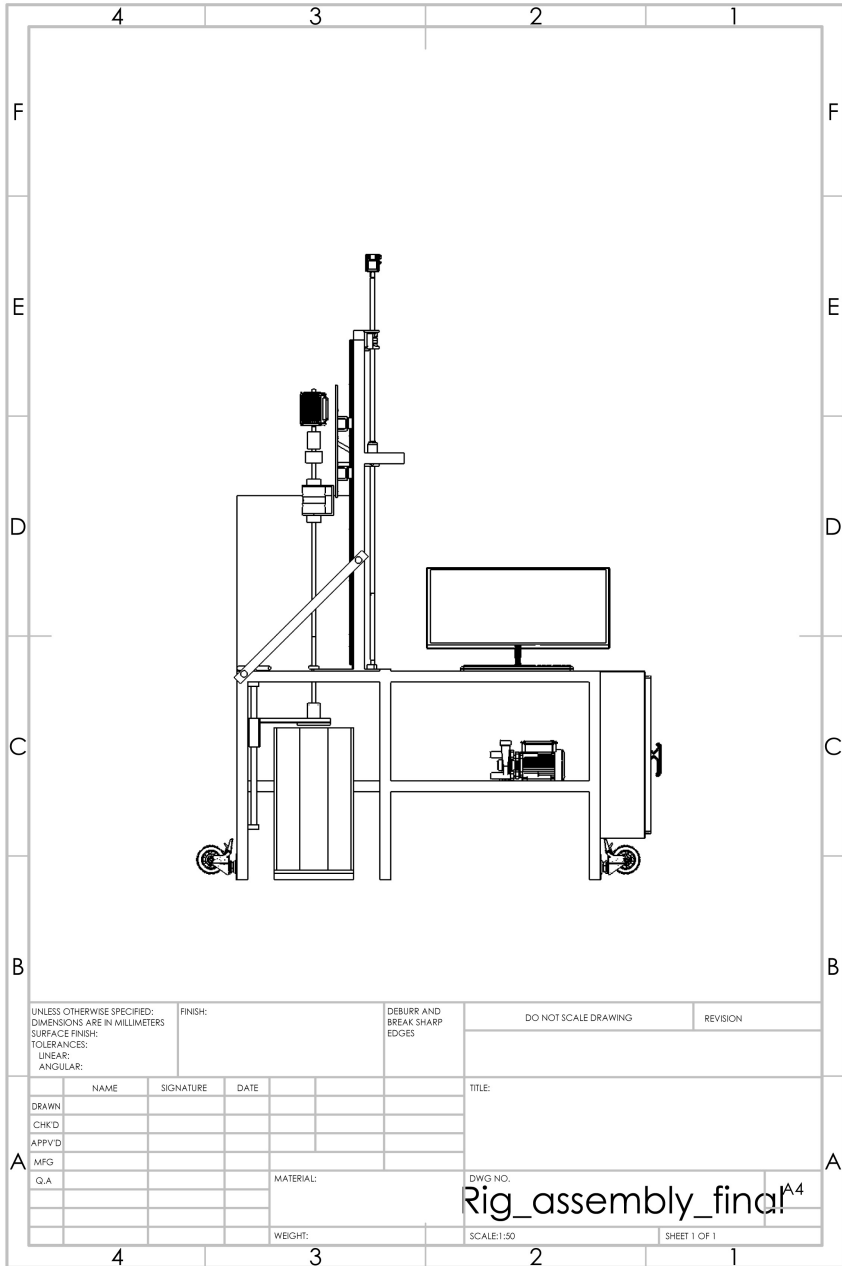
Figure C.10: Complete rig construction with all equipment.
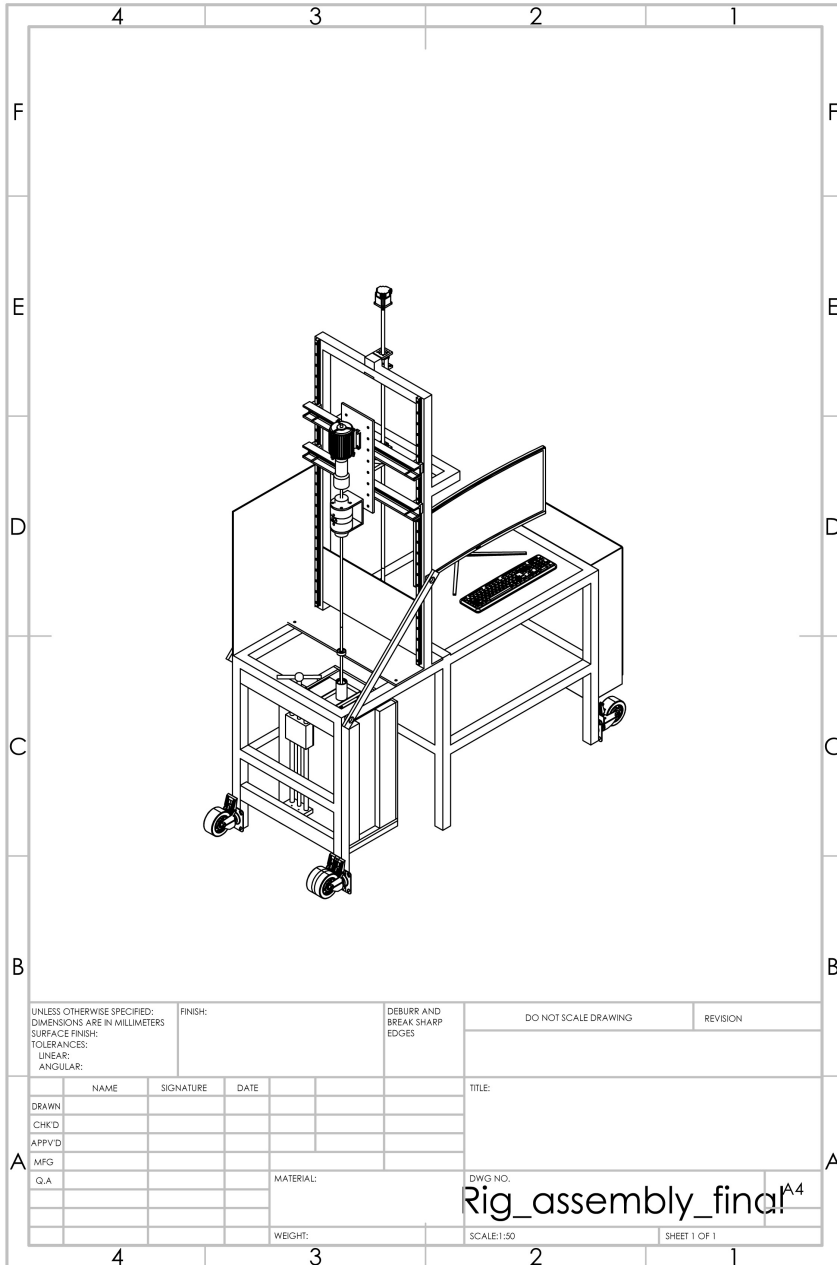
Figure C.11: Complete rig construction with all equipment.
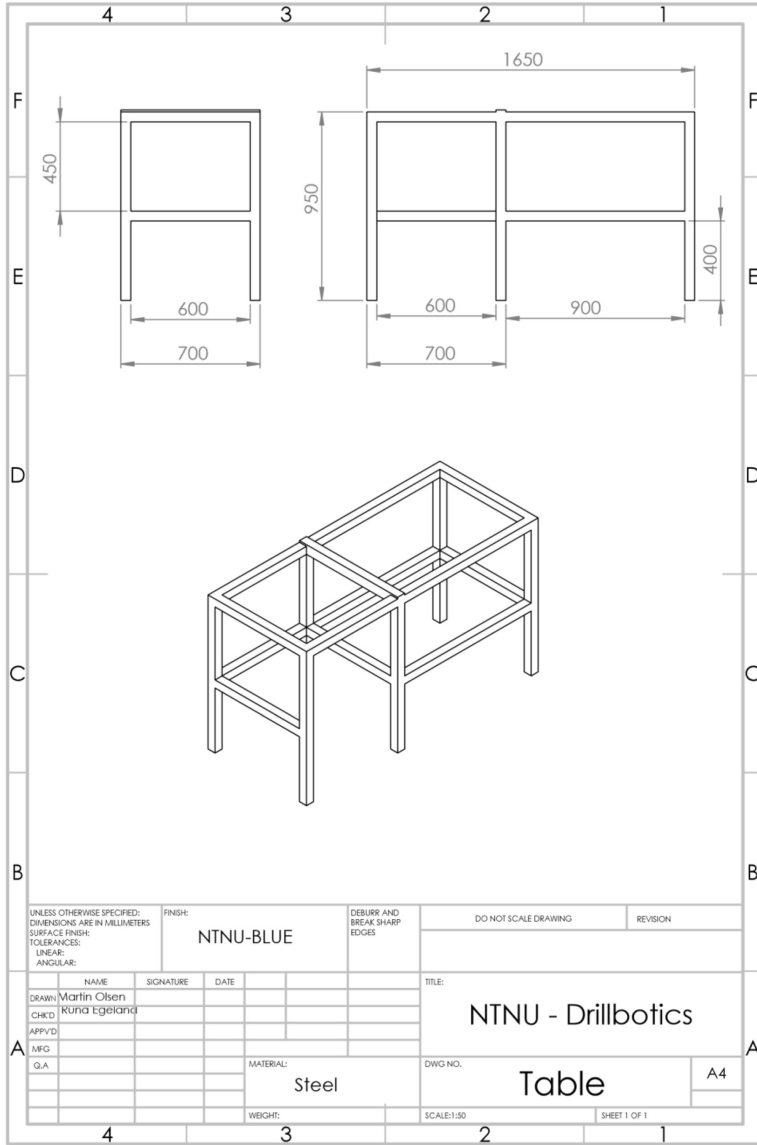
Figure C.12: Rig framework.
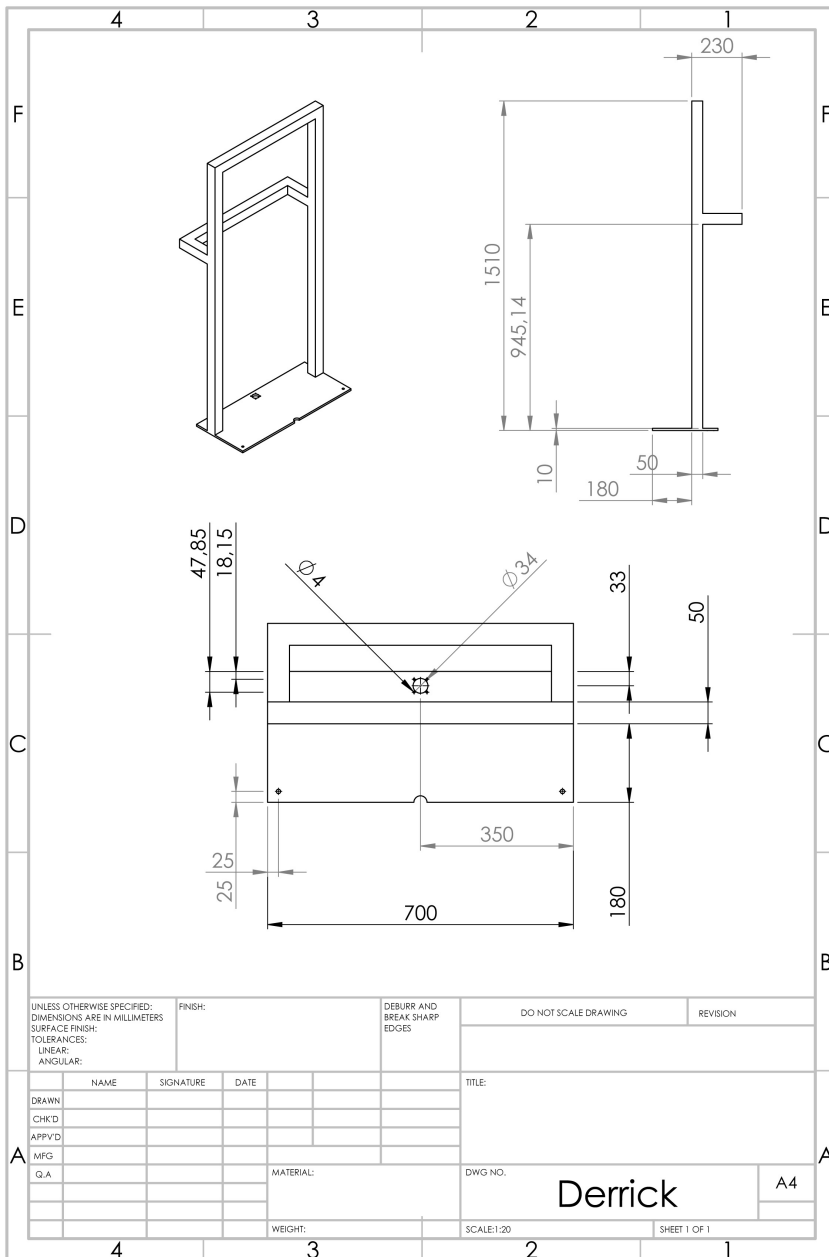
Figure C.13: Complete derrick structure.

Figure C.14: Derrick base.
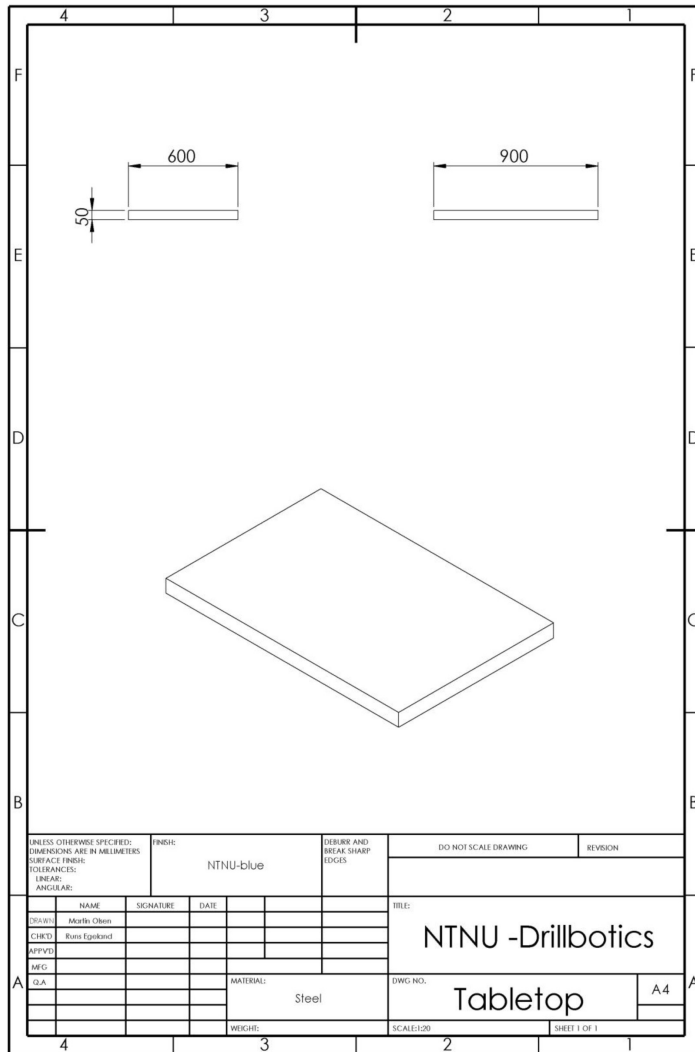
Figure C.15: Tabletop.
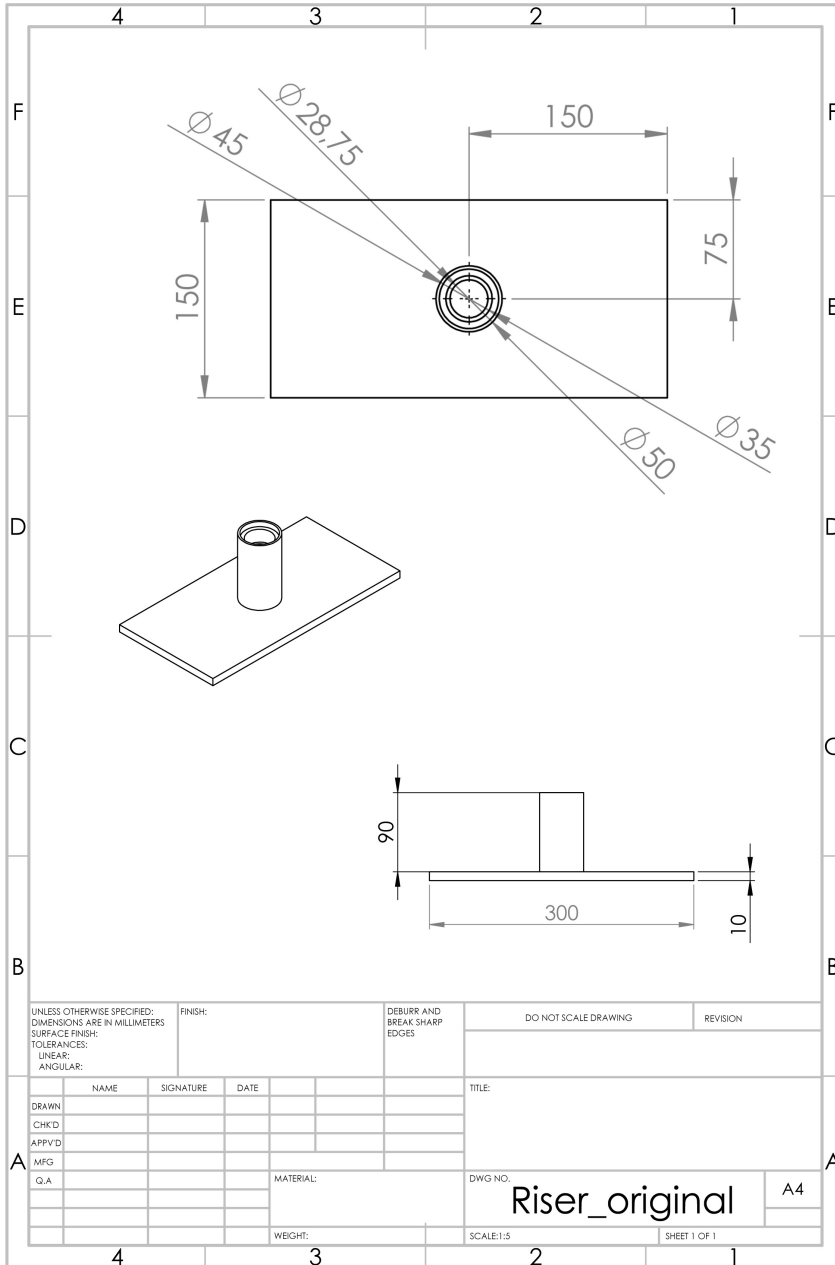
Figure C.16: Guide base for dynamic guide base.
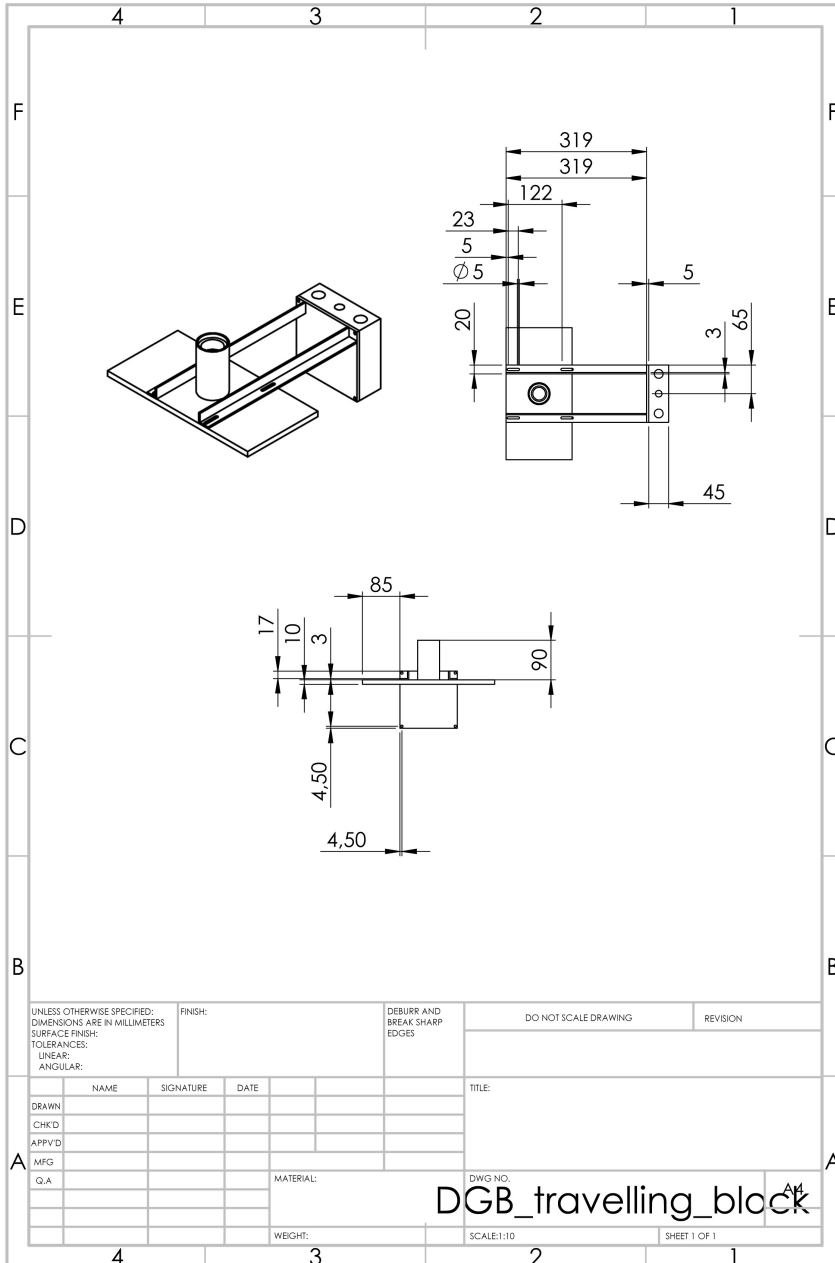
Figure C.17: Travelling block for dynamic guide base.
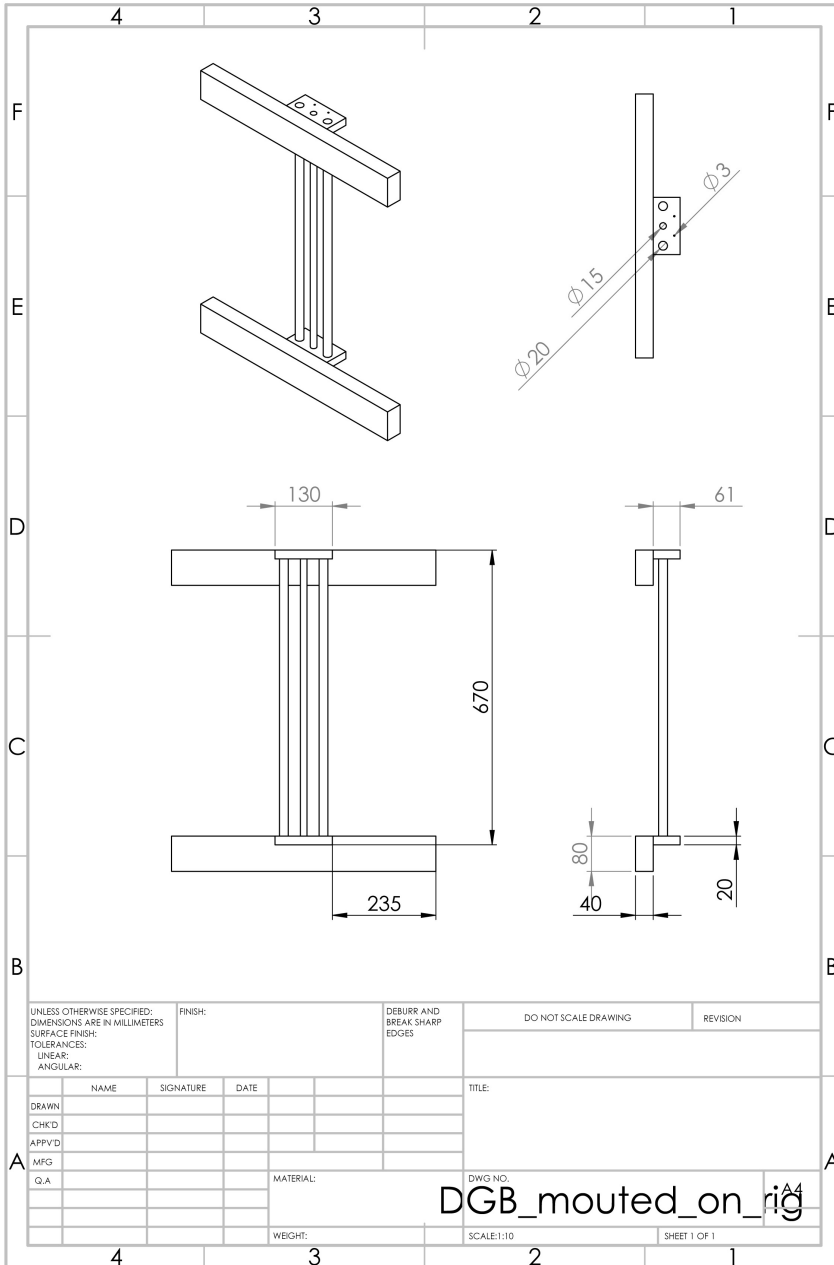
Figure C.18: Rig mount for dynamic guide base.
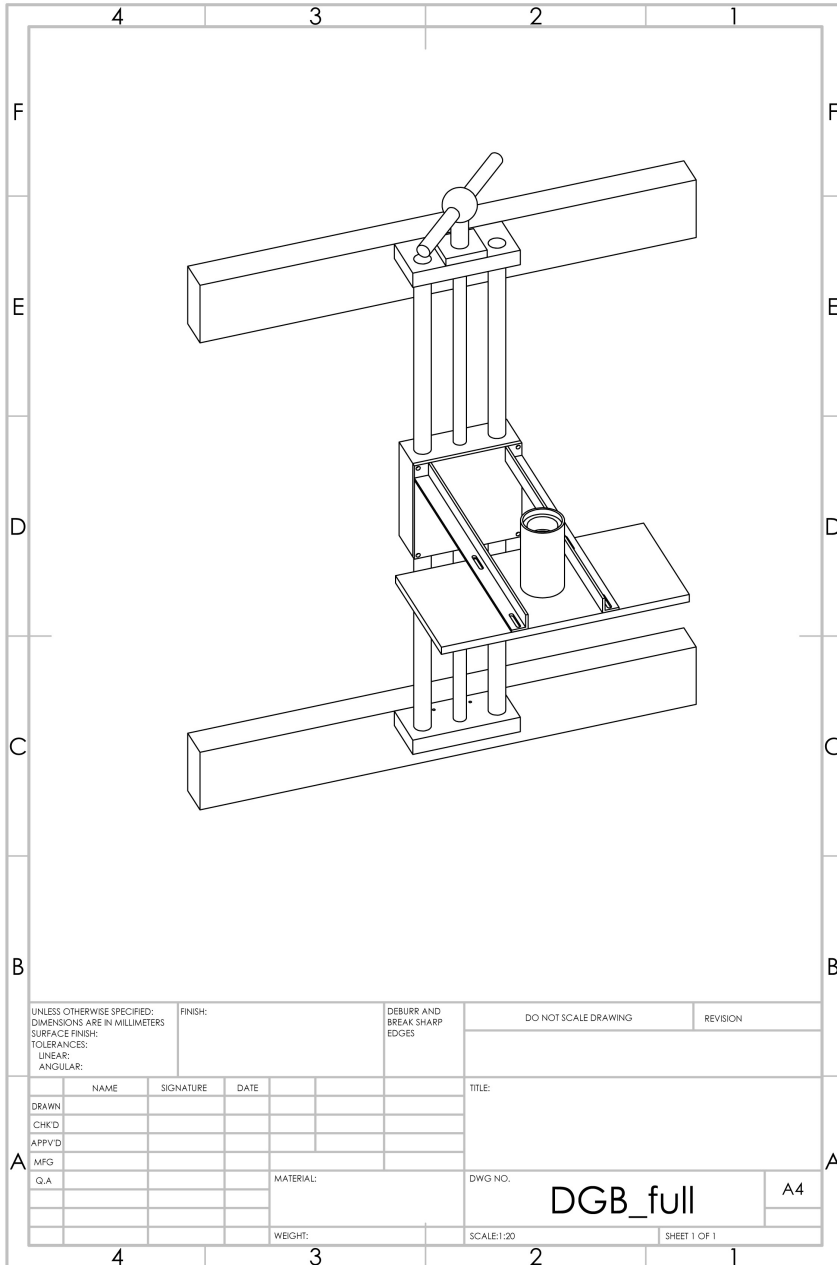
Figure C.19: Complete dynamic guide base.
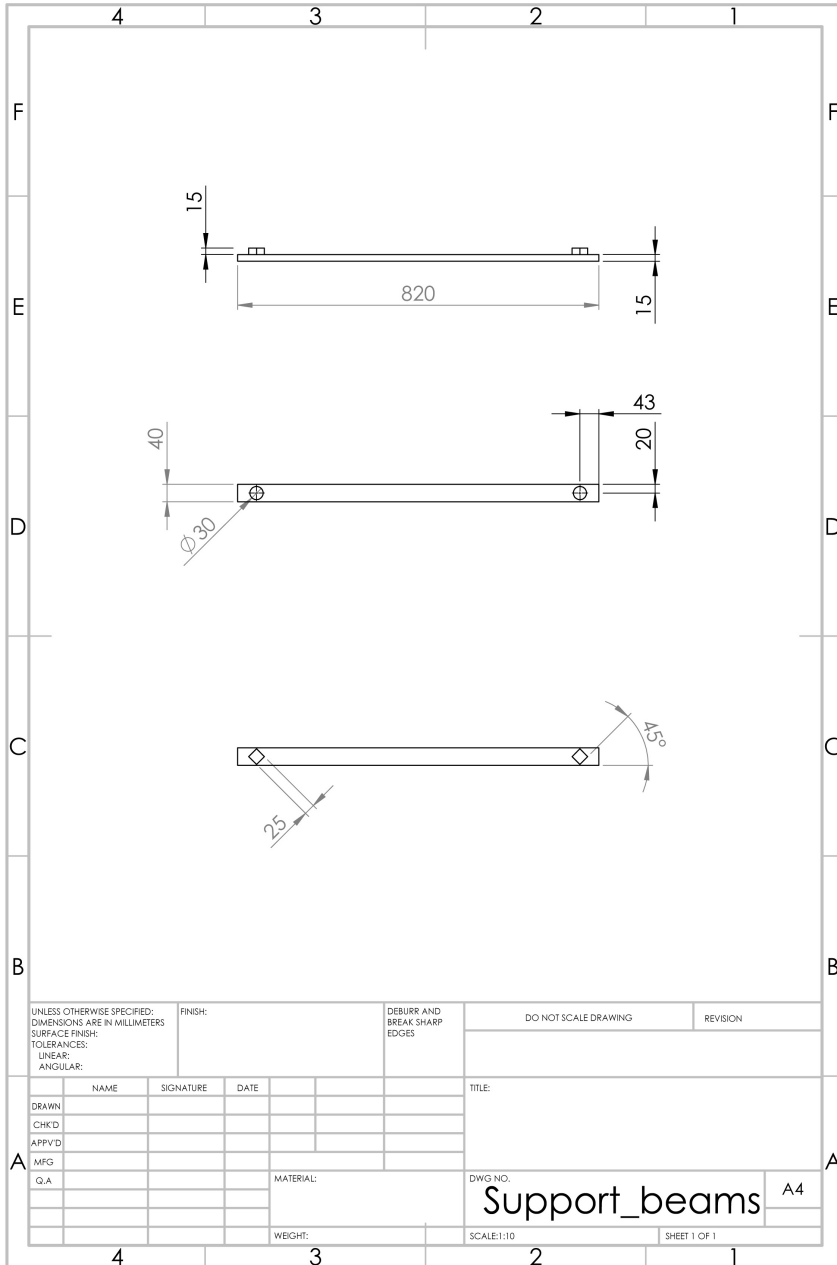
Figure C.20: Support beam.
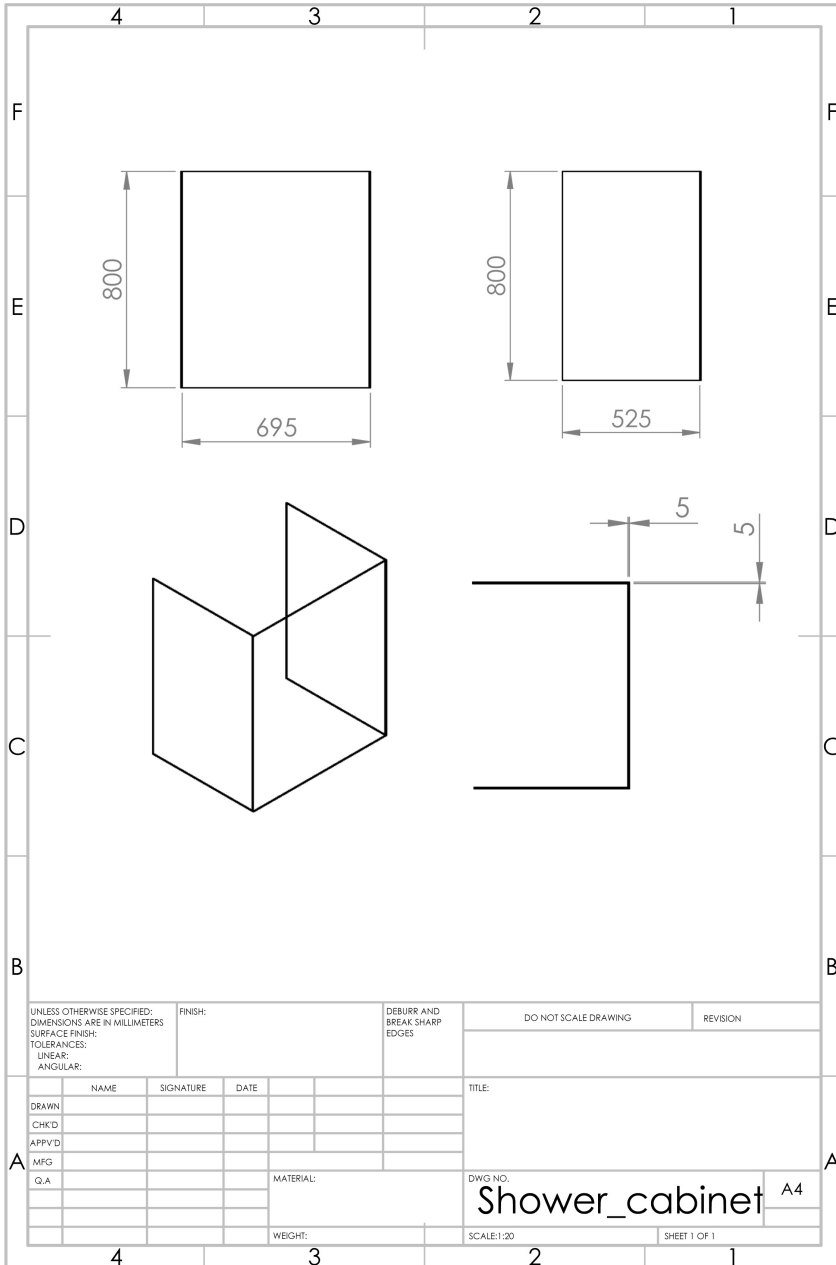
Figure C.21: Protective acrylic glass above RKB.
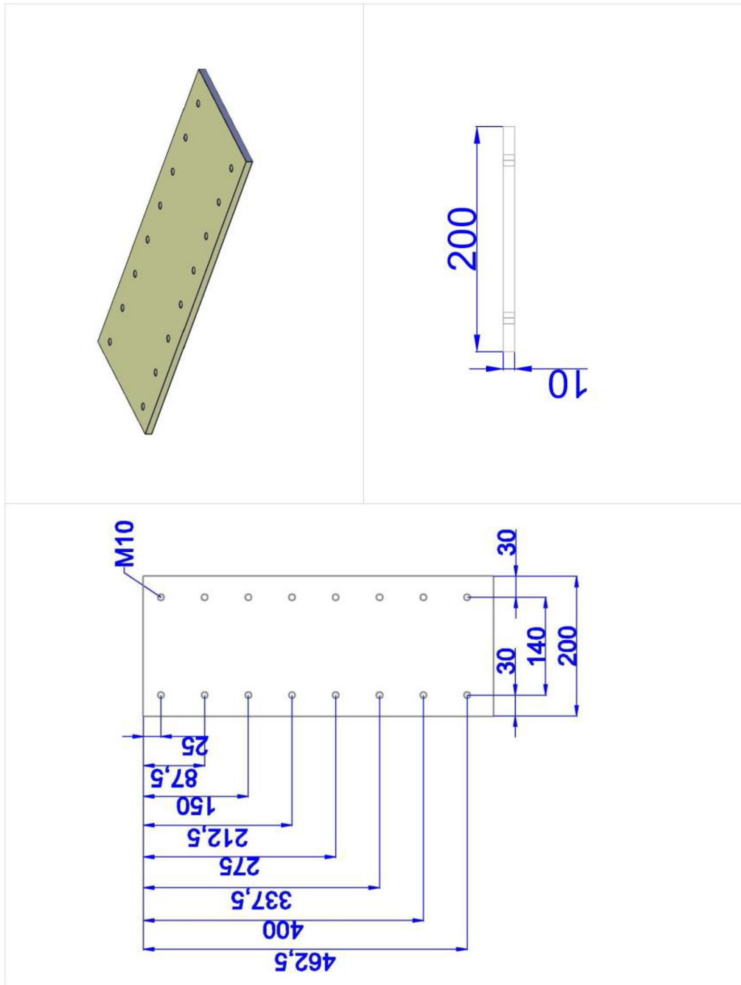
Figure C.22: Carriage mount for top drive motor.
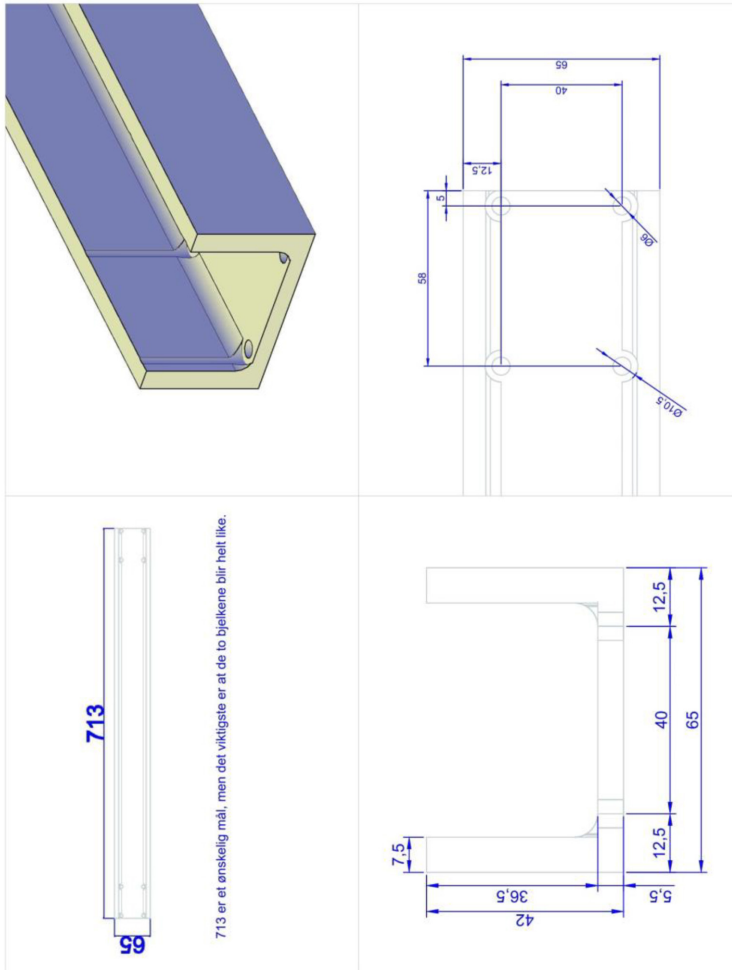
Figure C.23: Strut for carriage.
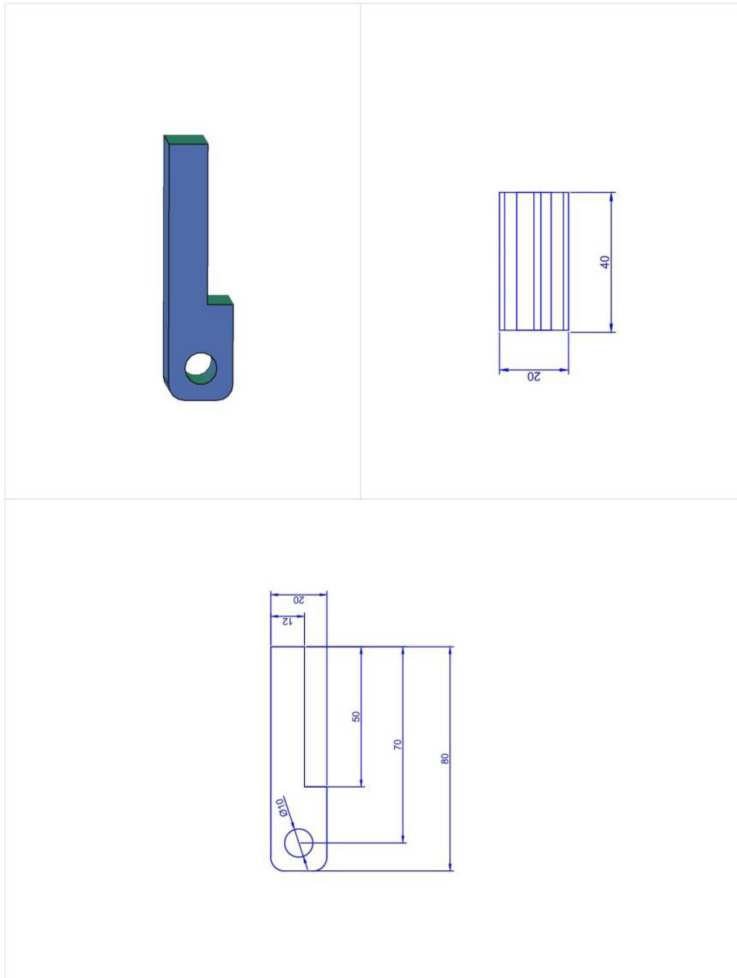
Figure C.24: Hinge first part.
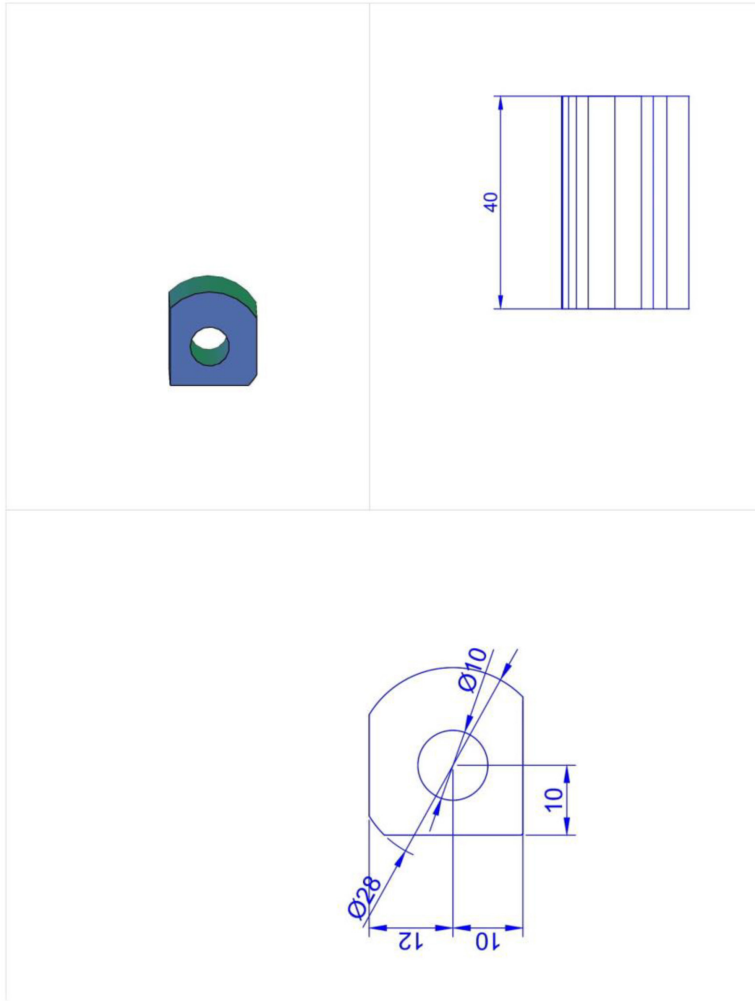
Figure C.25: Hinge second part.
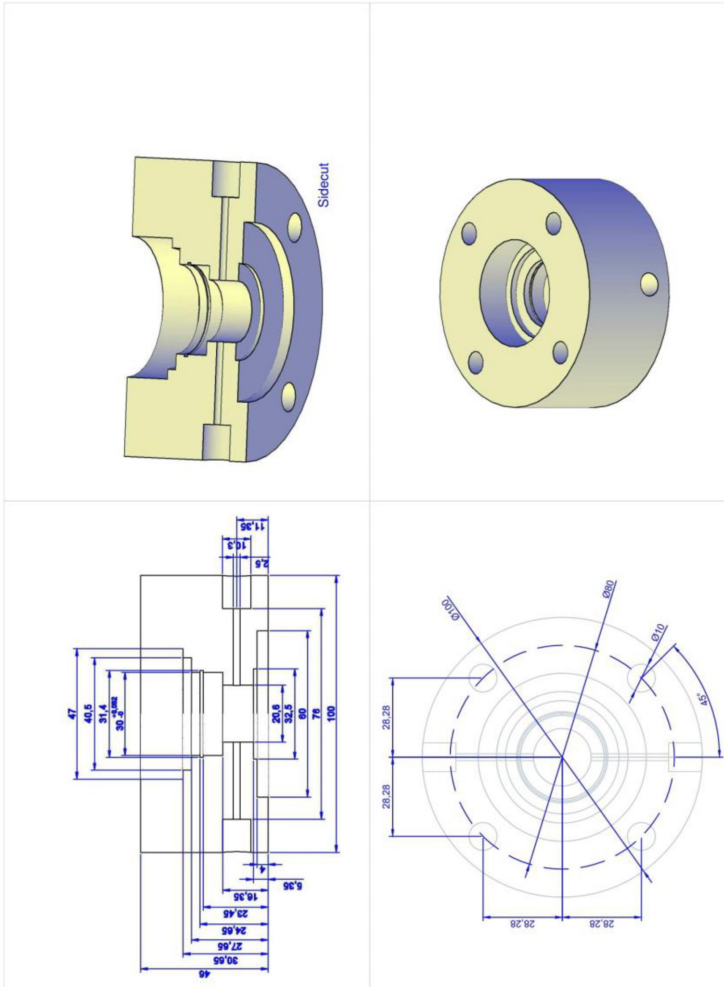
Figure C.26: Top and bottom part of swivel.

Figure C.27: Middle part of swivel.
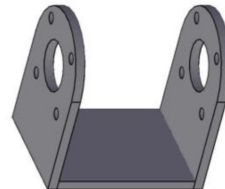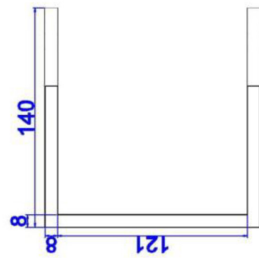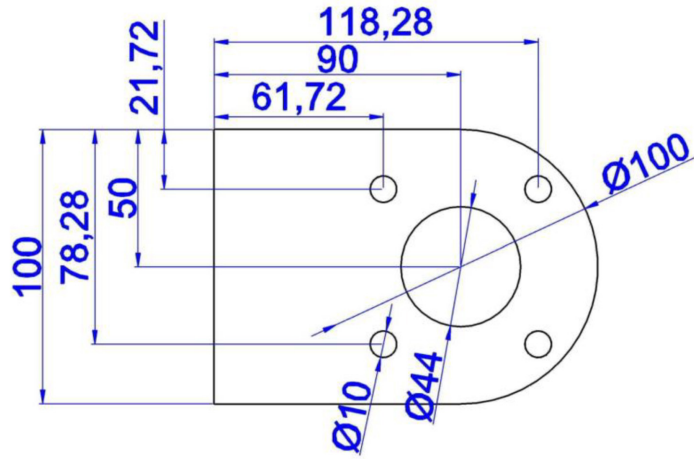
Figure C.28: Holder for swivel.
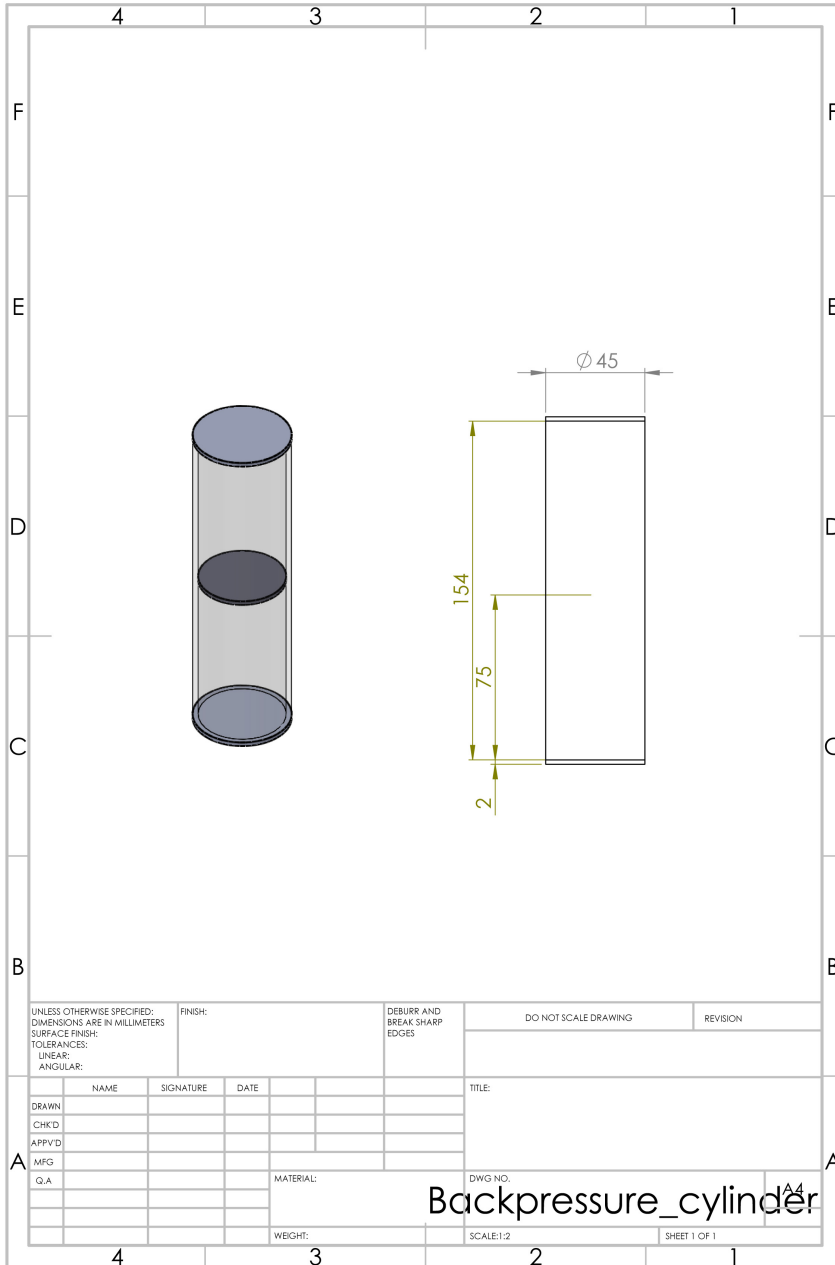
Figure C.29: Pressure chamber for backpressure in swivel.
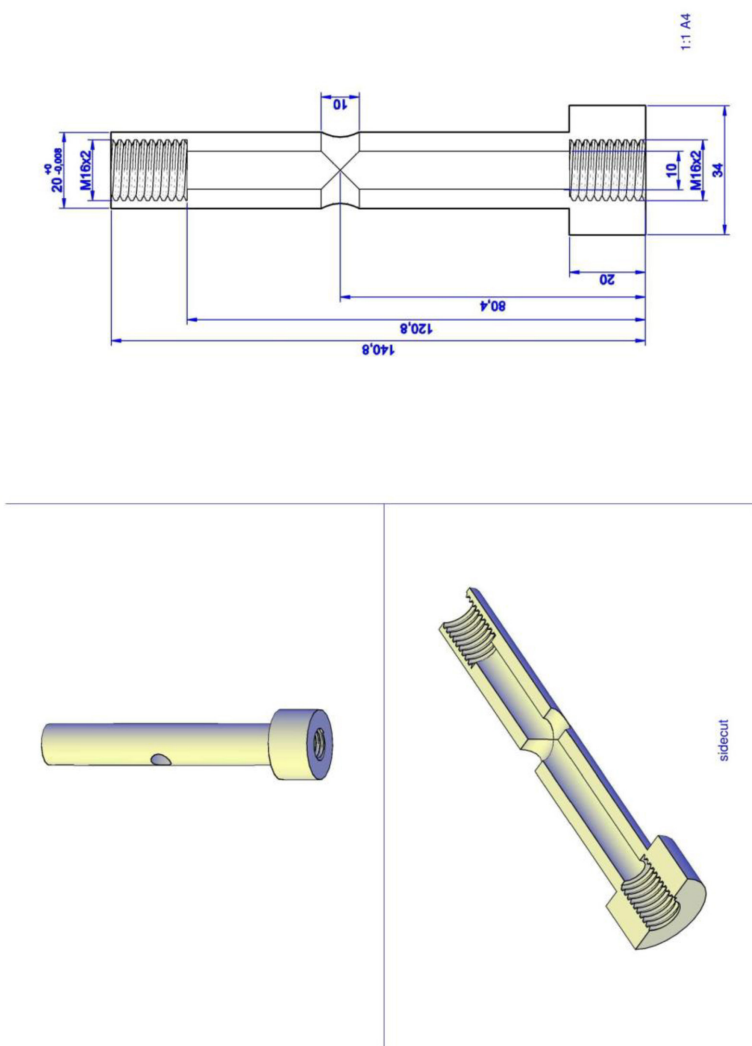
Figure C.30: Hollow shaft for water.
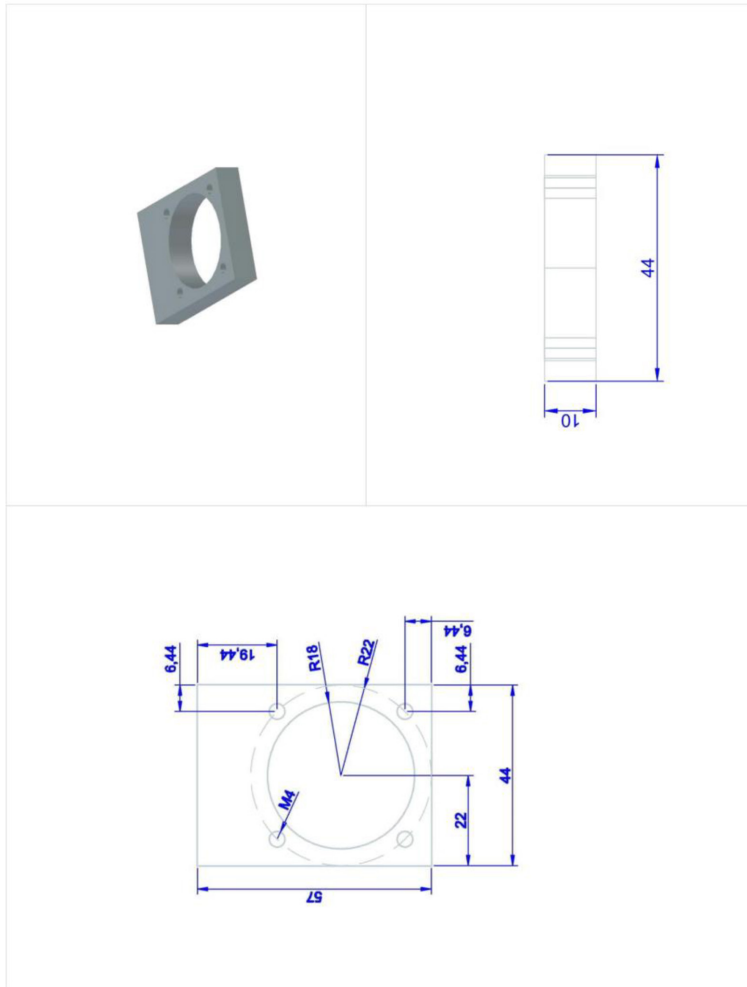
Figure C.31: Bottom mount for hoisting motor.
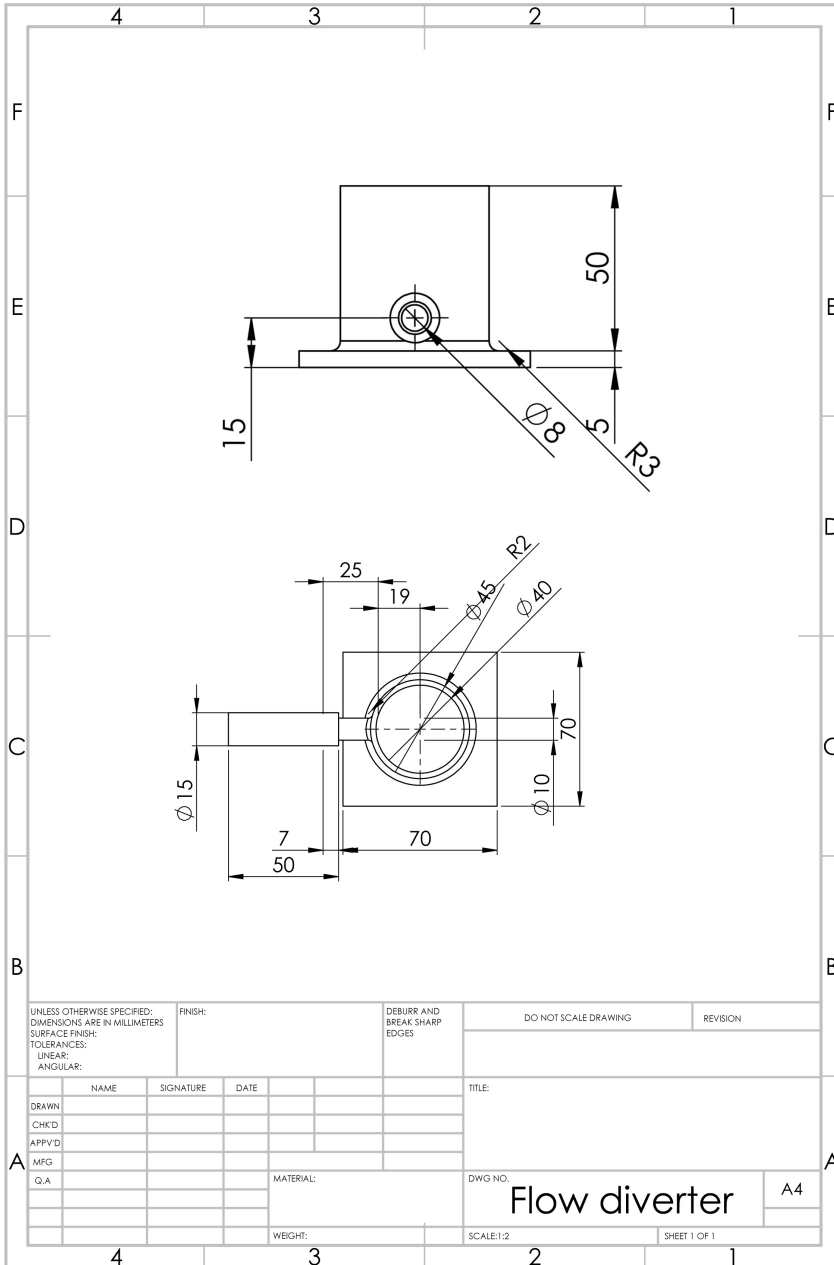
Figure C.32: Bell nipple.

C.5.2   Bottom Hole Assembly Specifications

R10

2

M20x1
6.5 mm

3,80

3,80

51

30

D

10

3/8" NPT

R7,25

R8

R11,37

	NAME	SIGNATURE	DATE			TITLE:	
DRAWN							
CHK'D							
APPV'D							
MFG							
Q.A				MATERIAL:		DWG NO.	

UNLESS OTHERWISE SPECIFIED:
DIMENSIONS ARE IN MILLIMETERS
SURFACE FINISH:
TOLERANCES:
  LINEAR:
  ANGULAR:

FINISH:

DEBURR AND
BREAK SHARP
EDGES

DO NOT SCALE DRAWING

REVISION

282

Main body - cross section view

A4

WEIGHT:

SCALE:1:1

SHEET 1 OF 1

Main body - top view

R8,57

R2,37

3/8" NPT
5 revolutions

18

8

3

7

1

2

∅4

R4,37

R11,37

M8x1
5 revolutions

Dyn Sub Top - cross section vie

35°

55°

R14,25

$\emptyset$17,1?

$\emptyset$4,73

R11,37

		NAME	SIGNATURE	DATE			TITLE:			
	DRAWN									
	CHK'D									
	APPV'D									
	MFG									
	Q.A			MATERIAL:			DWG NO.			A4

Dyn Sub Top - top view

WEIGHT: SCALE:2:1 SHEET 1 OF 1

Dyn Sub Bottom - cross section v

R4,37

R2,37

M8x1
5 revolutions

1

2

R2

21

8

7

4

10

R8,57

R11,37

3/8" NPT

Ø20,73
R14,25
Ø8,73
Ø4,74
R11,37
Ø12,73

Dyn Sub Bottom - top view

	NAME	SIGNATURE	DATE				TITLE:
DRAWN							
CHK'D							
APPV'D							
MFG							
Q.A				MATERIAL:			DWG NO.

WEIGHT:

SCALE:1:1

SHEET 1 OF 1

A4
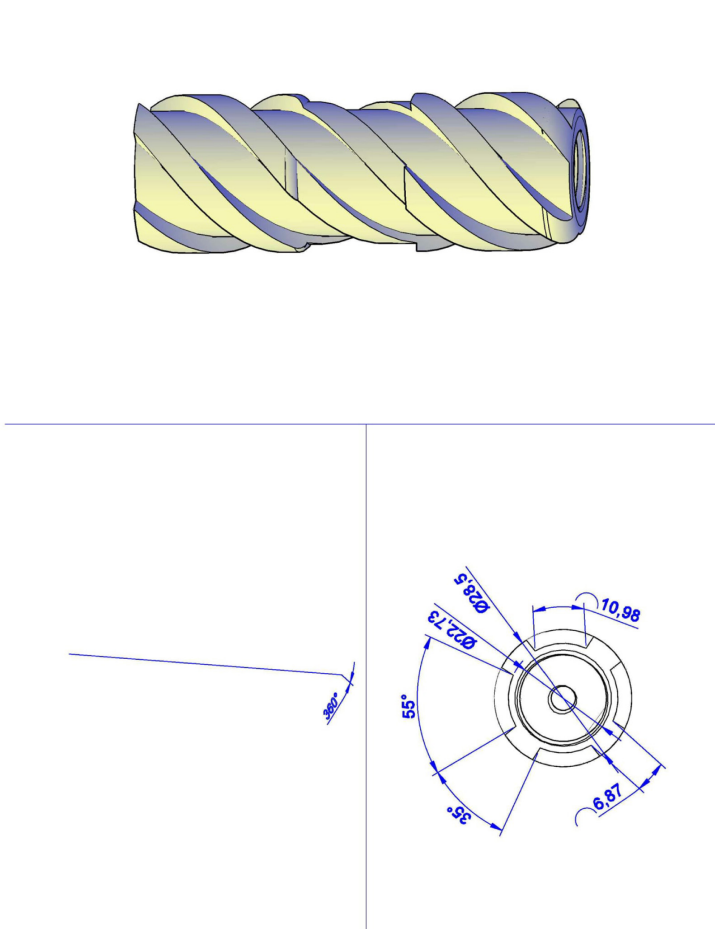
Figure C.33: Old BHA body external view.

Figure C.34: Old BHA body cross section view.
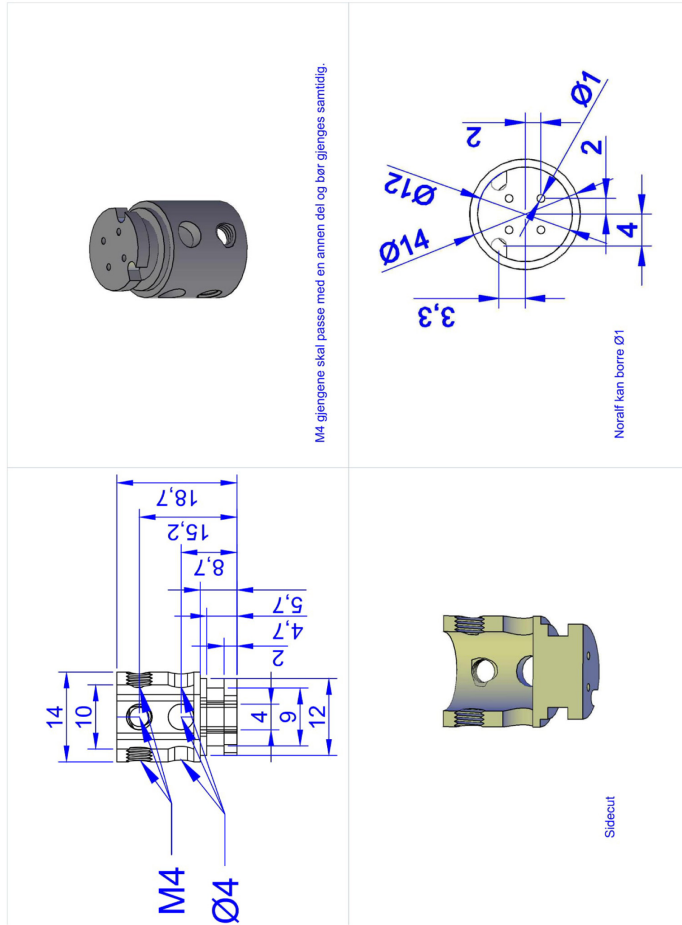
Figure C.35: Middle part of old BHA.
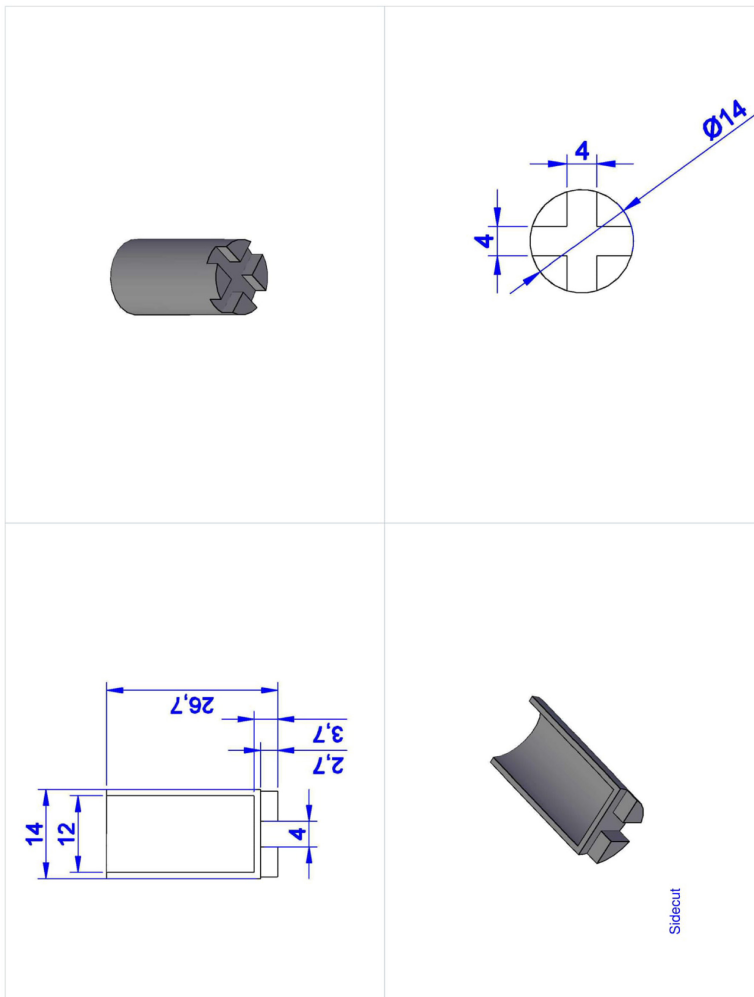
Figure C.36: Old BHA sensor cover.
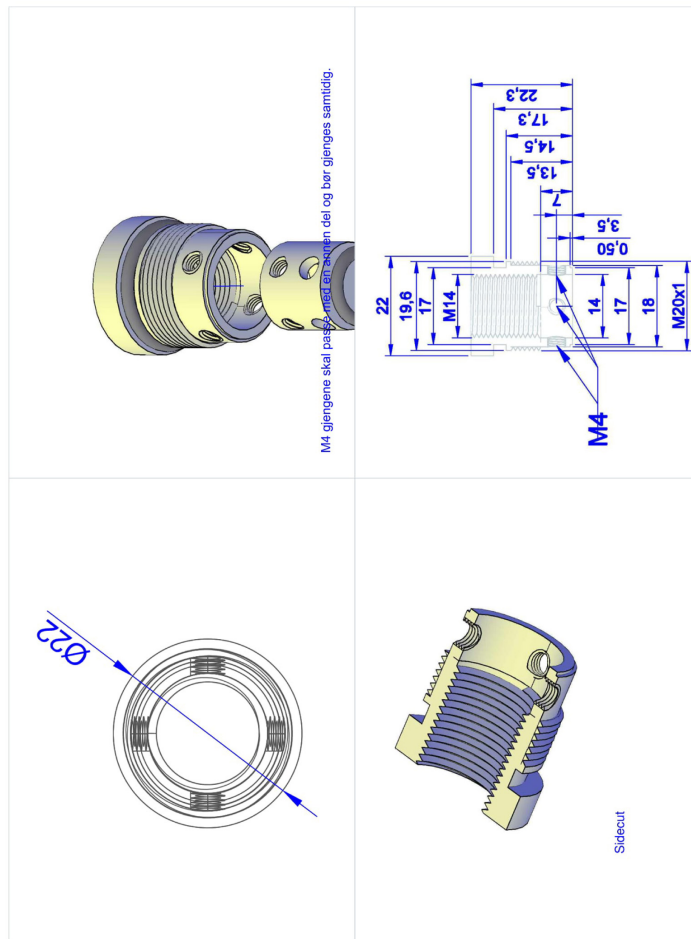
Figure C.37: Old BHA upper part.
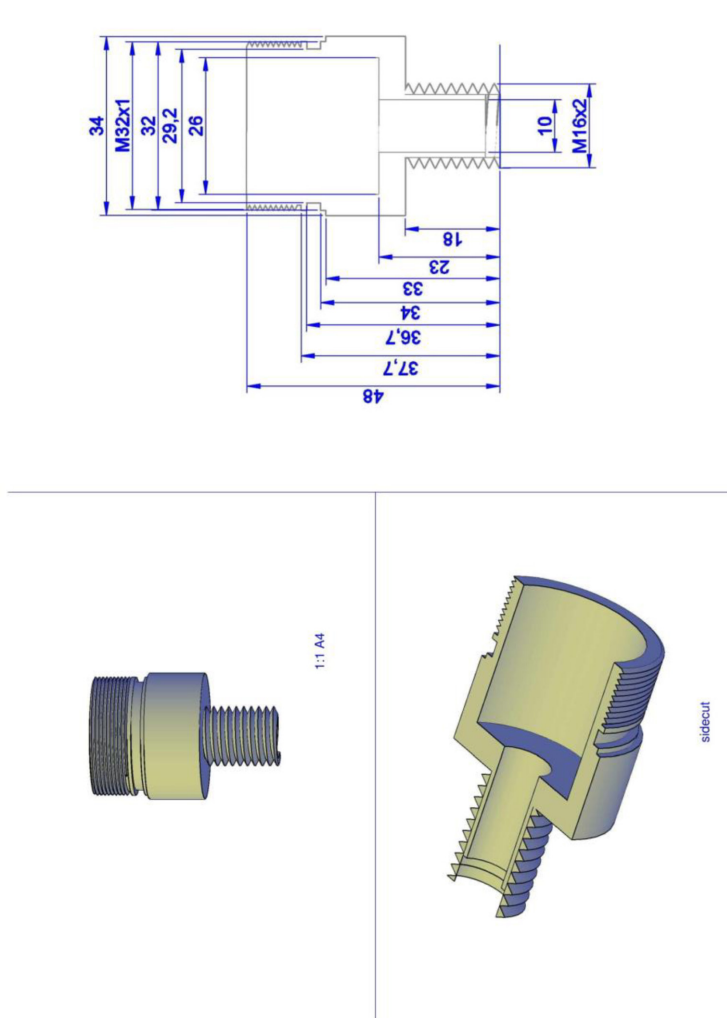
Figure C.38: Old BHA sensor housing.
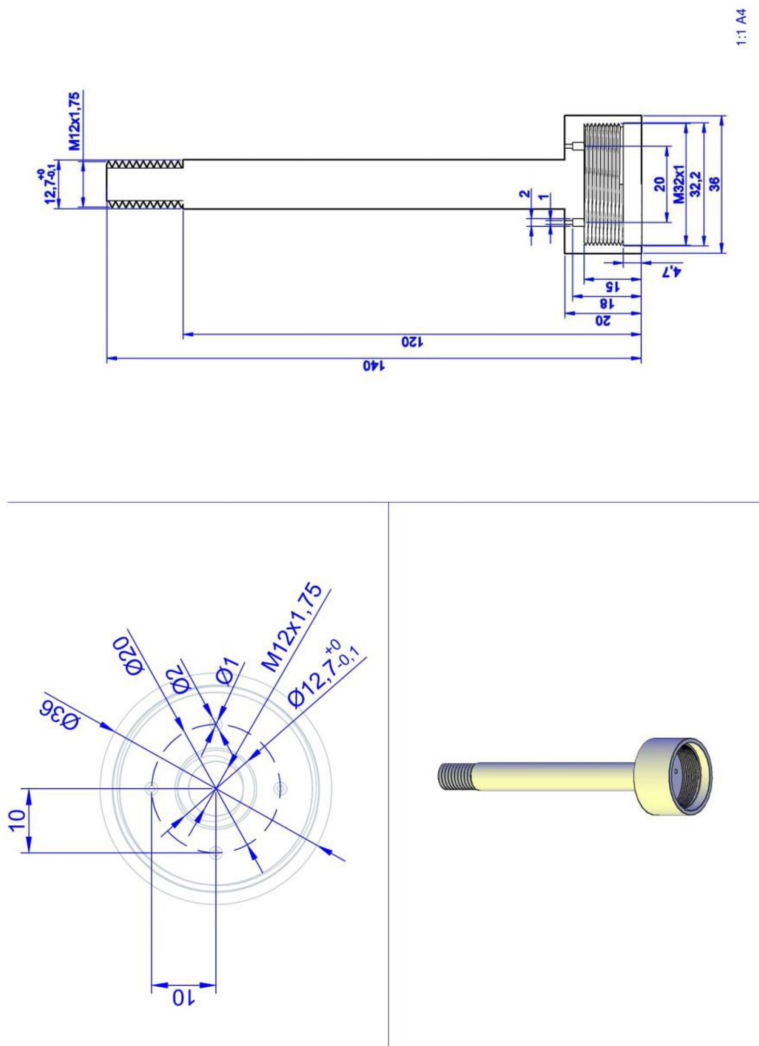
Figure C.39: Shaft for sensor wiring to old BHA.

C.5.3 Drill Bit Specifications

RILLING N

14,04

8,90

13,81

54,66

21,20

NTNU

10,63

R8,57

	NAME	SIGNATURE	DATE			TITLE:		
DRAWN								
CHK'D								
APPV'D								
MFG								
Q.A				MATERIAL:		DWG NO.		

296

NTNU_PDC_main

A4

WEIGHT:

SCALE:1:2

SHEET 1 OF 1

TRUE R3

R9

⌀22,76

R6,71

R14,03

R13,74

⌀16,67

⌀21,76

⌀10

⌀8

R14.25

TRUE R7

TRUE R7

14,25

9,74

8

6

41,74

18

16

UNLESS OTHERWISE SPECIFIED: DIMENSIONS ARE IN MILLIMETERS SURFACE FINISH: TOLERANCES: LINEAR: ANGULAR:	FINISH:		DEBURR AND BREAK SHARP EDGES	DO NOT SCALE DRAWING		REVISION	

	NAME	SIGNATURE	DATE			TITLE:		
DRAWN								
CHK'D								
APPV'D								
MFG								
Q.A				MATERIAL:		DWG NO.	A4	

Alibaba_PDC_main

WEIGHT: | SCALE:1:1 | SHEET 1 OF 1

C.5.4   Motors and Sensors Specifications

Figure C.40: HIWIN ball screw product specifications [62].
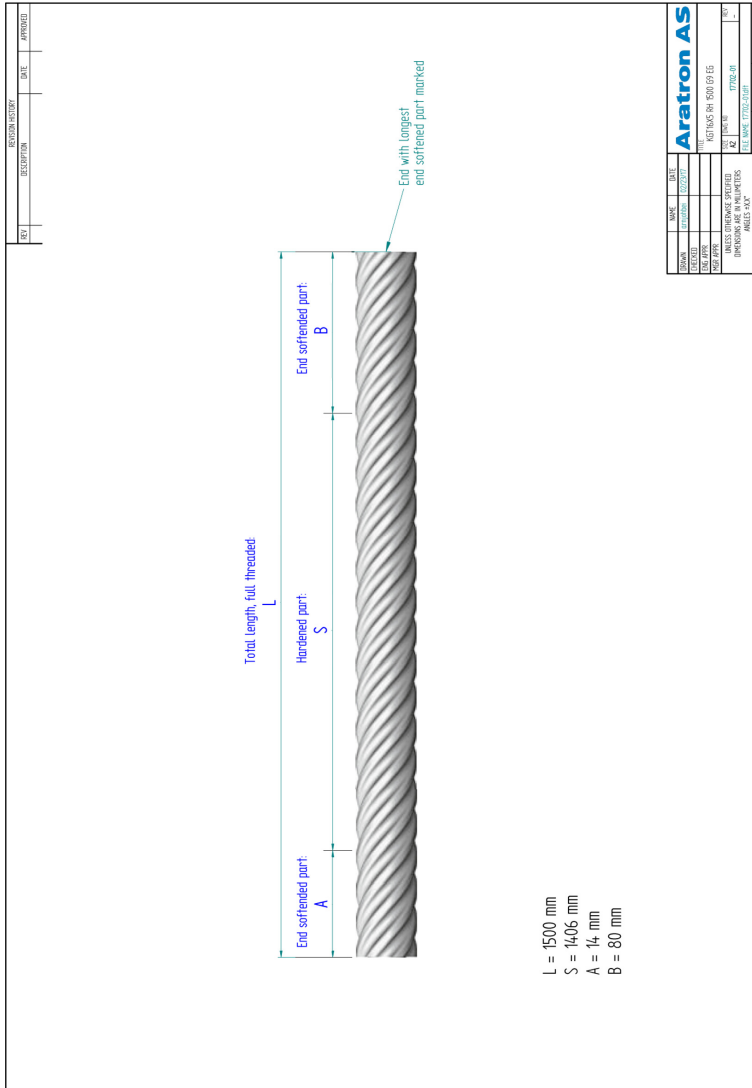
Figure B.1.5: Ball screw [8].

Figure C.41: HIWIN ball screw product specifications [62].

F S W TYPE
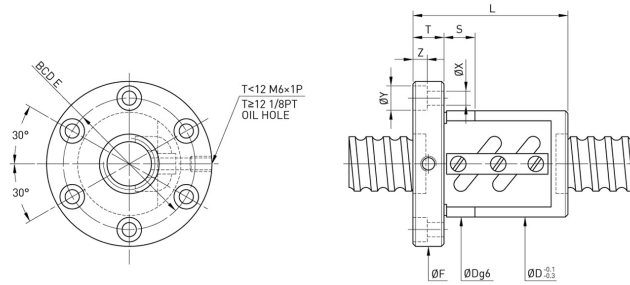
| Model	Size Nominal Dia.	Size Lead	Ball Dia.	PCD	RD	Circuits	Stiffness kgf/μm K	Dynamic Load 1x10^6 revs C (kgf)	Static Load Co (kgf)	Nut D	Nut L	Flange F	Flange T	Flange BCD-E	Bolt X	Bolt Y	Bolt Z	Fit S
12-4B1	12	4	2.381	12.25	9.792	2.5x1	8	383	638	30	38	50	10	40	4.5	8	4	12
12-4C1				12.25	9.792	3.5x1	9	511	893	30	44	50	10	40	4.5	8	4	12
12-5B1		5		12.25	9.792	2.5x1	8	383	638	30	40	50	10	40	4.5	8	4	12
14-5B1	14			14.6	11.324	2.5x1	10	710	1216	34	40	57	11	45	5.5	9.5	5.5	12
15-10A1	15	10	3.175	15.6	12.324	1.5x1	9	474	781	34	48	57	11	45	5.5	9.5	5.5	12
15-20A1		20		15.6	12.324	1.5x1	9	474	781	34	62	58	12	45	5.5	9.5	9.5	12
16-4B1		4	2.381	16.25	13.792	2.5x1	14	439	870	34	38	57	11	45	5.5	9.5	5.5	12
16-5B1	16			16.6	13.324	2.5x1	16	763	1400	40	45	64	12	51	5.5	9.5	5.5	12
16-5B2				16.6	13.324	2.5x2	33	1385	2799	40	60	64	12	51	5.5	9.5	5.5	12
16-5C1		5	3.175	16.6	13.324	3.5x1	22	1013	2013	40	50	64	12	51	5.5	9.5	5.5	12
20-5B1	20	5	3.175	20.6	17.324	2.5x1	19	837	1733	44	45	68	12	55	5.5	9.5	5.5	12
20-5B2				20.6	17.324	2.5x2	39	1519	3465	44	60	68	12	55	5.5	9.5	5.5	12
20-6B1		6	3.969	20.8	16.744	2.5x1	20	1137	2187	48	48	72	12	59	5.5	9.5	5.5	12
20-6C1				20.8	16.744	3.5x1	28	1512	3041	48	66	72	12	59	5.5	9.5	5.5	12
25-4B2	25	4	2.381	25.25	22.792	2.5x2	38	976	2776	46	48	69	11	57	5.5	9.5	5.5	12
25-5B2		5	3.175	25.6	22.324	2.5x2	46	1704	4417	50	60	74	12	62	5.5	9.5	5.5	12
25-5C1				25.6	22.324	3.5x1	35	1252	3085	50	50	74	12	62	5.5	9.5	5.5	12
25-6B1		6	3.969	25.8	21.744	2.5x1	24	1255	2735	53	44	76	11	64	5.5	9.5	5.5	12
25-6B2				25.8	21.744	2.5x2	48	2308	5523	56	68	82	12	69	6.6	11	6.5	12
25-6C1				25.8	21.744	3.5x1	35	1690	3844	56	55	82	12	69	6.6	11	6.5	12
25-10B1		10	4.763	26	21.132	2.5x1	25	1592	3237	60	65	86	16	73	6.6	11	6.5	12
25-10B2				26	21.132	2.5x2	46	2888	6472	58	97	85	15	71	6.6	11	6.5	12
25-12B1		12	3.969	25.8	21.744	2.5x1	24	1271	2761	53	60	78	11	64	6.6	11	6.5	12
28-5B1	28	5	3.175	28.6	25.324	2.5x1	26	984	2466	55	45	85	12	69	6.6	11	6.5	12
28-5B2				28.6	25.324	2.5x2	50	1785	4932	55	60	85	12	69	6.6	11	6.5	12
28-6A2		6		28.6	25.324	1.5x2	29	1150	2960	55	55	85	12	69	6.6	11	6.5	12
28-12B2		12	4.763	29	24.132	2.5x2	51	3060	7299	60	110	86	12	73	6.6	11	6.5	12
28-16B1		16		29	24.132	2.5x1	25	1686	3649	62	84	89	12	75	6.6	11	6.5	12
32-5B2	32	5	3.175	32.6	29.324	2.5x2	55	1886	5666	58	60	84	12	71	6.6	11	6.5	12
32-5C1				32.6	29.324	3.5x1	39	1388	3967	58	50	84	12	71	6.6	11	6.5	12
32-6B2		6	3.969	32.8	28.744	2.5x2	56	2556	7020	62	68	88	12	75	6.6	11	6.5	12
32-6C1				32.8	28.744	3.5x1	39	1888	4936	62	55	88	12	75	6.6	11	6.5	12
32-8B2		8	4.763	33	28.132	2.5x2	59	3284	8453	66	86	100	16	82	9	14	8.5	15
32-8C1				33	28.132	3.5x1	41	2428	5948	66	70	100	16	82	9	14	8.5	15
32-10B2		10	6.350	33.4	26.91	2.5x2	60	4810	11199	74	98	108	16	90	9	14	8.5	15
32-10C1				33.4	26.91	3.5x1	44	3519	7785	74	78	108	16	90	9	14	8.5	15
32-12A2		12		33.4	26.91	1.5x2	37	3051	6612	74	97	108	18	90	9	14	8.5	15
32-12B2				33.4	26.91	2.5x2	59	4810	11199	74	110	108	18	90	9	14	8.5	15

Remark: Stiffness values listed above value are derived from theoretical formula while axial load is 30% of dynamic load rating without preload.

Figure C.42: HIWIN ball screw nut product specifications [62].

(5) HGW-CC / HGW-HC
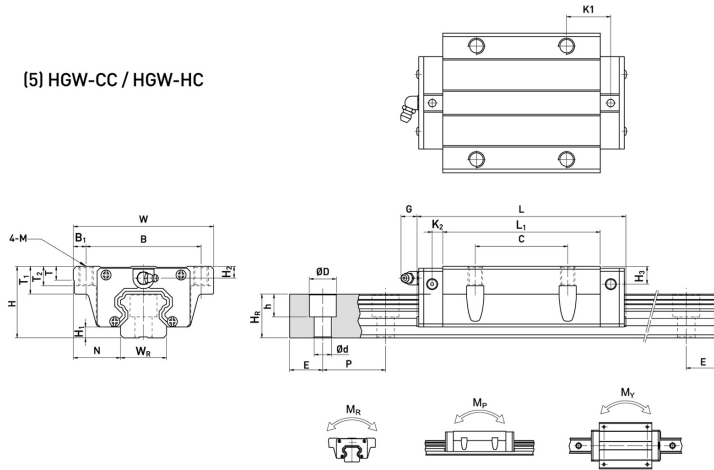
Model No.	Dimensions of Assembly (mm)				Dimensions of Block (mm)															Dimensions of Rail (mm)							Mounting Bolt for Rail (mm)	Basic Dynamic Load Rating C (kN)	Basic Static Load Rating C₀ (kN)	Static Rated Moment			Weight	
	H	H_1	N	W	B	B_1	C	L_1	L	K_1	K_2	G	M	T	T_1	T_2	H_2	H_3	W_R	H_R	D	h	d	P	E	(mm)	C (kN)	C_0 (kN)	M_R kN-m	M_P kN-m	M_Y kN-m	Block kg	Rail kg/m
HGW 15CC	24	4.3	16	47	38	4.5	30	39.4	61.4	8	4.85	5.3	M5	6	8.9	6.95	3.95	3.7	15	15	7.5	5.3	4.5	60	20	M4x16	11.38	16.97	0.12	0.10	0.10	0.17	1.45
HGW 20CC	30	4.6	21.5	63	53	5	40	50.5	77.5	10.25	6	12	M6	8	10	9.5	6	6	20	17.5	9.5	8.5	6	60	20	M5x16	17.75	27.76	0.27	0.20	0.20	0.40	2.21
HGW 20HC								65.2	92.2	17.6																	21.18	35.90	0.35	0.35	0.35	0.52	
HGW 25CC	36	5.5	23.5	70	57	6.5	45	58	84	11.8	6	12	M8	8	14	10	6	5	23	22	11	9	7	60	20	M6x20	26.48	36.49	0.42	0.33	0.33	0.59	3.21
HGW 25HC								78.6	104.6	22.1																	32.75	49.44	0.56	0.57	0.57	0.80	
HGW 30CC	42	6	31	90	72	9	52	70	97.4	14.25	6	12	M10	8.5	16	10	6.5	10.8	28	26	14	12	9	80	20	M8x25	38.74	52.19	0.66	0.53	0.53	1.09	4.47
HGW 30HC								93	120.4	25.75																	47.27	69.16	0.88	0.92	0.92	1.44	
HGW 35CC	48	7.5	33	100	82	9	62	80	112.4	14.6	7	12	M10	10.1	18	13	9	12.6	34	29	14	12	9	80	20	M8x25	49.52	69.16	1.16	0.81	0.81	1.56	6.30
HGW 35HC								105.8	138.2	27.5																	60.21	91.63	1.54	1.40	1.40	2.06	
HGW 45CC	60	9.5	37.5	120	100	10	80	97	139.4	13	10	12.9	M12	15.1	22	15	8.5	20.5	45	38	20	17	14	105	22.5	M12x35	77.57	102.71	1.98	1.55	1.55	2.79	10.41
HGW 45HC								128.8	171.2	28.9																	94.54	136.46	2.63	2.68	2.68	3.69	
HGW 55CC	70	13	43.5	140	116	12	95	117.7	166.7	17.35	11	12.9	M14	17.5	26.5	17	12	19	53	44	23	20	16	120	30	M14x45	114.44	148.33	3.69	2.64	2.64	4.52	15.08
HGW 55HC								155.8	204.8	36.4																	139.35	196.20	4.88	4.57	4.57	5.96	
HGW 65CC	90	15	53.5	170	142	14	110	144.2	200.2	23.1	14	12.9	M16	25	37.5	23	15	15	63	53	26	22	18	150	35	M16x50	163.63	215.33	6.65	4.27	4.27	9.17	21.18
HGW 65HC								203.6	259.6	52.8																	208.36	303.13	9.38	7.38	7.38	12.89	

Note : 1 kgf = 9.81 N

Figure C.43: HIWIN linear roller guide product specifications [63].

GST helical gearboxes

Technical data

		063C32 063C42	071C32 071C42	080C32 080C42	090C32	100C12	100C32	112C22	132C12 132C22 132C32
g		123	139	156	176	194		218	258
g$_1$	MFEMAXX	100	109	150	157	166		176	195
	MFEMABR	107	118	132	137	147		158	187
k$_1$	MFEMAXX	187	207	224.5	274	324		319	403
k$_2$		120			145	180		222	265
Δk	MFEMABR	40	52	73	68	76		90	109.5
	MFFMAXX		128			109		102	115
	MFFMABR	170	165	183	181	170		183	201.5
k									
GST03		329							
GST04		371	391	413					
GST05		401	421	443	503	553			
GST06		427	447	469	529	579		580	
GST07				525	585	635		636	728
GST09					648	698		699	791
GST11						755		756	848
GST14								846	938

	a	h[1]	o[1]	p[1]
GST03	2	65	90	101
GST04	0	80	100	132
GST05	1	100	115	158.5
GST06	2	125	145	198
GST07	3	160	180	251
GST09	4	200	222	311
GST11	4	250	270	385
GST14	6	315	328	479

|	d k6	d m6	d$_2$	l	l$_1$	l$_2$	u	t	i	i$_5$	o$_1$	b$_5$	b$_7$	c$_5$	e$_5$	f$_5$	m	n	n$_1$	s$_5$
GST03	14		M5	28	4	20	5	16	34	40	127	60	91	11	105	84	20			6.6
	20		M6	40	5	28	6	22.5	46	52	139									
GST04	20		M6	40	5	28	6	22.5	43	53	174	76	105	18	129	112	24.5	20	36	9
GST05	25		M10	50	4	40	8	28	53	66	214	90	125	23	155	139	32.5	26	49	11
GST06	30		M10	60	6	45	8	33	64	79	243	106	160	28	196	157	38	35	52	13.5
GST07	40		M16	80	7	63	12	43	84	104	302	130	200	34	247	196	48.5	45	66	18
GST09	50		M16	100	8	80	14	53.5	105	1275	370	165	245	44	298	239	54	48	74	18
GST11		60	M20	120	8	100	18	64	125	155	433	200	300	54	368	280	69	65	80	22
GST14		80	M20	160	15	125	22	85	165	200	533	250	380	65	460	340	85	85	91	26

6.4

[1] k$_2$!

Figure C.44: Lenze hoisting motor product specifications (Lenze GST03-2M VBR 063C42) [64].

Dimensions

GST☐☐-2M VBR
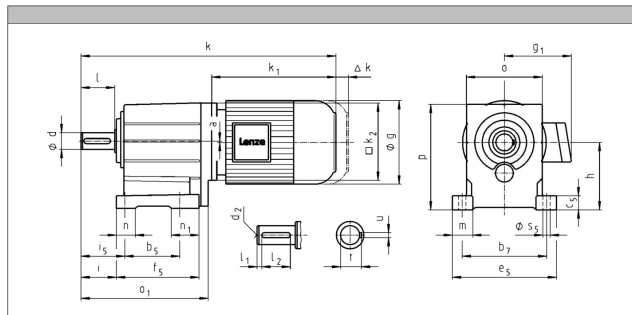
Technical data

Gearbox size		GST03	GST04	GST05	GST06	GST07	GST09	GST11	GST14
Max. torque	[Nm]	45	73	172	375	710	1623	2848	5920
Ratio range		2.6 - 59	1.6 - 45	1.6 - 335	2 - 435	2 - 417	2 - 412	4 - 412	4 - 412
Dimensions									
Solid shaft	[mm]	14 x 28 20 x 40	16 x 32 20 x 40	20 x 40 25 x 50	25 x 50 30 x 60	30 x 60 40 x 80	40 x 80 50 x 100	60 x 120	80 x 160
Flange	[mm]	120 140 160	120 140 160	120 140 160 200	160 200	200 250	250 300	300 350	350 400

Figure C.45: Lenze hoisting motor product specifications (Lenze GST03-2M VBR 063C42) [64].
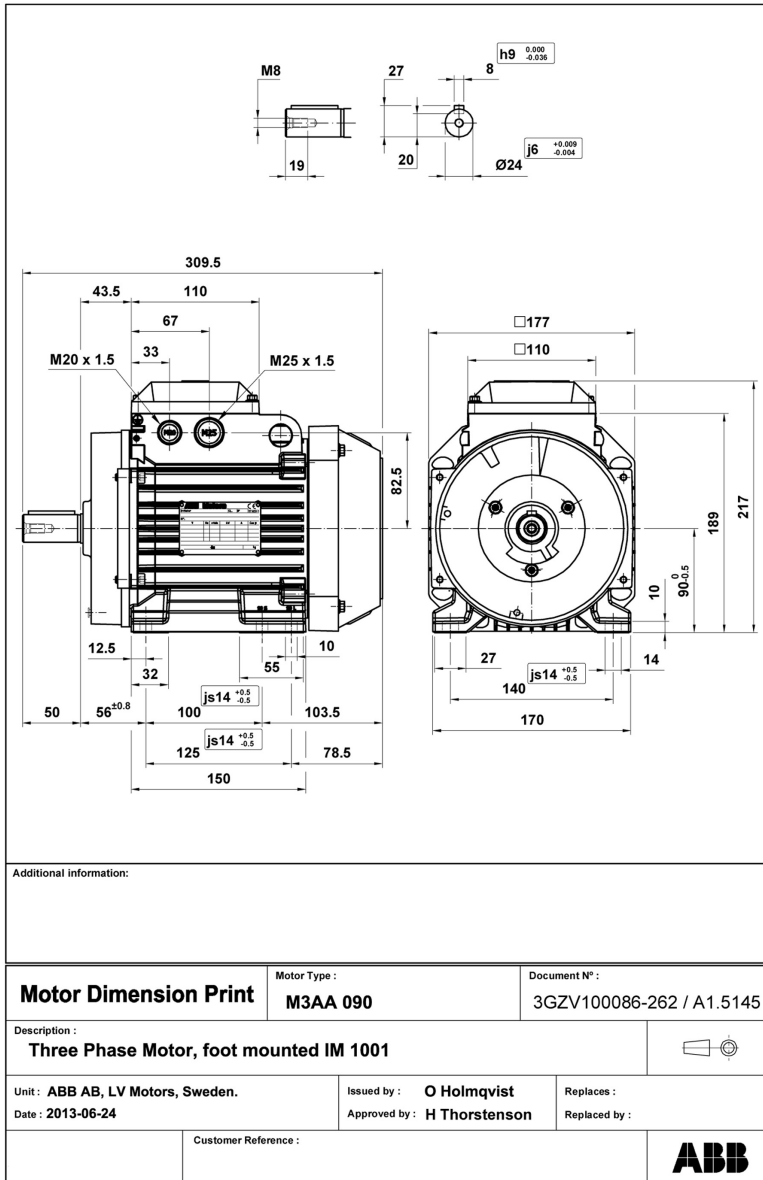
Figure C.46: ABB top drive motor product specifications (3GAA091520-ASJ) [65].

3GAA091520-ASJ

ABB

General Information

Product ID:	3GAA091520-ASJ
ABB Type Designation:	M3AA 90LB 2
Catalog Description:	No Description Available

Additional Information

ABB Type Designation:	M3AA 90LB 2
Bearing:	6205-2Z/C3
Bearing NDE:	6204-2Z/C3
Country of Origin:	Poland (PL)
	Finland (FI)
	Romania (RO)
Customs Tariff Number:	85015220
Direction of Rotation:	Both sides
Gross Weight:	21 kg
IC Class:	IC411
IE Class Data (50 Hz):	IE Class IE3
	Full Load (100%) 85.9 %
	Partial Load (75%) 85.8 %
	Partial Load (50%) 83.8 %
IM Class:	IMB3 IM1001
IP Class:	IP55
Insulation Class:	ICLF
Made To Order:	No
Minimum Order Quantity:	1 piece
Order Multiple:	1 piece
Package Level 1 Units:	0 carton
Poles (High):	2
Product Name:	3-Phase squirrel cage motor
Product Net Weight:	18 kg
Quote Only:	No
Replaced Product ID (OLD):	3GAA091613-ASJ
Selling Unit of Measure:	piece
Stocked At (Warehouses):	Central Stock Europe
	Central Stock Nordic
	Central Stock Spain
	CSI
Temperature Class Default:	--
Terminator Box Location:	D-End top
Two Speed Motor:	No
Voltage Code:	S

Electrical Data:

Conn	Temp Class	Freq	Voltage	Power	Speed	Current	Power Factor	Efficiency	Torque	IS/IN
Y	--	50 Hz	400 V	2.20 kW	2903 r/min	4.70 A	0.790	85.90 %	7.20 N·m	7.40
D	--	50 Hz	230 V	2.20 kW	2902 r/min	8.20 A	0.790	85.90 %	7.24 N·m	7.40
Y	--	50 Hz	415 V	2.20 kW	2911 r/min	4.80 A	0.750	85.90 %	7.20 N·m	7.60

Figure C.47: ABB top drive motor product specifications (3GAA091520-ASJ) [65].
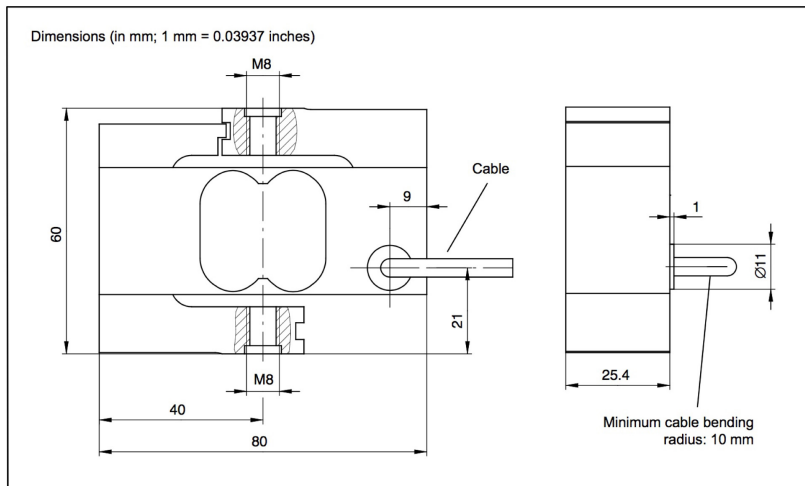
Figure C.48: HBM load cell product specification (HBM S2M 500 N, CLOP AE301) [66].
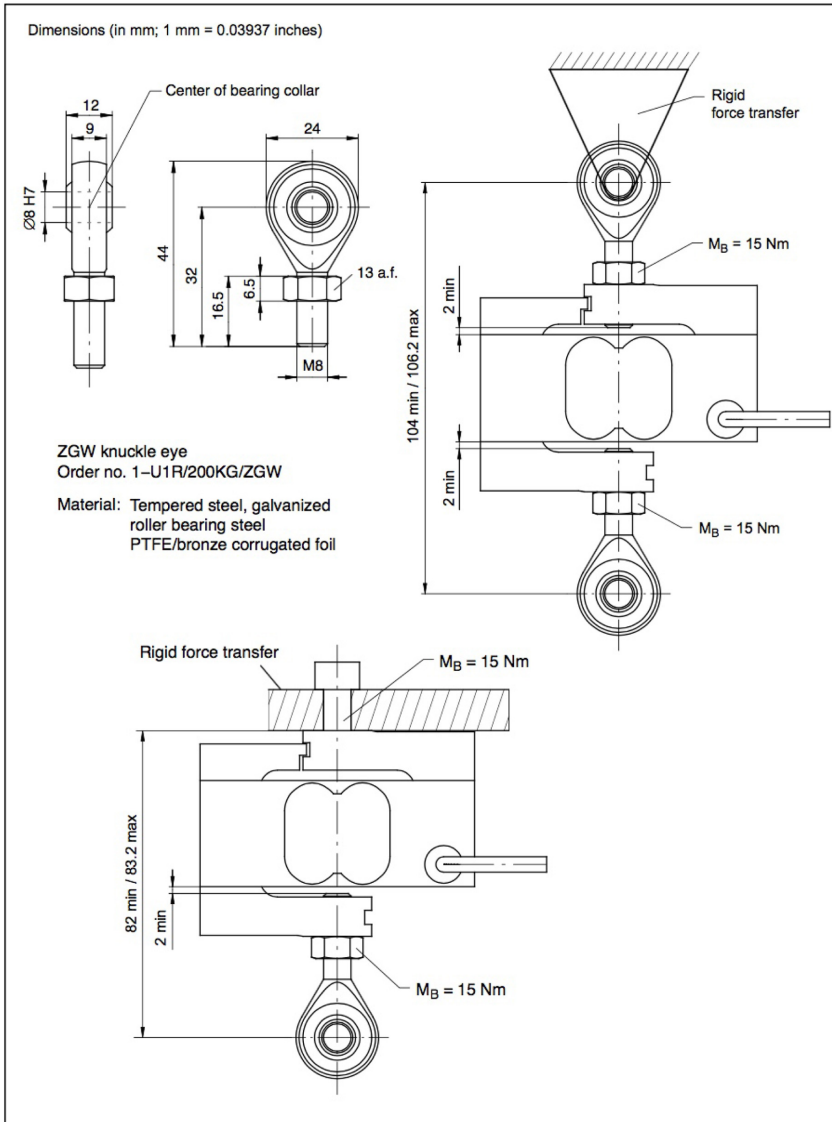
Figure C.49: HBM load cell product specification (HBM S2M 500 N, CLOP AE301) [66].
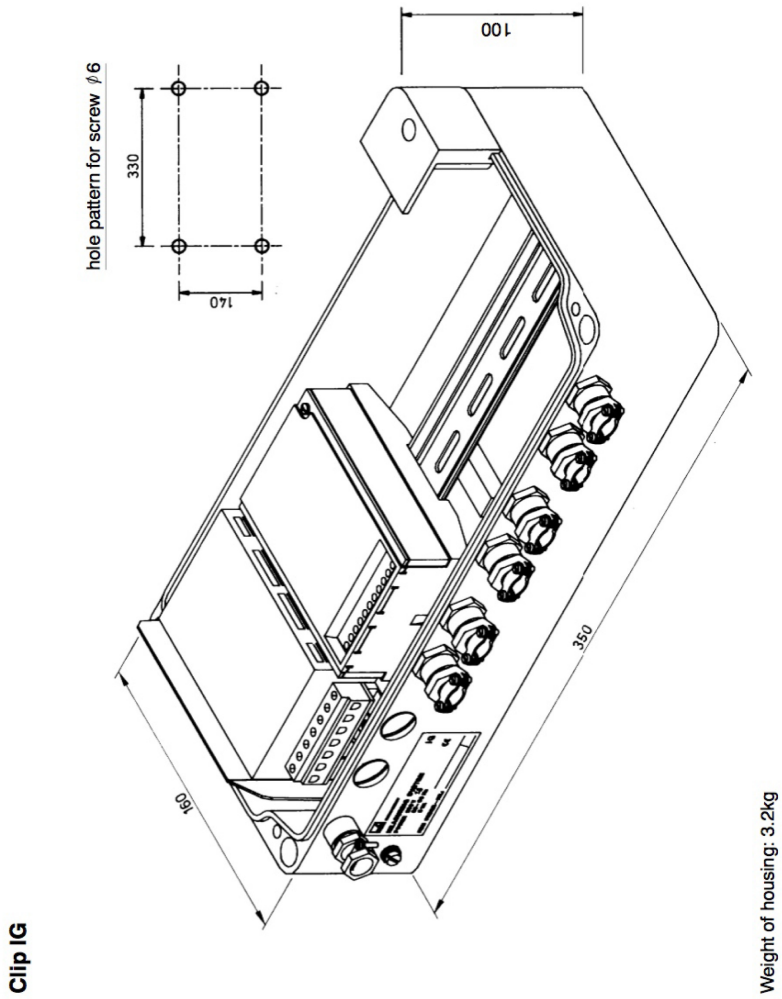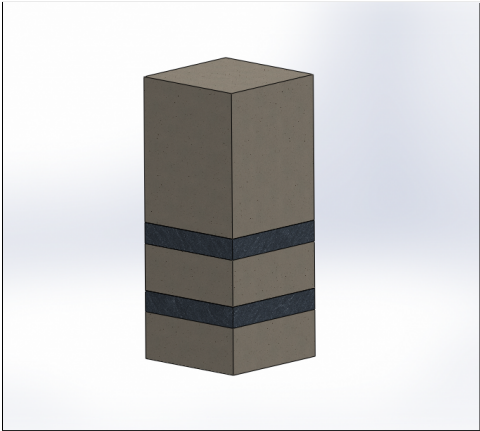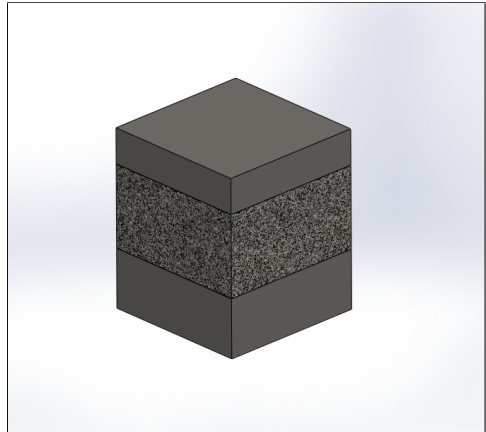
Figure C.50: HBM load cell product specification (HBM S2M 500 N, CLOP AE301) [66].
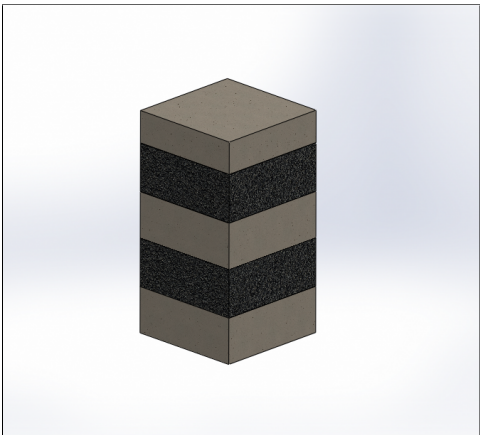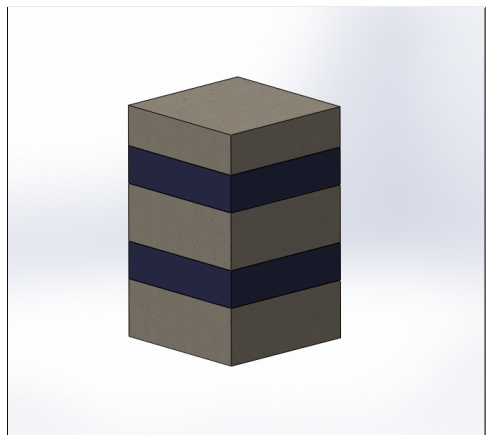
C.6   Standardized Formations

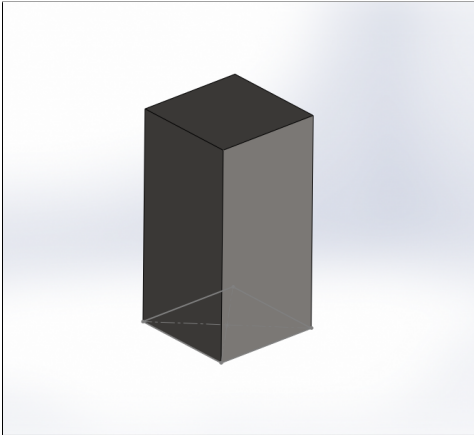**(a)** Shale1. Made of cement (10 cm), shale (4.5 cm), cement (10 cm), shale (4.5 cm) and cement (31 cm).

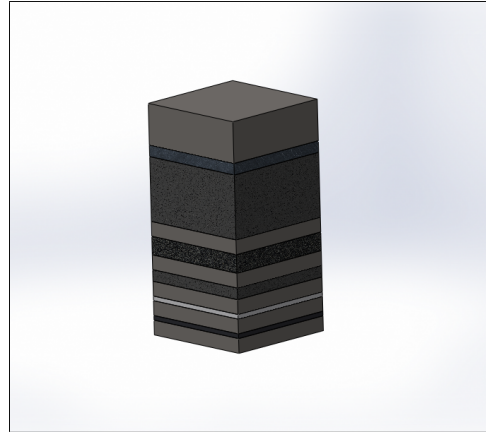
(b) Granite1. Made of cement (10 cm), granite (14 cm), cement (6 cm) on top.

(c) Basalt1. Made of cement (10 cm), basalt (10.5 cm), cement (10 cm), basalt (10.5 cm) and cement (7 cm).

(d) Tiles1. Made of cement (10 cm), basalt (6.5 cm), cement (10 cm), basalt (6.5 cm) and cement (7 cm).

(a) Cement 1. Made of 50 cm cement.

(b) Made with black tile (1.2 cm) white tile (1.2 cm) basalt (3.2 cm) mica shale (4.6 cm) and shale (15.9 cm). Every layer is spaced with 3 cm of cement.
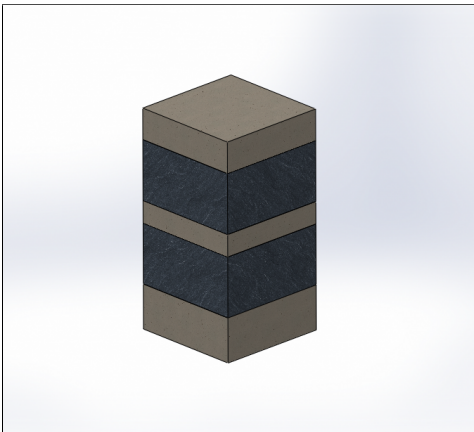
(c) Shale2. Made of cement (10 cm), shale (13.5 cm), cement (5 cm), shale (13.5 cm) and cement (7 cm)

(d) Mixed1. Made with three inclined layers of tile (1.2 cm), basalt (2.5 cm) and shale (7 cm). The inclination angle is between 23°and 28 °.

Figure C.52: The figures shows the rock samples made for drilling tests including layer type and thickness. The order is described from the bottom and up.

Appendix D

Software

D.1 File Handling

D.1.1 LabVIEW File Storage VI

Fig 8.45 shows the main VI block diagram's shutdown sequence and file saving sequence when saving data during drilling in internal memory and releasing the data when the user terminates the run. At each iteration in the while loop (when the rig is active) all data point scalars are build to a 1D array. This 1D array is appended to previous data and builds a 2D array through an auto-indexed tunnel in the while loop. Due to the data flow in LabVIEW, the prompt is executed after the shutdown sequence. If the user selects "OK" on the prompt, all data is passed to the "Save File" VI. The "Save File" VI consists of several subroutines and is described in section D.1.2.

D.1.2 Save to File Main VI

Fig D.1 shows the main VI for processing and saving data from a drilling run. For all the subVIs in the main save to file.vi, the front panel is of little interest as they do not show up in the main GUI. The data flow and program functionality is mainly determined from the block diagrams of the subVIs. The block diagram of the save to file.vi depicts the use of modularity in the LabVIEW programming environment. Notice that there are several copies of Format File Property.vi and Add Column to String.vi. Saving these modules as subVIs makes the code more readable and scalable. In short, "Format File Property.vi", "Add Column to String.vi", "Add End of Line to String.vi" creates the text file header information, "Create Data file.vi" creates the data file and directory, "MultChannel Write.vi" writes the data from the input numeric 2D array, and "Close Data file.vi" closes the data file.

The block diagram and connector pane of Format File Property.vi, Add Column to String.vi, and Add end of Line to String.vi are shown in **Fig D.2**. These subVIs create the header
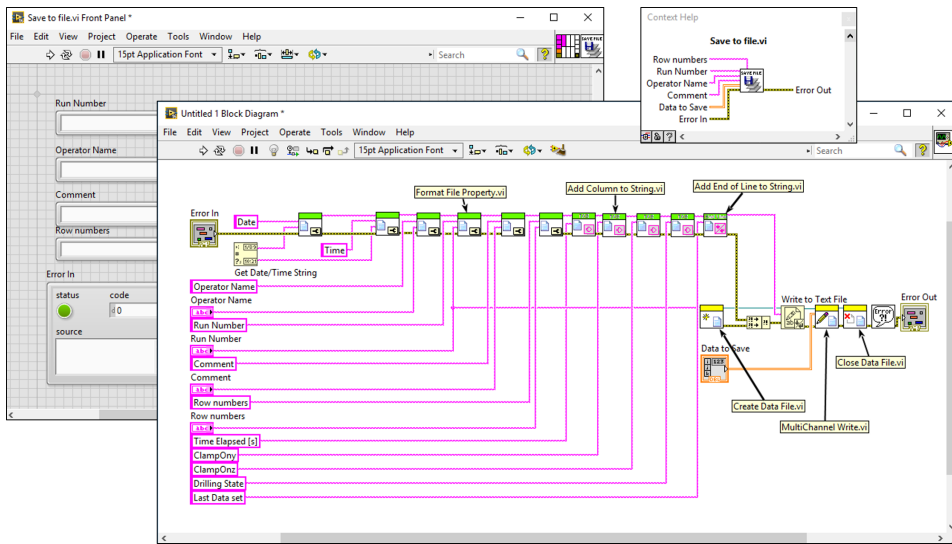
Figure D.1: Save to file.vi block diagram, connector pane and example front panel.

information of the final text file with the stored data. As shown in the block diagram, the subVIs take in a string, appends columns and or rows to the string and outputs it for further processing. The Format File Property.vi adds one row of two columns to an existing string input, the first being the file property name, such as "Operator name", and the second being the file property value, e.g. "Andreas". The output of the subVI is a tab delimited string with an end of line at the end for an extra row. The Add Column to String.vi adds a string value, e.g. "Time Elapsed [s]", and a tab constant to the string input. The Add End of Line to String.vi does the same, but adds an end of line constant instead of a tab constant. Adding a header row for more information or an extra data set for storage in the text file is simple with the modular design. One only needs to add a subVI and wire the extra input. Hard coding the file processing is possible, but will result in a messy block diagram and results in no scalability.

The "Create Data File.vi" checks if a folder called "Drilling Data" exists in the same relative directory as the main VI. If the folder doesn't exist, the folder is created, if not it is ignored. The file name is auto-generated with the format "Drilling Data <Date>, Run Number: <Run no>.txt" where the run number is taken from the user input of the prompt.

"MultiChannel Write.vi" (**Fig D.4**) appends the numeric 2D data set to the text file by using the built in LabVIEW functions "Array to spreadsheet String" and "Write to text file". Note that the precision of the data stored in the text.file is determined in this subVI. The 2D array is of double precision, more than necessary for post drilling data storage. 4 decimal points are used in the Drillbotics code. "Close Data file.vi" (**Fig D.5**) closes the data file.
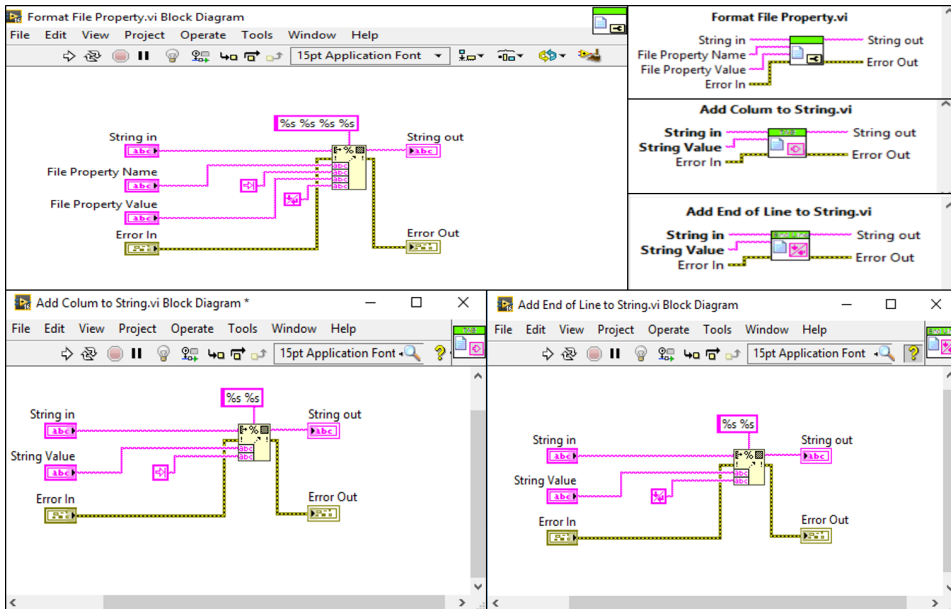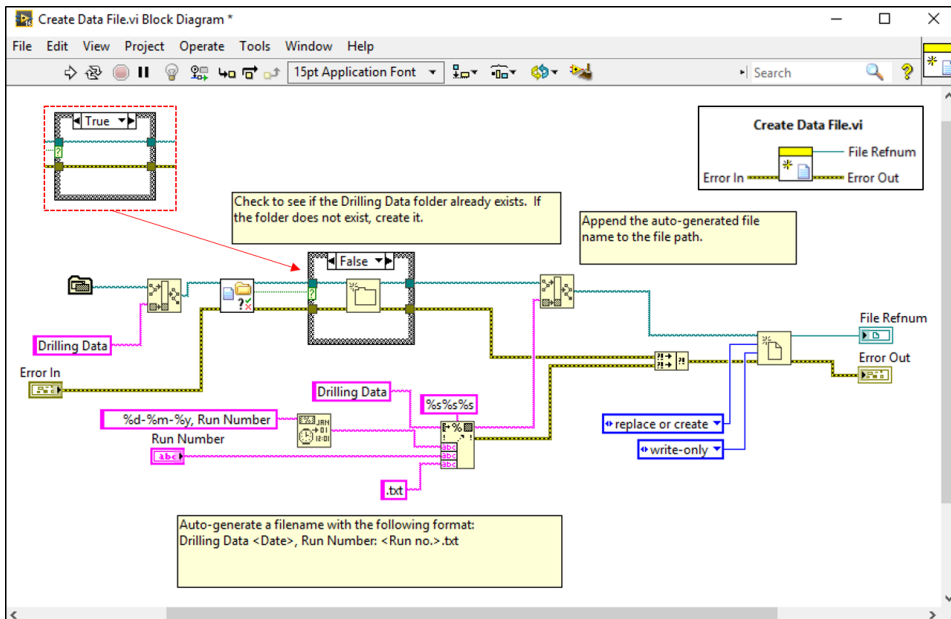
Figure D.2: Adding Header data.

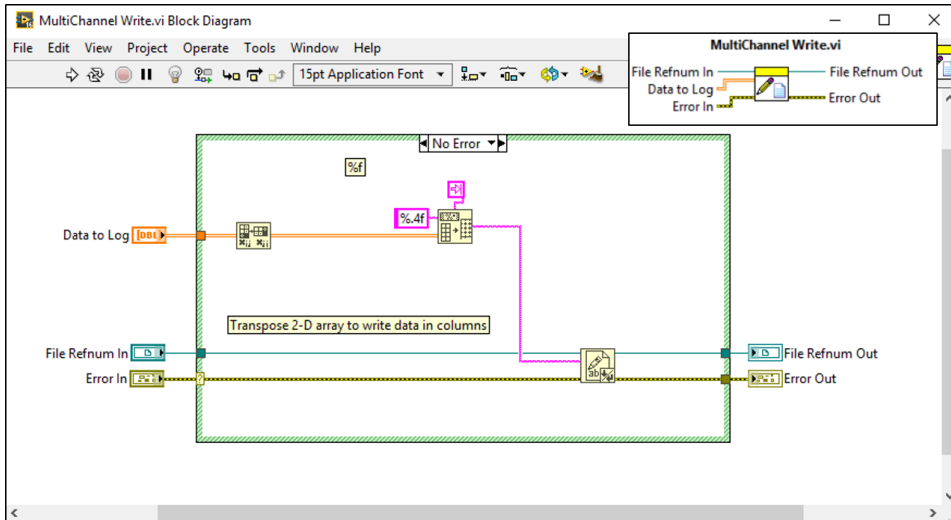**Figure D.3:** Creating data file and placing it in the chosen directory.
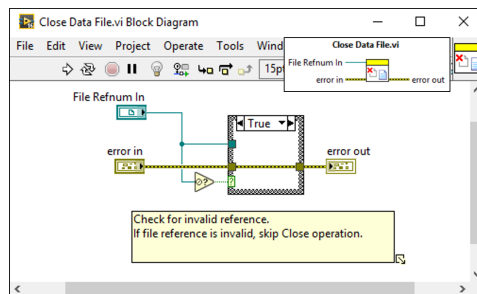
Figure D.4: Writing multiple data sets to the file

Figure D.5: Closing the data file

D.1.3 Matlab File Handling

Fig 8.46 in section 8.8 shows the flow chart of the file handling process. The possibility of post drilling analysis is enabled by saving all data in a text file and running the Matlab script. It is a script developed as an easy to use application for visualizing any drilling run. The only input is the run number and the date of the run. Since the file processing in LabVIEW saves the file in an auto-generated folder with an auto-generated filename based on date and the run number, the file is automatically retrieved in Matlab and processed. Time series of the collected data is plotted on two monitors and the figures are saved as .fig formats. The header information is also displayed on the command window for a quick recap of the drilling test, its purpose and results. The header information and figures are published to a PDF document. All figures and the pdf-report are saved in auto-generated folder by date and run number. The data from the auto generated text file can easily be retrieved from the stored MATLAB figures. Running the MATLAB script "PlotAndPublishData." plots all figures on the monitors and publishes the report. The correct folder for the LabVIEW generated text file is chosen in the script "PlotDrillingDataFromTextFile.". The codes are given below

D.1.4 Plot And Publish Data: MATLAB Script

```matlab
% This script is ment to be run with "
    PlotDrillingDataFromTextFile.m"
% There, the correct subfolder i chosen and the data from
    LabVIEW is
% published in a PDF as a drilling report. Only change Day,
    Month, Year and
% Run_number. Make sure that correct folder script is
    chosen in
% "PlotDrillingDataFromTextFile.m"

clear
close all
clc
% Run to publish in chosen file format
% Change Day, Month, Year and Run_number to retrieve data
    file saved
% from LabVIEW.
Day='09'; Month='06'; Year='18';
Run_number='4';
Date_short=strcat(Day,Month,Year);
% Retrieve correct file name.
% Format: 'Drilling Data XX-XX-XX, Run Number X.txt'
global filename filename2
filename=strcat('Drilling Data',{' '},Day,'-',Month,'-',
    Year,{', '},...
    'Run Number',{' '},Run_number,'.txt');
```

```matlab
21  filename=char(filename); % Convert to character vector
22
23  filename2=strcat('Drilling Data',{' '},'Down Hole',{' '},
        Day,'-',Month,...
24      '-',Year,{', '},'Run Number',{' '},Run_number,'.txt');
25  filename2=char(filename2); % Convert to character vector
26
27  % Specify file location
28  Current_folder=pwd; % Current folder
29  filepath=strcat(Current_folder,'\',Date_short);
30  filepath_publish=strcat(filepath,'\','Summary PDF');
31
32  % Format options for publication of code
33  options=struct('format','pdf','showCode',false,...
34      'outputDir',filepath_publish);
35
36  % Publish to chosen file format
37  My_DOC=publish('PlotDrillingDataFromTextFile_02_06_18.m',
        options);
38  Description % Print description to Command Window
39
40  % Find and extract Run Number from Description
41  str2find='Run Number: ';
42  strIndex=strfind(Description,str2find);
43  charLength=length(str2find);
44
45  str2find2='Comment: ';
46  strIndex2=strfind(Description,str2find2);
47  % Run_number=Description(strIndex+charLength:strIndex2-2)
        ,-2 for line shift
48  % Rename autogiven filname to relevant name
49  fileName1=strcat('Drilling Data Run',{' '},Run_number); %
        as cell array
50  fileName1=char(fileName1); % Convert from cell array to
        character vector
51  newFileName=strcat(fileName1,'.pdf');
52  newFilePath=strcat(filepath_publish,'\',newFileName);
53  movefile(My_DOC,newFilePath);
54
55  % Save figures as .fig (matlab editable figures)
56  % Add all figures to one graphic array
57  figures=[f1 f2 f3 f4 f5 f6 f7 f8 f9 f10 f11 f12];
58  figures_name=strcat(fileName1,'.fig'); % save as .fig
59  % Make folder if it doesn't exist. saveas()needs
        preexisting folder to work
```

```matlab
60  if exist(strcat(filepath,'\Figures'),'dir')==7 % Does
        subfolder exist?
61  else
62      mkdir(filepath,'Figures'); % creates subfolder if it
            doesn't exist
63  end
64
65  subfolder=char(strcat('Run Number',{' '},Run_number));% new
        sub folder name
66  relFigFilepath=[filepath '\Figures\' subfolder '\'];
67  if exist(relFigFilepath,'dir')==7 % Does subfolder already
        exist?
68  else
69      mkdir(strcat(filepath,'\Figures'),subfolder); % creates
            subfolder
70  end
71  saveas(figures,[relFigFilepath figures_name])
72
73  % Distribute figures evenly on screen
74  distFig('Screen','Main','Only',[1,2,3,4,5,6])
75  distFig('Screen','External','Only',[7,8,9,10,11,12])
```

D.1.5 Plot Drilling Data from Text File: MATLAB Script

```matlab
1
2  R1=8;          % Row offset start (start row minus 1)
3  C1=0;          % Column offset start (start column minus 1)
4  C2=33;         % Column offset end (end column minus 1)
5  CDH2=7;        % Column offset end for DH data
6  plotting=1; % 1 if values should be plotted
7
8  global filename filename2 % Retrieves global variable
9  filename       % Write out file name of LabVIEW file
10 filename2      % Write out file name of LabVIEW file for DH
       Data
11 % Choose path where data is stored from LabVIEW. Uncomment
       the filepath to
12 % enable data lake
13
14 % DrillDataPath='C:\Users\Drillbotics\Desktop\LabVIEW
       Drillbotics 2018\...
15 % Test Rock Response\Drilling Data\';
16 % DrillDataPath='C:\Users\Drillbotics\Desktop\LabVIEW
       Drillbotics 2018\...
```

```
17  % GUI\30_04_18\Drilling Data\';
18  % DrillDataPath='C:\Users\Drillbotics\Desktop\LabVIEW
        Drillbotics 2018\...
19  % Autotuning_PID\Drilling Data\';
20  % DrillDataPath='C:\Users\Drillbotics\Desktop\LabVIEW
        Drillbotics 2018\...
21  % PID testing\Drilling Data\';
22  % DrillDataPath='C:\Users\Drillbotics\Desktop\LabVIEW
        Drillbotics 2018\...
23  % Identification Tests\Drilling Data\';
24  % DrillDataPath='C:\Users\Drillbotics\Desktop\LabVIEW
        Drillbotics 2018\...
25  % Hoisting Motor cDAQ\Drilling Data\';
26  % DrillDataPath='C:\Users\Drillbotics\Desktop\LabVIEW
        Drillbotics 2018\...
27  % DAQ_Low_Level\Drilling Data\'
28  % DrillDataPath='C:\Users\Drillbotics\Desktop\LabVIEW
        Drillbotics 2018\...
29  % Autonomous mode\Drilling Data\'
30  % DrillDataPath='C:\Users\Drillbotics\Desktop\LabVIEW
        Drillbotics 2018\...
31  %CompetitionScript\Drilling Data\'
32  % % filename='Drilling Data 23-04-18, Run Number 2.txt';
33  filename=strcat(DrillDataPath, filename);
34  filename2=strcat(DrillDataPath, filename2);
35
36  %% Drilling Test Information
37  fileID=fopen(filename);
38  C=textscan(fileID,'%s %s %s %s %s %s %s %s %s %s %s %s',
        'Delimiter','\t');
39  [Date, Time, Operator, Run_Number, Comment, Row_numbers]=C
        {2}{1:6};
40
41  Description=sprintf...
42      ('Date: %s\nTime: %s\nOperator:%s\nRun Number: %s\
            nComment: %s\n',...
43      Date, Time, Operator, Run_Number, Comment) % Do not put
            ";", for publishing
44  %%
45  delimiter='\t';                    % Tab delimiter
46  R2=str2double(Row_numbers)+6; % Row numbers pluss offset
        from header
47  data=dlmread(filename, delimiter,[R1 C1 R2 C2]); % Read
        textfile to matrix
48  fclose(fileID);                  % Close text file
```

```matlab
49
50
51   fileID=fopen(filename2);
52   C=textscan(fileID,'%s %s %s %s %s %s %s %s %s %s %s %s','
         Delimiter','\t');
53   [Date,Time,Operator,Run_Number,Comment, Row_numbers]=C
         {2}{1:6};
54   R2=str2double(Row_numbers)+6;
55   %Read textfile to matrix
56   dataDH=dlmread(filename2,delimiter,[R1 C1 R2 CDH2]);
57   fclose(fileID);              % Close text file
58
59   time_elapsed=data(:,1);      % Time elapsed [s]
60   WOB_SP=data(:,2);            % WOB SP [s]
61   WOB_M_RAW=data(:,3);         % WOB raw data (unfiltered) [kg
         ]
62   WOB_M_filtered=data(:,4);    % WOB filtered data [kg]
63   Pressure_SP=data(:,5);       % Pressure set point [bar]
64   Pressure_M=data(:,6);        % Measured pressure [bar]
65   Pump_motor_RPM=data(:,7);    % Pump motor RPM
66   TD_RPM_SP=data(:,8);         % Top drive RPM set point
67   TD_RPM_M=data(:,9);          % Top drive measured RPM
68   TD_Torque_SP=data(:,10);     % Top drive torque set point [
         Nm]
69   TD_Torque_M=data(:,11);      % Top drive measured torque  [
         Nm]
70   TD_Torque_Lim=data(:,12);    % Top drive torque limit [Nm]
71   Hoist_RPM_SP=data(:,13);     % Hoisting motor RPM set point
72   Hoist_RPM_M=data(:,14);      % Hoisting motor RPM measured
73   Hoist_Torque_M=data(:,15);   % Hoisting Torque measured [Nm]
74   Hoist_Torque_Lim=data(:,16); % Housting torque limit [Nm]
75   Position=data(:,17);         % Bit position [mmRKB]
76   Position(1:19)=Position(20);
77   ROP=data(:,18);              % ROP [cm/min] measured
78   MSE=data(:,19);              % MSE [MPa] calculated
79   theta1=data(:,20);           % Estimator variable 1
80   theta2=data(:,21);           % Estimator variable 2
81   theta3=data(:,22);           % Estimator variable 3
82   ROP_regressand=data(:,23);   % ROP regressand for auto
         drilling [cm/min]
83   %accx=data(:,24);            % Down hole sensor
         accelerometer x
84   %accy=data(:,25);            % Down hole sensor
         accelerometer y
```

```
85  %accz=data(:,26);                % Down hole sensor
         accelerometer z
86  %gyrox=data(:,27);               % Down hole sensor gyro x
87  %gyroy=data(:,28);               % Down hole sensor gyro y
88  %gyroz=data(:,29);               % Down hole sensor gyro z
89  ClampON_x=data(:,30);        % ClampON accelerometer x
90  ClampON_y=data(:,31);        % ClampON accelerometer y
91  ClampON_z=data(:,32);        % ClampON accelerometer z
92  Drilling_state=data(:,33);   % Drilling state
93  formation_index=data(:,34);  % Formatin index identified
         rock type
94
95  time_elapsed_DH=dataDH(:,1);
96  accx=dataDH(:,2);      % Down hole sensor accelerometer x
97  accy=dataDH(:,3);      % Down hole sensor accelerometer y
98  accz=dataDH(:,4);      % Down hole sensor accelerometer z
99  gyrox=dataDH(:,5);     % Down hole sensor gyro x
100 gyroy=dataDH(:,6);     % Down hole sensor gyro y
101 gyroz=dataDH(:,7);     % Down hole sensor gyro z
102 temp=dataDH(:,8);      % Sensor card temperature
103
104 Delta_t=time_elapsed(2:end)-time_elapsed(1:end-1);%
         Calculate time increment
105 Delta_t=[Delta_t; Delta_t(end)]; % Add element to make
         equal size
106
107 xsec=10; % Seconds to base ROP calculations on
108 fs_t=0.01; % sampling time  [s] Used 100 hz -> 0.01 s
109 xsecsamples=xsec/0.01; % number of samples to calculate ROP
         from
110 pos_t2=Position(1+xsecsamples:end);
111 pos_t1=Position(1:end-xsecsamples);
112 deltaPos=pos_t2-pos_t1; % change in position within xsec
         seconds
113 ROP_from_pos=zeros(length(time_elapsed),1); % Pre allocate
         for memory
114 ROP_from_pos(1+xsecsamples:end,1)=deltaPos/xsec; %DPos/Dt
115 ROP_from_pos=ROP_from_pos*6; % from mm/sec to cm/min
116
117 % Moving average of measurements
118 mov_avg_HL=30; % Moving average half length
119 DT_MA=movmean(Delta_t,mov_avg_HL*2+1);
120 WOB_MA=movmean(WOB_M_RAW,mov_avg_HL*2+1);
121 TD_Torque_MA=movmean(TD_Torque_M,mov_avg_HL*2+1);
122 ROP_from_pos_MA=movmean(ROP_from_pos,mov_avg_HL*2+1);
```

```
123  %% Plotting of data
124  if plotting==1
125
126  f1=figure('Name','Delta t','NumberTitle','off');
127  plot(time_elapsed,Delta_t)
128  hold on
129  plot(time_elapsed,DT_MA,'LineWidth',2)
130  grid on       % Plot major grid lines
131  xlabel('Time Elapsed [s]')
132  ylabel('\Delta t_{sampling}')
133  title('Sampling time vs Time Elapsed')
134  legend('Sampling time (s)',string(strcat('Moving Average'
         ,...
135      {' '},num2str(mov_avg_HL),' point half length')))
136
137  f2=figure('Name','WOB','NumberTitle','off');
138  plot(time_elapsed,WOB_M_RAW,':', 'color',
         [128,128,128]/256,...
139      'LineWIdth',0.5);
140  hold on
141  plot(time_elapsed,WOB_SP,'LineWidth',1)
142  plot(time_elapsed,WOB_MA,'k-')
143  plot(time_elapsed,WOB_M_filtered,'color','[0 0.447 0.741]',
         'LineWidth',1)
144  grid on       % Plot major grid lines
145  legend('WOB Raw [kg]','WOB Set Point [kg]',...
146      string(strcat('Moving Average',{' '},...
147  num2str(mov_avg_HL),' point half length')),'WOB measured [
         kg]')
148  xlabel('Time Elapsed [s]')
149  ylabel('WOB [kg]')
150  title('WOB')
151
152  f3=figure('Name','Pressure','NumberTitle','off');
153  plot(time_elapsed,Pressure_M)
154  grid on
155  xlabel('Time Elapsed [s]')
156  ylabel('Pressure [bar]')
157  legend('Measured Pressure')
158  title('Pressure')
159
160  f4=figure('Name','Top Drive','NumberTitle','off');
161  subplot(2,1,1) % Create first subplot
162  plot(time_elapsed,TD_RPM_M)
163  hold on
```

```matlab
164  plot(time_elapsed,TD_RPM_SP);
165  grid on % Plot major grid lines
166  xlabel('Time Elapsed [s]')
167  ylabel('Top Drive RPM')
168  legend('TD RPM M','TD RPM SP')
169  title('Top Drive Torque & RPM')
170  subplot(2,1,2) % Create second subplot
171  plot(time_elapsed,TD_Torque_M)
172  hold on
173  plot(time_elapsed,TD_Torque_MA)
174  plot(time_elapsed,TD_Torque_Lim)
175  grid on % Plot major grid lines
176  xlabel('Time Elapsed [s]')
177  ylabel('Top Drive Torque [Nm]')
178  legend('TD Torque M',...
179      string(strcat('Moving Average',{' '},...
180      num2str(mov_avg_HL),' point half length')),'TD Torque
            Limit')
181
182  f5=figure('Name','Hoisting Motor','NumberTitle','off');
183  subplot(2,1,1) % Create first subplot
184  plot(time_elapsed,Hoist_RPM_M)
185  hold on
186  plot(time_elapsed,Hoist_RPM_SP);
187  grid on % Plot major grid lines
188  xlabel('Time Elapsed [s]')
189  ylabel('Hoisting Motor RPM')
190  legend('Hoisting Motor RPM M','Hoisting Motor RPM SP')
191  title('Hoisting Motor Torque & RPM')
192  subplot(2,1,2) % Create second subplot
193  plot(time_elapsed,Hoist_Torque_M)
194  hold on
195  plot(time_elapsed,Hoist_Torque_Lim)
196  grid on % Plot major grid lines
197  xlabel('Time Elapsed [s]')
198  ylabel('Hoisting Motor Torque [Nm]')
199  legend('Hoisting Motor Torque M','Hoisting Motor Torque
        Limit')
200
201  f6=figure('Name','ROP, MSE & Position','NumberTitle','off')
        ;
202  subplot1=subplot(2,1,1); % Create first subplot
203  yyaxis left
204  plot(time_elapsed,ROP)
205  ylabel('ROP [cm/min]')
```

```matlab
206  yyaxis right
207  semilogy(time_elapsed ,MSE, 'Parent' , subplot1 )
208  % ylim(subplot1 ,[0  3000])
209  ylabel('MSE [MPa]')
210  legend('ROP measured' , 'MSE calculated')
211  xlabel('Time Elapsed [s]')
212  title('ROP, MSE & Position')
213  subplot(2,1,2)
214  plot(time_elapsed , Position )
215  set(gca,'Ydir','Reverse')    % Reverse y-axis
216  ylabel('Position [mmRKB]')
217  xlabel('Time Elapsed [s]')
218  legend('Position')
219
220  f7=figure('Name','Estimator','NumberTitle','off');
221  subplot(2,1,1)
222  plot(time_elapsed , theta1 )
223  hold on
224  plot(time_elapsed , theta2 )
225  plot(time_elapsed , theta3 )
226  ylabel('Estimator Regressors')
227  xlabel('Time Elapsed [s]')
228  legend('\theta_1','\theta_2','\theta_3')
229  title('Estimator Parameters')
230  subplot(2,1,2)
231  yyaxis left
232  plot(time_elapsed ,ROP)
233  ylabel('ROP [cm/min]')
234  yyaxis right
235  plot(time_elapsed , ROP_regressand )
236  ylabel('ROP Regressand [cm/min]')
237  xlabel('Time Elapsed [s]'),
238  legend('ROP Measured' , 'ROP Regressand')
239
240  f8=figure('Name','Acceleration','NumberTitle','off');
241  subplot(2,1,1)
242  yyaxis left
243  plot(time_elapsed_DH , accx )
244  hold on
245  plot(time_elapsed_DH , accy )
246  ylabel('Acceleration - x & y')
247  yyaxis right
248  plot(time_elapsed_DH , accz )
249  ylabel('Acceleration - z')
250  xlabel('Time Elapsed [s]')
```

```
251  legend ('DH Acc_x [g]','DH Acc_y [g]','DH Acc_z [g]')
252  title ('Acceleration')
253  subplot (2,1,2)
254  yyaxis left
255
256  plot (time_elapsed_DH, temp)
257  ylabel ('Temperature [C]')
258  legend ('Sensor Card Temperature')
259
260  f9=figure ('Name','Gyroscope','NumberTitle','off');
261  yyaxis left
262  plot (time_elapsed_DH, gyrox)
263  hold on
264  plot (time_elapsed_DH, gyroy)
265  ylabel ('Gyro x and y')
266  xlabel ('Time Elapsed [s]')
267  yyaxis right
268  plot (time_elapsed_DH, gyroz)
269  legend ('Gyro_x [rad/sec]','Gyro_y [rad/sec]','Gyro_z [rad/
         sec]')
270  title ('Gyroscope')
271
272  f10=figure ('Name','Drilling State','NumberTitle','off');
273  % subplot (2,1,1)
274  plot (time_elapsed, Drilling_state)
275  yticks ([0 1 2 3 4 5])
276  yticklabels ({'Init (tagg)','Hoist Up','Start Rotation','
         Identification',...
277      'Drilling','Trip Out'})
278  ylabel ('Drilling State')
279  xlabel ('Time Elapsed [s]')
280  title ('Drilling State')
281
282  f11=figure ('Name','ROP','NumberTitle','off');
283  subplot (2,1,1)
284  plot (time_elapsed,ROP);
285  hold on
286  plot (time_elapsed,ROP_from_pos)
287  plot (time_elapsed,ROP_from_pos_MA)
288  grid on      % Plot major grid lines
289  legend ('ROP LabVIEW', string (strcat ('ROP based on position'
         ,{' '},...
290      num2str (xsec),' seconds')),...
291      string (strcat ('Moving Average from position',{' '},...
292      num2str (mov_avg_HL),' point half length')))
```

```matlab
293   xlabel('Time Elapsed [s]')
294   ylabel('ROP [cm/min]')
295   title('ROP Comparison')
296   subplot(2,1,2)
297   plot(time_elapsed,Position)
298   set(gca,'Ydir','Reverse')    % Reverse y-axis
299   ylabel('Position [mmRKB]')
300   xlabel('Time Elapsed [s]')
301   legend('Position')
302   title('Position')
303
304   f12=figure('Name','Formation Index','NumberTitle','off');
305   plot(time_elapsed,formation_index)
306   yticks([0 1 2 3 4]);
307   yticklabels({'Unknown','Cement','Shale','Basalt','Granite'
          })
308   xlabel('Time Elapsed [s]')
309   ylabel('Formation Index')
310
311   end
```

D.1.6   Example of Auto-Generated Drilling Report

```
filename =

    'Drilling Data 04-06-18, Run Number 2.txt'


filename2 =

    'Drilling Data Down Hole 04-06-18, Run Number 2.txt'


DrillDataPath =

    'C:\Users\Drillbotics\Desktop\LabVIEW Drillbotics
 2018\CompetitionScript\Drilling Data\'
```

Drilling Test Information

```
Description =

    'Date: 04.06.2018
    Time: 12.58
    Operator: Andreas
    Run Number: 2
    Comment: Ran throguh the competition sample with NTNU bit. 50 kg
 and 1300 rpm
    '
```

Plotting of data

Sampling time vs Time Elapsed
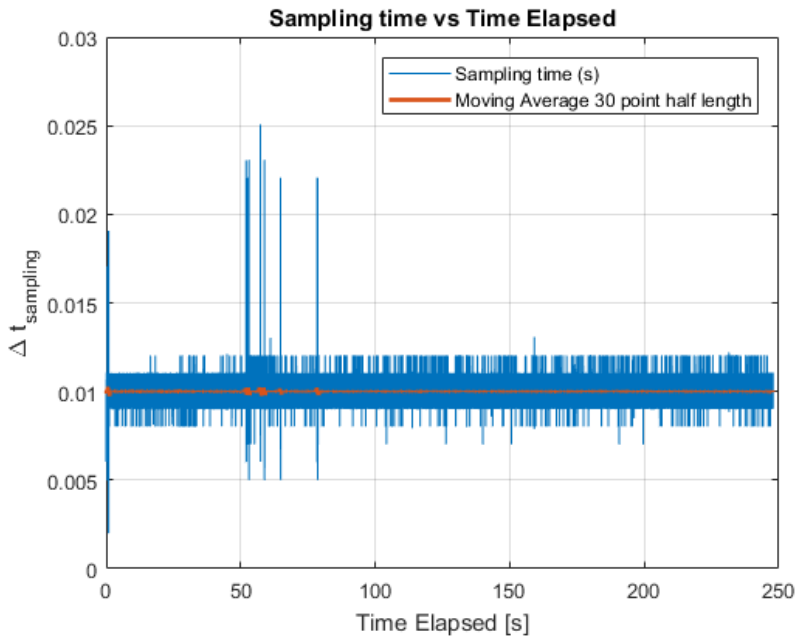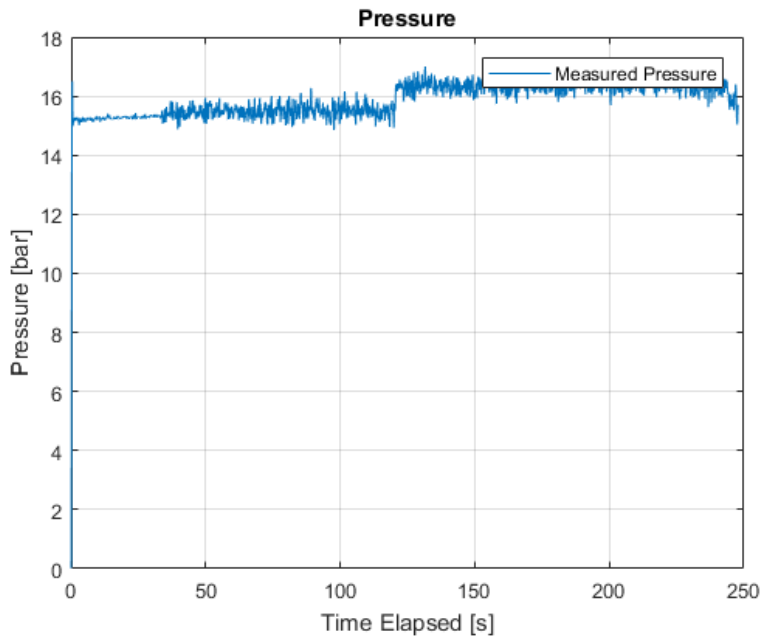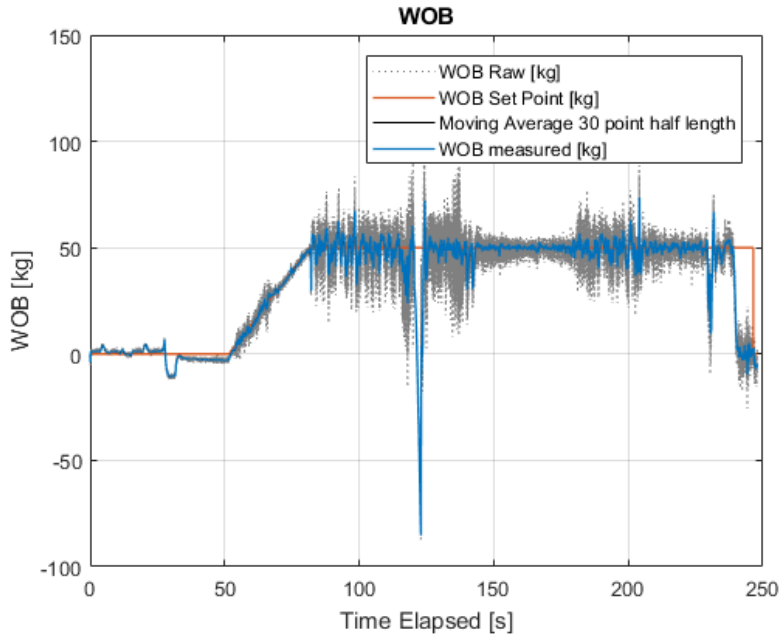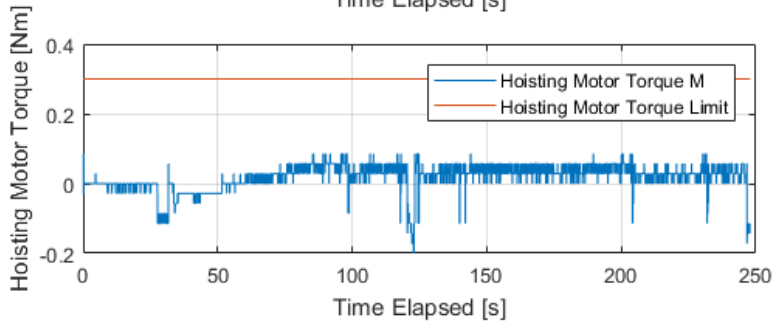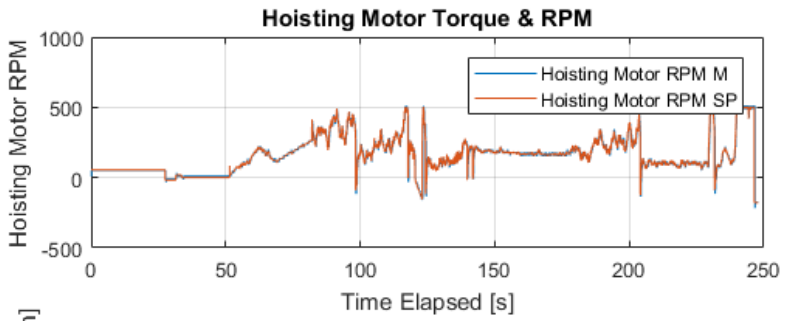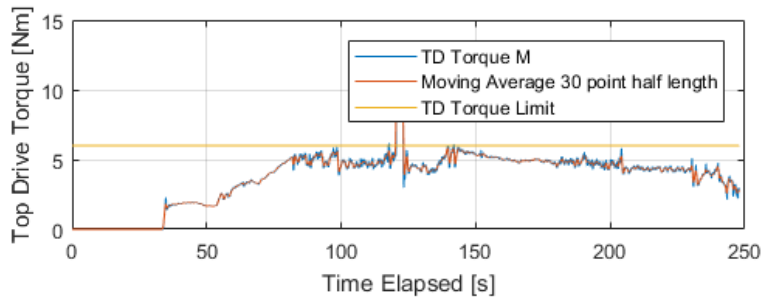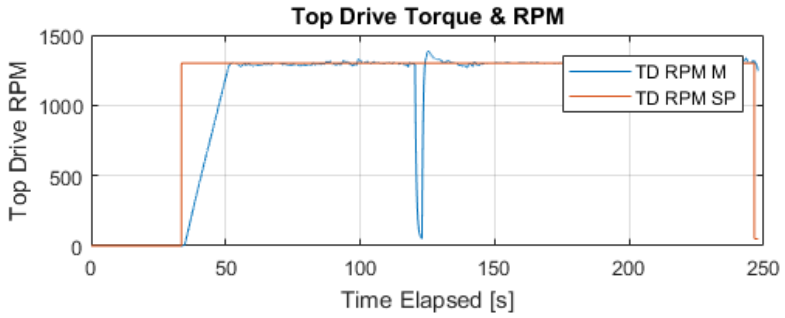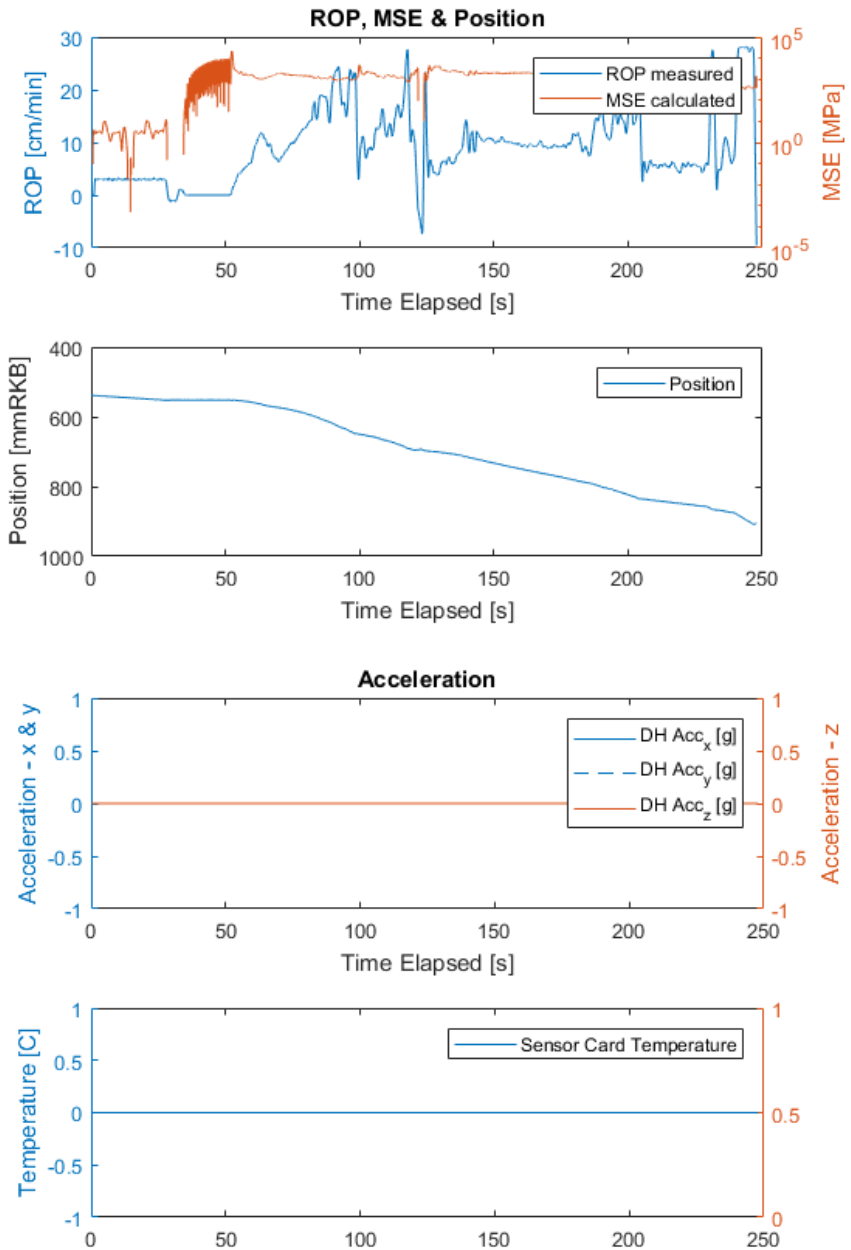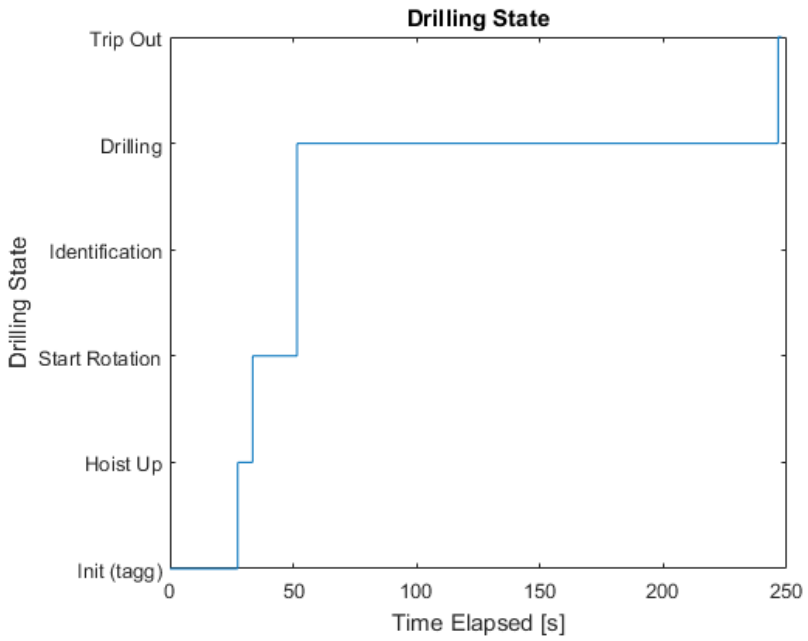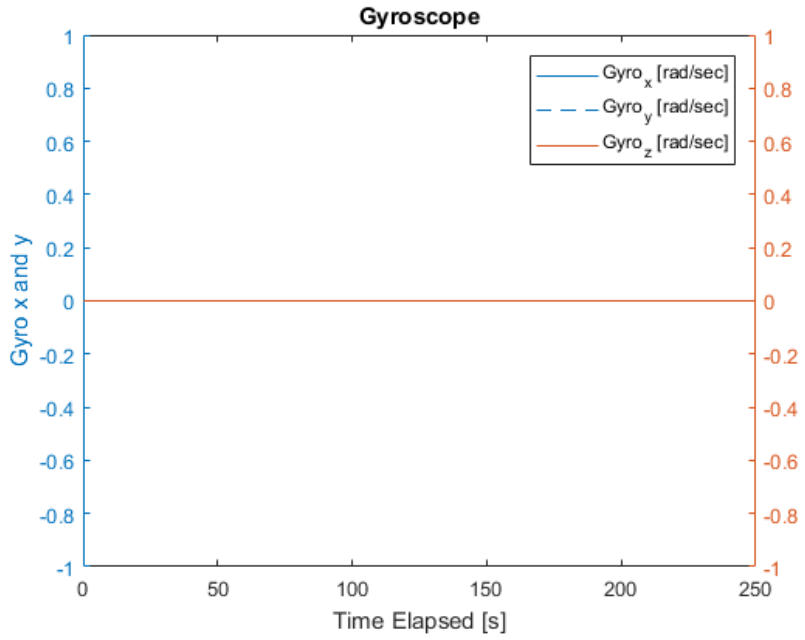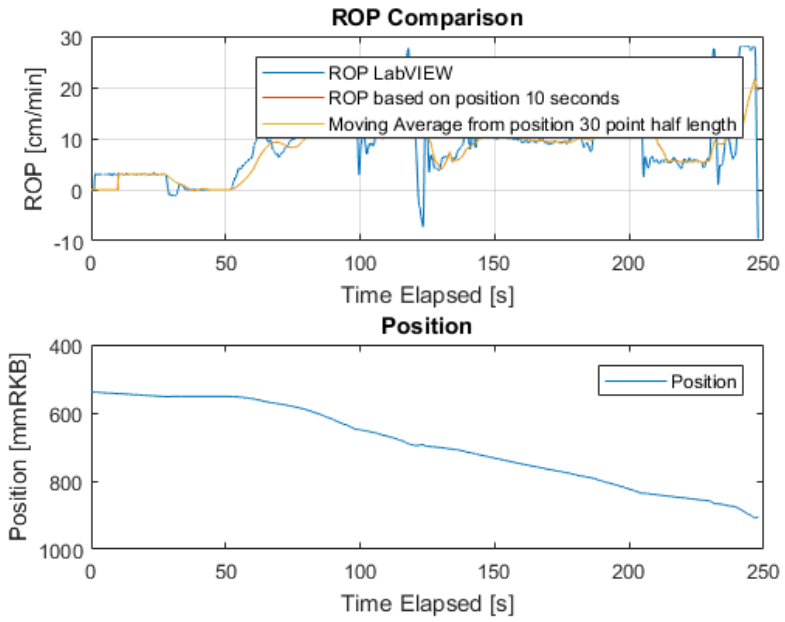
Published with MATLAB® R2017a

7
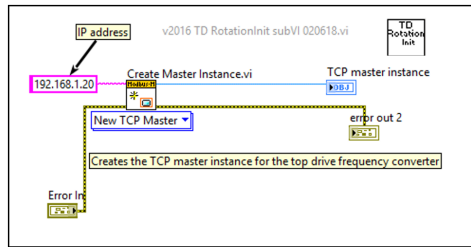
Figure D.6: Initializing the top drive motor connection with the top drive frequency converter using a TCP master instance.
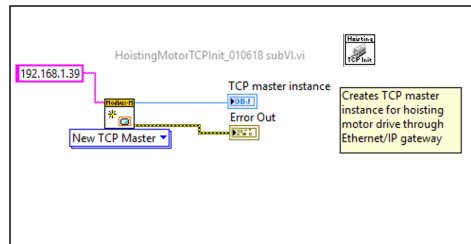
Figure D.7: Initializing the hoisting motor connection with the Modbus TCP - Ethernet/IP gateway and hoisting motor drive.

D.2   SubVI's of LabVIEW
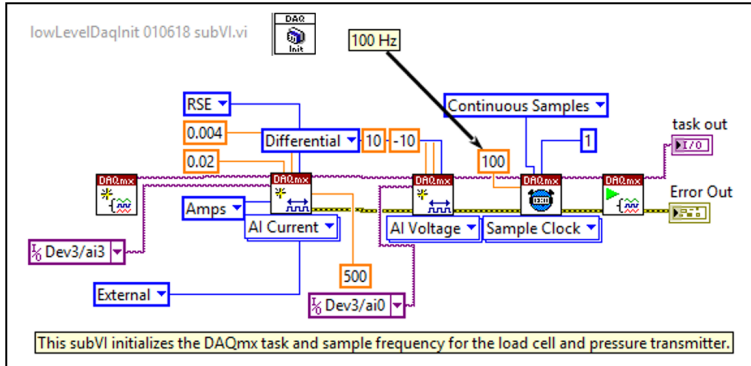
Figure D.8: Initializing the DAQmx connection for reading load cell and pressure gauge data through the NI-USB-6009.
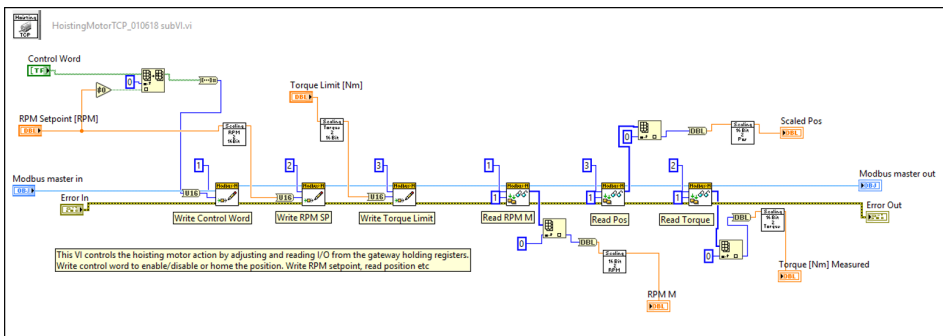
Figure D.9: SubVI for controlling the rotation of the hoisting motor, as well as reading torque, speed and position. Speed set point is also done in this VI.
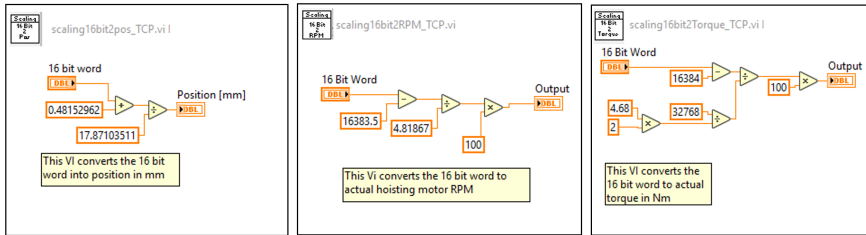
(a) Conversion from 16 bit word to position in mm. **(b)** Conversion of 16 bit word to RPM **(c)** Conversion of 16 bit word to torque in NM
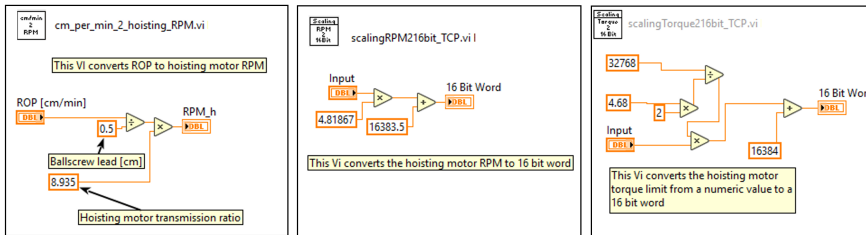
(d) Conversion from cm in min to hoisting motor RPM. **(e)** Conversion of hoisting motor RPM to 16 bit word **(f)** Conversion from torque in Nm to 16 bit word.

Figure D.10: SubVIs used for cenverting and scaling in the main VI.
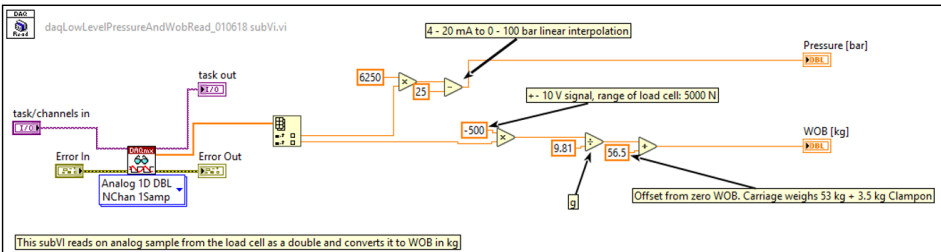
Figure D.11: This subVI is used to read the NI USB-6009 raw data, and converts the measurement of current and voltage to pressure and WOB.
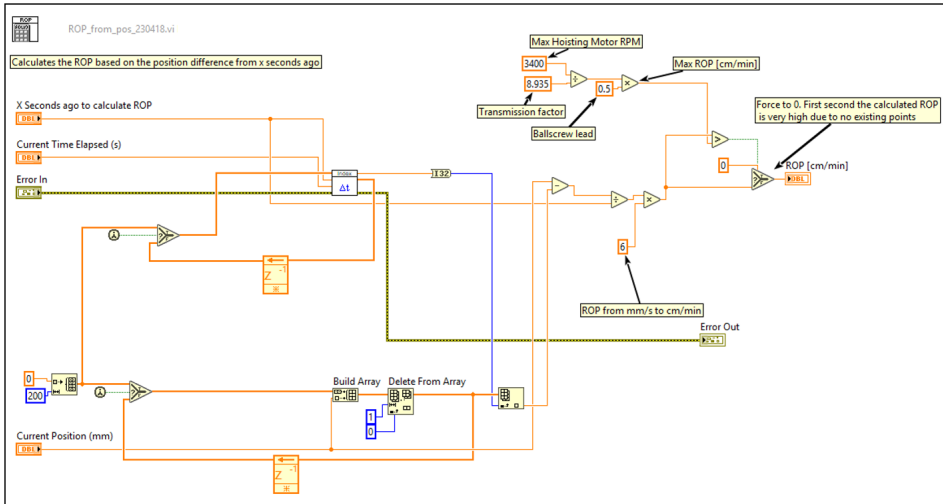
Figure D.12: This subVI calculated the ROP based on the change in measured position.
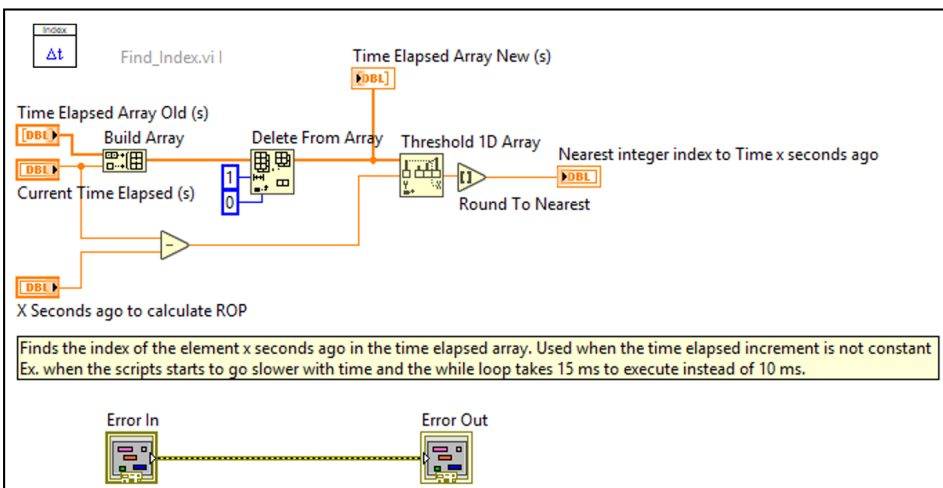
Figure D.13: This subVI is used to find the index in the time elapsed array which has a value of current time minus x second. Execution time in not necessarily a constant 100 Hz. This VI ensures that the ROP is calculated from an exact time increment.
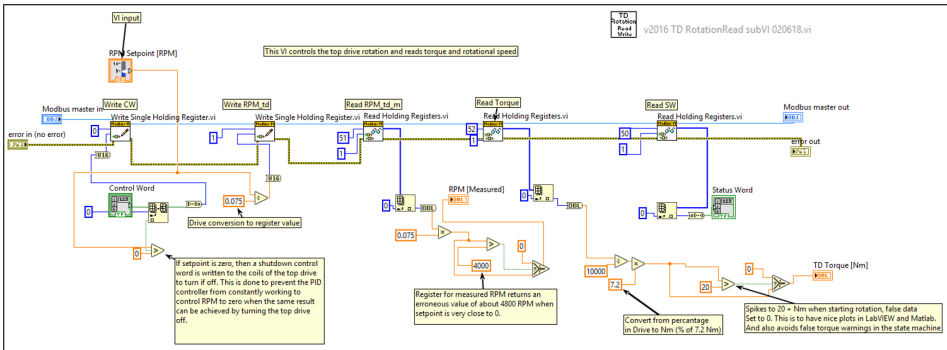
Figure D.14: This subVI controls the top drive rotation. The torque limits is written to the drive, together with the RPM set point. Torque and rotational speed are also read.
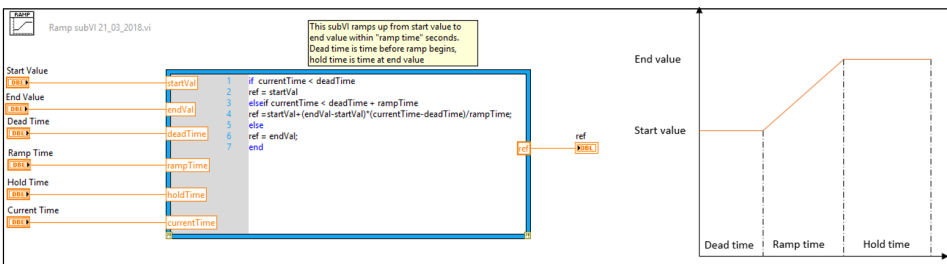
Figure D.15: The subVI generated an arbitrary ramp based on the used input. Is used for ramping WOB set point and rotational speed set point.
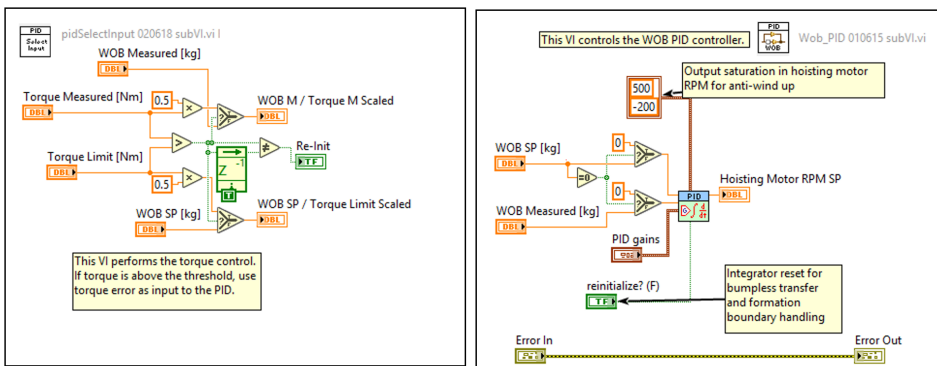
(a) subVI used to determine the input of the PID subVI. Implements the torque control where the torque error is used if torque is above the threshold.

(b) subVI used to automatically regulate the hoisting motor rotational speed such that the WOB is close to the intended set point. Implements anti-wind up.

Figure D.16: SubVIs used for the PID controller.
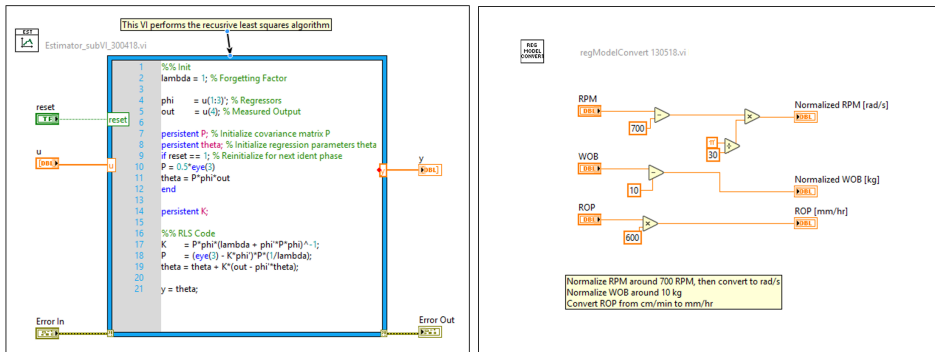
(a) The recursive least squares estimator is implemented in this subVI. A mathscript node is used in LabVIEW to perform the calculations.

(b) The estimator uses ROP in mm/hr and rotational speed as radians per second. This subVI scales the input.
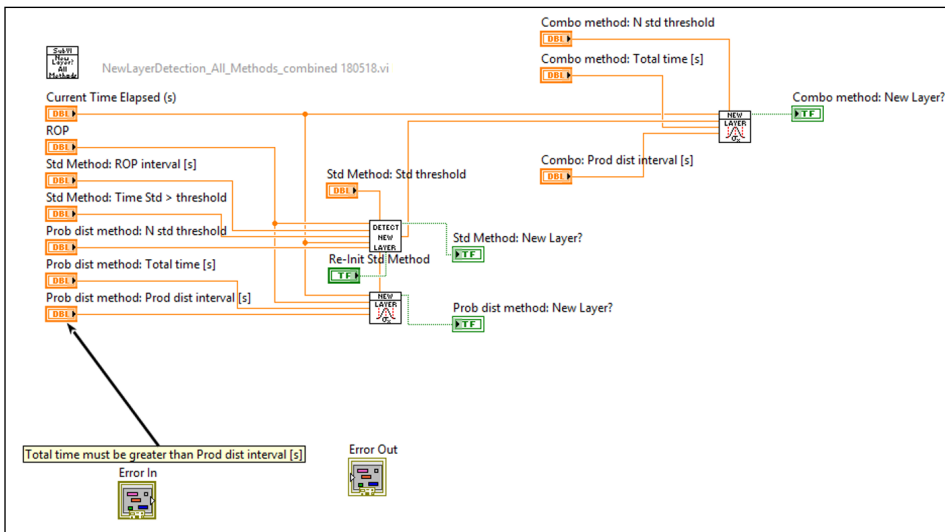
Figure D.17: SubVIs used for the estimator.

Figure D.18: Three methods for detecting a new formation boundary is implemented in this single VI. Note that the "combo" method is not used nor discussed in the thesis.
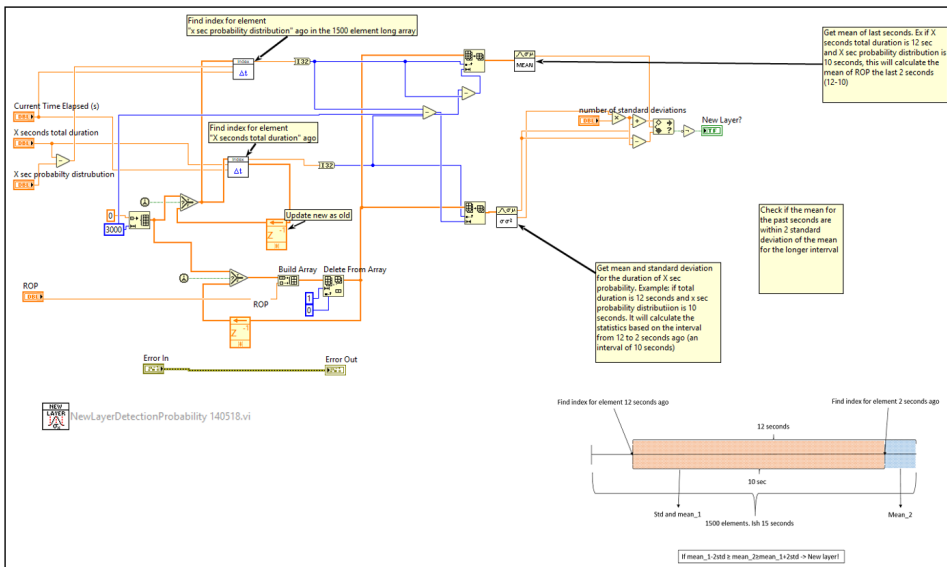
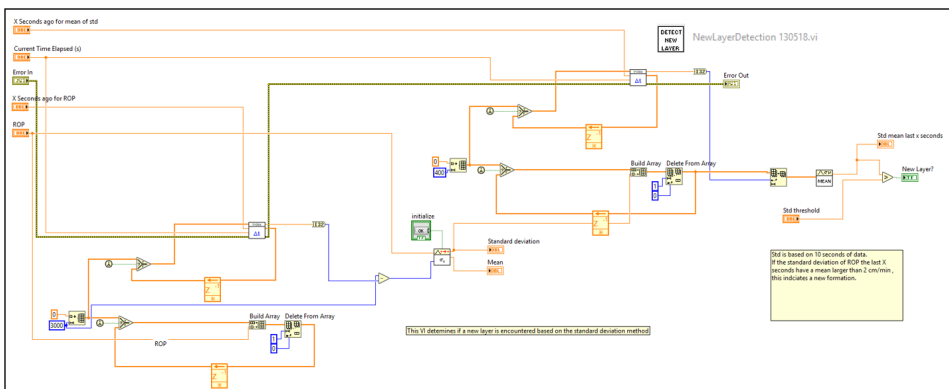**Figure D.19:** SubVI for detecting a new formation based on the frequency distribution of the ROP and a sample mean.

Figure D.20: SubVI for detecting a new formation based on the standard deviation of the past X seconds.
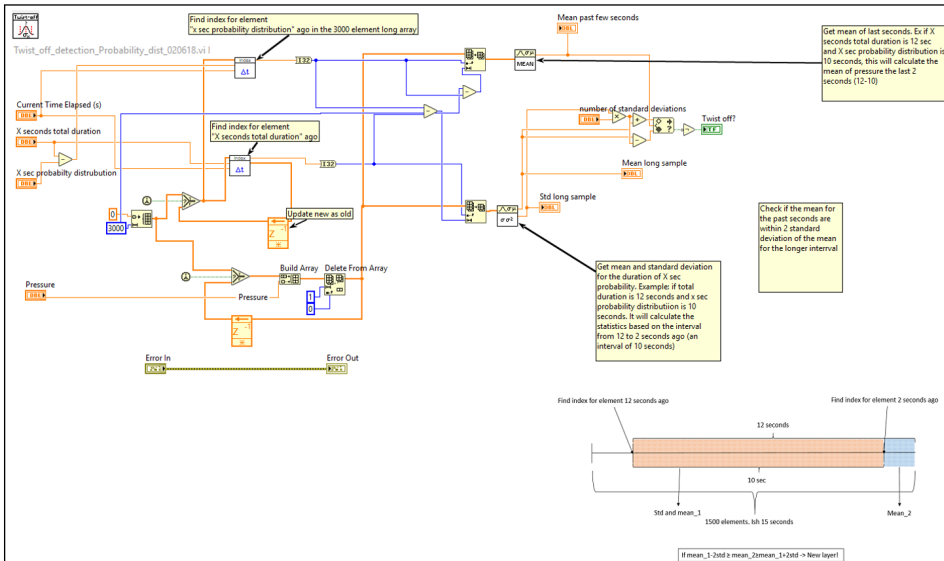
Figure D.21: SubVI used to indicate twist off based on a measured pressure drop. Uses the same principle as the layer detection method based on a frequency distribution.
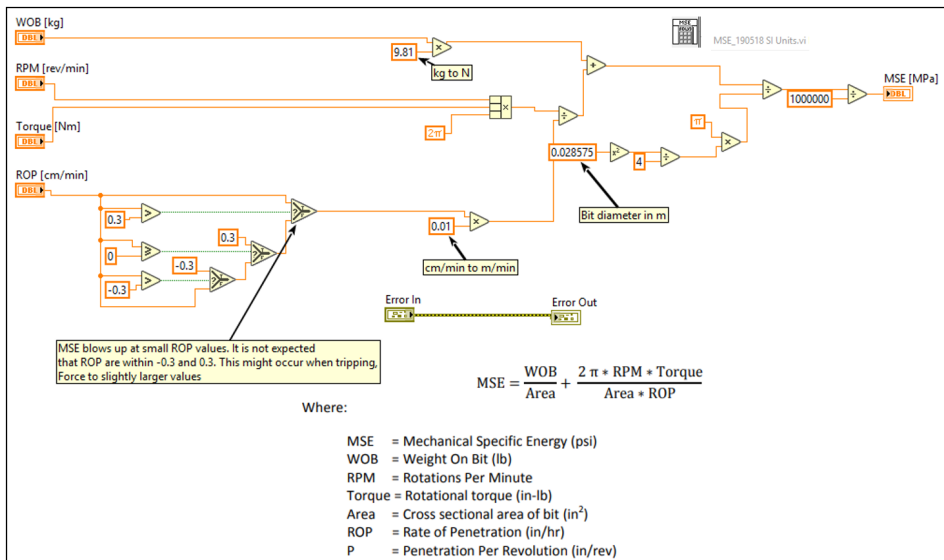

$$MSE = \frac{WOB}{Area} + \frac{2\,\pi * RPM * Torque}{Area * ROP}$$

Where:

MSE = Mechanical Specific Energy (psi)
WOB = Weight On Bit (lb)
RPM = Rotations Per Minute
Torque = Rotational torque (in-lb)
Area = Cross sectional area of bit (in^2)
ROP = Rate of Penetration (in/hr)
P = Penetration Per Revolution (in/rev)

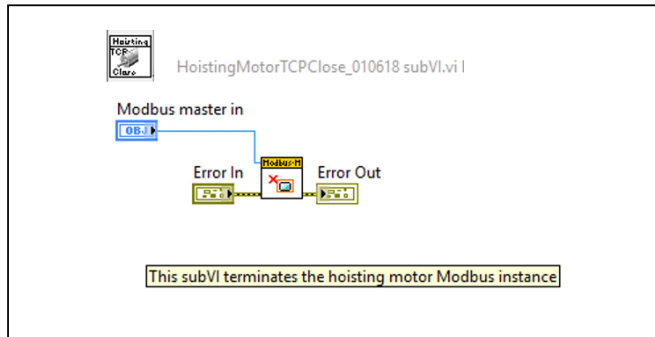**Figure D.22:** MSE is calculated using this subVI. The MSE is given in MPa.

Figure D.23: The Modbus - Ethernet/IP communication is terminated using this subVI. There is no equivalent subVI to terminate the top drive modbus communication as it is done in each iteration of the while loop, as seen in **Fig. D.14**
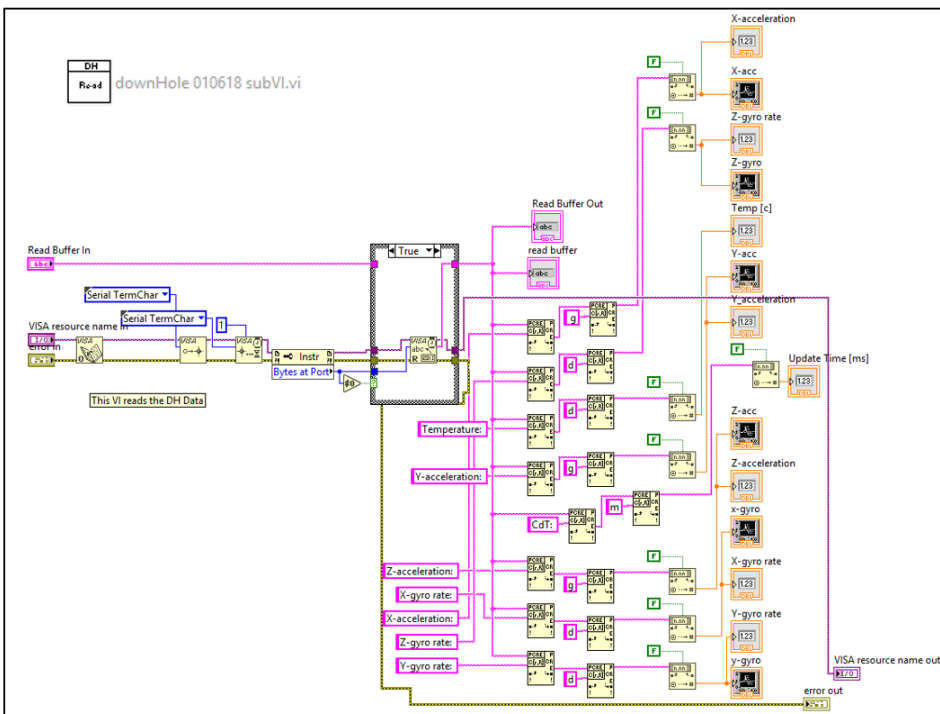

Figure D.24: The down hole sensor data are acquired in this subVI.